ESMAR FABEN SOUZA

Development of pH- and temperature-sensitive microgel particles: synthesis monitoring, characterisation and application as potential oral carriers

São Paulo

2019

ESMAR FABEN SOUZA

Development of pH- and temperature-sensitive microgel particles: synthesis monitoring, characterisation and application as potential oral carriers

Versão Corrigida

(Versão original encontra-se na unidade que aloja o Programa de Pós-graduação)

Tese apresentada à Escola Politécnica da Universidade de São Paulo para obtenção do título de Doutor em Ciências

São Paulo

2019

28

Janus

Universidade de São Paulo

ATA DE DEFESA

Ata de defesa de Tese do(a) Senhor(a) Esmar Faben Souza no Programa: Engenharia Química, do(a) Escola Politécnica da Universidade de São Paulo.

Aos 12 dias do mês de abril de 2019, no(a) realizou-se a Defesa da Tese do(a) Senhor(a) Esmar Faben Souza, apresentada para a obtenção do título de Doutora intitulada:

"Desenvolvimento de partículas de microgéis sensíveis ao pH e à temperatura: monitoramento da síntese, caracterização e aplicação como potencial carreador oral de fármacos"

Após declarada aberta a sessão, o(a) Sr(a) Presidente passa a palavra ao candidato para exposição e a seguir aos examinadores para as devidas arguições que se desenvolvem nos termos regimentais. Em seguida, a Comissão Julgadora proclama o resultado:

Nome dos Participantes da Banca	Função	Sigla da CPG	Resultado
Reinaldo Giudici	Presidente	EP - USP	APROVADO
Claudia Sayer	Titular	UFSC - Externo	aprovado
Liliane Maria Ferrareso Lona	Titular	UNICAMP - Externo	aprovada
Amilton Martins dos Santos	Titular	EEL - USP	aprovado
Leandro Gonçalves de Aguiar	Titular	EEL - USP	Aprovado

Resultado Final: APROVADO

Parecer da Comissão Julgadora *

Eu, Elias Alves de Almeida _____, lavrei a presente ata, que assino juntamente com os(as) Senhores(as). São Paulo, aos 12 dias do mês de abril de 2019.

Claudia Sayer

Liliane Maria Ferrareso Lona

Amilton Martins dos Santos

Leandro Gonçalves de Aguiar

Reinaldo Giudici
Presidente da Comissão Julgadora

* Obs: Se o candidato for reprovado por algum dos membros, o preenchimento do parecer é obrigatório.

A defesa foi homologada pela Comissão de Pós-Graduação em _____ e, portanto, o(a) aluno(a) _____ jus ao título de Doutora em Ciências obtido no Programa Engenharia Química.

_____
Presidente da Comissão de Pós-Graduação

ESMAR FABEN SOUZA

Development of pH- and temperature-sensitive microgel particles: synthesis monitoring, characterisation and application as potential oral carriers

Versão Corrigida

(Versão original encontra-se na unidade que aloja o Programa de Pós-graduação)

Tese apresentada à Escola Politécnica da Universidade de São Paulo para obtenção do título de Doutor em Ciências

Área de Concentração:
Engenharia Química

Orientador:
Prof. Dr. Reinaldo Giudici

São Paulo

2019

Este exemplar foi revisado e corrigido em relação à versão original, sob responsabilidade única do autor e com a anuência de seu orientador.

São Paulo, _____ de _____ de _____

Assinatura do autor: _____

Assinatura do orientador: _____

Catalogação-na-publicação

Souza, Esmar Faben
Development of pH- and temperature-sensitive microgel particles: synthesis monitoring, characterisation and application as potential oral drug carriers / E. F. Souza -- versão corr. -- São Paulo, 2019.
221 p.

Tese (Doutorado) - Escola Politécnica da Universidade de São Paulo. Departamento de Engenharia Química.

1.Microgéis multisensíveis 2.Polimerização por precipitação 3.Carreadores oral de fármacos 4.Técnicas espectroscópicas 5.Monitoramento da síntese I.Universidade de São Paulo. Escola Politécnica. Departamento de Engenharia Química II.t.

To my mother, my stepfather, my aunt Margarethe,
my sister Lorena, and my boyfriend Lucas,
special people in my life.

ACKNOWLEDGEMENTS

Ao professor Dr. Reinaldo Giudici, pela oportunidade, orientação, apoio, e por toda confiança depositada em mim.

Aos professores do Departamento de Engenharia Química da Escola Politécnica da USP pelo conhecimento transmitido, em especial ao professor Dr. Roberto Guardani e a professora Drª Idalina Vieira Aoki.

Aos técnicos do Departamento de Engenharia Química pelo suporte. Ao Adir (técnico do Departamento de Engenharia Elétrica da EP/USP) e ao Fernando (do Laboratorio de corrosão do Departamento de Engenharia Química da EP/USP) pelas análises com o MEV.

Aos colegas da Universidade de São Paulo pela colaboração acadêmica e amizade, em particular ao grupo de polímeros.

À Maria Giuliana pela amizade e suporte, e pelas correções e sugestões de melhoria desse trabalho.

Às minhas alunas de iniciação científica, Daniela e Marcela, pela colaboração experimental ao longo desse trabalho.

À minha mãe, meu padrasto, minha Tia Margarethe e minha irmã pelo amor incondicional e constante apoio; Ao meu namorado e companheiro Lucas pelo amor, carinho, apoio e paciência.

Agradeço aos meus amigos José Eduardo e Flávia pelo companheirismo, amizade e palavras de incentivo. Às minhas amigas Cristhiane Assenhaimer e Beatriz Sanabria, que mesmo longe me apoiaram com suas palavras motivadoras.

Ao CNPq pela concessão da bolsa de doutorado direto (processos n° 141163/2015-1 e 165775/2018-1). Agradeço também às agências financiadoras CAPES e FAPESP.

E a todos que colaboraram direta ou indiretamente, na execução deste trabalho.

We come here to be philosophers; and I hope you will always remember a result happens,

especially if it be new, you should say, "what is the cause? Why does it occur?"

and you will in the course of time find out the reason.

(Michael Faraday “The chemical history of a candle”)

RESUMO

SOUZA, E.F. **Development of pH- and temperature-sensitive microgel particles:** synthesis monitoring, characterisation and application as potential oral drug carriers. Versão corrigida. 2019. 221 p. Tese (Doutorado em Ciências) – Departamento de Engenharia Química, Escola Politécnica da Universidade de São Paulo, São Paulo, 2019.

Microgéis multisensíveis são partículas poliméricas covalentemente reticuladas, com uma dimensão coloidal, e com capacidade para mudar o seu volume através de vários estímulos externos, como por exemplo, pH, força iônica, temperatura e campos magnéticos ou elétricos. Devido a essas características, estas partículas têm recebido grande atenção, principalmente na aplicação como carreadores de fármacos. O objetivo deste estudo foi sintetizar partículas de microgéis sensíveis ao pH e à temperatura através da polimerização por precipitação dos monômeros N-isoproprilacrilamida e ácido acrílico, que tivessem tamanho definido, distribuição de tamanho estreita, morfologia esférica e estabilidade coloidal, para serem utilizadas como carreadores oral de fármacos. Com o intuito de proporcionar melhor biocompatibilidade e biodegradabilidade no material sintetizado, foram realizados alguns ensaios acrescentando o biopolímero quitosana durante a polimerização dos monômeros citados anteriormente. O presente trabalho também teve como objetivo contribuir para uma melhor compreensão da relação entre a síntese de microgéis e suas propriedades utilizando técnicas espectroscópicas para monitorar a formação dos microgéis. Uma nova abordagem foi proposta para monitorar as variáveis de processo, conversão de monômero e tamanho médio das partículas de microgel, durante a polimerização por precipitação através de espectrofotômetros NIR e UV-VIS-NIR acoplados a uma sonda. Além disso, a influência das condições da reação nas características físico-químicas das partículas de microgel foi extensivamente investigada, bem como o seu potencial como carreador oral de insulina. Os resultados do monitoramento indicaram o enorme potencial das técnicas espectroscópicas utilizadas, permitindo o controle da polimerização com aquisição rápida e direta dos dados em tempo real. Em geral, os microgéis sensíveis ao pH e à temperatura foram sintetizados com sucesso, e algumas formulações mostraram-se adequadas para aplicação como veículos de fármaco através da via oral. No entanto, os resultados preliminares da liberação in vitro não foram satisfatórios,

e um estudo mais aprofundado entre a interação do fármaco com as partículas e o método de liberação é recomendado. Em conclusão, com uma compreensão adequada da influência das condições do processo (nesse caso, da concentração dos reagentes) nas propriedades físico-químicas dos microgéis, é possível ajustá-las para obtenção de microgéis multissensíveis com características adequadas para a aplicação desejada.

Palavras-chave: Microgéis multisensíveis, polimerização por precipitação, carreadores oral de fármacos, técnicas espectroscópicas, monitoramento da síntese.

ABSTRACT

SOUZA, E.F. **Development of pH- and temperature-sensitive microgel particles:** synthesis monitoring, characterisation and application as potential oral drug carriers. Versão corrigida. 2019. 221 p. Tese (Doutorado em Ciências) – Departamento de Engenharia Química, Escola Politécnica da Universidade de São Paulo, São Paulo, 2019.

Multi-sensitive microgel particles are covalently crosslinked polymeric chains with a colloidal dimension that can rapidly change their volume through various external stimuli such as pH, ionic strength, temperature, and magnetic and electric field. Due to these characteristics, increasing attention has been focus on the development of multi-sensitive microgels, mainly for application as drug delivery carriers. This study aimed to synthesise pH- and temperature-sensitive microgel particles, based on precipitation polymerisation of N-isopropylacrylamide and acrylic acid, with a defined size, narrow size distribution, spherical morphology and colloidal stability to be used as an oral drug carrier. In order to provide better biocompatibility and biodegradability in the synthesised material, some assays were performed, adding the chitosan biopolymer during the polymerisation of the monomers previously mentioned. This thesis also intended to contribute to a better understanding of the relationship between the microgel synthesis and their properties using spectroscopic techniques to monitor the microgel formation. A new approach was proposed to monitoring the process variables, monomer conversion and average particle size of the microgel particles, during precipitation polymerisation using NIR and UV-VIS-NIR high-resolution spectrophotometers coupled with a probe. Besides, the influence of reaction conditions in the physicochemical characteristics of microgel particles was extensively investigated as well as their potential as an oral drug carrier for insulin. The monitoring results pointed out the enormous potential of these spectroscopy techniques to monitor the precipitation polymerisation process, allowing control over the polymerisation reaction with quickly and directly acquisition of data in real-time. In general, pH- and temperature-sensitive microgels were successfully synthesised, and many formulations showed to be suitable for application as oral drug carriers. However, the preliminary *in vitro* release results were not satisfactory, and a more in-depth study between the interaction of the drug with the particles as well as the method of release is recommended. In conclusion, with a proper understanding of the

influence of the process conditions (e.g., reagent concentrations) on the physicochemical properties of the microgels, it is possible to tailor the multi-sensitive microgels for the desired application.

Keywords: Multi-sensitive microgels, precipitation polymerisation, oral drug carrier, spectroscopic techniques, synthesis monitoring.

LIST OF FIGURES

LIST OF TABLES

LIST OF ABBREVIATIONS

AA	Acrylic Acid
AAm	Acrylamide
AFM	Atomic Force Microscopy
BSA	Bovinum Serum Albumin
BuA	Butyl Acrylate
COE	Constant Offset Elimination
Cs	Chitosan
DDS	Drug Delivery System
DLS	Dynamic Light Scattering
DSC	Differential Scanning Calorimetry
EE	Entrapment Efficiency
EGA	Ethylene Glycol Acrylate
EGDA	Ethylene Glycol Diacrylate
EGDMA	Ethylene Glycol Dimethacrylate
EGMA	Ethylene Glycol Methacrylate
ELS	Electrophoretic Light Scattering
EP	Emulsion Polymerisation
FCC	Free-radical Crosslinking Copolymerisation
FD	First Derivative
FRET	Fluorescence Resonance Energy Transfer
FTIR	Fourier Transforms Infrared
GI	Gastrointestinal
HDSC	High-sensitivity Differential Scanning Calorimetry
HEMA	Hydroxyethyl Methacrylate
H-NMR	Nuclear Magnetic Resonance
HPMA	N-(2-hydroxypropyl) methacrylate
Hq	Hydroquinone
IHM	Indirect Hard Modelling
IR	Infrared
IS	Internal Standard
ITC	Isothermal Titration Calorimetry
IU	Insulin Units
KBr	Potassium Bromide
KPS	Potassium Persulfate
LCST	Lower Critical Solution Temperature
MAA	Methacrylic Acid
MLR	Multiple Linear Regression
MBA	N,N’-methylenebisacrylamide
NIPAM	N-isopropylacrylamide
NIR	Near-Infrared
M-M N	Min-Max Normalization
MPT-2	Multipurpose Titrator
MSC	Multiplicative scatter correction
NN	Neural Networks

NPs	Nanoparticles
NSDP	No Spectra Data Pre-processing
NVCL	N-vinylcaprolactam
NVP	N-vinyl-2-pyrrolidone
PALS	Phase Analysis Light Scattering
PCA	Principal Component Analysis
PCR	Principal Component Regression
PCS	Photon Correlation Spectroscopy
PDI	Polydispersity Index
PEGDA	Poly(ethylene glycol) Diacrylate
PLS	Partial Least Square
PP	Precipitation Polymerisation
PRESS	Prediction Residual Error Sum of Squares
PSD	Polydispersed Size Diameter
QELS	Quasi-elastic Light Scattering
RMSECV	Root Mean Square Error of Cross-Validation
SANS	Small-angle Neutron Scattering
SAXS	Small-angle X-ray Scattering
SEC	Size Exclusion Chromatography
SED	Secondary Electron Detector
SEM	Scanning Electron Microscopy
SEP	Surfactant-free Emulsion Polymerisation
SLS	Static Light Scattering
SOP	Standard Operating Procedures
TEA	Triethanolamine
TEM	Transmission Electron Microscopy
TGA	Thermogravimetric Analysis
TMPTA	Trimethylolpropane Triacrylate
UPEs	Unsaturated Polyesters
UV-Vis	Ultraviolet-Visible
UV-VIS-NIR	Ultraviolet-Visible-Near Infrared
VAc	Vinyl acetate
VN	Vector Normalisation
VPTT	Volume Phase Transition Temperature
WHO	World Health Organization
ZP	Zeta Potential

LIST OF SYMBOLS

a	Radius of the particle
ABS	Absorbance
A'	Baseline constant
b_0 and b	Regression coefficients
$\hat{b}_0$ and $\hat{b}$	Predicted regression coefficients
B'	Intercept constant
D	Translational diffusion coefficient of the particles
D_h	Average particle size
Dh_{max}	Maximum value for average particle size (hydrodynamic diameter)
Dh_{min}	Minimum value for average particle size (hydrodynamic diameter)
e	Residue
E	Energy of the system
E_v	Energy associated with the vth quantum level
$f(ka)$	Henry function
G(t)	Autocorrelation function
h	Plank constant
$I(t_0)$ and $I(t_0 + t)$	Scattered light intensities at instants (t_0) and $(t_0 + t)$
k	Force constant of the bond
k	Debye length
k	Number of principal factors or components
K_B	Boltzmann's constant
m_1	Mass 1 for body harmonic oscillator
m_2	Mass 2 for body harmonic oscillator
M	Number of samples in the calibration set
M_{CS}	Mass of the collect sample
M_{DR}	Mass of the dry polymer
M_{NPS}	Mass of non-polymeric solids
n	Refractive index of the dispersant
q	Light scattering wave vector
r	Internuclear distance
r_e	Internuclear distance at equilibrium
R^2	Determination coefficient
T	Absolute temperature
U_E	Electrophoretic mobility
v	Fundamental vibrational frequency
v	Vibrational quantum number (0,1,2,….)
V	Potential energy
x^2	Displacement of the vibrating atoms
x^3	Higher-order terms of displacement
X	Monomer conversion in polymer
X	NIR spectrum
X_{max}	Maximum value for monomer conversion
X_{min}	Minimum value for monomer conversion
y	Anharmonicity constant of the vibration

$y_{i,exp}$	Experimental value
$y_{i,pred}$	Value predict by the calibration model
y_{m0}	Mass fraction of monomers in the reaction medium
$\bar{y}_{exp}$	Average of the experimental values
Y	Process response
$\hat{Y}$	Predicted process response
Γ	Decay constant of the exponential curve generated by the autocorrelation function
ε	Dielectric constant of the medium
ζ	Zeta potential
η	Viscosity of the dispersing medium
θ	Scattering angle
λ	Wavelength
λ_0	Wavelength of the incident light
μ	Reduced mass
$[I]$	Insulin concentration
$[I]_{free}$	Free concentration of insulin
$[I]_{initial}$	Initial concentration of insulin

CONTENTS

1. Introduction

1.1. Motivation

Microgel particles are covalently crosslinked polymeric chains with a colloidal dimension that are swollen by a good solvent (SAUNDERS; VINCENT, 1999; BALACEANU et al., 2013). One of the most important characteristics of these particles is their intrinsic ability to rapidly change their volume (i.e., swell or unswell) through various external stimuli such as pH (SNOWDEN et al., 1996; LALLY et al., 2007; ZHANG; LIU; ZHA, 2011; YUAN; WANG; CHEN, 2014), ionic strength (SNOWDEN et al., 1996), temperature (SNOWDEN et al., 1996; DIMITROV et al., 2007; LU; LIU; ZHA, 2013; KAWAGUCHI, 2014; YUAN; WANG; CHEN, 2014), magnetic and electric field (MÉNAGER et al., 2004; NOJD et al., 2013; YUAN; WANG; CHEN, 2014) and osmotic pressure (FERNÁNDEZ-NIEVES et al., 2003). Because of this unique characteristic, microgels have acquired high importance in several areas of science, for example in the drug and genes delivery (MUNDARGI; RANGASWAMY; AMINABHAVI, 2011; BAI et al., 2012; SAMAH; HEARD, 2013; GANGULY et al., 2014), catalysis (AJMAL; FAROOQI; SIDDIQ, 2013; FAROOQI et al., 2015; IQBAL et al., 2016), sensors (HAN; ZHANG; SERPE, 2015), and oil recovery (AL-MANASIR, 2009).

In the biomedical and pharmaceutical fields, microgels sensitive to temperature and pH have been the object of numerous studies (MUNDARGI; RANGASWAMY; AMINABHAVI, 2011; BAI et al., 2012; FAROOQI et al., 2013; SAMAH; HEARD, 2013; HAIDER et al., 2014; RWEI et al., 2015). This interest is supported by the fact that the human body exhibits pH variations along the gastrointestinal tract, as well as in some specific regions, such as specific tissues (such as tumour sites) and subcellular compartments (SCHMALJOHANN, 2006). For example, polyacids offer opportunities in pH-dependent release for oral delivery since these are uncharged at low pH (e.g., in the stomach, pH=1-2.5), resulting in network collapse (dehydrated structure), low drug release rate, and protection against acid-catalysed drug hydrolysis. At higher pH, on the other hand (e.g., in the small intestine, pH=6.6-7.5), dissociation of the acid groups causes network swelling as a result of electrostatic interactions, thereby facilitating drug release in a part of the gastrointestinal tract where it is absorbed more effectively, and where the drug is more stable against hydrolytic degradation (MALMSTEN, 2006; MALMSTEN; BYSELL; HANSSON, 2010).

Thus, microgels particles offer unique advantages as carrier system for drug delivery, mainly for oral drug delivery of biomacromolecules such as proteins and peptides, since they are generally hydrophilic and highly hydrated, which allows such drugs to be incorporated into them with only moderate conformational changes and limited aggregation, facilitating maintained biological effect of the biomacromolecular drug (MALMSTEN; BYSELL; HANSSON, 2010).

The most studied protein is insulin that is the drug used to treat *Diabetes mellitus*, a significant global public health problem. In this way, the oral delivery of insulin is an attractive option compared to the actual method of insulin administration (subcutaneous injections), due to the ease of administration and the absence of pain, leading to greater convenience and adhesion, and a reduced risk of infection.

Taking into account the needs in the development of an oral carrier for insulin, this work aimed to test the potential of pH- and temperature-sensitive microgel particles based on acrylic acid (AA) and N-isopropylacrylamide (NIPAM) to protect the insulin in an acid environment (simulating the stomach) and release them in the alkaline medium (simulating the small intestine). Besides the characteristic of great pH-response, the polymers based on AA also presents excellent mucoadhesives properties (ELSAYED, 2012; CHATURVEDI et al., 2013), helped to increase the area available between the intestine cells, permitting the movement of molecules across the layers (CHATURVEDI et al., 2013).

Nevertheless, it is important to understand many physical, chemical, and biological characteristics of the particles for designing a microgel to deliver a specific drug at a specific rate in a specific physiological context (SMEETS; HOARE, 2013). Also, the control over these characteristics allows improving the drug binding and release kinetics, long-term stability and shelf-life, biocompatibility, biodistribution and targeting, bioaccumulation and degradation, and functionalisation (SMEETS; HOARE, 2013).

In particular, particle size and size distribution can help to regulate the release of the drug over a period and to understand how it affects the bioavailability and thereby determine the dosage of the drug. The microgel size can be controlled by choosing appropriate polymerisation techniques and polymerisation conditions (SMEETS; HOARE, 2013).

The most used method to synthesise microgel particles is precipitation polymerisation (PP) (PICH; RICHTERING, 2010). PP is a traditional polymerisation technique that enables the generation of monodisperse spheres in a single step, without the use of stabilisers or surfactants, and without an additional process, step or apparatus. Furthermore, it is possible to control the mean diameter, porosity, degree of crosslinking, and the physical nature of the particles by manipulating the conditions of the reaction medium (PICH; RICHTERING, 2010).

PP produces monodisperse microgel particles, due the short period (order of minutes) of particle nucleation in the absence of surfactant, the particles are stabilised by the electrostatic stabilisation provided by an ionic initiator and/or reactive functional co-monomer (PELTON; HOARE, 2011), and it is necessary highly diluted monomer concentration in the reaction medium (<5%) to maintain the colloidal stability (VEGA et al., 2013).

However, when the new formulations (different kind of monomers and proportion between them) are tested, the system can be destabilised by the occurrence of particle aggregation inside the reactor and agglomerates can be formed, being necessary to interrupt the process. Thus, due to the significant influence of the particle size in the stability of the reaction medium, it is very important to develop techniques for evaluating the microgel formation during the polymerisation and understand how the process conditions affect the microgel characteristic. In this way, monitoring some microgels features give us essential information for the control of the product quality, and allow improving the final characteristic of the product according to the desired application.

In particular, off-line monitoring of the formation of microgel particles by precipitation polymerisation can be challenging due to the highly diluted monomers concentrations (<5 wt%) and the short period (order of minutes) of particle nucleation that can make difficult the proper analysis. In this way, in-line monitoring can provide useful information about the process, allowing to reduce time delays and inaccuracy of analyses usually involved with sample preparation.

Recently, some authors have used spectroscopic techniques for monitoring the microgels formation during precipitation polymerisation. Meyer-Kirschner et al. (2016,2018) used Raman spectroscopy to monitor monomer and polymer content of poly(N-vinylcaprolactam) microgels, and the monomer and polymer fraction of the N-vinylcaprolactam (NVCL) and N-

isopropylacrylamide (NIPAM) copolymerisation during the precipitation polymerisation. They evaluated the spectra using multivariate indirect hard modelling (IHM) regression and concluded that in-line Raman spectroscopy associated with IHM regression could be an excellent technique for monitoring the reaction composition during polymerisation, and allow better control of functional microgels synthesis. The works of Kanter et al. (2016) and Meyer-Kirschner, Mitsos and Viell (2018) also show contributions in the monitoring of microgel formation during precipitation polymerisation. Kanter et al. (2016) used a novel probe design coupled with a dynamic light scattering equipment for in-line monitoring of particle size growth of poly(NIPAM) and poly(NVCL) particles during precipitation polymerisation. The results show good agreement with the offline dynamic light scattering measurements (reference method). Meyer-Kirschner, Mitsos and Viell (2018) have also monitored the microgel particle size during precipitation polymerisation of styrene using Raman spectroscopy technique. Both studies show good agreement between experimental and predicted values.

Although the studies present previously shown good results for in-line monitoring of microgel formation, there are many aspects that still need to be explored, and other spectroscopic techniques can be considered.

In this way, this work intends to contribute to the exploration of the potentialities of Near-infrared (NIR) and Ultraviolet-visible spectroscopy for monitoring the microgel formation by precipitation polymerisation. In principle, NIR spectroscopy would not be the most suitable choice for monitoring precipitation polymerisation due to the higher amount of water in the system, and it is well known that water has strong absorbance bands in the NIR region, which become difficult to visualise the characteristic bands of other compounds.

However, NIR spectra, like Raman spectra, show baseline variations due to light scattering by particles present in the heterogeneous medium, allowing correlations between the physical properties of the particles and the spectra to be made by the proper use of calibration methods.

1.2. Objectives

Although the microgel synthesis and characterisation are quite reported in the literature and drug delivery is the most cited application, there are few works about the understanding of

the microgel formation during the precipitation polymerisation, and the application of poly(NIPAM-co-AA) as insulin oral drug delivery. Moreover, most of the works on characterisation is focused on the swelling behaviour of sensitive microgels. However, the investigation of the interplay between particle size and size distribution, surface charge and morphology is very important and has not been well studied mainly for oral drug delivery system.

Thus, this thesis aimed to design pH- and temperature-sensitive microgel particles based on precipitation polymerisation of N-isopropylacrylamide and acrylic acid with a defined size, narrow size distribution, spherical morphology and stability to be used as an oral insulin carrier. Overall, the general objective is to contribute to a better understanding of the relationship between the microgel synthesis and their properties using spectroscopic techniques to monitor the microgel formation.

Consequently, the specific objectives were:

- To evaluate the feasibility of applying Near-infrared and ultraviolet-visible spectroscopic techniques to monitoring the average particle size and monomer conversion during the formation of microgel particles by precipitation polymerisation process;
- To understand how the variables of the reaction (reagent concentrations) influence the physicochemical characteristic (size, polydispersity index, charge, morphology) and swelling behaviour (in different pHs and temperatures) of the microgel particles;
- To synthesise poly(NIPAM-co-AA) with the biopolymer chitosan (Cs) for preliminary evaluation of the influence of this biopolymer in the microgel features;
- To select the best formulations among the studies to be used as an oral drug delivery;
- To study the potential application of microgel as oral drug delivery for insulin (model drug) by a preliminary analysis of insulin entrapment efficiency and *in vitro* release, as well as the influence of the drug in the size, polydispersity index, zeta potential and pH behaviour of microgel particles.

1.3. Thesis outline

This thesis was organised in six chapters, including this introductory chapter. This work also contains one section with the references in the final part of this document. Chapter 2 presents a literature review about microgel particles with focus in pH- and temperature-sensitive characteristics, and application as drug delivery system. Chapter 3 describes the study of the synthesis of pH- and temperature microgels particles using spectroscopic techniques to monitor the precipitation polymerisation. Chapter 4 shows a detailed study focused on the characterisation of pH- and temperature-sensitive microgel particles for being used as oral drug delivery system, as well as a preliminary study about the physicochemical characteristics of poly(NIPAM-co-AA)-Cs. Chapter 5 shows the preliminary study about the potential of poly(NIPAM-co-AA) as an oral drug carrier of insulin. Finally, Chapter 6 summarises the main conclusions, observations and hypothesis formulate during the discussion of the results, and suggestions for future works are proposed. Chapters 3, 4 and 5 of this thesis were prepared with the structure of scientific articles. Each of these chapters has individual sections composed of abstract, introduction, materials and methods, results and discussion and partial conclusions.

2. Background and Literature Review

2.1. Introduction

This thesis involved a study that is related to two relevant fields: (1) the polymerisation reaction engineering, with the monitoring of the polymerisation in heterogeneous systems, and (2) the biomedical/pharmaceutical area, through the application of polymers as the Drug Delivery System (DDS).

In this way, the present chapter shows the theories behind the development of the proposed work. Because of the different areas included in this project, it is important to provide an overview of some concepts that will allow the connection of these areas of research.

However, focused reviews of the literature more closely related to the specific topics studied in this thesis will be presented in each of the following Chapters.

2.2. Smart Polymers – Hydrogels

Hydrogels are cross-linked polymeric networks that show the capability of swell in water and still maintain a distinct three-dimensional structure.

The hydrogel research began in the 1960s with polymerisation of hydroxyethyl methacrylate and ethylene diacrylate by Wichterle and Lim (1960). The product obtained was the first material used in the biomedical application, in the production of the contact lenses.

Hydrogels are hydrophilic and water-insoluble materials. The hydrophilicity is due to the presence of hydrophilic groups such as: -OH, -COOH, -$CONH_2$, -SO_3H, among others, and the water-insoluble behaviour is attributed to the presence of the cross-linkages in their structure. Because of these characteristics, they can absorb large amounts of water or biological fluids and swell, while maintaining their network polymeric chain structure.

Due to their unique behaviour, there are several applications of these hydrogels in the industry, in particular in the pharmaceutical and medical fields, such as drug delivery system (DON et al., 2008; MAHKAM; ASSADI, 2010; SIMÕES S., FIQUEIRAS A., 2012; AHMAD et al., 2014), biosensors (MATEESCU et al., 2012; PEPPAS; BLARCOM, 2015), on-off switching materials (YOSHIDA et al., 1994; YAO et al., 2015), and adsorptive materials (GONÇALVES et

al., 2009). The most significant progress has been on the controlled release of drugs, because of some advantages of this material, such as:

- Excellent biocompatibility: due to their high water contents and soft consistency which is similar to natural tissues (PEPPAS; LEOBANDUNG; ICHIKAWA, 2000);
- Low toxicity;
- Elastomeric consistency: a factor that minimises friction between tissues and the hydrogel;
- High permeability: allowing the flow of body fluids through the hydrogel, due to the high porosity;
- Application in various routes of administration, such as ocular, nasal, oral, transdermal, subcutaneous and rectal, because of the capability of incorporation and controlled release of drugs of different polarities.

Hydrogels can be called "smart polymers" because they are physiologically-responsive; this means that the swelling behaviour depends on the external environment. These smart materials can be classified according to their specific stimuli, such as pH, temperature, ionic strength, light, sound, electromagnetic stimulation, or the concentration of specific substances like sugars (Figure 2.1).

Figure 2.1 - Factors influencing the swelling rate of hydrogel polymers.

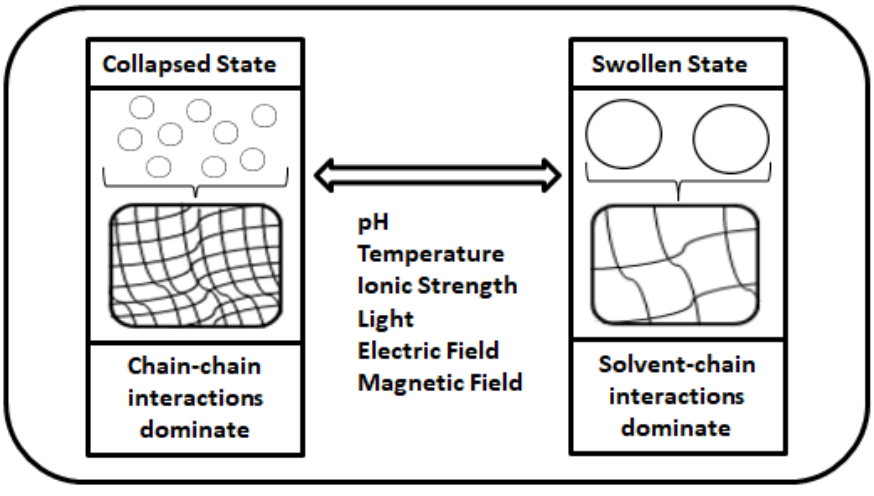

Source: author

Hydrogels can be classified in many ways, such as the type of crosslink (physically and chemically), type of stimuli (pH, temperature, light, pressure, among others), and size (macrogels, microgels and nanogels).

In this work, the focus is on the classification based on size. There are three class of hydrogels based on their size:

- Macrogels: particles visible to the naked eye (the size can be of the order of magnitude of millimetre and above);
- Microgels: particles of diameter in the range from 10 to 1000 nm, typically of colloidal nature;
- Nanogels: particles with 100 nm or less.

Macrogels and microgels have similar polymer chemistry, but their physical molecular arrangements are different. Microgel, as compared with macrogels, are differentiated as discrete gel-like particles, they have a much lower viscosity than macrogels and show very high surface areas (GALAEV; MATTIASSON, 2008).

Because of these interesting physicochemical properties, microgels and nanogels may have a significant advantage over macrogels in biomedical applications; they can improve swelling behaviour and controlling the drug release with more efficiency.

As the microgels are the material of study in this work, the following topics describe the relevant properties, methods of the synthesis and characterisation, and meaningful application of microgels.

2.3. Microgels: Definition and properties

Microgels have been defined as cross-linked polymer particles with a colloidal dimension that are swollen by a good solvent (SAUNDERS; VINCENT, 1999; BALACEANU et al., 2013). The term 'microgel' was first introduced by Baker (1949), in his work entitled "Microgel, a new macromolecule" (BAKER, 1949; SAUNDERS; VINCENT, 1999).

Microgels have also been described as superabsorbent polymers because they consist of a network of flexible cross-linked molecules that exhibits an intriguing combination of the physicochemical properties of bulk solids and liquids (GALAEV; MATTIASSON, 2008).

Aqueous microgels are generally spherical and consist of water swollen cross-linked polymer network. The water content in microgels can vary from 10 to 90% in weight; this variation depends upon the interplay between polymer-polymer and polymer-water interactions and, additionally, numerous factors such as temperature, pH, and ionic strength influence the behaviour of polymer chains inside the microgel. By taking into account these features, aqueous microgels can be considered as porous cross-linked polymeric particles that swell in water and adjust their dimensions, density, and related properties according to the surrounding conditions (PICH; RICHTERING, 2010).

Another important characteristic of the microgels is their stable structures. Covalent or strong physical forces stabilise the polymeric network. On the other hand, like any colloidal dispersion, microgels can aggregate (flocculate or coagulate). However, they are very resistant to aggregation (i.e., colloidally stable) because the surfaces often bear electrical charges and dangling surface chains (hairs). In general, microgel particles tend to be more colloidally stable in the swollen form where Van der Walls attraction is diminished, and surface hairs can sterically stabilise the microgels (PELTON; HOARE, 2011).

Microgels show a unique blend of properties combining useful aspects of conventional macrogels (microgels swell with water or another solvent, and can be "intelligent" or "responsive") with useful properties of colloidal dispersions (free-flowing liquids, respond very rapidly to environmental changes, among others). In this way, several researchers have worked to understand how the composition of microgels affect their characteristics, and how these characteristics can be used in many applications, mainly in the biomedical-pharmaceutical field.

Microgel can be built from a large variety of monomers, which allows precise control of their responsive properties (BALACEANU et al., 2013). Responses to different stimuli can be engineered into a microgel by choice of monomers, comonomers and/or cross-linkers (LYON et al., 2011). Table 2.1 shows the natural polymers and synthetic monomers most often used in the synthesis of microgels for biomedical applications.

Table 2.1 – Natural polymers and synthetic monomers most often used in the synthesis of microgels.

Synthetic monomers	Natural polymer
Hydroxyethyl methacrylate (HEMA)	Chitosan
N-(2-hydroxypropyl) methacrylate (HPMA)	Alginate
N-vinyl-2-pyrrolidone (NVP)	Fibrin
N-isopropylacrylamide (NIPAM)	Collagen
N-vinylcaprolactam (NVCL)	Gelatin
Vinyl acetate (VAc)	Hyaluronic acid
Acrylic Acid (AA)	Dextran
Methacrylic acid (MAA)	
Ethylene glycol acrylate/methacrylate (EGA/EGMA)	
Ethylene glycol diacrylate/dimethacrylate (PEGDA/PEGDMA)	

Source: adapted from Lin and Metters (2006)

2.4. Multi-sensitive microgels

The ultimate goal of the stimuli-sensitive controlled release is the ability to integrate the system to respond to more than two stimuli (PEPPAS; LEOBANDUNG; ICHIKAWA, 2000). This integration allows to combine the advantages of the two stimuli and to make these new systems more specific and directional, showing maximum therapeutic efficacy and minimal toxicity.

Based on the concept of multi-sensitive microgels, a brief description of the monomers utilised in the production of drug delivery systems sensitive to pH and temperature is given in the following subtopics. After presenting the main characteristics of the materials used in this work, it will be discussed how these materials interact with each other to form microgels with dual-sensitive properties.

2.4.1. Acrylic acid (AA)

Acrylic acid (AA) and derivatives are widely used in industrial processes. In particular, acrylic acid is one of the most important compounds used in water-soluble polymers, showing a vast range of applications.

The popularity of this monomer is due to its economic and physical-chemical characteristics. On the economic side, AA is less expensive than other acrylic compounds, because of the simplicity of its production method.

On the other side, there is a variety of pharmaceutical and cosmetic products with AA in their composition (known as Carbomer) due to gelling and mucoadhesive properties. Carbomers are used as a thickener, that is, to stabilise emulsions, and increase the viscosity of the solutions. As an example of products currently marketed containing poly(acrylic acid) are: CataflanPro® Emulgel® and Feldene® Gel (topical anti-inflammatory drugs); Isotrex® and Differin® (products for the treatment of acne and reduction of expression lines); Nenê Dent® N Gel (to alleviate the effects of first dentition) (VILLANOVA; ORÉFICE; CUNHA, 2010).

Over the past few decades, increasing attention has been focus on the development of a drug delivery system, and particular attention has been concentrated in a system with stimuli-responsive behaviour. Microgels based on acrylic acid are classified as anionic microgel, because of the carboxylic groups linked in the polymer particle chain, which are ionisable and sensitive to pH and ionic strength. In this way, acrylic acid is a promising candidate for developing microgels sensitive to pH.

In the case of pH-sensitive microgels, the most important parameter is the relationship between the pKa of the polymer and the pH of the surrounding medium, this means that when the pH is higher than the pKa, the ionised structure will provide greater electrostatic repulsion of the network and increase the swelling properties. Figure 2.2 shows the influence of the pH on the particle size for a specific pKa.

Figure 2.2 - The relationship between pH and pKa on the particle size of the microgels

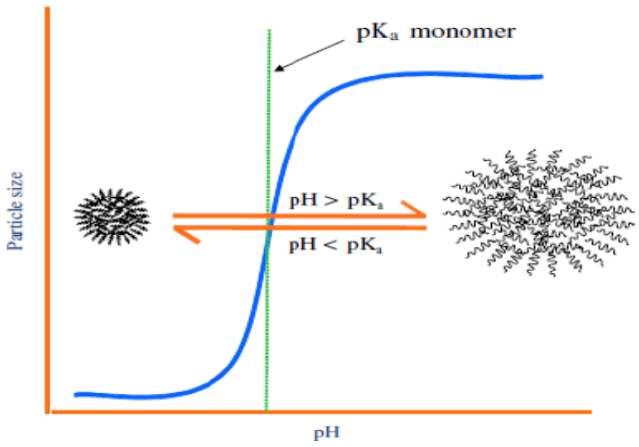

Source: from SNOWDEN et al. (1996)

In the case of poly(acrylic acid), its pKa is around 4.2. This means that the poly(acrylic acid) particles exposed to a medium with a pH above 4.2 will tend to swell. In contrast, at pH

below 4.2, the polymer shrinks. This behaviour can be used to protect drugs and proteins in the oral delivery system. When in the stomach (low pH), microgel will protect the drug; and in the intestine (higher pH), the polymer will open the structure and release the drug initially loaded inside of the particles. Figure 2.3 illustrates this behaviour of anionic microgels in mediums with different pHs.

Figure 2.3 - Drug delivery mechanism through pH-sensitive microgels in the gastrointestinal tract

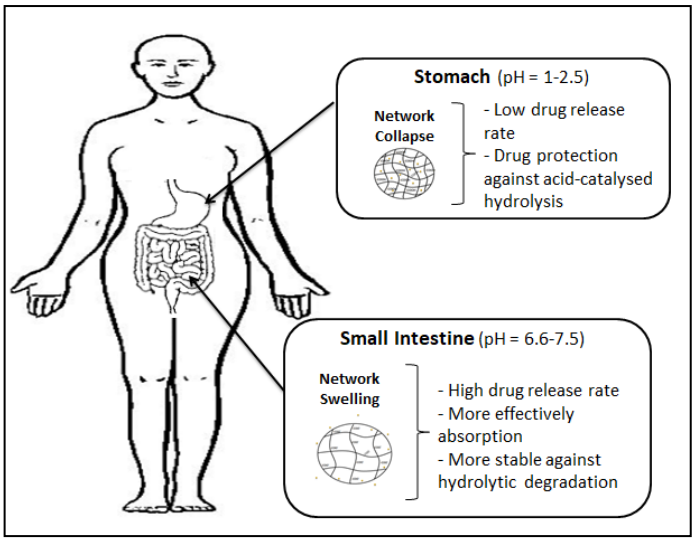

Source: Author

2.4.2. N-isopropylacrylamide (NIPAM)

Microgel particles based on N-isopropylacrylamide (NIPAM) are the most well studied water-swellable microgel system. These microgels can change their structure when exposed to mediums at different temperatures. Their temperature sensitivity in aqueous solution is caused by an interplay of hydrophilic and hydrophobic interactions between the microgel chains and water molecules (SCHNEIDER et al., 2014).

The abrupt and reversible nature of poly(N-isopropylacrylamide) (poly NIPAM) phase transition, as well as the biocompatibility and the proximity between the values of its Lower Critical Solution Temperature (LCST) (31-34°C) and the human body temperature (35-37°C), have attracted several researchers to the study of this polymer, mainly for biomedical application (ACCIARO; GILÁNYI; VARGA, 2011; LANZALACO; ARMELIN, 2017).

When the temperature is raised above the LCST, the polymer network collapses, expelling most of its water content and any potentially dissolved molecule from the gel structure

(ACCIARO; GILÁNYI; VARGA, 2011); it means that this polymer changes from a hydrophilic state below this temperature, to a hydrophobic state above it (DIMITROV et al., 2007) (Figure 2.4-A). In the poly(NIPAM) microgels, this behaviour is due to their chemical groups; it has a hydrophilic amide group and a hydrophobic isopropyl group (Figure 2.4-B).

Figure 2.4 – Representation of (A) the effect of the relationship between the surrounding temperature and LCST of the microgel in their particle size and (B) the phase transition mechanism of poly(NIPAM).

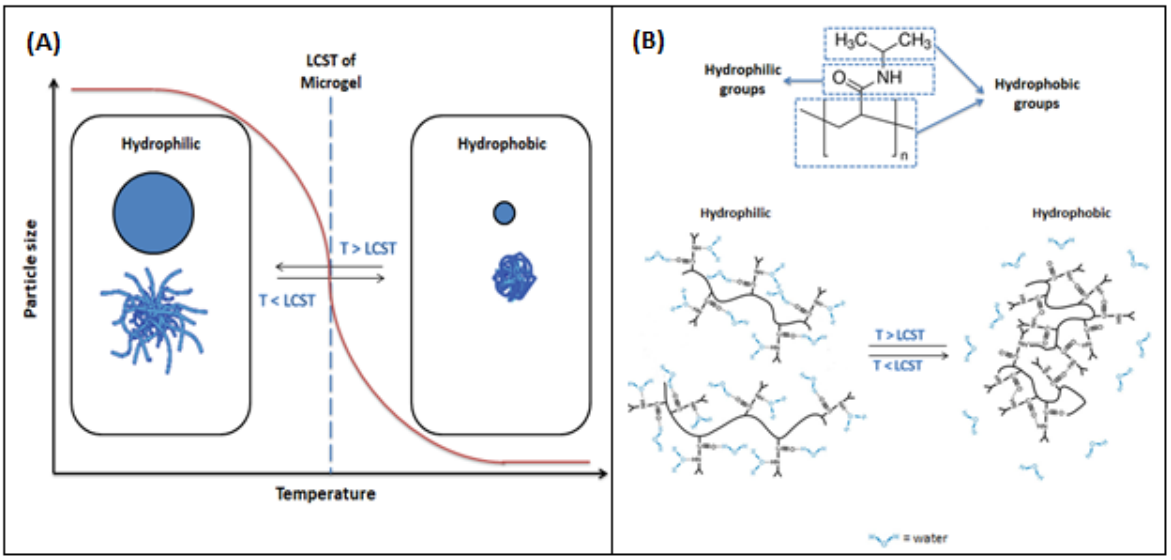

Source: Adapted from LANZALACO and ARMELIN (2017)

2.4.3. Chitosan (Cs)

One of the inherent limitations in the use of pH-responsive synthetic polymers in biomedical applications is the non-biodegradability of these materials. In some cases, if the polymer does not degrade inside the body, it must be removed surgically, implying high cost and risk to the patient (SAMGENKO; ULBERG; KOROTYCH, 2011).

Thus, attention has been focused on the development of pH-sensitive hydrogels with biodegradability, that is a property that degrades *in* vivo some materials in small fragments that can be excreted by the body.

Therefore, with the intention to incorporate biological properties in sensitive polymers, such as biodegradability, biocompatibility and low toxicity, attention has been focused on the development of biodegradable, pH-sensitive hydrogels based on polypeptides, proteins and polysaccharides, with particular attention to a polysaccharide denominated chitosan (Cs).

Chitosan is a cationic biopolymer. Polymer networks with pendant cationic groups function contrarily to polymer networks with pendant anionic groups. In this case, these materials remain collapsed in basic medium and swollen in the acid medium due to electrostatic repulsion between the positively charged groups. Thus, the most important parameter is the relationship between the pKb of the polymer and the pH of the environment. When the pH is lower than pKb, the amine groups change from NH_2 to NH_3, a situation which increases the electrostatic repulsion that consequently increases the hydrophilicity and swelling of the materials based on chitosan (PEPPAS; LEOBANDUNG; ICHIKAWA, 2000).

2.4.4. Microgel based on acrylic acid, N-isopropylacrylamide and chitosan: combination of pH and temperature-sensitive properties

pH and temperature have been the solution variables of the most significant scientific and technological interest, primarily because these variables can be changed in typical biological and chemical systems. The ability of the polymer to respond both to pH and temperature offers additional control over the polymer phase behaviour. In this way, a highly diverse set of "smart" materials can be prepared, which will be able to mimic the responsive macromolecules found in nature (DIMITROV et al., 2007).

Although the capability to change their structure when exposed in media with different pHs, microgel based on homopolymer poly(acrylic acid) has limited application when used in the biomedical field because this particle shows high colloidal instability and non-spherical morphology. This limitation can be manipulated by the introduction of the monomer N-isopropylacrylamide (NIPAM) into the polymer backbone at the synthesis step. As the poly(NIPAM) is a temperature-sensitive polymer, when NIPAM is copolymerised with an anionic monomer containing carboxylic acid groups (e.g., acrylic acid), the result is a polymer sensitive to pH and temperature with better colloidal stability that can help to regulate the microgel size. This combination can be used in the biomedical applications because of the hydrophilicity of the acrylic acid, that can increase the volume phase transition temperature (VPTT) (or low solution critical temperature, LSCT) for a temperature close to the human body temperature (35-37 °C).

Poly(N-isopropylacrylamide-co-acrylic acid) [poly(NIPAM-co-AA)] microgels have been well studied (SNOWDEN et al., 1996; ZHANG et al., 2007; BURMISTROVA et al., 2011; FAN; BRADLEY; VINCENT, 2012; FAROOQI et al., 2013; HAIDER et al., 2014).

The combination of the poly(acrylic acid) and the chitosan are promising in the oral delivery of peptides and proteins because they are mucoadhesive polymers, i.e., they can open the tight epithelial junctions of the intestine which are mainly responsible for enhancing the paracellular absorption of the hydrophilic macromolecules. Hu et al. (2007) and Lay, Aung and Naing (2011) studied the physicochemical properties of polymers based on acrylic acid and chitosan.

Despite the many studies in the literature about microgels based on acrylic acid and N-isopropylacrylamide, there are few studies about microgels based on acrylic acid, N-isopropylacrylamide and chitosan that were produced in one step. Marques et al. (2013) analysed the stability and rheological behaviour of suspensions with different compositions of N-isopropylacrylamide, acrylic acid and chitosan under different conditions of pH and temperature; these dual-sensitive particles were obtained by one-pot method via free-radical precipitation copolymerisation. The results show that it is possible to produced pH and temperature sensitive particles and control the stability of the material through adjustment of the medium, taking into account the desired application.

Therefore, depending on the desired application, it is important to investigate the stability range of microgels under different conditions of the medium. In the case of the pH- and temperature-sensitive microgels, it is necessary to study the behaviour of these particles under different pH, temperature, and salt concentration.

2.5. Microgel Synthesis

The goals of microgel synthesis include controlling the particle size distribution, colloidal stability, and the distribution of specific functional groups such as cross-linker, charge groups, or reactive centres for further chemical derivatisation (PELTON; HOARE, 2011).

Monodispersed size is very important in order to improve the performance of stimuli-sensitive microgels in various applications. In particular, when the microgels are used for biomedical application, especially, as drug delivery system (DDS), particle size and particle size distribution are two of the most important characteristics, because the distribution of particles in the organism and the interaction with biological cells are directly affected by their size. Additionally, if microgels exhibit a monodisperse size distribution, the drug release

kinetics can be manipulated, facilitating the formulation of sophisticated and intelligent DDS (BAI et al., 2006).

Microgel synthesis can be classified into three categories based on particle formation mechanism. Those formed by (PELTON; HOARE, 2011):

- Homogeneous nucleation: microgel particles are generated from initially homogeneous (or nearly so) solutions;
- Emulsification: aqueous droplets of a "pregel" solution are formed in an oil or brine phase and, in the second step, the droplets are polymerised and/or cross-linked into a microgel;
- Complexation: microgels are prepared by mixing two dilute, water-soluble polymers that form complexes in water.

In this work, microgels are prepared by homogeneous nucleation strategy. In this case, a solution of soluble monomers, including a crosslinking agent, is fed into the reactor and microgel particles form over the course of polymerisation (PELTON; HOARE, 2011). These microgels are insoluble in the aqueous medium.

Microgel preparations involving homogeneous nucleation include the following types of polymerisation (PELTON; HOARE, 2011):

- Emulsion polymerisation (EP);
- Surfactant-free emulsion polymerisation (SEP) and precipitation polymerisation (PP);
- Microgel formation from the dilute polymer solution.

Taking into account the final characteristics of the particles and their application in this work, precipitation polymerisation is the only one capable of generating monodisperse particles in a single step, without the use of stabilisers or surfactants, and without further process, step or apparatus. Also, it is possible to control important physicochemical properties of aqueous microgels, such as size and size distribution, surface charge, microstructure (porosity), the degree of crosslinking, and the physical and chemical nature of the particles through the reaction conditions (PICH; RICHTERING, 2010).

2.5.1. Precipitation Polymerization (PP)

Despite surfactant-free emulsion polymerisation and precipitation polymerisation have the same mechanism of particles formation, many authors consider that precipitation polymerisation is the best term when the polymeric system consists of higher water-soluble monomers. As in this work, the monomers to be used are water-soluble; once again, the precipitation polymerisation is the best conventional alternative to produce microgels.

Precipitation polymerisation is probably the most frequently used technique for microgel synthesis (PICH; RICHTERING, 2010). Several studies have been reported in the literature on the preparation of highly crosslinked polymeric microspheres and microgels by precipitation polymerisation (CUI et al., 2009). This technique was first utilised by Philip Chibante in 1978 for preparation of microgels based on N-isopropylacrylamide (PELTON; CHIBANTE, 1986; PICH; RICHTERING, 2010). During the precipitation polymerisation, all ingredients are dissolved in a solvent (water), including the monomer (s), crosslinker agent and initiator, to form a homogeneous mixture in which initiation of polymerisation takes place, and as the polymerisation takes place the system becomes heterogeneous, in which case the polymer particles obtained are not soluble in the medium.

An important characteristic of this polymerisation is that it is necessary highly diluted monomers concentrations (no more than 5%); in other words, the system is composed by a high amount of continuous phase. The continuous phase must have a high dielectric constant (e.g., water), and an ionic initiator is employed (e.g., $K_2S_2O_8$). In this case, thermal decomposition of the ionic initiator ($S_2O_8^{2-}$) initiates free-radical polymerisation, that is, these sulphate radicals attack water-soluble monomers followed by radical propagation and chain growth (PICH; RICHTERING, 2010).

In the step of chain growth, when microgel particles reach the critical size, they become stabilised by an electrostatic stabilisation mechanism. This stabilisation occurs from the charges originating from the initiator fragments (e.g., sulphate groups) that were incorporated into polymer chains during the nucleation and growth process. At this stage, microgel particles are in a collapsed state but still contain much water. Polymerisation continues within the particles until other radical species enter the growing particle and termination occurs (SAUNDERS; VINCENT, 1999; PICH; RICHTERING, 2010).

When the polymerisation is completed, and the reaction mixture cools down to room temperature, microgel particles swell (temperature below VPTT of polymer chains) and develop a “hairy” morphology. At temperatures below VPTT, microgels are stabilised by steric mechanisms due to the formation of hydrogen bonds between polymer segments and water molecules (PICH; RICHTERING, 2010).

In general, the key feature of PP is that the particle nucleation period is very short (order of minutes) which ensures a narrow particle size distribution. The final particle size achieved by PP increases with electrolyte concentration and decreasing initiator concentration (SAUNDERS; VINCENT, 1999). Figure 2.5 shows the principal features of the reaction mechanism for precipitation polymerisation.

Figure 2.5 - Mechanism of microgel formation by precipitation polymerisation: (a) Initiation of polymerisation and chain growth, (b) precipitation and homogeneous nucleation, (c) particle growth and (d) particle swelling.

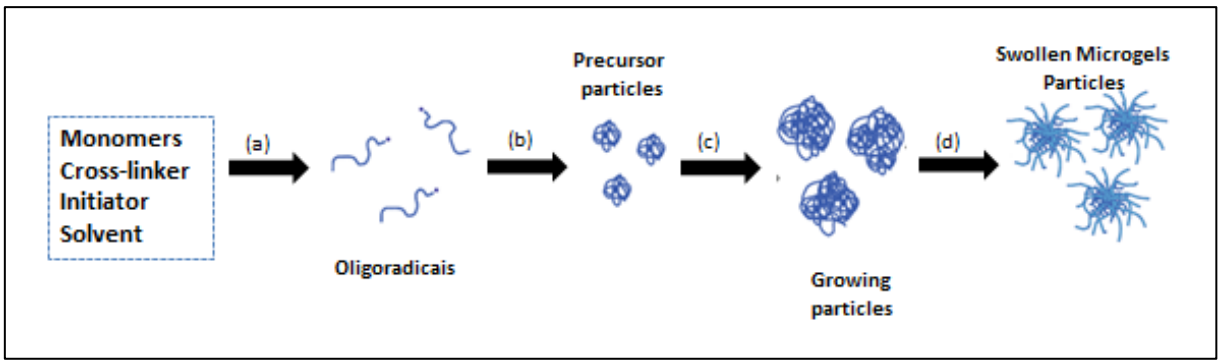

Source: adapted from Pich and Richtering (2010) and Klinger and Landfester (2012)

In conclusion, precipitation polymerisation is a versatile technique and offers several advantages for the preparation of aqueous microgels (PICH; RICHTERING, 2010):

1. The polymerisation process can be carried out as a batch, semi-batch, or continuous process, providing the possibility to optimise reaction conditions and obtain microgels with desired properties;
2. Microgel size can be controlled over a broad range (from 100 nm to 3µm) by the use of surfactants or ionisable co-monomers;
3. Microgel particles with narrow size distribution can be obtained;
4. Different co-monomers can be integrated into the microgel network during the polymerisation process;
5. Hybrid colloids can be prepared by encapsulation of nanoparticles (NPs) during microgel formation.

2.6. Microgel Characterisation

Microgel characterisation is an important topic. A suitable way of characterisation is required for efficient product performance and quality assurance of produced batches.

The main characteristics to be studied in particles for pharmaceutical application includes size/size distribution, morphological evaluation, molar mass distribution, concentration, degradation, structure/crystallinity, composition, porosity/surface area, surface charge, pH, the determination of the amount of drug-associated in the particle structure, the kinetics of the drug release, and also evaluation of the stability in function of the storage time.

Table 2.2 highlights some of the essential characterisation parameters form microgels and the methods used to measure them.

Table 2.2 - Characterisation parameters for microgels.

Parameter	Techniques of measurements
Size and size distribution	Dynamic light scattering (DLS) Scanning electron microscopy (SEM) Transmission electron microscopy (TEM)
Morphology	Scanning electron microscopy (SEM) Transmission electron microscopy (TEM) Atomic Force Microscopy (AFM)
Swelling behaviour	Fluorescence resonance energy transfer (FRET)
Stability	Ultraviolet-visible spectroscopy (UV-Vis) Turbidimetric methods
Molecular weight	Size Exclusion Chromatography (SEC) Static Light Scattering (SLS) Ultracentrifugation
Internal structural	Small-angle X-ray scattering (SAXS) Small-angle neutron scattering (SANS)
Surface charge	Conductometric and potentiometric titration
Structural/quantitative analysis	Fourier transforms infrared (FTIR) Raman spectroscopy Nuclear magnetic resonance (H-NMR)
Thermal properties	Thermogravimetric analysis (TGA)
Thermodynamic properties	Isothermal titration calorimetry (ITC) High-sensitivity differential scanning calorimetry (HDSC) Differential scanning calorimetry (DSC)
Rheology	Rheometry

Source: adapted from Galaev and Mattiasson (2008)

The theory about the characterisation techniques used in this work was described in Chapter 4.

2.7. Microgel application

The field of smart polymers and their application is developing at a high-speed rate. There are a variety of possible applications for microgel particles such as coatings, agriculture, oil recover, and medicine (AL-MANASIR, 2009; MALMSTEN; BYSELL; HANSSON, 2010; SAMAH; HEARD, 2013; GANGULY et al., 2014; FAROOQI et al., 2015; HAN; ZHANG; SERPE, 2015; IQBAL et al., 2016). Some of the applications have already been achieved (e.g., rheological control additives); whereas much more is yet to be developed. Microgel particles are versatile systems and are expected to play an important role in pollution control, in surface coatings, and in pharmaceutical industries in years to come (SAUNDERS; VINCENT, 1999).

Chen, Chen and Wang (2010) prepared pH-responsive hydrogels based on N-isopropylacrylamide and acrylic acid by an aqueous dispersion polymerisation process for the selective isolation of haemoglobin from human blood. They characterised these hydrogels about the influence of some characteristic of them in the adsorption of proteins (Bovinum Serum Albumin, BSA, and haemoglobin). The results showed that the hydrogels exhibit excellent binding selectivity to study proteins in determined pH regions. The satisfactory results allow the research group to conclude that poly(NIPAM-co-AA) hydrogels can be used as an excellent sorbent in the separation and purification of biomolecules.

In the medical and pharmaceutical field, as with macroscopic polymer gels, microgels may be designed to respond to several stimuli, including temperature, ionic strength, pH, the presence of divalent ions, specific metabolites, and external fields. Given the small size of these gel particles, they have potential also in areas where macroscopic polymer gels have not found useful, for example, in parenteral administration (injectable). They are also expected to provide advantageous effects on other administration routes, including oral and nasal administration, due to their small size (MALMSTEN, 2011).

Another application of the microgel in the medical and pharmaceutical field is as drug delivery system. Microgels have particular potential as delivery systems for protein and other biomacromolecular drugs. They are generally hydrophilic and contain much water, which allows proteins to be incorporated into the microgels with only moderate conformational changes and with limited aggregation, thus facilitating maintained biological effect of the protein drug (MALMSTEN, 2011).

2.8. Drug Delivery System (DDS)

In 1968 Alza Corporation (Palo Alto, CA, USA) created the term drug delivery system (DDS) to introduce the concept of a system of sustained release of the drug, which would provide the desired pharmacological action with minimal side effects. The main characteristics desired for a controlled release system are the ability to absorb the drug and to release it in a controlled manner in a specific site of action (OLIVEIRA, 2011).

In other words, DDS is an administration system developed to prolong the release time of the drug in the body, sustain its concentration in the plasma and temporal and spatial location of the molecules in vivo, through the application of biological and chemical. In this way, cyclical changes in the concentrations are eliminated, and the biological availability of drug interaction is increased. Also, the toxicity reduction can be achieved, suppression of adverse reactions and the number of doses administered daily (VILLANOVA; ORÉFICE; CUNHA, 2010).

A controlled DDS should have some key features to be considered ideal, that include biocompatibility, mechanical resistance, patient comfort, and absorption of high amounts of drugs during the preparation, no accidental dressing of the drug, easy production and the possibility of sterilisation (OLIVEIRA, 2011).

Such delivery system offers numerous advantages compared to conventional dosage forms, including improved efficacy, reduced toxicity, and improved patient compliance and convenience (UHRICH et al., 1999). This improvement can take the form of increasing therapeutic activity compared to the intensity of side effects, reducing the number of drug administrations required during treatment, or eliminating the need for specialised drug administration (e.g., repeated injections). Two types of control over drug release can be achieved, temporal and distribution control (UHRICH et al., 1999).

In temporal control, drug delivery system aims to deliver the drug over an extended duration or at a specific time during treatment. Controlled release over an extended duration is highly beneficial for drugs that are rapidly metabolised and eliminated from the body after administration. Figure 2.6 shows an example in which the concentration of the drug at the site of activity within the body is compared after immediate release from 4 injections administered at 6 hours intervals and after extended release from a controlled release system (UHRICH et al., 1999).

Figure 2.6 - Comparison of drug concentration in the range of therapeutic action after the conventional mechanism (thin line) and the controlled delivery mechanism (thick line).

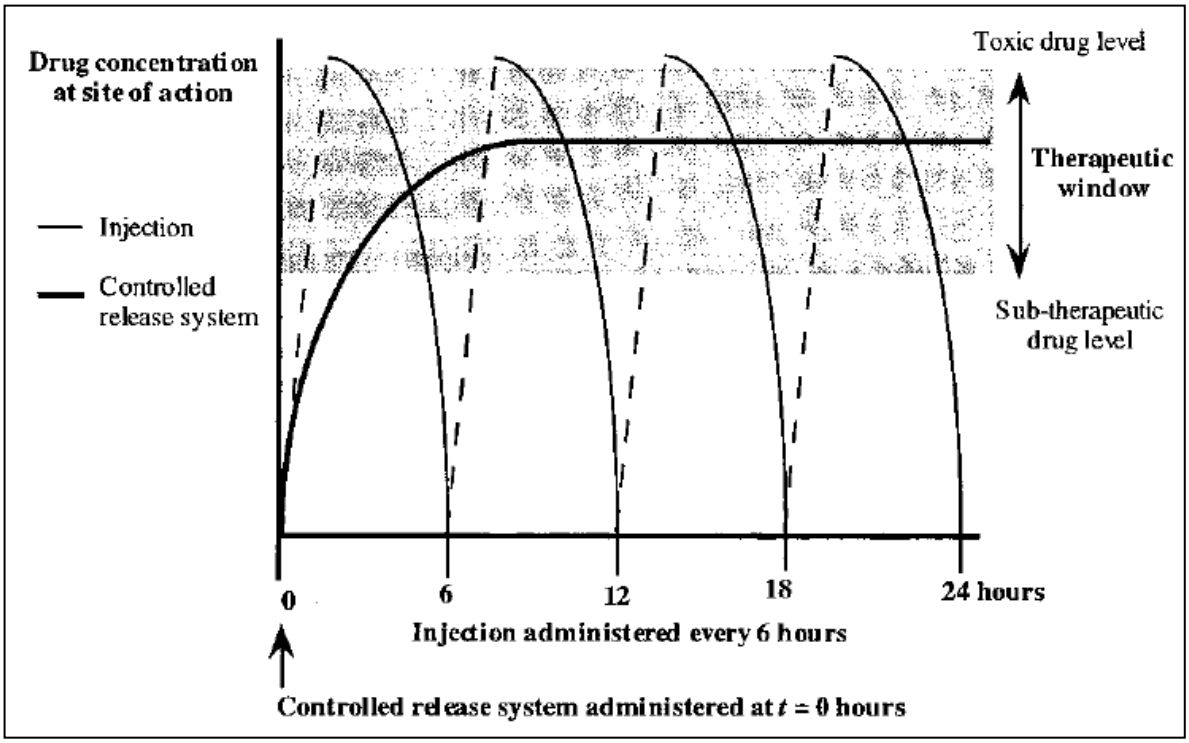

Source: from Uhrich et al. (1999)

Figure 2.6 shows that drug concentration may fluctuate widely during the 24 hour period when the drug is administered through injections; the drug concentration is only a period within the therapeutic window (where the drug has a therapeutical action but does not produce damage or collateral effects). In the controlled release system, the concentration of the drug remains within the therapeutic window the majority of the 24 hours after administration of the drug (UHRICH et al., 1999).

As a result of new and increasing demands, some strategies have been proposed to achieve drug delivery systems for effective therapy, and microgels have attracted considerable attention as an excellent candidate for controlled release of drugs.

In the context of oral delivery, research has been directed in particular at: (i) reducing the side effects of certain drugs, especially non-steroidal anti-inflammatory drug, which often cause irritation to gastrointestinal mucosa; (ii) protection of degradable drugs in the gastrointestinal tract, such as peptides, proteins and/or hormones, and increasing their bioavailability (SCHAFFAZICK et al., 2003; MALMSTEN, 2011).

2.9. Concluding remarks

This Chapter presented a general overview of the basic concepts of microgels, their production by polymerisation, and the main characterisation techniques. Emphasis was given on the microgels that are responsive to changes in pH and temperature. The pH- and thermosensitive properties of these microgels make them suitable for pharmacological applications in the design of efficient drug delivery systems. Discussion of more specific literature is further presented in each of the next Chapters, within the framework of the topic under study in each part of this thesis.

3. Synthesis of Microgel Particles with At-line and In-line Monitoring using Spectroscopy Techniques

Abstract

This chapter reports the results of the monitoring of the precipitation copolymerisation reactions of acrylic acid (AA) and N-isopropylacrylamide (NIPAM) through Ultraviolet-Visible-Near infrared (UV-VIS-NIR) and Near-infrared (NIR) spectroscopy techniques. The monitored variables analysed were the monomer conversion and the average particle diameter of the microgels. UV-Vis-NIR high-resolution spectrophotometer was used for at-line monitoring, and five calibration models were constructed. These models were based on a simple linear relationship between studied variables and the information contained in the visible and near-infrared spectra. The calibration models for monomer conversion showed a determination coefficient (R^2) above 0.91, while the models for average particle size had a determination coefficient above 0.84. A linear relationship between monomer conversion and average particle size was also verified, with a determination coefficient equal to 0.665. The calibration models for spectra collected from NIR spectrophotometer were based on Partial Least Square (PLS) regression method, and showed a determination coefficient equal to 0.934, and a root mean square error of cross-validation (RMSECV) equal to 0.0939 for the cross-validation of the monomer conversion calibration model, while for the average particle size calibration model, the cross-validation showed R^2 equal to 0.8024 and RMSECV equal to 18.4 nm. In general, the results of the external validation of all calibration models developed showed a good correlation between the predicted and the experimental data. When aggregation of the microgel particles occurs in the reactor, the NIR model was able to identify this phenomenon. In conclusion, the spectroscopic techniques used in this work show great potential for estimating the monomer conversion and the average particle size of the microgel particles during the precipitation polymerisation, allowing control over the polymerisation reaction with quick and direct acquisition of data.

3.1. Introduction

Microgel particles have been received much attention by researchers, mainly because of their characteristic of changing their structure (swelling or shrinking) according to the changes in the properties of the medium, such as pH, temperature, and ionic strength. This

unique characteristic allows these particles to be used in many areas of application. One of these areas is the pharmaceutical field, with the focus in design polymer particles as drug delivery systems (DDS) that can deliver the drug in a specific site in the human body (SAMAH; HEARD, 2013; SMEETS; HOARE, 2013; GANGULY et al., 2014).

The challenges of developing an appropriate DDS for the desired application begin in the production method, on what the monitoring of some important characteristics of the particles is essential for better control of the interaction between the carrier and the drug. For example, with the knowledge of how the variables of the reaction (reagent concentrations, reaction temperature and pH, agitation speed) influence the physical and chemical characteristic of the particles, such as size and size distribution, allow improving the release kinetics of the drug in the human organism (SMEETS; HOARE, 2013).

The most used method to synthesise microgel particles is precipitation polymerisation (PP) (PICH; RICHTERING, 2010). PP is a free radical polymerisation that begins as a homogeneous mixture of monomers, initiator and solvent; as the reaction occurs, the system becomes heterogeneous by the formation of polymer particles insoluble in the medium (PELTON; HOARE, 2011; PICH; RICHTERING, 2010). Due to the absence of surfactant, the particles are stabilised by the electrostatic stabilisation mechanism provided by an ionic initiator and/or reactive functional co-monomer (PELTON; HOARE, 2011). However, to maintain this colloidal stability, it is necessary highly diluted monomer concentration in the reaction medium (<5%); i.e., the system is composed of a high amount of solvent, most typically water (VEGA et al., 2013).

Although the PP produces monodisperse microgel particles due the short period (order of minutes) of particle nucleation, when the concentration of monomers present in the reaction medium increases, particles with larger sizes and broader distribution sizes can be produced, causing instability in the medium and the aggregation of microgel particles, giving rise to larger sized particles.

Thus, due to the significant influence of the particle size in the stability of the reaction medium, it is very important to develop techniques for evaluating the microgel formation during the polymerisation. Monitoring some microgel features give us essential information for the control of the product quality, and allow improving the final characteristic of the product (in this case, it is the microgels particle size) according to the desired application.

Despite the large volume of research in the field of microgel particles by precipitation polymerisation, most of the information is about characterisation (BURMISTROVA et al., 2011; MARQUES et al., 2013) and potential applications (SAMAH; HEARD, 2013). However, in the area of polymer reaction engineering, some aspects of the polymerisation mechanism have received little attention, such as how the concentration of reagents and process conditions affect the particle size, particle size distribution and morphology. In this way, kinetic modelling and process control are considered important tools for understanding the mechanisms involved in microgels formation and allow to achieve better composition control of the characteristics of the final particles. For this reason, in this chapter, the kinetic behaviour of the precipitation polymerisation will be discussed with the focus on monitoring of the process.

3.1.1. Spectroscopy Techniques for Monitoring of Polymerisation Process

Spectroscopic techniques are considered attractive and promising analytical tools for analyses conducted in research, control or industrial laboratories (BAETEN; DARDENNE, 2002).

The possibility of coupling the instruments with suitable fibre optics makes spectroscopy techniques much more attractive for process and monitoring. These sensors permit data to be obtained continuously and in real time, allowing actions to be taken quickly to ensure the desired quality of the product and even to avoid a run-away reaction.

The instruments could be applied “at-line” in the laboratory control, “on-line” with the use of measurements through optically clear windows and dedicated sampling techniques, and “in-line” with the use of the specific probe for the measurement inside a pipe or a tank/reactor (BAETEN; DARDENNE, 2002). In-line and on-line sensors offer enhanced information content about the process that might be overlooked with off-line analysis (FONSECA; DUBE; PENLIDIS, 2009). Figure 3.1 shows the different types of monitoring techniques which are dependent on the location of the analytical system about the process unit.

Figure 3.1 – Types of monitoring techniques.

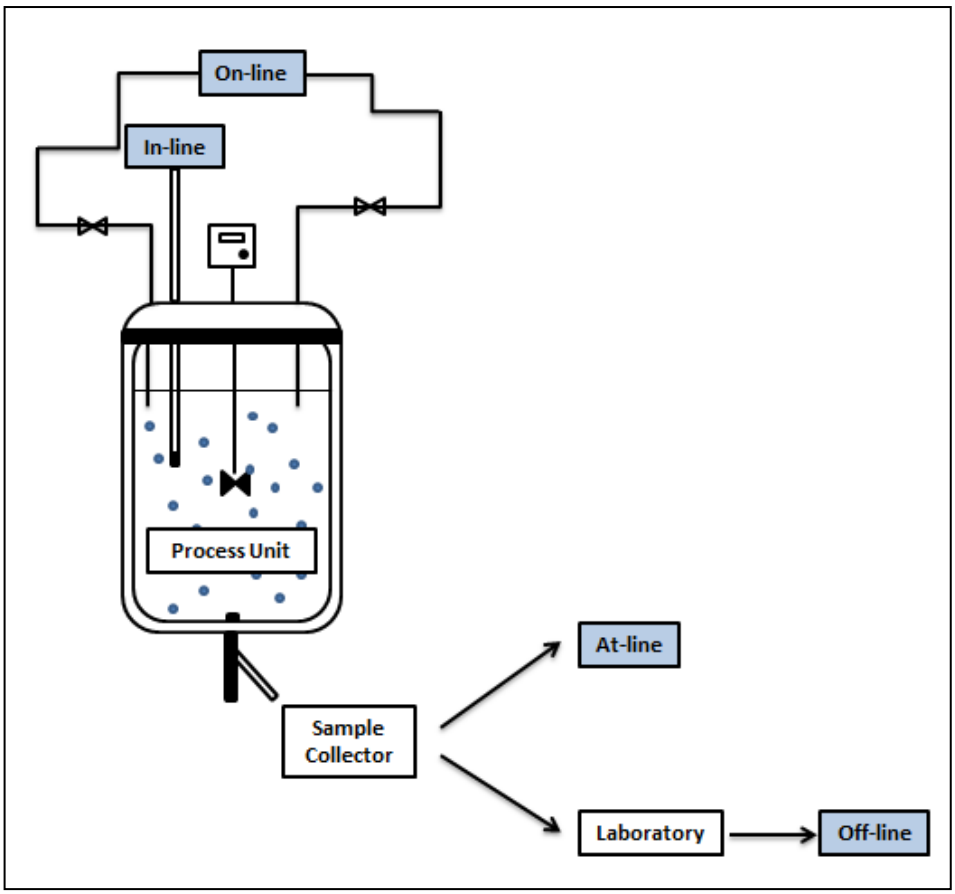

Source: Author

In the field of the polymerisation process, there is an increasing demand for the production of polymers with specific properties that must be controlled during the reaction, being necessary the monitoring of the desired feature. However, some difficulties can be found in the off-line and on-line monitoring, such as the complex and viscous nature of some polymerisation systems, and delays and poor reliability in sampling and measurement (KAMMONA; CHATZI; KIPARISSIDES, 1999). In this way, to achieve higher quality, faster processing times, better end-use properties or simply for a deeper understanding of polymerisation kinetics, the control of different features in real-time has become a necessity (FONSECA; DUBE; PENLIDIS, 2009). The breakthrough in the field of online and in-line polymer reactions and quality monitoring was achieved when conventional sensing techniques were coupled to fibre optics, thus giving rise to the possibility of making in situ measurements for many applications (KAMMONA; CHATZI; KIPARISSIDES, 1999).

In particular, off-line monitoring of the formation of microgel particles by precipitation polymerisation can be challenging due to the highly diluted monomers concentrations (<5

wt%) and the short period (order of minutes) of particle nucleation that can difficult the proper analysis. In this way, in-line monitoring can provide information about the process allowing to reduce time delays and inaccuracy of analyses usually involved with sample preparation.

In literature, there are some works about the monitoring of microgel/macrogels reactions; most focus on the concentration of monomers and polymers in the reaction medium.

Table 3.1 and Table 3.2 show the bibliography about this topic.

Table 3.1 - Literature overview about monitoring of microgels formation.

Polymerisation System	Monomers	Technique[4]	Variables Monitored	References
-[1]	Acrylamide	UV-VIS	Gelation mechanism	(KARA; PEKCAN, 2001)
-[1]	N-isopropylacrylamide	UV-VIS	Phase separation	(KARA; OKAY; PEKCAN, 2002)
UV-curing reactions	Adipic Acid, Trimethylol Propane, Neopentyl Glycol	FTIR	Reaction kinetics	(NEBIOGLU; SOUCEK, 2006)
Visible light photopolymerization	Vinyl monomers[2], Divinyl monomers[3]	NIR	Reaction kinetics and final conversion values	(STANSBURY; DING; NEWMAN, 2006)
Precipitation Polymerisation	N-isopropylacrylamide N-vinylcaprolactam	DLS with a fibre-optical backscatter probe	Particle growth	(KANTER et al., 2016)
Visible light induced polymerisation	Ethylene glycol diacrylate, 1-vinyl-2-pyrrolidone, Triethanolamine	UV-Vis/FT-NIR	Chromophore and monomers reactive groups concentration	(KAASTRUP et al., 2016)

[1] The article does not explain what kind of polymerisation they used, only that it is free-radical crosslinking copolymerisation (FCC); [2] ethyl acrylate, ethyl methacrylate 2-hydroxyethyl methacrylate, isobornyl methacrylate; [3] triethylene glycol dimethacrylate, tetraethylene glycol dimethacrylate, urethane dimethacrylate, 2,2-bis[p-(2-hydroxy-3-methacryloxyprop-1-oxy)phenyl]propane. [4] UV-VIS: Ultraviolet-visible; FTIR: Fourier Transform Infrared; NIR: Near Infrared; DLS: Dynamic Light Scattering.

Table 3.2 – Continuation of the literature overview about monitoring of microgels formation.

Polymerisation System	Monomers	Technique[4]	Variables Monitored	References
Precipitation Polymerisation	N-vinylcaprolactam	Raman	Monomer and polymer content	(MEYER-KIRSCHNER et al., 2016)
Precipitation Polymerisation	N-vinylcaprolactam and N-isopropylacrylamide	Raman	Monomers, microgel and water fraction (wt%)	(MEYER-KIRSCHNER; MITSOS; VIELL, 2018a)
Precipitation Polymerisation	Polystyrene	Raman	Particle size	(MEYER-KIRSCHNER; MITSOS; VIELL, 2018b)
Precipitation Polymerisation	N-vinylcaprolactam and N-isopropylacrylamide	Turbidity and Raman	Monomer and polymer fraction for reaction temperatures 60-80 °C	(MEYER-KIRSCHNER et al., 2018)

[4] UV-VIS: Ultraviolet-visible; FTIR: Fourier Transform Infrared; NIR: Near Infrared; DLS: Dynamic Light Scattering.

Kara and Pekcan (2001) used a UV-VIS spectrometer to in-situ and real-time monitoring of the free-radical crosslinking copolymerisation (FCC) of acrylamide (AAm) and N,N'-methylenebisacrylamide (MBA). The objective of their study was to follow the gelation mechanism during hydrogel formation that was performed with various MBA contents at different wavelengths. The gelation was related to the photon transmission intensity. Another work in the same research group (KARA; OKAY; PEKCAN, 2002) also used the UV-VIS spectrometer to monitor phase separation during the formation of poly(N-isopropylacrylamide) gels. During polymerisation, the transmitted light intensity at 450 nm and the temperature were recorded simultaneously. Both works show a better understanding of the microgelation mechanism and phase transition through the photon transmission and temperature measurements during the hydrogel formation.

Nebioglu and Soucek (2006) investigated the effects of the reactive diluent (trimethylolpropane triacrylate, TMPTA) and terminal acrylate unsaturation in Ultraviolet-curing unsaturated polyesters (UPEs) on microgel formation. For this study, the authors used Dynamic Light Scattering (DLS) and time-resolved Fourier Transform Infrared (FTIR) to monitor the particle size and reaction kinetics of gelation and free-radical network formation

of microgels. The authors also observed the morphology of the UV-cured films by Atomic Force Microscopy (AFM) and Scanning Electron Microscopy (SEM). The results of the DLS studies showed that the smaller sizes of microgels were due to the primary UPE acrylate coils, and the larger sizes correspond to the formation of microgels by the reaction of UPE acrylates and TMPTA. In the time-resolved FTIR results, the concentration of reactive diluent shows to be the most important factor in the microgel formation, mainly in the gel point of UV-curing polyesters. The authors also confirmed the formation of the cluster through the reaction between microgels.

In the work of Kanter et al. (2016), they also used DLS to monitor the particle size during the microgel formation. The differential of this work was that the measurements were performed in-line with a novel probe design coupled with a dynamic light scattering equipment allowing the monitoring of the particle size growth during precipitation polymerisation of poly(N-isopropylacrylamide) and poly(N-vinylcaprolactam). The in-line measurements were compared with a reference method (offline dynamic light scattering) and showed good agreement between them.

Stansbury, Ding and Newman (2006) prepared nanogel particles based on a variety of monovinyl and divinyl monomers with a chain transfer agent using toluene as solvent. The reaction was monitored using real-time near-infrared spectroscopy in transmission mode, with the intention to analyse the degree of conversion during the thermal polymerisation process. The results show a decrease in the NIR peak intensity during the reaction; this decrease corresponds to the disappearance of the methacrylate vinyl bond (=C-H) (first overtone at 1663 nm). The authors concluded that NIR monitoring is a convenient method to monitor the polymerisation reaction.

In the work of Kaastrup et al. (2016), they used real-time dual UV-Vis/FT-NIR spectroscopy to monitor the visible-light-induced polymerisation of poly(ethylene glycol) diacrylate (PEGDA) hydrogels initiated by eosin in the presence of triethanolamine (TEA) and oxygen. The results show that the monitored data allow the determination of the duration of the inhibition period, the rates of eosin consumption in different stages of the reaction, and the rate of polymerisation. According to the authors, the developed method could be applied to analyse the dynamic morphology of a wide range of polymer networks.

Recently, many works have been developed in the research group of Meyer-Kirschner and coworkers about the in-line monitoring of precipitation polymerisation using Raman spectroscopy (MEYER-KIRSCHNER et al., 2016, 2018, MEYER-KIRSCHNER; MITSOS; VIELL, 2018a, 2018b). They applied Raman to monitor monomer and polymer content of poly(N-vinylcaprolactam) microgels, and the monomer and polymer fraction during copolymerisation of N-vinylcaprolactam and N-isopropylacrylamide. The spectra were evaluated by multivariate Indirect Hard Modelling (IHM) regression. Specifically, the work of Meyer-Kirschner, Mitsos and Viell (2018a) discussed a strategy to optimise the Raman spectra treatment through a novel method to determine the analyte-specific signal-to-noise ratio (SNR) from a single multicomponent spectrum with overlapping peaks based on multivariate IHM regression. The particle size during precipitation polymerisation was also monitored by Raman; the spectra of aqueous polystyrene were treated with a hybrid model based on IHM and data-driven partial least squares regression and shown good fits with experimental data. In conclusion, according to the authors, in-line Raman spectroscopy associated with IHM regression could be an excellent technique for monitoring functional microgel synthesis by precipitation polymerisation.

According to the studies presented previously, there has not yet been reported literature on the monitoring of microgel formation by precipitation polymerisation using NIR spectroscopic techniques. The main difficulty is the high amount of solvent, most typically water, which has two strong absorbance bands in the NIR region, which make difficult to visualise the characteristic bands of other compounds.

However, NIR spectra are influenced by the presence of particles in heterogeneous mediums due to the high ratio of scattering/absorption. Although this peculiar characteristic sometimes has been considered as a negative effect, this scattering allows analysing the physical properties of the particles, such as size and morphology. In this way, NIR spectroscopy can be an excellent tool for in-line monitoring of microgel particle size evolution in precipitation polymerisation.

The monitoring of precipitation polymerisation process presented in this work was carried out with spectroscopic equipment coupled with sensors that provide in-line and at-line information, and off-line data obtained by gravimetric method and dynamic light scattering (DLS) technique. In-line monitoring was conducted through Near InfraRed (NIR), and at-line

monitoring through UltraViolet – Visible – Near Infrared (UV-Vis-NIR) spectroscopy. The off-line data were used to validate the acquired spectra.

Visible and Near-infrared spectroscopy offers many significant advantages for process monitoring and has been used since the 1980s (REY-BAYLE et al., 2017). The following is a brief description of each spectroscopic technique used in this work.

3.1.1.1. Ultraviolet-Visible (UV-Vis)

Ultraviolet-Visible (UV-Vis) spectroscopy is a well-known analytical technique. The UV-Vis is a part of the electromagnetic spectrum that corresponds to the excitation of the outer electrons of atoms and molecule, from lower to higher energy levels, where this energy level depends on the bonds present in the sample (FONSECA; DUBE; PENLIDIS, 2009). It commonly provides knowledge about π-electron systems, conjugated unsaturation, aromatic compounds and conjugated non-bonding electron systems (KUMAR, 2006). Ultraviolet has the wavelength range from 200 to 400 nm, while visible region belongs to the range from 400 to 800 nm.

Beer-Lambert law offers a valuable and straightforward method for quantitative analysis. In practice, a calibration curve is constructed by plotting absorbance at a given wavelength versus molar concentration, and then the calibration curve is used to obtain the concentration of analyte from the measured absorbance (KUMAR, 2006).

UV-Vis spectroscopy is a versatile technique with many applications (BASET et al., 2011; BEGUM et al., 2018). In the field of polymerisation, UV-Vis spectroscopy can be used as a reliable and straightforward method for characterisation of microgel features (BOUTRIS; CHATZI; KIPARISSIDES, 1997; FAN; BRADLEY; VINCENT, 2012; BEGUM et al., 2018).

In this work, we tested the capability of UV-Vis-NIR spectrophotometer with a coupled probe to monitoring at-line the production of microgel particles by precipitation polymerisation. In preliminary tests, we identified changes in the spectra data during the polymerisation process, in this way, we decided to explore this information and associate them with the physical and chemical properties of the microgels during the polymerisation. Also, this monitoring was used as a comparative method with Near-infrared data, looking for a better understanding of microgel formation and advances in the monitoring of precipitation polymerisation.

3.1.1.2. Near - InfraRed spectroscopy (NIR)

NIR spectroscopy is a vibrational spectroscopic method in the Infrared spectral region and based on molecular overtones and combinations bands of the fundamental molecular vibrations of the considerate molecular groups (C-H, N-H, O-H and S-H). Molecular overtones correspond to the transition from the fundamental vibrational state to the second (first harmonic) or the third (second harmonic) excited vibrational state or a higher vibrational state. Molecular overtones and combinations bands are typically weaker than their corresponding fundamental transitions (KAMMONA; CHATZI; KIPARISSIDES, 1999).

The NIR region extends from the end of the visible spectral region (800 nm or 12500 cm^{-1}) to the beginning of the fundamental Infrared (IR) spectral region (2500 nm or 4000 cm^{-1}) (METROHM, 2013). In this region, most of the organic and some inorganic compounds show good reflectance or transmission properties. Table 3.3 shows the characteristic regions of the NIR spectra.

Table 3.3 - Near InfraRed bands of organic compounds in wavelength (nm) and wavenumber (cm^{-1})

Wavelength (nm)	Wavenumber (cm^{-1})	Group absorption
2500-2200	4000-4545	C-H combination
2200-1800	4545-5556	O-H and N-H combinations
1800-1600	5556-6250	C-H 1st overtone
1600-1420	6250-7042	O-H and N-H 1st overtone
1420-1300	7042-7692	C-H combination
1300-1100	7692-9091	C-H 2nd overtone; O-H combination
1100-800	9091-12500	N-H 2nd overtone; O-H 2nd overtone; C-H 3rd overtone

Source: adapted from Metrohm (2013)

The simplest classical model employed to have a didactic insight on the interaction of radiation and matter in the NIR spectral region is given by Hook's law (PASQUINI, 2003). Hook's law states that for two bodies harmonic oscillator ($m_1 \; and \; m_2$), the energy of the system (E) is (AENUGU et al., 2011):

$$E = \frac{h}{2\pi}\sqrt{\frac{k(m_1 + m_2)}{m_1 m_2}} \tag{3.1}$$

where h is plank constant, and k is force constant of the bond.

The molecular vibration can be described by a simplified model supposing a harmonic oscillator for which the potential energy (V) is a quadratic function of the displacement of the vibrating atoms (x^2) (Equation (3.2) (PASQUINI, 2003). The parabolic function is symmetrical about the equilibrium bond length r_e (METROHM, 2013).

$$V = \frac{1}{2}k(r - r_e)^2 = \frac{1}{2}kx^2 \tag{3.2}$$

where r is internuclear distance and r_e is the internuclear distance at equilibrium.

Quantum mechanical considerations using the Schrodinger equation show that the vibrational energy for the harmonic oscillator has no continuum for vibrational energy levels, but only certain discrete energy levels (METROHM, 2013).

$$E_{\mathrm{v}} = hv\left(\mathrm{v} + \frac{1}{2}\right) \tag{3.3}$$

where E_{v} is the energy associated with the vth quantum level, v is the fundamental vibrational frequency, and v is a vibrational quantum number (0,1,2,….). In the classical model, this frequency is defined by:

$$v = \frac{1}{2\pi}\sqrt{\frac{k}{\mu}} \tag{3.4}$$

where μ is reduced mass:

$$\mu = \frac{m_1 m_2}{m_1 + m_2} \tag{3.5}$$

However, although the harmonic model may help the understanding of vibrational spectroscopy, it produces some undesirable limitations for NIR spectroscopy, because it

does not allow transitions to the energy level Δv > 1. Transitions with Δv greater than or equal to 2 are forbidden by the harmonic/quantum model; thus, many of the phenomena observed in the NIR region (such as bands associated with combinations and overtones) should not exist (PASQUINI, 2003; JUNIOR, 2008).

This deviation from the harmonic model is known as anharmonic oscillation, and this behaviour can be approximated to the diatomic molecules through an extension of the Equation (3.2 by adding higher-order terms of displacement (METROHM, 2013).

$$V = \frac{1}{2}kx^2 + \frac{1}{2}k_a x^3 + \frac{1}{2}k_b x^3 + \cdots \tag{3.6}$$

with k_a, k_b << k.

Applying the correction in Equation (3.6, the Schrödinger equation provides the following term for the vibrating energy of the molecule:

$$E_{\mathrm{v}} = hv\left(\mathrm{v} + \frac{1}{2}\right) - yhv\left(\mathrm{v} + \frac{1}{2}\right)^2 \tag{3.7}$$

in which y is the anharmonicity constant of the vibration.

The anharmonicity now allows the occurrence of transitions with Δv > 1 and the existence of combination bands between vibrations. These two types of bands are the most common absorption bands in the NIR spectral region. Additionally, the vibrational energy levels are no longer equidistant and energy differences decrease with increasing quantum number v (PASQUINI, 2003; METROHM, 2013).

NIR spectroscopy presents some measurement modes which the analysis can be affected depending on the type of analyte. These NIR modes are diffuse reflection, diffuse transmission, transflection and transmission (Figure 3.2), and they differ in light behaviour when reflected in the sample being analysed.

Figure 3.2 - Different kind of NIR measurements methods

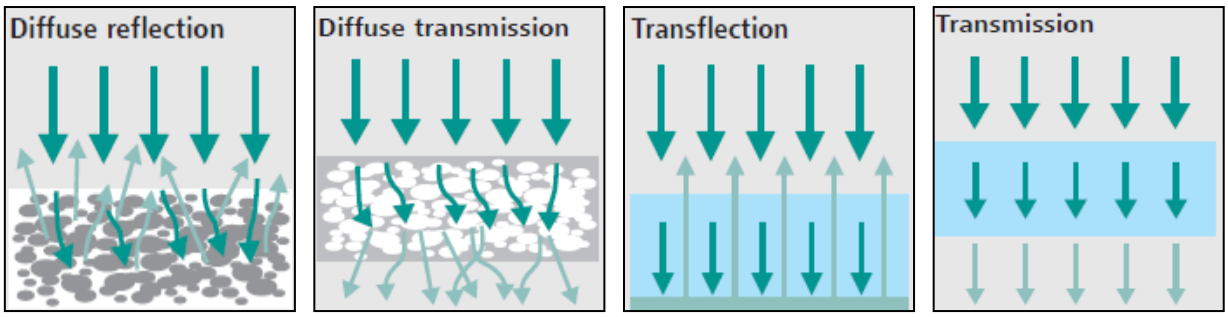

Source: adapted from Metrohm AG (2013)

In the diffuse reflection, NIR light penetrates the sample and interacts with the matter. The NIR energy that is not absorbed is reflected to the detector (diffusely). It is more suitable to measure solids (e.g., cream, paste, granulates, coarse and fine powers), and does need sample preparation. In the case of diffuse transmission, NIR light penetrates the samples and, due to the particles, the light is scattered throughout the sample. The nonabsorbed NIR light is transmitted through the sample reaching the detector. It is more suitable to measure solid dosage forms (tablets and capsules), and like diffuse reflection does need sample preparation. In transmission, the sample is placed between the NIR light source and the detector. NIR light is transmitted through the sample, and the nonabsorbed NIR energy continues to reach the detector. It is suitable for clear liquids, suspensions and solutions. Transflection is a combination of transmission and reflection. A reflector is placed behind the sample, used to reflect the nonabsorbed NIR light back to the sample and then to the detector. It is more suitable for liquids and gels (METROHM AG, 2013).

The advantages of NIR spectroscopy are numerous and diversified. There are many characteristics of this technique that makes it attractive as an alternative to traditional and more time-consuming analytical methods, such as:

- Simple and rapid analysis;
- Not require pollutant solvents;
- Direct, non-invasive and nondestructive.

NIR also provides easy manipulation and fast acquisition of physical and chemical information with levels of accuracy and precision that are comparable to primary reference methods (METROHM, 2013). Chemical information is characterised by the main bonds

present in the monomer consumed and in the polymer formed, while physical information is observed through the slope of the spectrum baseline.

Many successful applications of NIR monitoring on different kinds of polymerisation processes have been reported (Table 3.4 and Table 3.5). Previous works have shown the potential of NIR for monitoring polymerisation reactions, in which the evidence of a correlation between polymer particle size and near-infrared spectroscopy was extensively studied with a focus on emulsion and miniemulsion polymerisation.

Table 3.4 - Literature about monitoring of polymerisation process utilising Near Infrared spectroscopy.

Polymerisation System	Monomers	Calibration Method	Variables Monitored	References
Suspension Polymerisation	Styrene	PLS (Partial Least Squares) NN (Neural Networks)	Average Particle size	(SANTOS; LIMA; PINTO, 1998)
Solution Polymerisation	Methyl Methacrylate	PLS	Conversion	(CHERFI; FÉVOTTE, 2002)
Solution Polymerisation	Styrene	MLR (Multiple Linear Regression) and Kalman Filter	Monomer conversion and average molecular weight of polymer resins	(FONTOURA et al., 2003)
Emulsion Polymerisation	Vinyl acetate (VAc) and butyl acrylate (BuA)	Multivariate PLS	Residual monomers concentration; Average particle size; global conversion and polymer	(CHICOMA et al., 2010)
Emulsion Polymerisation	Styrene Vinyl acetate (VAc) and butyl acrylate (BuA)	PLS	Average particle size	(CHICOMA; SAYER; GIUDICI, 2011)

Table 3.5 – Continuation of literature about monitoring of polymerisation process utilising Near Infrared spectroscopy.

Polymerisation System	Monomers	Calibration Method	Variables Monitored	References
Emulsion Polymerisation	Methyl Methacrylate	PLS Method	Monomer and polymer content, and particle size	(SILVA; CHICOMA; GIUDICI, 2011)
Suspension Polymerisation	Vinyl Acetate and Acrylic Acid	PLS	Copolymer composition	(PEREIRA et al., 2011)
Miniemulsion Polymerisation	Acrylamide	PLS	Monomer concentration; global conversion and average particle size	(COLMÁN et al., 2014)
Miniemulsion Polymerisation	Styrene	PLS	Monomer conversion and particle size	(AMBROGI; COLMÁN; GIUDICI, 2017)

Santos; Lima and Pinto (1998) used NIR spectroscopic technique for in-line monitoring of the average particle size in styrene suspension polymerisation. According to the results, the NIR spectra are sensitive to changes in the operation conditions, and through empirical models (Partial Least Squares (PLS) and Neural Networks (NN)) it is possible to correlate experimental data with the NIR spectra. In this way, the models allow obtaining information about the evolution of the average particle in suspension polymerisation.

Cherfi and Févotte (2002) used the fibre-optic NIR spectroscopy technique to monitor the online conversion of methyl methacrylate in poly(methyl methacrylate) during the solution polymerisation. The calibration model was constructed using Partial Least Squares (PLS) to relate the experimental data (gravimetric) to the NIR spectral data. The obtained calibration results in a nine-factor model with a correlation coefficient equal to 99.45% and a standard error of calibration equal to 1.95%. According to the authors, on-line NIR spectroscopy is an accurate, robust, versatile and suitable technique for monitoring conversion in an industrial polymerisation plant.

Fontoura et al. (2003) report the first use of NIR spectroscopy to simultaneously control of styrene solution polymerisation and monitor the reaction evolution. The monitored

variables were monomer conversion and polymer molecular weight distribution. The calibration model for monomer conversion was constructed using Multiple Linear Regression (MLR) to relate the gravimetric data with the NIR spectra. A good correlation between both data was observed, with a correlation coefficient equal to 99.0%. The molecular weight distribution was estimated by the Kalman filter. The results show good agreement between the Kalman Filter estimations and the experimental data. Based on the results, the authors concluded that NIR spectroscopy with the help of the Kalman Filter estimator could be used successfully for in-line and *in situ* monitoring of monomer conversion and polymer average molecular weight.

The monitoring of emulsion polymerisation using NIR spectroscopy was studied by Chicoma et al. (2010), and Chicoma, Sayer and Giudici (2011). The authors monitored the vinyl acetate and butyl acrylate copolymerisation in a tubular reactor (pulsed sieve plate continuous reactor) and styrene homopolymerisation in a semi-batch stirred tank. The results showed good correlations between the predicted and experimental values.

Silva et al. (2011) studied the monitoring of emulsion polymerisation of methyl methacrylate with a Near-Infrared Spectrophotometer operated in the transflectance mode. Three calibration models based on the PLS method were developed for relating the information contained in the NIR spectra to the off-line analysis. The monitored variables were monomer content, polymer content, and particle size. The results showed good prediction between the experimental data and the NIR calibration model. According to the authors, the results prove that NIR spectroscopy can be a satisfactory alternative for on-line monitoring of important variables in the emulsion polymerisation process.

Pereira et al. (2011) used NIR spectroscopy technique for in-line monitoring of vinyl acetate and acrylic acid during suspension copolymerisation. The results showed that NIR technique could be successfully used to monitor the monomer and polymer concentration during polymerisation.

In the work of Colmán et al. (2014), NIR spectroscopy was used for on-line monitoring of inverse miniemulsion polymerisation of acrylamide. The variables analysed were monomer concentration, conversion and average particle size. The reactions were conducted at different temperatures and concentrations and types of surfactants and initiators. The authors obtained excellent results for the monitoring of acrylamide concentration with the

determination coefficient of 0.994. However, the results of particle size monitoring were not as satisfactory, with a coefficient of determination equal to 0.76, and the root mean squared error of calibration equal 14.4 nm. In conclusion, the models were feasible and capable of identifying disturbances in the reaction medium, and estimated complex phenomena, such as particle nucleation and coalescence.

Ambrogi; Colmán and Giudici (2017) used in-line near-infrared and at-line Raman spectroscopy to monitor the monomer conversion and average size during miniemulsion polymerisation of styrene. Based on the results, the authors concluded that the spectroscopic techniques used to monitor the miniemulsion polymerisation allowed the real-time measurements of the studied variables.

As present in the literature review, NIR spectroscopy has been shown good results in the applications of monitoring and analysis of many kinds of polymerisation processes. However, no work was done on the evolution of the conversion and particle size during precipitation polymerisation reactions, reinforcing the importance of the exploration of the viability of this spectroscopic technique to monitor this kind of polymerisation.

3.2. Material and Methods

3.2.1. Materials

The preparation of microgels by precipitation polymerisation involved the following reagents (Table 3.6): acrylic acid (AA, 99% purity), N-isopropylacrylamide (NIPAM, 97% purity), N,N'-methylenebisacrylamide (MBA, 99% purity), potassium persulfate (KPS, 99% purity). Hydroquinone (Hq) was used to short-stop the reaction in the collected samples. These reagents were purchased from Sigma Aldrich and Vetec and were used as received. Deionised water obtained from reverse osmose system (Chanitex Diaphragm pump SML 8816 and PA-E Water storage tank RO-1070) was employed as the polymerisation medium.

Table 3.6 - Empirical formulas of the precipitation polymerisation reagents.

Compound	Chemical Structure	Function
Acrylic Acid (AA)	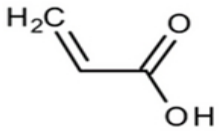	Monomer
N-isopropylacrylamide (Nipam)	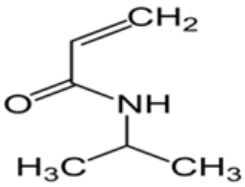	Monomer
N,N' – Methylenebisacrylamide (MBA)	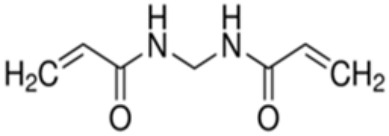	Cross-linking agent
Potassium Persulfate (KPS)	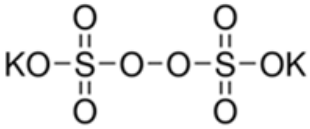	Initiator
Hydroquinone (Hq)	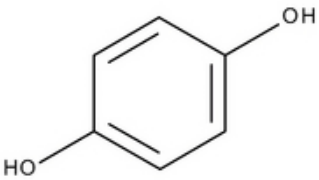	Inhibiting agent

3.2.2. Experimental Procedure

3.2.2.1. Experimental Unit

The precipitation polymerisation process was carried out in reactors with two different volumes: a 250 and a 500 mL jacketed well-mixed reactor (borosilicate glass reactor), both equipped with the following elements (Figure 3.3):

1. Reflux condenser: to avoid the monomer losses due to evaporation during the reaction, mainly of acrylic acid;

2. Mechanical stirrer (TECNAL Te-039/1): for mixing reaction medium;

3. Nitrogen inlet: to eliminated the oxygen from the system. The oxygen is one of the major inhibitors of radical polymerisation reactions;

4. Thermocouple: for temperature monitor of the reaction medium;

5. NIR probe: for in-line monitoring of the polymerisation reaction;

6. Thermostatic bath (TECNAL Te-184): to control the temperature of the reaction medium through the circulation of water inside the reactor jacket.

Figure 3.3 - Experimental Unit of the precipitation polymerisation process. A stirred batch reactor equipped with an immerse NIR probe.

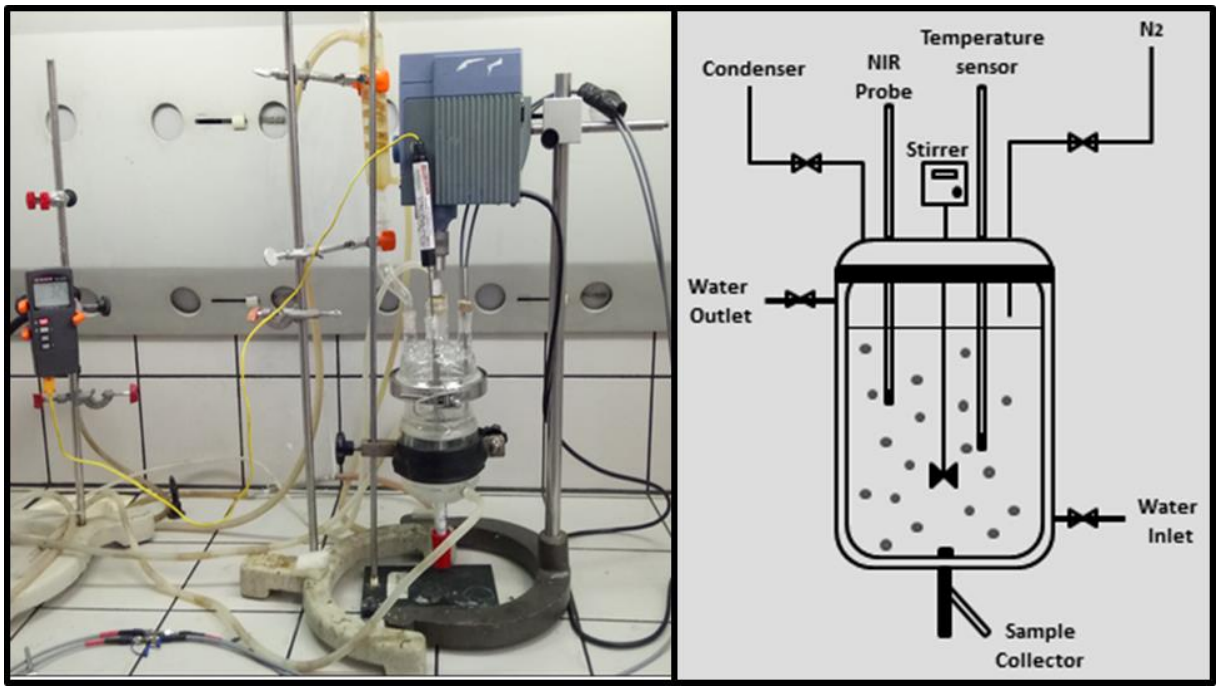

Source: Author

3.2.2.2. Preparation of Microgels

The microgels were synthesised by free radical precipitation polymerisation of AA, NIPAM and MBA using KPS as a hydrosoluble initiator. First, all reagents were weighed and dissolved in distilled water. The mixture composed of the monomers (AA and NIPAM), the cross-linking agent (MBA) and the solvent (water) was added to the reactor under constant stirring at 300 rpm and N_2 purge until the system reached the temperature of 70 °C.

When the system reached the desired temperature, the initiator dissolved in a small amount of water (5 mL) was added to the reaction medium, initiating the polymerisation process. The reaction was carried out for 4 hours. The microgels obtained were purified by ultracentrifugation and washed with water to remove unreacted monomers and initiator. The purification process was repeated three times.

The procedure described for the microgel synthesis was based on the literature (PELTON; CHIBANTE, 1986; ZHANG et al., 2009; MARQUES et al., 2013).

3.2.2.3. Measurements

During the reaction time, samples of the reaction medium were collected at predetermined intervals. These samples were used to measure off-line the conversion of monomers in polymers by gravimetry method and the average particle size by dynamic light scattering (DLS). Simultaneously, at-line and in-line measurements of the UV-VIS-NIR and NIR spectra, respectively, were continuously registered.

3.2.2.3.1. Monomer conversion determination

The monomer conversion was determined by gravimetric analysis. This method consists of analysing the relationship between the mass of the polymer present in the sample and the mass of monomer fed.

For this purpose, during the predetermined reaction time, aliquots of around 15 ml were withdrawn from the reactor, and the collected samples were placed in test tubes with 1% hydroquinone solution and weighed. The tubes and the hydroquinone solution were pre-weighed. Then, the samples were dried in a 65 °C oven with air circulation (TE-394/2, Tecnal) for 24 hours. After this period, the dry residue obtained was weighed and returned to the oven until the weights of the samples remained constant.

The conversion (X) was calculated according to Equation 3.8.

$$X = \frac{M_{DR} - M_{NPS}}{M_{CS} \times y_{m0}} \quad \textbf{(3.8)}$$

where, $\boldsymbol{M_{DR}}$ is the mass of the dry residue; $\boldsymbol{M_{NPS}}$ is the mass of non-polymeric solids (potassium persulfate and hydroquinone); $\boldsymbol{M_{CS}}$ is the mass of the collected sample; and $\boldsymbol{y_{m0}}$ is the mass fraction of monomers in the reaction medium at the beginning of polymerisation.

However, in this work, we face two problems for determining the conversion: first, we have solid monomers, making it difficult to separate them from the dried polymer. Second, the monomer concentration is very low, making it difficult to quantify the polymer formed.

To overcome these difficulties, we first chose to increase the volume of the batch so that a larger sample volume could be collected. The samples were then centrifuged and filtered to remove all non-polymeric solids. The filter used was the Amicon filter with Eppendorf (10 kD, 500 µL/2 mL). Figure 3.4 shows an example of gravimetric results with and without centrifugation and filtration.

Figure 3.4 - Comparison between gravimetric results without centrifugation/filtration (Full circle) and with centrifugation/filtration (Empty circle).

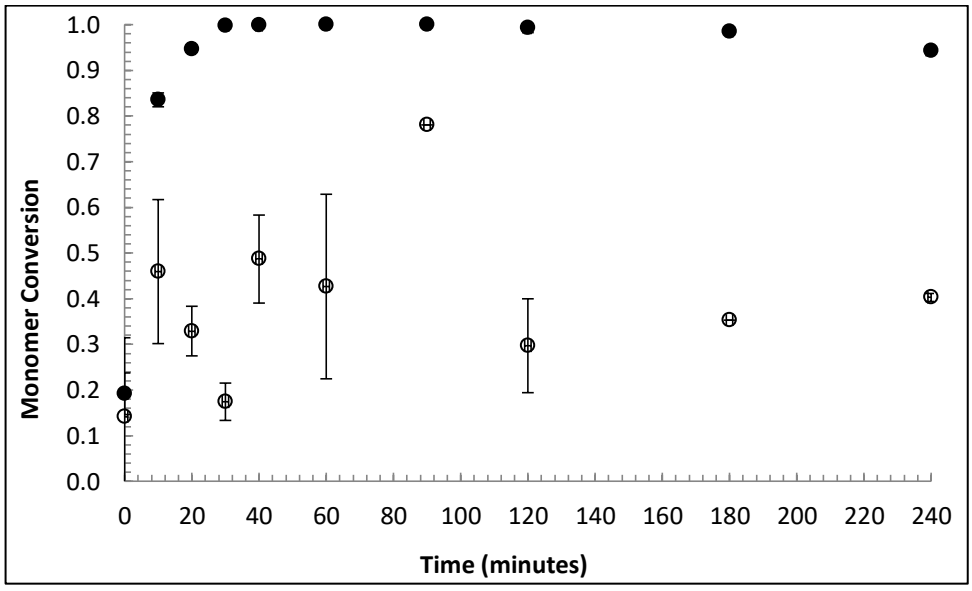

According to Figure 3.4, it is observed that the centrifugation and filtration steps can significantly increase the gravimetric conversion measurement error and diminishing the

values of monomer conversion considerably. This decrease can be associated with loss of material during the purification procedure or loss of soluble polymer fraction. Due to these problems, it was decided to treat the data taking into account only the gravimetric results without the previous centrifugation/filtration of the samples.

3.2.2.3.2. Average particle size determination

Average particle size was determined by the dynamic light scattering method (or photon correlation spectroscopy) at a 90° angle, using Zetasizer Nano ZS90 equipment; Malvern Instruments, Malvern, UK. The diffraction pattern analysis was performed according to the Mie theory, with a refractive index of 1.33 for the diluent. The samples were previously diluted with MiliQ water (1:100), respecting the appropriate concentration for the reading range of the equipment.

3.2.2.3.3. Spectroscopy Techniques

Ultraviolet-visible and near-infrared spectroscopy techniques were used to monitor at-line and in-line, respectively, the precipitation polymerisation reactions of acrylic acid and N-isopropylacrylamide.

a) Ultra-Violet-visible (UV):

UV-Vis-NIR high-resolution spectrophotometer (HR2000+ES, Ocean Optics) with Deuterium and Halogen light sources (DH-2000-BAL, Ocean Optics) and a dip probe (T300-RT-UV-VIS) was used to at-line monitoring of the precipitation polymerisation kinetics in the wavelength range from 200 to 1100 nm (Figure 3.5). The dark noise (a signal obtained without the passage of light through the optical fibre to the detectors) and the reference signal (water spectrum) were collected before every experiment and subtracted from the measurement signal.

Figure 3.5 - A: UV-VIS-NIR spectrophotometer setup; B: dip probe with 6.35 mm of diameter, 127 mm of length, and 2 mm of the light optical path; C: deuterium and halogen light sources.

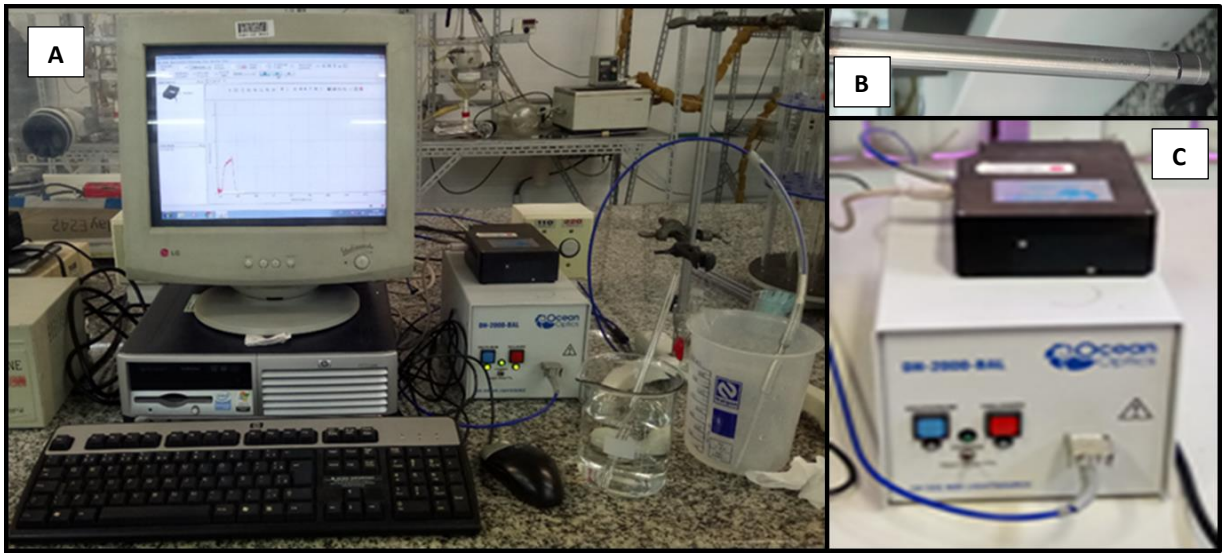

Source: Author

b) Near-InfraRed (NIR):

The NIR spectra were collected in-line using a FTLA 2000 spectrophotometer (ABB) equipped with a Hellma 661.622-NIR transflection probe (with an overall optical path length of 1 mm) immersed into the reaction medium (Figure 3.6).

Data acquisition was conducted by using the Grams/LT (7.00) software (Thermo Galactic/Thermo Fischer Instrument), while for the processing of spectral data, manipulation of the spectra, elaboration of the calibration models, data preprocessing and validation (internal and external), the built-in software Opus-NT (version 3.1) was used, through the Quant 2 tool.

The instrument was configured to scan the spectral region from 4000 to 14000 cm^{-1}. Three spectra were collected at each predetermined time during the reaction, with a resolution of 256 cm^{-1} using ambient air (empty reactor) as a reference.

Figure 3.6 – A: NIR setup; B and C: transflection probe with an overall optical path length of 1 mm.

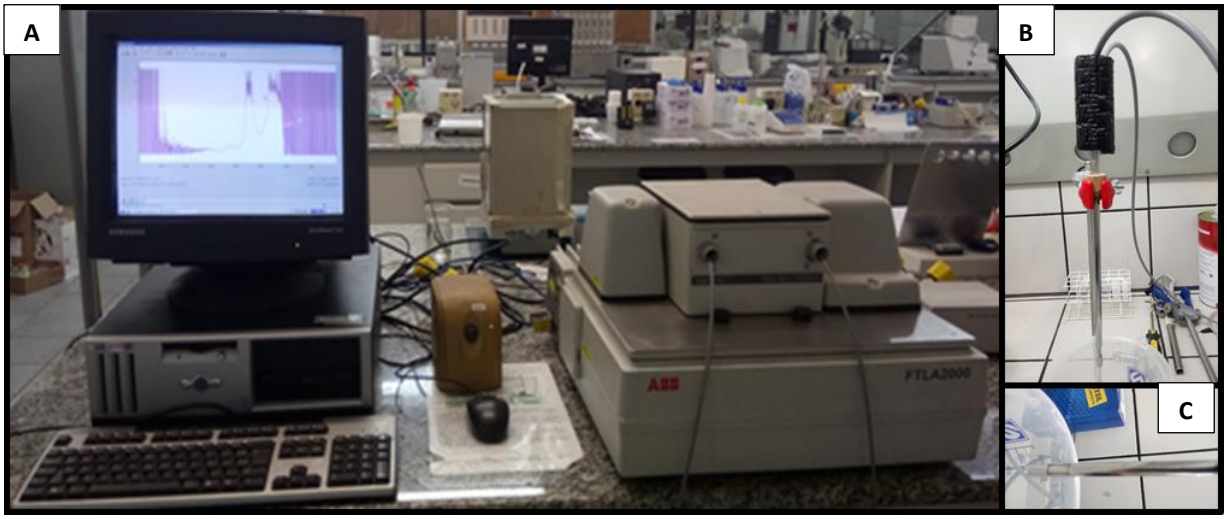

Source: Author

3.2.3. Calibration Model Development

3.2.3.1. Near Infrared Spectroscopy (NIR)

Due to the complex nature of NIR spectra, the information acquired in-line is not a direct measurement of the monitored variables, thus requiring mathematical and statistical procedures, along with careful calibration, to correlate them with the desired physical and chemical properties being monitored (SILVA; CHICOMA; GIUDICI, 2011). This resource is known as chemometrics.

For this, two calibration models were developed for relating the information contained in the NIR spectra (the absorbances at different wavenumber) to the off-line measured values of each of the monitored variables (global monomer conversion and diameter particle size).

For the construction of the calibration models, in most cases, it is considered that there is a linear relationship between the monitored parameters and the intensities of the NIRs spectra (or the first or second derivatives of the NIR spectra) at specific wavenumber. This linearity is represented by the following equation (Equation 3.9), which is based on estimating the regression coefficients b_0 and b:

$$Y = b_0 + X^T b + e \tag{3.9}$$

where Y corresponds to the process response (e.g., polymer concentration and particle size), X is the NIR spectrum, and e is the residue which contains the calibration and experimental errors. The resulting prediction equation can be written as:

$$\hat{Y} = \hat{b}_0 + X^T \hat{b} + e \tag{3.10}$$

The 'hat' symbol means that the quantity is estimated (or predicted).

In practice, all NIR data sets are collinear, which means that there are large correlations between spectral readings at different wavelengths. From statistic, this is known to be a serious problem which makes it difficult to obtain precise estimates $\hat{b}_0$ and $\hat{b}$ and consequently good predictions of $\hat{Y}$ (NAES; MARTENS, 1988).

In this way, for data treatment, a variety of chemometric algorithms based on linear calibration technique can be used with the intention to handle such collinear data, such as Multiple Linear Regression (MLR), Principal Component Regression (PCR), Principal Component Analysis (PCA), and Partial Least Squares (PLS).

MLR is the most straightforward approach to the construction of the calibration model, and it is usually employed when the set of wavelengths used in the calibration model is previously defined. This usually occurs when a single process response (such as monomer conversion) can be measured as a function of a single process disturbance (batch time if it is assumed that the initial process conditions are held constant) (SANTOS et al., 2005; JUNIOR, 2008). The PCR and PLS methods are usually employed when the user does not (or cannot) define the particular set of wavelengths that should be used to calibrate the model. These models are generally employed when the process responses (e.g., individual conversion of monomer to copolymerisations) are a function of multiple process perturbations (e.g., batch time and initial composition of the chemical components) (SANTOS et al., 2005; JUNIOR, 2008).

PCA is used to explain the variability in a single data block. It calculates latent vectors that are uncorrelated, called principal components, and that describes the direction of the most significant variability in the data set (KAMMONA; CHATZI; KIPARISSIDES, 1999). PCR is a more advanced method for multivariate analysis and, in this analytical technique, the model is

constructed where there is a maximum variability of the spectral data. PLS is the most suitable method for the treatment of complex samples that have many sources of the unknown; this method is based on the best correlation between the spectral data and the monitored parameters. PLS is more robust than MLR and PCR; it means that the model's parameters do not change very much when new calibration samples are taken from the total population (GELATI; KOWASLSKI, 1986).

As mentioned previously (sub-section 3.2.2.3.3-b), the NIR data treatment is done through the software Opus-NT utilising the PLS regression. Based on the literature (SANTOS; LIMA; PINTO, 1998; CHERFI; FÉVOTTE, 2002; ARAUJO et al., 2008; CHICOMA et al., 2010; CHICOMA; SAYER; GIUDICI, 2011; PEREIRA et al., 2011; SILVA; CHICOMA; GIUDICI, 2011; COLMÁN et al., 2014) the PLS shown to be the most used method for the construction of calibration models based on NIR spectra. For a better mathematical understanding of the PLS method, it is recommended to consult the work of Gelati and Kowaslski (1986).

In this work, cross-validation is used to estimate the relative predictive powers of models generated by adding PLS dimensions (latent variables). The principle of cross-validation is to calculate a prediction residual error sum of squares (PRESS) as a function of the number of dimensions are incorporated into the model. In principle, as significant dimensions are incorporated into the model, the predictive ability of the calibration model will improve, and the PRESS will decrease (GOSSEN; MACGREGOR; PELTON, 1993). This dimension is known as “factor”, or latent variables (PLS), or “principal components” (PCA), and results from the product of two vectors (loadings and scores) that incorporate the most relevant information from spectral data (ARAUJO et al., 2008), i.e., each factor or latent variable is a linear combination of the spectral absorbances.

Theoretically, if more and more factors are used, one eventually gets the least-squares solution for the training data. However, the goal of building a PLS model is to give predictions on new observations. If too many factors are used, the model would fit the training samples too well, and therefore, it fits the noise in the training data as well. The cross-validation method is used to avoid over-fitting on training data. A typical way of doing cross-validation is to leave one or several samples out at a time, and then train the model with the remaining samples. After training, the model is tested with the samples which are not used in training. This procedure is repeated until every sample has been left out once.

Summing up all the test errors over each factor, the optimal number of factors is chosen as the location of the minimum of the sum of test errors. One can see that the cross-validation method is quite laborious, but it is useful in determining the number of factors (QIN; McAVOY, 1992).

For an elaboration of the multivariate calibration model, the following steps were necessary: 1. Classification of the calibration and validation set; 2. Spectral band evaluation; 3. Preprocessing of spectra data; 4. Evaluation of chemometric parameters; and 5. External Validation.

3.2.3.1.1. Classification of the calibration and Validation Set

The first step to build a chemometric model is to pick a sufficiently large number of samples that contain information significant for the system. For this, it is essential to select the samples that will be part of the calibration and validation set. The calibration set contains data that are representative of the samples to be analysed, and the validation set is utilised for evaluating the performance of calibration. The samples belonging to the validation set were not used in the stage of construction of the model. Table 3.7 shows the information about the formulations of samples used in this chapter; these samples belong to the experimental set number 4 that was better explained in section 4.2.2 (Chapter 4).

Table 3.7 - Information about the formulation of samples used in the calibration and validation of NIR monitoring. Reactions conditions: 70°C (temperature), 300 rpm (agitation speed).

Sample (run)	AA ($mmol.L^{-1}$)	NIPAM ($mmol.L^{-1}$)	MBA ($mmol.L^{-1}$)	KPS ($mmol.L^{-1}$)	Y_{m0} (%)
Calibration					
S18	10	120	2	5	1.44
S24	40	200	2	5	2.51
S26.1	25	160	4	7.5	2.01
Validation					
S19	10	120	6	10	1.50
S20	10	200	2	10	2.31
S21	10	200	6	5	2.37
S22	40	120	2	10	1.64
S25	40	200	6	10	2.56
S26.2	25	160	4	7.5	2.01
S26.3	25	160	4	7.5	2.01

3.2.3.1.2. Spectral Band Evaluation

In this step, it is important to determine the appropriate spectral range where there is a good correlation between changes in spectra and the property of interest. In some cases, the relation between the spectra and the monitored variable is well defined. However, in others, this relationship is not very clear, being necessary to use statistical analysis for the evaluation of the better spectral band for construction of a calibration model.

3.2.3.1.3. Preprocessing of Spectral Data

Multiple spectra are typically acquired to determine reproducibility for each calibration sample. If the spectra of the same sample are not identical, a data preprocessing procedure must be chosen, which makes them more similar (BRUKER OPTIK GMGH, 2000). In this way, a data preprocessing is a necessary stage in performing a calibration, with removal or reduction of the irrelevant source of random or systematic variations in spectra, such as noise and shifts in the baseline, among others.

Preprocessing the data is essential to ensure a good correlation between the spectral data and the concentration values. For this, the following methods can be applied (BRUKER OPTIK GMGH, 2000):

- Linear Offset Subtraction: shifts the spectra to set the y-minimum to zero;
- Straight Line Subtraction: fits a straight line to the spectrum and subtracts it. This accounts for a tilt in the recorded spectrum;
- Vector normalisation: normalises a spectrum by first calculating the average intensity value and subsequent subtraction of this value from the spectrum. Then the sum of the squared intensities is calculated, and the spectrum is divided by the square root of this sum. This method is used for example account for different sample thickness;
- Min-max normalisation: first subtracts a linear offset and then sets the y-maximum to a value of 2 by multiplication with a constant. Used similar to the vector normalisation.
- Multiplicative Scatter Correction: performs a linear transformation of each spectrum; often used for spectra measured in diffuse reflection;
- First Derivative: calculates the first derivative of the spectrum. This emphasises on steep edges of a peak. This method is used to emphasise pronounced, but small features over a broad background. Spectral noise is also enhanced;

- Second Derivative: similar to the first, but with a more drastic result.

3.2.3.1.4. Evaluation of the Chemometric Parameters

The final choice of the model and the preprocessing technique was based on the predictive ability of the models, evaluated by the chemometric parameters between the estimated and experimental values. These chemometric parameters are: Root mean square error of cross-validation (RMSECV) and determination coefficient (R^2). These parameters can be calculated according to the following equations:

$$RMSECV = \sqrt{\frac{1}{M}\sum_{i=1}^{M}\left(y_{i,exp} - y_{i,pred}\right)^2} \tag{3.11}$$

$$R^2 = 1 - \sum_{i=1}^{M}\left(\frac{y_{i,exp} - y_{i,pred}}{y_{i,exp} - \bar{y}_{exp}}\right)^2 \tag{3.12}$$

where M is the number of samples in the calibration set, $y_{i,exp}$ is the experimental value, $y_{i,pred}$ is the value predicted by the calibration model, and $\bar{y}_{exp}$ is the average of the experimental values.

R^2 gives the value of variance between the experimental and predicted data. For better calibration, this value should be approximately 1. RMSECV is a cross-validation parameter that judges the quality of the method; that is, it is a quantitative value that represents the proximity between the experimental and prediction data.

In this step, other parameters must be considered for appropriate choices of the calibration model, such as the number of principal factors or components (k) to be used in the model, detection of outliers, and anomalous samples.

The determination of the number of principal components is a crucial point for the quality of the calibration model. Using an insufficient number of principal components leads to poor reproduction of the spectral data, and therefore, the model will not be able to recognise changes in the spectral features. This is called underfitting. Including too many principal components, on the other hand, adds spectral noise to the regression and does not increase the amount of valuable information (overfitting) (BRUKER OPTIK GMGH, 2000).

The number of principal factors (k) in the PLS method was determined by the standard cross-validation (leave-one-out) procedure. In this procedure, parts of the calibration set are left out of the calculation used to fit the model (with a certain number of k) to the data. Then the model is used to estimate the values of the left-out samples. This procedure is repeated several times for different sets, and the RMSECV between the predicted and the real values are calculated. The number of k is chosen as the minimum of the plot of RMSECV versus k.

3.2.3.1.5. Validation

Finally, an external validation needs to be done for a confirmation that the calibration model selected was adequate. This external validation is based on the comparison between the model predictions with a different set of data that was not used previously in the calibration procedure.

3.3. Results and Discussion

The aim of studying at-line and in-line monitoring using spectroscopic techniques, respectively, UV-Vis-NIR and NIR, were to evaluate the ability of these techniques to monitor the changes in important process variables, such as monomer conversion and average particle size, during the process of production of microgel particles by precipitation polymerisation.

For the selection of the experiments used in the calibration models, the minimum, medium and maximum points of the fractional experimental design, respectively, runs S18, S26.1 and S25 were first chosen. However, the spectra of samples belonging to experiment S25 were not in agreement with off-line measurements, mainly about the average particle size.

As can be seen in Figure 3.7, throughout the reaction period, the samples belonging to S25 showed an observed heterogeneity, in which the medium became less milky due to the aggregation of the microgel particles. This aggregation was caused by the higher initial concentration of monomers together with the high concentration of initiator in the reaction medium. This combination increases the number of microgels, consequently the instability in the medium, and finally microgel aggregation.

Figure 3.7 – (A) Samples collected during the polymerisation of experiment S25; Microgels aggregates in (B) the stirrer blades and (C) the bottom of the reactor.

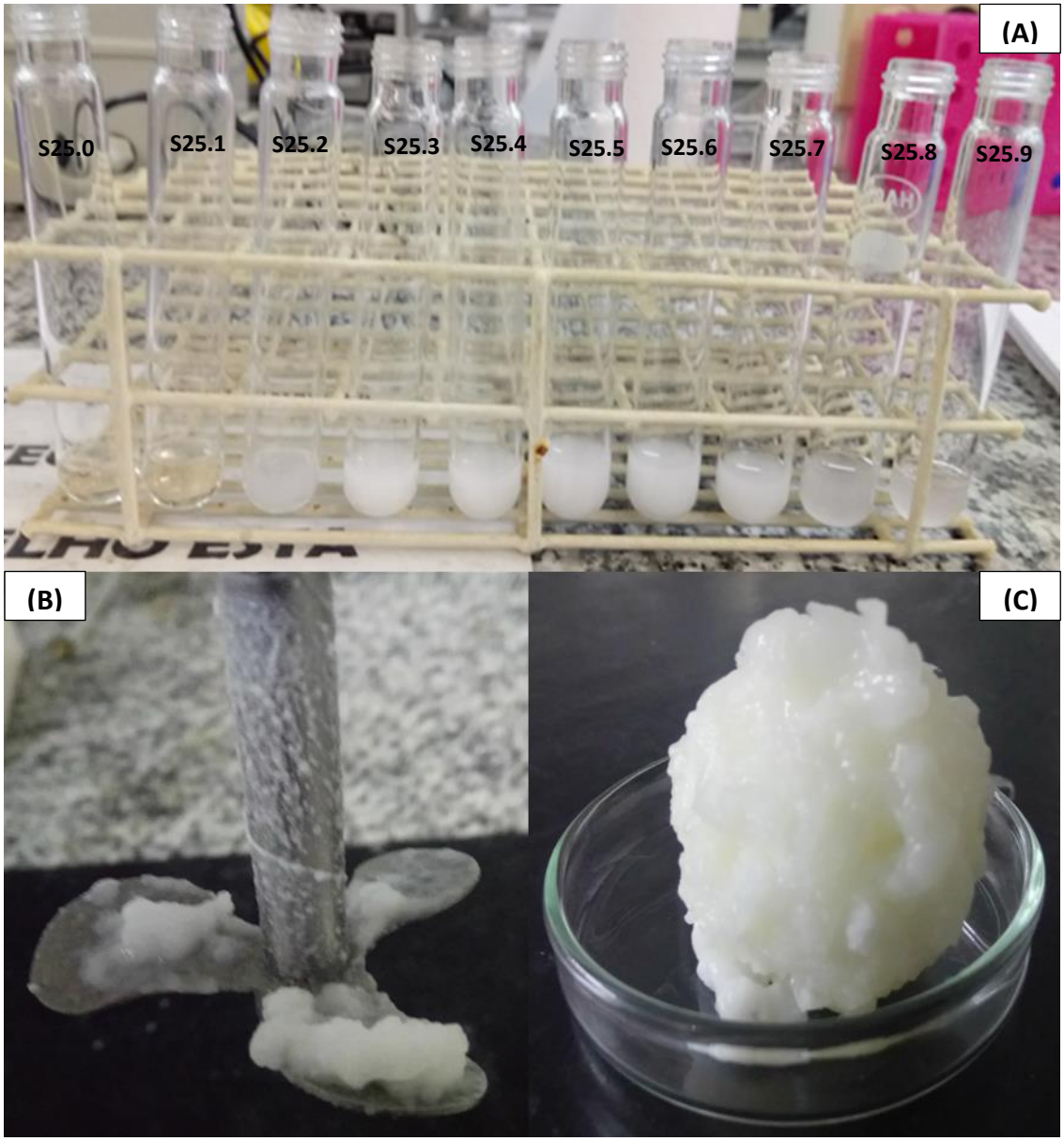

Then, it was decided to substitute the sample S25 (Y_{m0} equal to 2.56) for the sample S24 (Y_{m0} equal to 2.51), which also shows a high initial concentration of monomers, but has a lower concentration of crosslinking agent and initiator, making the particles more stable and with a lower tendency of aggregation. Table 3.8 shows the monitoring parameters (minimum and maximum values) of the samples used in the construction of calibration models and the external validation of them.

Table 3.8 - Values of the variable (Y_{m0}) and the parameters analysed (X_{min}, X_{max}, Dh_{min} and Dh_{max}) of the samples belonged the calibration and external validation sets.

Sample (run)	Y_{m0} (%)	X_{min}	X_{max}	Dh_{min}	Dh_{max}
Calibration					
S18	1.44	0.1090	1.0000	122.8	301.3
S24	2.51	0.0043	0.9623	278.0	352.3
S26.1	2.01	0.0000	1.0000	180.9	320.7
Validation					
S19	1.50	0.1587	1.0000	192.8	354.9
S20	2.31	0.1302	1.0000	220.7	331.9
S21	2.37	0.2874	0.9235	224.1	432.5
S22	1.64	0.4772	1.0000	271.2	357.4
S23	1.71	0.0738	0.9973	81.11	348.3
S25	2.56	0.0722	0.8976	219.9	524.5
S26.2	2.01	0.1920	1.0000	243.4	455.9
S26.3	2.01	0.6349	1.0000	233.5	348.0

Y_{m0} is the initial mass fraction of AA, NIPAM and MBA in the reaction medium; X_{min} and X_{max} are the minimum and maximum values for monomer conversion, respectively; Dh_{min} and Dh_{max} are the minimum and maximum values for average particle size (hydrodynamic diameter), respectively. X_{min}, X_{max}, Dh_{min} and Dh_{max} are data obtained during the reaction time for each experiment.

3.3.1. Ultraviolet-Visible-Near Infrared (UV-Vis-NIR)

Figure 3.8 shows the spectra of the experiments used in the calibration model. These spectra represent the spectroscopic behaviour of the samples during the reaction time.

Figure 3.8 - Spectra of the experiments used in the construction of the calibration model (S18, S24 and S26.1). The direction of the red arrow represents the time evolution of the reaction.

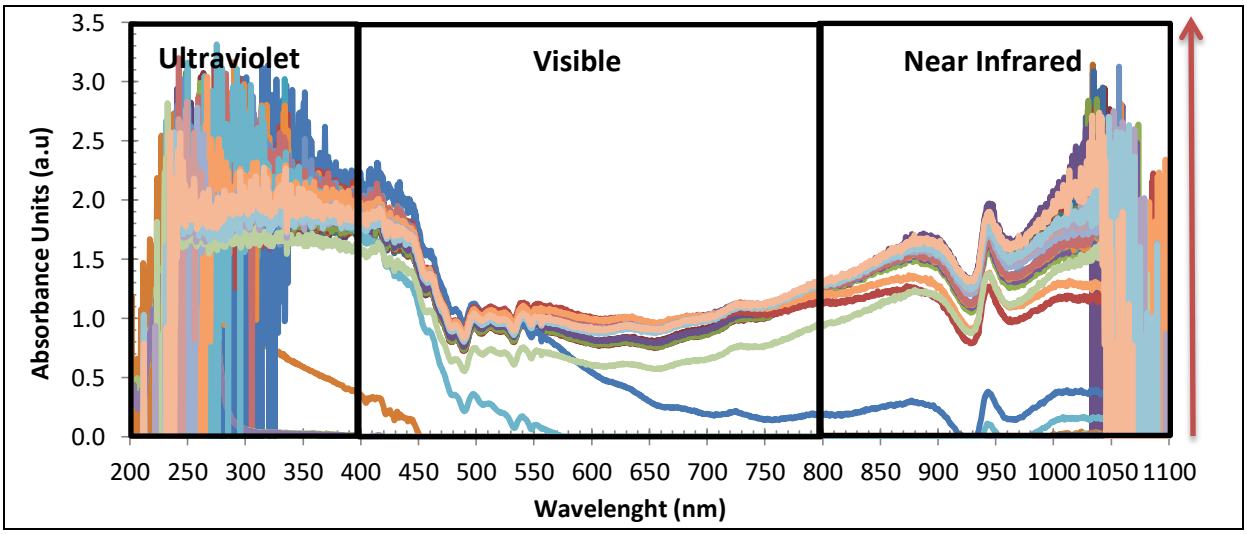

To correlate the global conversion and the average particle diameter with the spectral information using the UV-Vis-NIR high-resolution spectrophotometer, the relation between the areas corresponding to a specific wavelength range and the parameters to be monitored was analysed. This area was calculated by the trapezoidal rule.

For the construction of the models, we tried to choose a range in which the best linear adjustments were observed. Figure 3.9 shows how these spectroscopic regions were divided for the construction of calibration models, and Table 3.9 shows the results from these tests.

Figure 3.9 – Some regions using in the construction of the models. A represents the ultraviolet region (A.1: 335.98-399.57 nm). B represents visible region (B.1: 400.4-449.61nm; B.2: 450.54-489.59; B.3: 488.66-557 nm; B.4: 556.54-594.14; B.5: 594.14-799.86). C represents Near Infrared region (C.1:800.30-920.31 nm; C.2:920.31-933.42 nm; C.3: 933.42-1019.36). The direction of the red arrow represents the time evolution of the copolymerisations used in the calibration models (S18, S24 and S26.1).

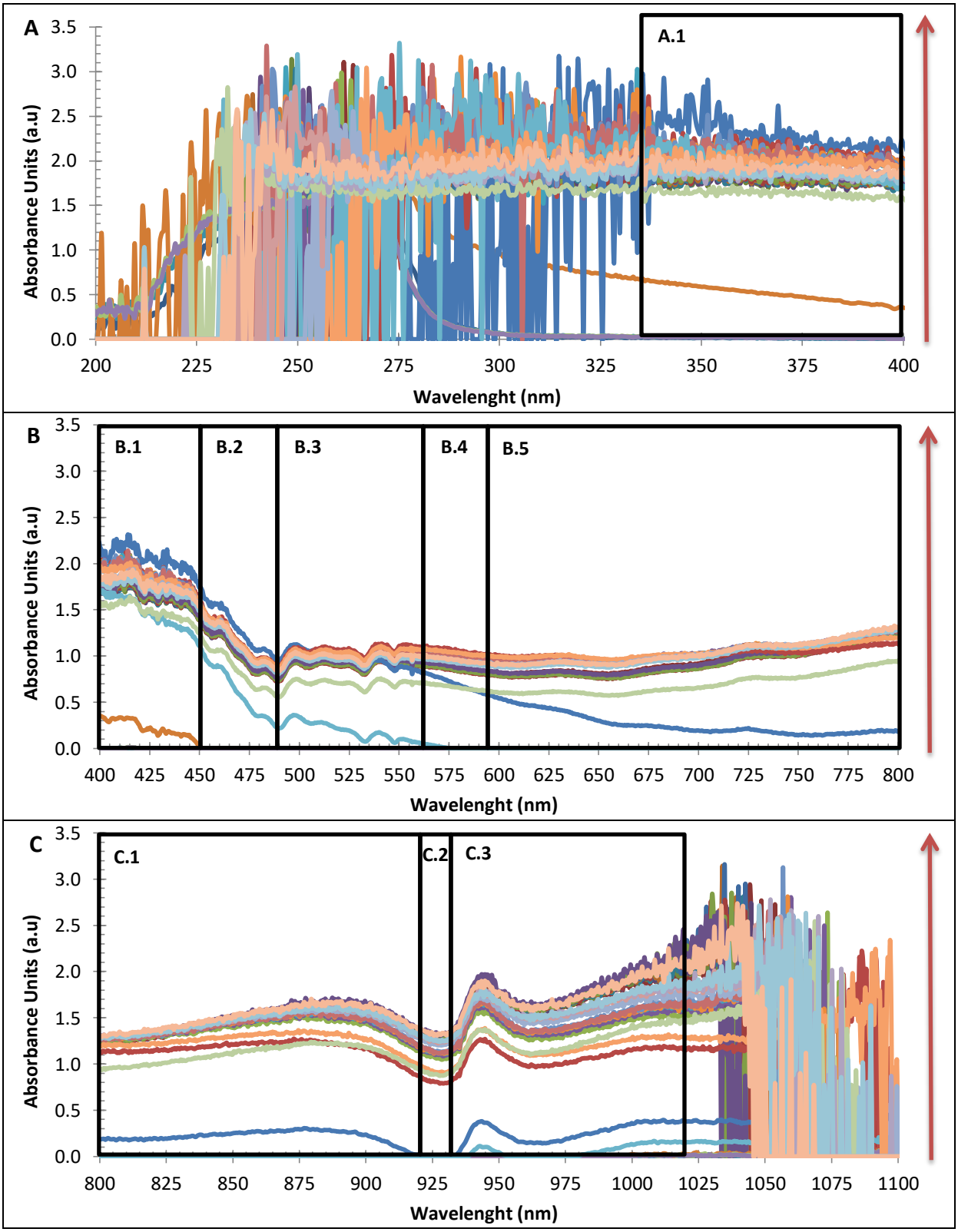

Table 3.9 - Results of the correlation coefficient (R^2) for monomer conversion (X) and average particle size (Dh) calibrations models using different spectroscopic regions and wavelength (λ).

Test	Spectral Region	λ range (nm)	R^2 (X model)	R^2 (Dh model)
1	All spectral range	186.56-1114.49	0.9446	0.6368
2	All spectral range	335.98-1019.36	0.9378	0.6747
3	Ultraviolet	200.04-399.57	0.7604	0.1997
4	Ultraviolet	335.98-399.57	0.6714	0.0809
5	Visible	400.40-799.86	0.9115	0.4995
6	Visible	400.40-449.61	0.7415	0.1991
7	Visible	450.54-489.59	0.7867	0.2877
8	Visible	488.66-557.00	0.8562	0.3812
9	Visible	556.54-594.14	0.6828	0.2614
10	Visible	594.14-799.86	0.9164	0.5610
11	Near Infrared	800.30-1114.49	0.7100	0.4460
12	Near Infrared	800.30-1019.36	0.9059	0.8161
13	Near Infrared	800.30-920.31	0.9219	0.7630
14	Near Infrared	920.31-933.42	0.8718	0.8193
15	Near Infrared	933.42-1019.36	0.8762	0.8551
16	Near Infrared	963.92-1001.65	0.8742	0.8566
17	Near Infrared	942.58*	0.9007	0.8457

* Abs peak

According to the linear coefficient results shown in Table 3.9, we choose to present the better models in the Visible (test 10) and NIR (test 13, 16 and 17) spectroscopic region. For monomer conversion, we constructed two calibration models denominated Model 1 (test 10) and Model 2 (test 13). For the average particle size, the models were denominated Model 4 (test 16) and Model 5 (test 17). Although the tests with all spectral region have the best results for R^2, we chose to leave it out and work with the separate regions so that we can compare them.

In the case of calibration models for average particle diameter, the NIR region is unique that shows better values for R^2 (Test 12-17). Moreover, an analysis of the data shows that there is a simple linear correlation between the experimental data of monomer conversion and particle size. Thus, an alternative approach is to use the calibration model to obtain the conversion from the spectra, and then use the so-obtained conversion to obtain the corresponding particle size from the simple linear correlation between conversion and particle size (Figure 3.10).

Figure 3.10 - Prediction of average particle size based on the calibration models for monomer conversion.

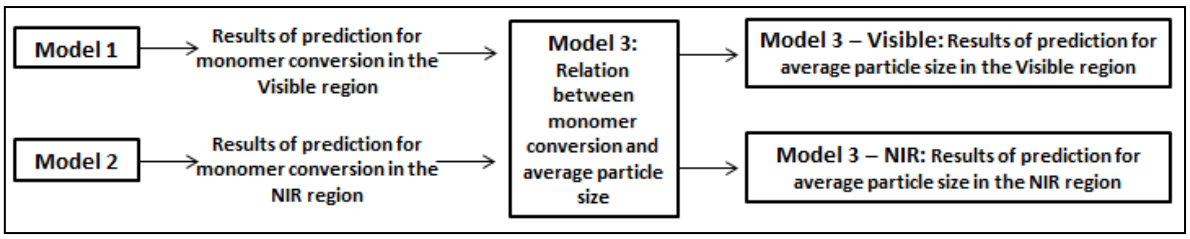

Figure 3.11 and Figure 3.13 show the calibrations models for monomer conversion and average particle size, respectively. Figure 3.12 shows the relation between monomer conversion and average particle size.

Figure 3.11 – Calibration models for monomer conversion. Model 1: Visible region (594.14-799.86 nm) with a linear coefficient equal to 0.9164. Model 2: Near Infrared Region (800.3-920.31 nm) with a linear coefficient equal to 0.9219.

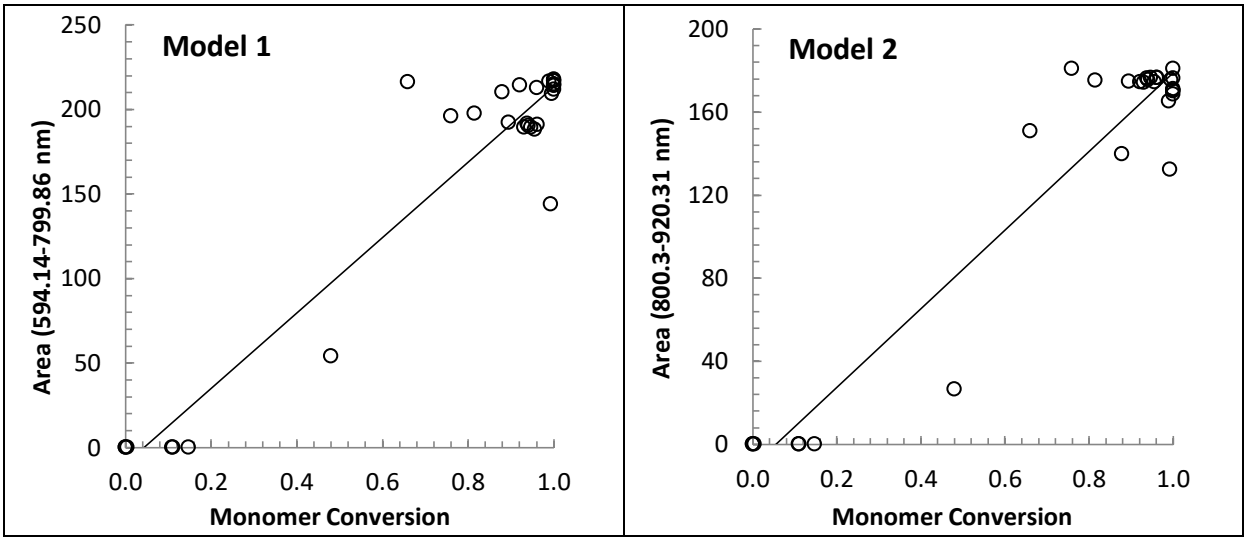

Figure 3.12 – Model 3: Linear correlation between monomer conversion and average particle size (R^2=0.665).

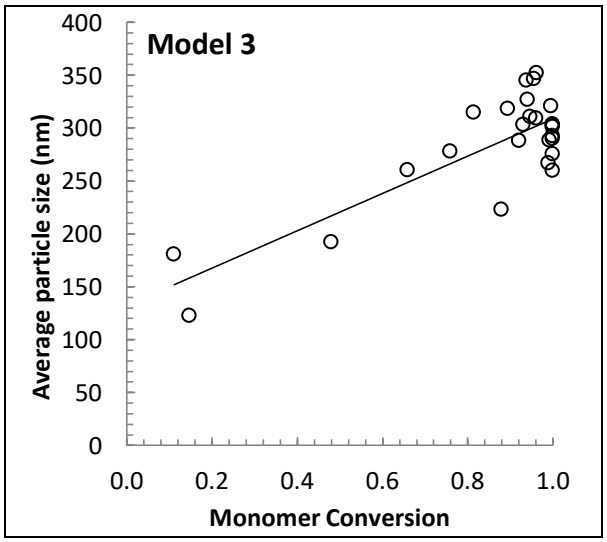

Figure 3.13 - Calibrations models for average particle size. Model 4: Nir region (963.92-1001.65 nm) with a linear coefficient equal to 0.8566. Model 5: Absorbance peak in the NIR region (942.58 nm) with a linear coefficient equal to 0.8457.

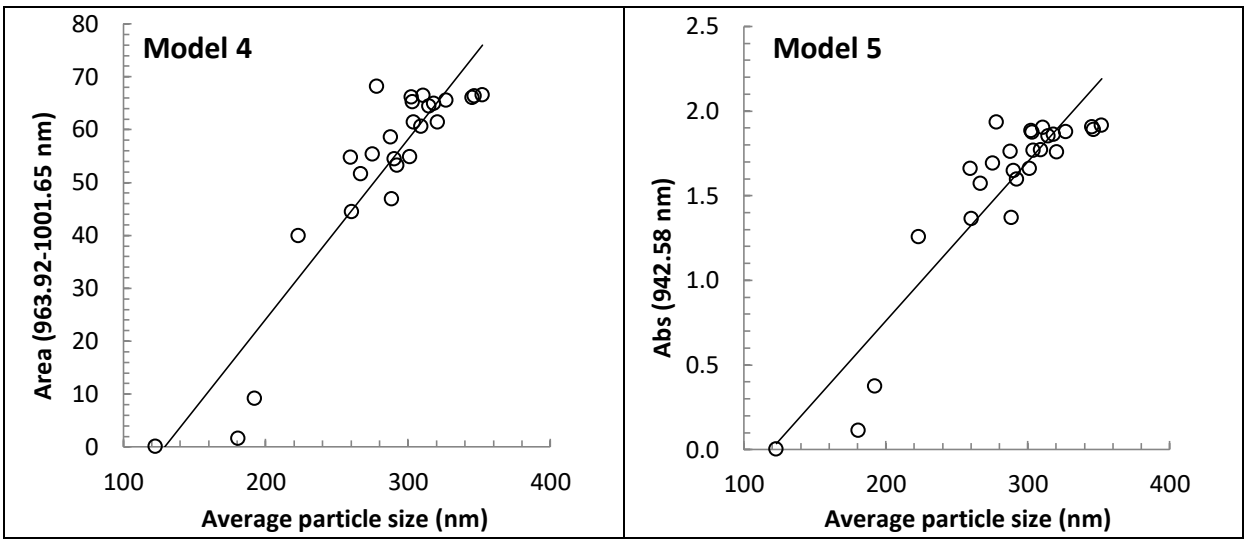

Figure 3.14 shows the internal validation of the calibration models for global conversion and average particle size (Model 1-5). These validations were done with the samples used in the construction of the calibration models.

According to the results of internal validation, there are some discrepancies when experimental data were compared with the predicted models. For global conversion results, these differences are higher in the first minutes of the reaction. It can be explained by the inaccuracy of the experimental data because of the possible existence of the unreacted monomers in the dried polymer samples. Another reason for this difference between the experimental data and the predicted models can be explained by the instability of the medium (it becomes heterogeneous) at the beginning of the reaction due to homogeneous nucleation. In experiment 26.1, the calibration models 1 and 2 predict a decrease in monomer conversion at 60 minutes of reaction, a behaviour not shown by the experimental values of conversion; probably, this point is an outlier.

The models of the average particle size for experiments S18 and S26.1 are similar to experimental data. However, in the experiment S24, the deviations are higher. One possible explanation is that this experiment has a total monomer concentration higher than others, in this way; there are more particles in the reaction medium, consequently more tendency to aggregation and a higher polydispersity index (broad particle size distribution).

Figure 3.14 – Internal validation. Samples used in the construction of the calibration models: S18 (Y_{m0} equal 1.44), S24 (Y_{m0} equal 2.51) and S26.1 (Y_{m0} equal 2.01). Left column: monomer conversion results; Right column: average particle size results.

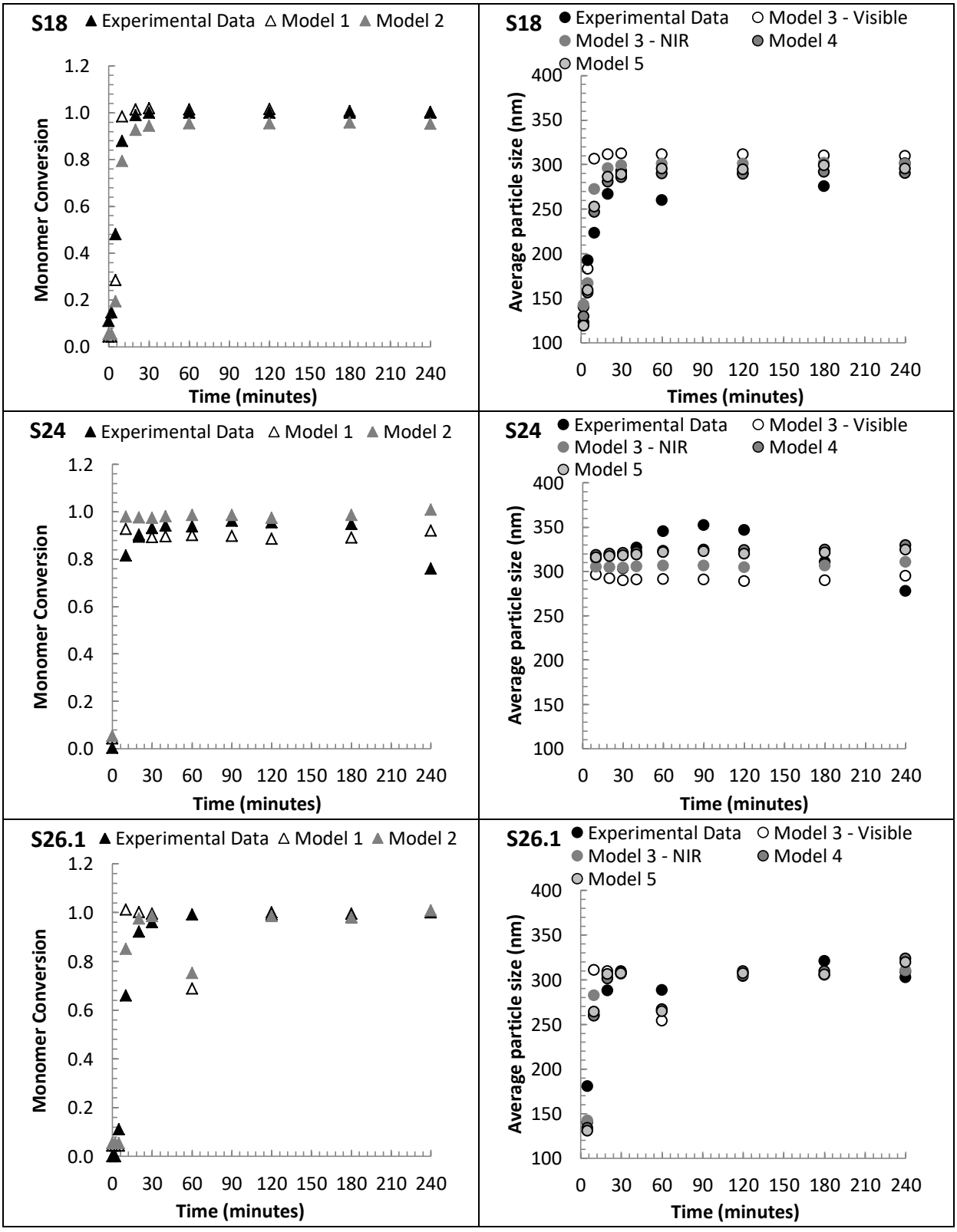

About the overall performance of the predictive models, they are very similar, except for prediction of average particle size in experiment S24. It means that all spectrum regions used in the calibration models have similar behaviour, so any part of the spectrum can be used for predicting the analysed parameters.

Figure 3.15 shows the results of the external validation of the experiments with an initial concentration of monomers close to the minimum point of the experimental design.

It is possible to observe the same behaviour found in the internal validation, which for some runs the values of the prediction in the first stage of reaction are different of the experimental data. In experiment S23, the monomer conversion predicted by the models in the range from 10 to 120 minutes show results above the maximum value of the conversion. In this case, these spectra collected during these periods cannot be considered for the estimation of monomer conversion because they probably were not described by corresponding models. Another relevant point in Figure 3.15 is that the models are not sensitive to the concentration of the particles in the sample. In experiment S19, at the final time of reaction; it is possible to observe a decrease in the experimental data for monomer conversion and average particle size that is not followed by the models. Probably, these are errors in the experimental measurements. Also, in run S23, an outlier is identified for the conversion at time 40 minutes.

Figure 3.15 – External Validation: S19 (Y_{m0} equal to 1.50), S22 (Y_{m0} equal to 1.64) and S23 (Y_{m0} equal to 1.71).

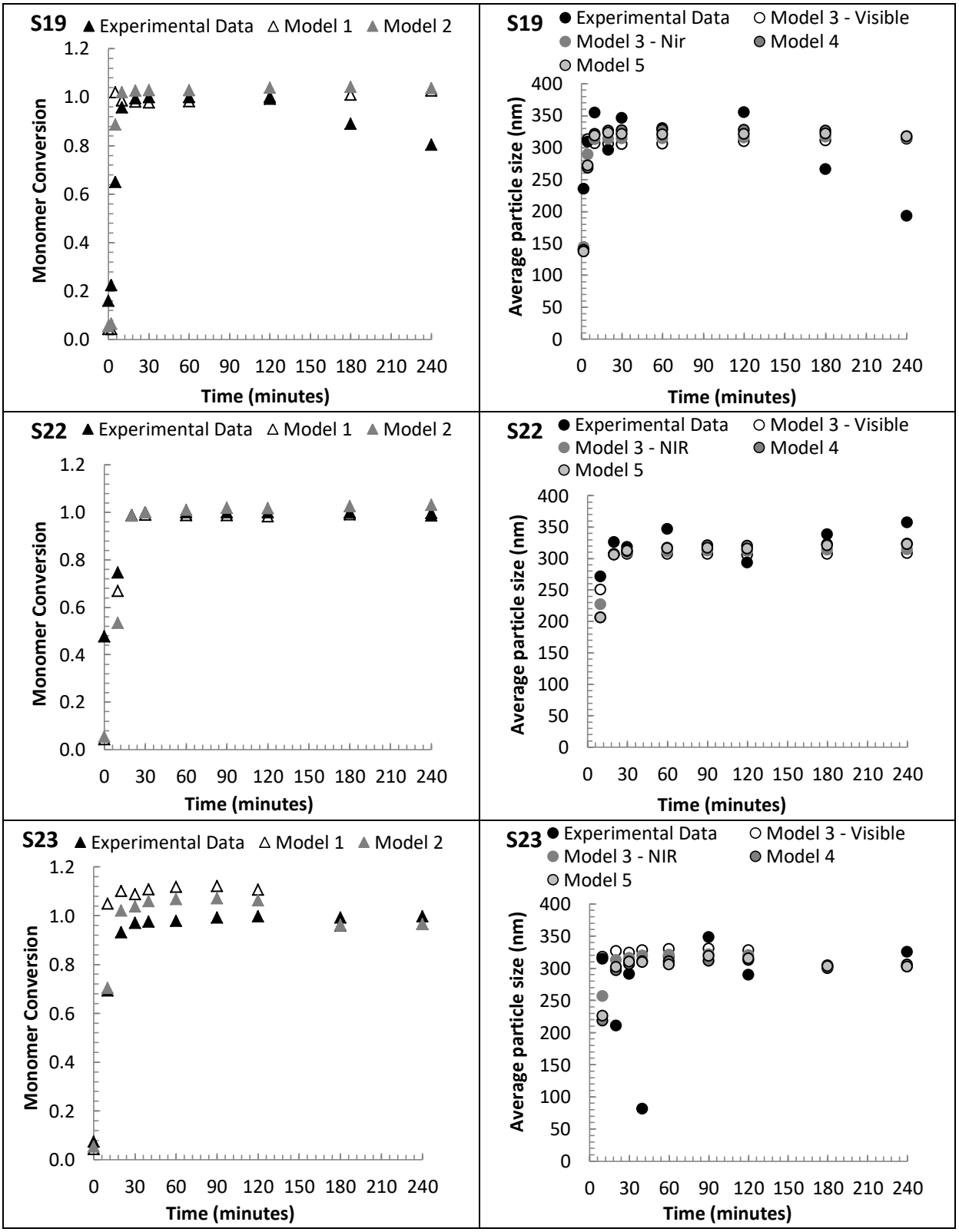

Figure 3.16 shows the results of the external validation of the experiments with an initial concentration of monomers at the central point of the experimental design.

Figure 3.16 – External Validation. The samples belong to the central point of the experimental design have the initial concentration of reagents equal to 2.01.

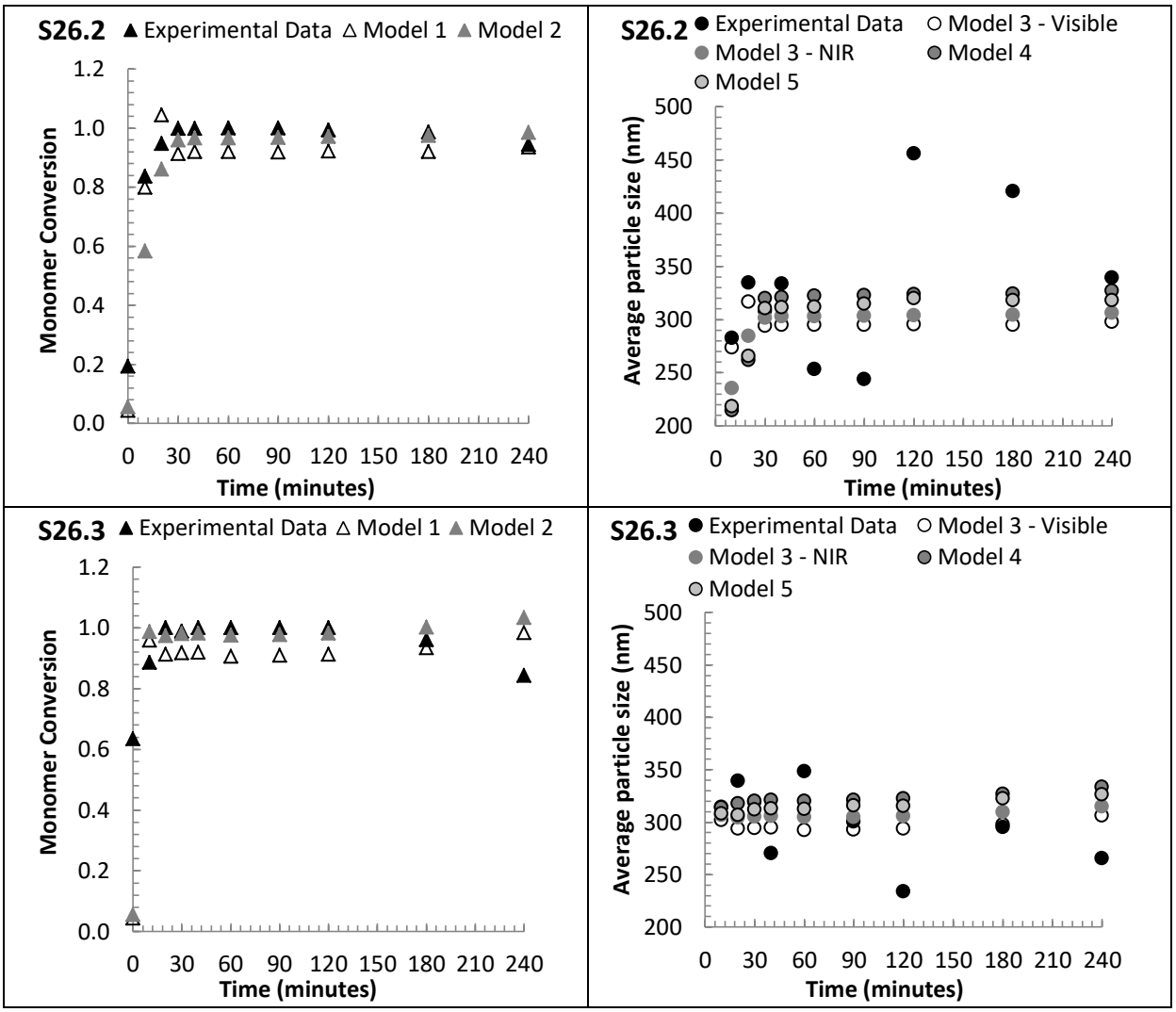

According to Figure 3.16, there is a good correspondence between the predicted models and the experimental data for monomer conversion. However, the same is not observed for average particle size, because the experimental results did present larger fluctuations over time that does not reflect the true, expected behaviour of the experimental data, indicating the occurrence of experimental errors of measurement or sampling.

Figure 3.17 shows the results of the external validation of the experiments with an initial concentration of monomers close to the maximum point of the experimental design.

Figure 3.17 – External Validation: S21 (Y_{m0} equal 2.37) and S25 (Y_{m0} equal 2.56).

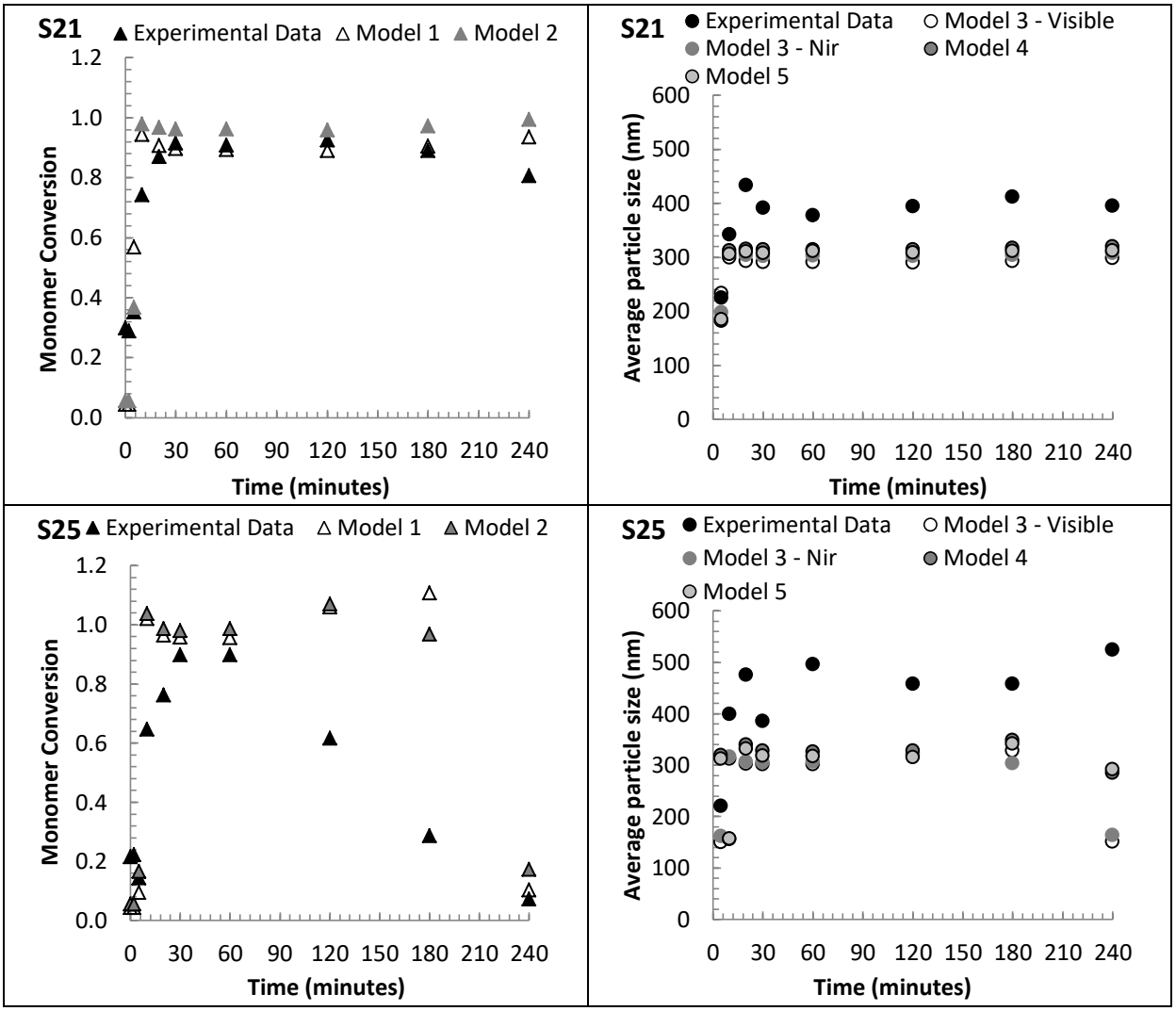

According to the results in Figure 3.17 for the experiments with higher total monomer concentration, it is observed that there is a significant difference between the experimental data and the data predicted by the models. Analysing the monomer conversion results, the models still can follow the profile obtained with the experimental data of the experiment S21. However, this behaviour is not observed about the experiment S25, which, as previously mentioned, presents an observed heterogeneity due to the formation of aggregates. It is important to say that the formation of aggregates in the reactor causes difficulties for the sampling during the reaction time. For this reason, these samples

withdrawn from the reactor do not represent the real monomer conversion of the microgel particles, but the concentration of polymer in the aqueous part into the reactor.

About the average particle size, the experimental values are higher than the values predicted by the models, but the profile remains similar. It means that in this case, the models probably represent the real size of the particles inside the reactor during the reaction time, while the experimental data show the results of the aggregation of microgel particles in the samples withdrawn from the reactor. As expected, the difference between the experimental data and the predictions is higher in the experiment S25 than experiment S21, because of the higher concentration of total monomers and initiator in the formulation.

3.3.2. Near Infrared Spectroscopy (NIR)

Two calibration models based on the NIR spectra were developed and validated, aiming to ensure the accuracy estimate of the experimental data of the conversion of the monomers in polymers and average particle size of microgels. The off-line measurements were used for the construction of the calibration models and validation of them. The experimental data for monomer conversion ranged from 0.00 to 1.00, and for particle sizes ranged from 81.1 to 524.5 nm. The initial reagents (AA, NIPAM and MBA) concentration of the experiments ranged from 1.44 to 2.56 wt%. The experimental results for each run can be found in Table 3.10 and Table 3.13.

3.3.2.1. Identification of spectral bands

The PLS regression method is a “full spectrum method”. The chemometric model should improve with an increasing number of data points. However, in some cases, spectral noise or additional components present in the sample may cause the PLS algorithm to interpret these features, which can degrade the model. In these cases, it is advisable to limit the spectral range used for the PLS regression (BRUKER OPTIK GMGH, 2000).

The spectral bands can be chosen according to the intensity of the regions of absorption of the interest bonds in the reagents present in the microgels, in this case, which is in the regions 4000-4500 and 5855-6250 cm^{-1} corresponding of C=C bond. The spectral region from 7500-12000 cm^{-1} also can be analysed to obtain the physical information of the reaction medium. As previously mentioned, the entire spectrum region (12500-4000 cm^{-1}) can also be evaluated.

Figure 3.18 shows the NIR spectra for pure water and pure acrylic acid monomer. The spectrum of water presents characteristic bands that correspond to the absorption of O-H bond in the range from 7576.87 to 6050.75 cm^{-1} (first overtone with a max peak at 6871.40 cm^{-1}) and from 5446.06 to 4539.03 cm^{-1} (combination stretches with a max peak at 5136.81 cm^{-1}) while acrylic acid presents the main bands from 6180.33 to 5604.43 cm^{-1} and from 4754.99 to 4251.08 cm^{-1}.

Figure 3.18 - NIR spectra of acrylic acid (monomer) and water (solvent). The rectangles denoted with (A) and (B) represent the spectral region of the intensity of the acrylic acid, region A ranged from 6180.33 to 5604.43 cm^{-1}, and region B ranged from 4754.99 to 4251.08 cm^{-1}.

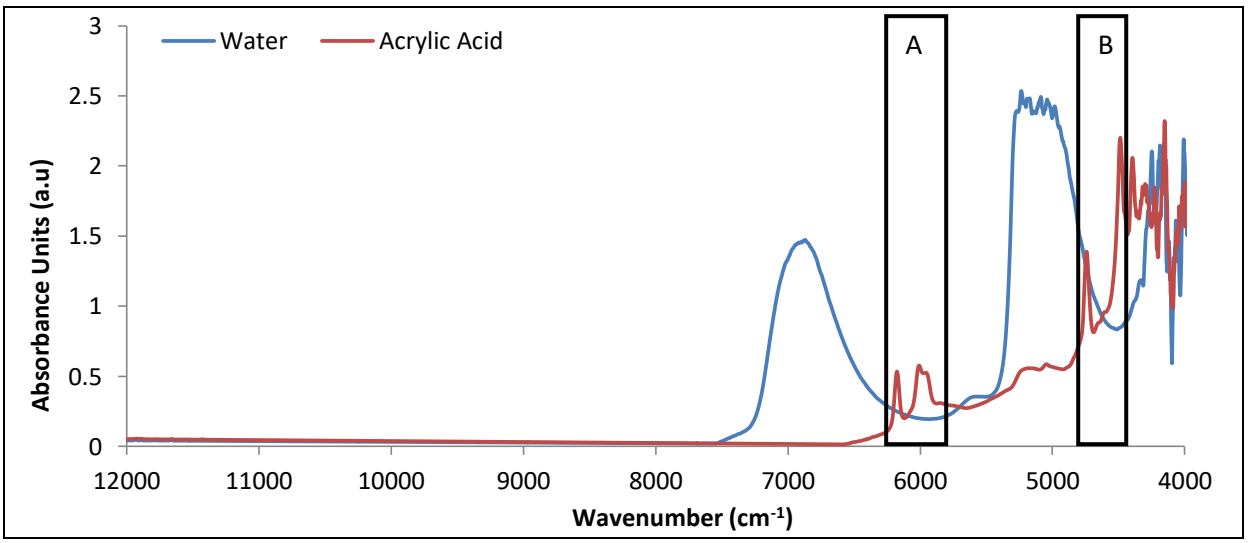

Figure 3.19 shows typical NIR spectra collected during a precipitation polymerisation, in which it is possible to obtain kinetic information about the formation of microgel particles. These spectra can be divided into two distinct regions: one with physical information and another with chemical information. In the physical region, it is possible to observe the qualitative effect of the presence of particles, in which a strong signal appears from 12000 to 7500 cm^{-1} as a deviation of the baseline (AMBROGI, 2015). In the region of chemical information, it is possible to observe that the bands correspond to the water is very intense, which become difficult to visualise the bands of consumption of the vinyl bonds (5855-6250 and 4400-4600 cm^{-1}). For this reason, the criterion used to define the best region that relates the information of the spectra and the parameters analysed was based on the better results of the calibration tests.

Figure 3.19 - NIR spectra of the precipitation polymerisation of acrylic acid and N-isopropylacrylamide. These spectra have physical and chemical information about the formation of polymer particles.

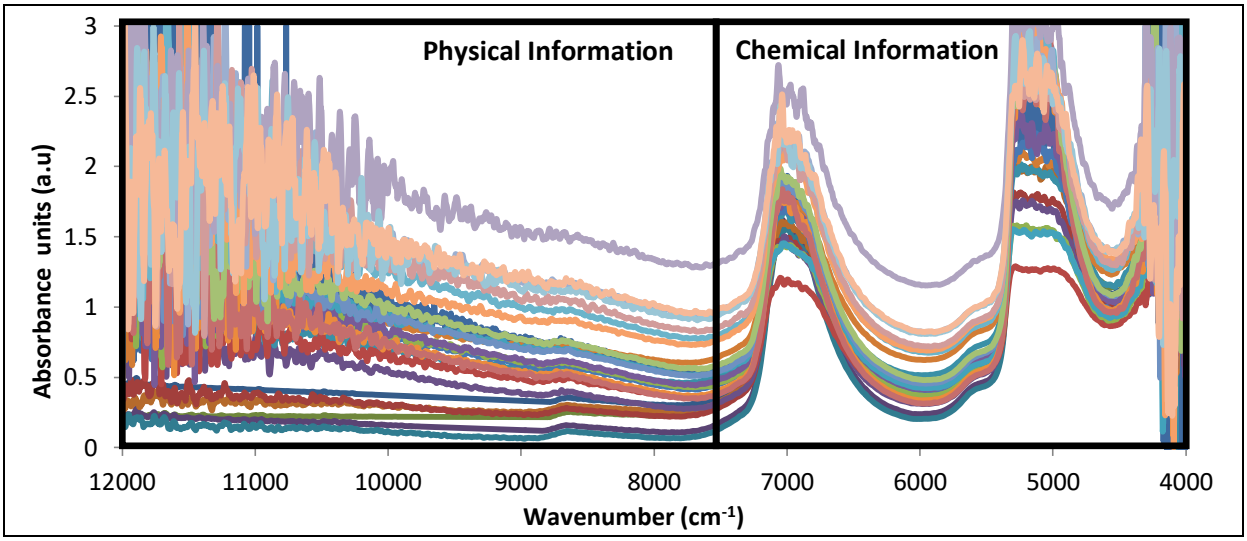

3.3.2.2. Elaboration of the NIR calibration model for monomer conversion

The selection of the set of reactions for the model calibration was made to include those that covered a more extensive conversion range. The data present in Table 3.10 correspond to the experiments used in the calibration model and the internal validation of them.

Table 3.10 – Experimental data for initial and final values of the global conversion of the experiments used in the calibration and internal validation.

Sample (run)	AA (wt%)	NIPAM (wt%)	MBA (wt%)	KPS (wt%)	Y_{m0} (wt%)	Initial Conversion	Final Conversion
Calibration							
S18	0.07	1.34	0.03	0.14	1.44	0.1090	1.0000
S24	0.28	2.20	0.03	0.13	2.51	0.0043	0.7599
S26.1	0.18	1.77	0.06	0.20	2.01	0.0000	1.0000
Validation							
S19	0.07	1.33	0.09	0.27	1.50	0.1587	0.8028
S20	0.07	2.21	0.03	0.26	2.31		
S21	0.07	2.21	0.09	0.13	2.37	0.2973	0.8059
S22	0.28	1.33	0.03	0.27	1.64	0.4772	0.9870
S25	0.28	2.20	0.08	0.26	2.56	0.2148	0.0722
S26.2	0.18	1.77	0.06	0.20	2.01	0.1920	0.9429
S26.3	0.18	1.77	0.06	0.20	2.01	0.6349	0.8429

Y_{mo}: Initial reagents concentration (AA, NIPAM, and MBA) about the entire reaction medium.

The experimental data of conversion collected in runs used for calibration are presented in Figure 3.20 (A), and those of the runs used for validation are present in Figure 3.20 (B).

Figure 3.20 - Experimental data for monomer conversion. Samples used in the calibration model and internal validation (A), and the external validation (B).

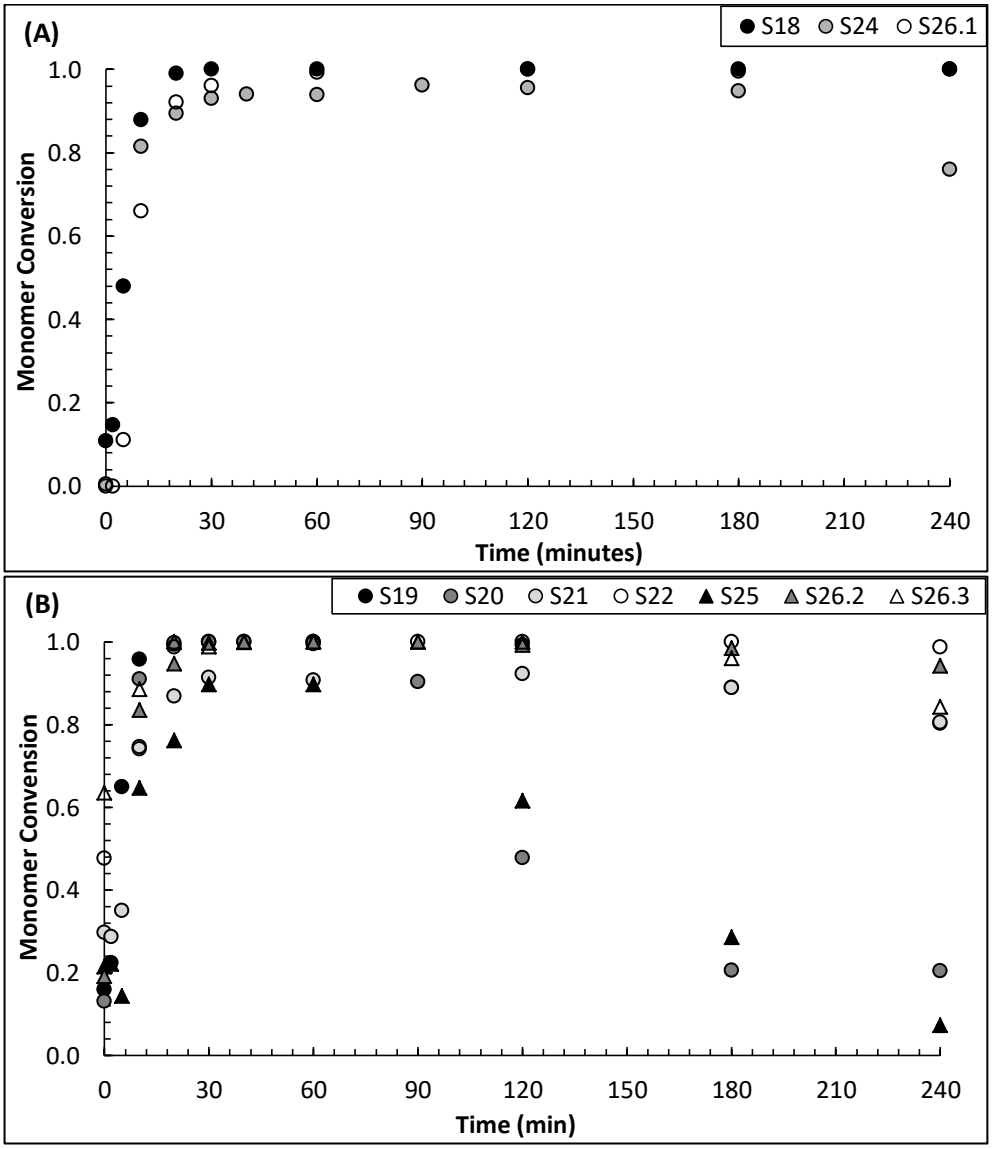

The quality of the calibration model can be improved through the application of pre-processing techniques in the spectral data. This step aims to remove unwanted variations in the data, such as noise, shifts in the baseline, in other disturbances. No general recommendations can be given about which data preprocessing method should be used. The best method is found empirically by trial and error (Bruker Optik GmbH, 2000).

Table 3.11 compares the result of different pre-processing methods applied to different frequency regions. It is important to emphasise that the results show in Table 3.11 and Table 3.12 do not take into account outlier points. In this step of the construction of the calibration model, it is important to detect such outliers because they can have a considerable influence

on the calibration equation and can consequently destroy the prediction ability of the predictor completely (NAES; MARTENS, 1988). However, some care needs to be taken when removing the alleged outliers, because in some cases, an outlier is not necessarily an erroneous observation; it can very well be an interesting case just belonging to another population than the majority of the samples (NAES; MARTENS, 1988). It must, therefore, be realised that if some samples are rejected from the calibration set as outliers, good predictions can then only be expected for future samples belonging to the population of calibration observations used (NAES; MARTENS, 1988). The best thing to avoid this situation is to collect enough observations from all subpopulation to ensure proper calibrations for the total population, but this can be very ambitious in practice (NAES; MARTENS, 1988).

Table 3.11 – Results for cross-validation of monomer conversion calibration models using different pre-processing methods and spectral range.

Validation	Preprocessing Method	Spectral range (cm^{-1})	Rank	RMSECV	R^2
1*	NSDP	12501.7-3998.1	2	0.117	89.22
2**	NSDP	12501.7-3998.1	2	0.111	90.32
3***	NSDP	12501.7-3998.1	2	0.107	91.18
4***	COE	12501.7-3998.1	2	0.110	90.57
5****	NSDP	12501.7-3998.1	2	0.104	91.60
6****	COE	12501.7-3998.1	2	0.108	90.98
7****	IS	12501.7-10000.2 6100.4-5448.5	2	0.130	86.89
8*****	M-M N	12501.7-3998.1	2	0.0975	92.76
9*****	COE	12501.7-3998.1	2	0.106	91.44
10*****	NSDP	12501.7-10000.2 6204.5-5695.4	2	0.100	92.44
11*****	M-M N	12501.7-10000.2 6204.5-5695.4	3	0.0939	93.40

Outliers nomenclature: 18-2.1 (replica 1 of the time 2 belongs to sample 18); *one outlier point; ** without one outlier (26.1-8.2); *** without two outliers (26.1-8.2 and 26.1-8.3); **** without three outliers (18-2.1, 26.1-8.2 and 26.1-8.3); **** without four outliers (18-2.1, 26.1-3.2, 26.1-8.2 and 26.1-8.3); ***** without five outliers (18-2.2, 18-4.2, 26.1-3.1, 26.1-32 and 26.1-3.3); NSDP: No Spectra Data Pre-processing; COE: Constant Offset Elimination; IS: Internal Standard; M-M N: Min-Max Normalization.

According to Table 3.11, validation 11 shows the best results for the chemometric parameters R^2 and RMSECV. It is important to say that calibrations models for range frequencies corresponding to the C=C bond of the monomers (4000-4500 and 5855-6250 cm^{-1}) were done. However, the results did not show good values for the chemometric parameters, probably, because there are not defined peaks corresponding to the monomers and/or polymers due to the strong absorbance bands of the water and the low concentration of monomer/polymer in the medium. As the PLS method is a full spectrum

method, the choice of the models corresponding the relation between experimental and NIR spectra data was based on the better results of rank, R^2 and RMSECV.

Table 3.12 shows the cross-validation results for different pre-processing method applied in the frequency range 12501.7-10000.2 and 6204.5-5695.4 cm^{-1}. These validations were run without the following outliers: 18-2.2, 18-4.2, 26.1-3.1, 26.1-3.2 and 26.1-3.3.

Table 3.12 – Comparison of different methods of data pre-processing. Frequency range: 12501.7-10000.2 and 6204.5-5695.4 cm^{-1}

Validation	Pre-processing Method	Rank	RMSECV	R^2
11	M-M N	3	0.0939	93.40
11.1	NSDP	2	0.100	92.44
11.2*	COE	2	0.111	90.76
11.3**	VN	2	0.0853	94.55
11.4*	IS	2	0.127	87.87

Outliers nomenclature: 18-2.1 (replica 1 of the time 2 belongs to sample 18); * Four outliers (18-2.1, 24-1.3, 26.1-8.2 and 26.1-8.3); ** One outlier (18-0.1); NSDP: No Spectra Data Pre-processing; COE: Constant Offset Elimination; VN: Vector Normalisation; M-M N: Min-Max Normalisation; IS: Internal Standard.

According to Table 3.12, validation 11.3 shows chemometric results a little better than validation 11; however, this validation has one more outlier. The more experimental points are excluded from the model, more robust the model is, and it may not be able to identify variations that could be significant. In this way, validation 11 still has better conditions for the calibration model.

Based on the pre-processing results presented Table 3.11 and Table 3.12, the calibration for the conversion of monomers in polymer was based on the spectral range from 12501.7 to 10000.2 cm^{-1} and from 6204.5 to 5695.4 cm^{-1}. The Min-Max Normalisation pre-processing method was chosen as the best spectral pre-processing method for monomer conversion calibration model. This choice was based on an appropriate combination of the lower RMSECV (0.0939) and the highest R^2 (93.40).

Figure 3.21 shows the cross-validation parity plot for monomer conversion. The graph compares the reference (experimental) and predicted monomer conversion of the samples S18, S24 and S26.1.

Figure 3.21 - Parity Plot for monomer conversion. Empty circle: Experimental values; Straight line: NIR prediction.

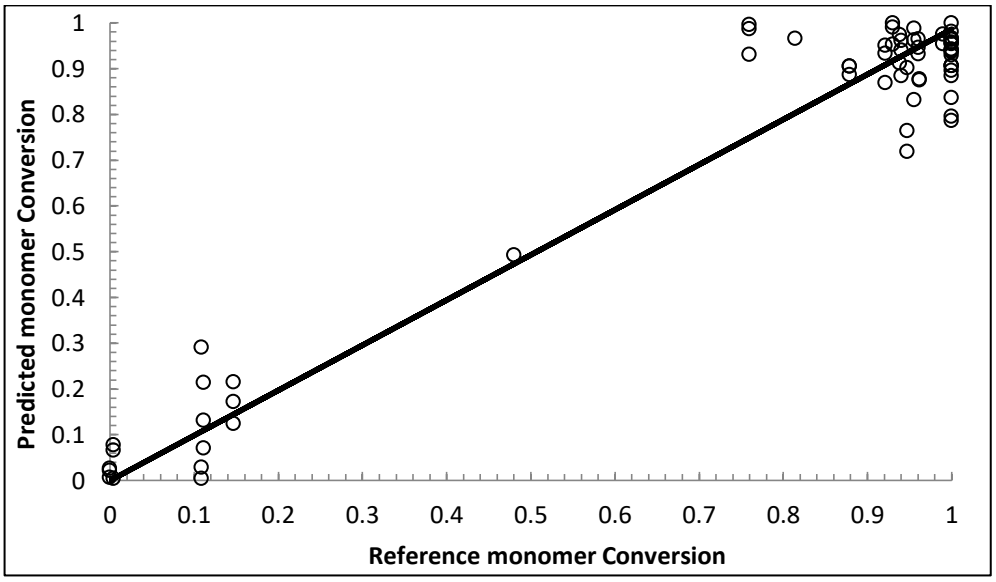

According to Figure 3.22 for the construction of the cross-validation parity plot shown in Figure 3.21, it was necessary 3 PLS vectors to predict the conversion of monomers in polymer from the NIR data. This value represents the optimum number of factors to maintain the quality of the chemometric model, and this is also known as “Rank” of the model.

Figure 3.22 – Rank for monomer conversion calibration model. The relationship between (A) determination coefficient and (B) root mean square error of cross-validation with rank.

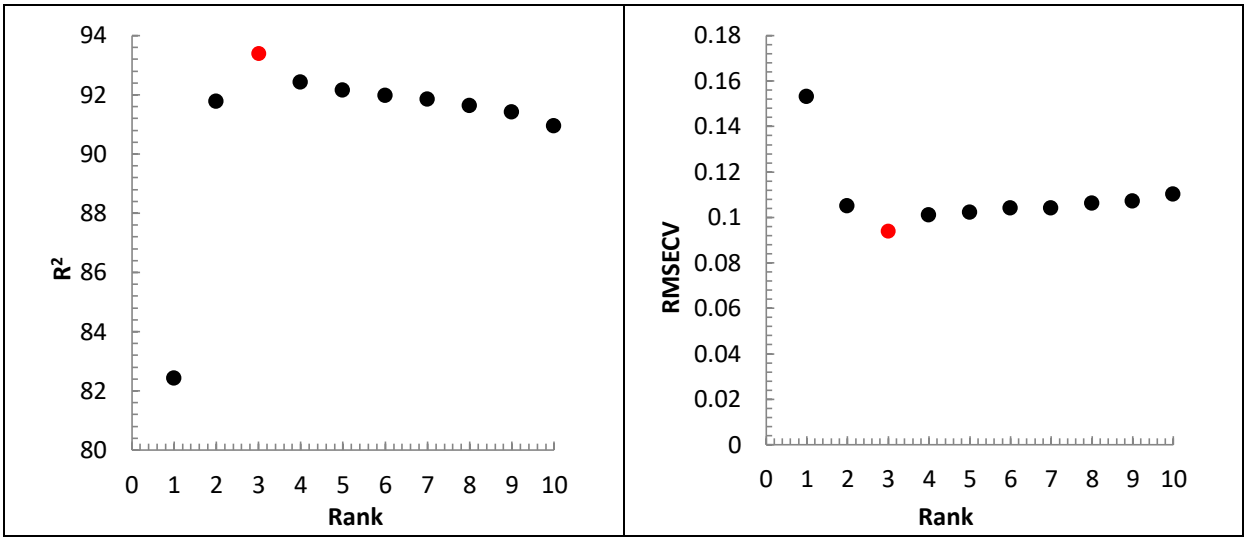

Figure 3.23 shows the comparison between the experimental data (offline measurements) by gravimetric and the prediction from the calibration model constructed with the spectra of NIR online measurement, for these internal validations were used the samples of the calibration model.

Figure 3.23 - Internal Validation. Full circle: Experimental data; Empty circle: NIR Prediction.

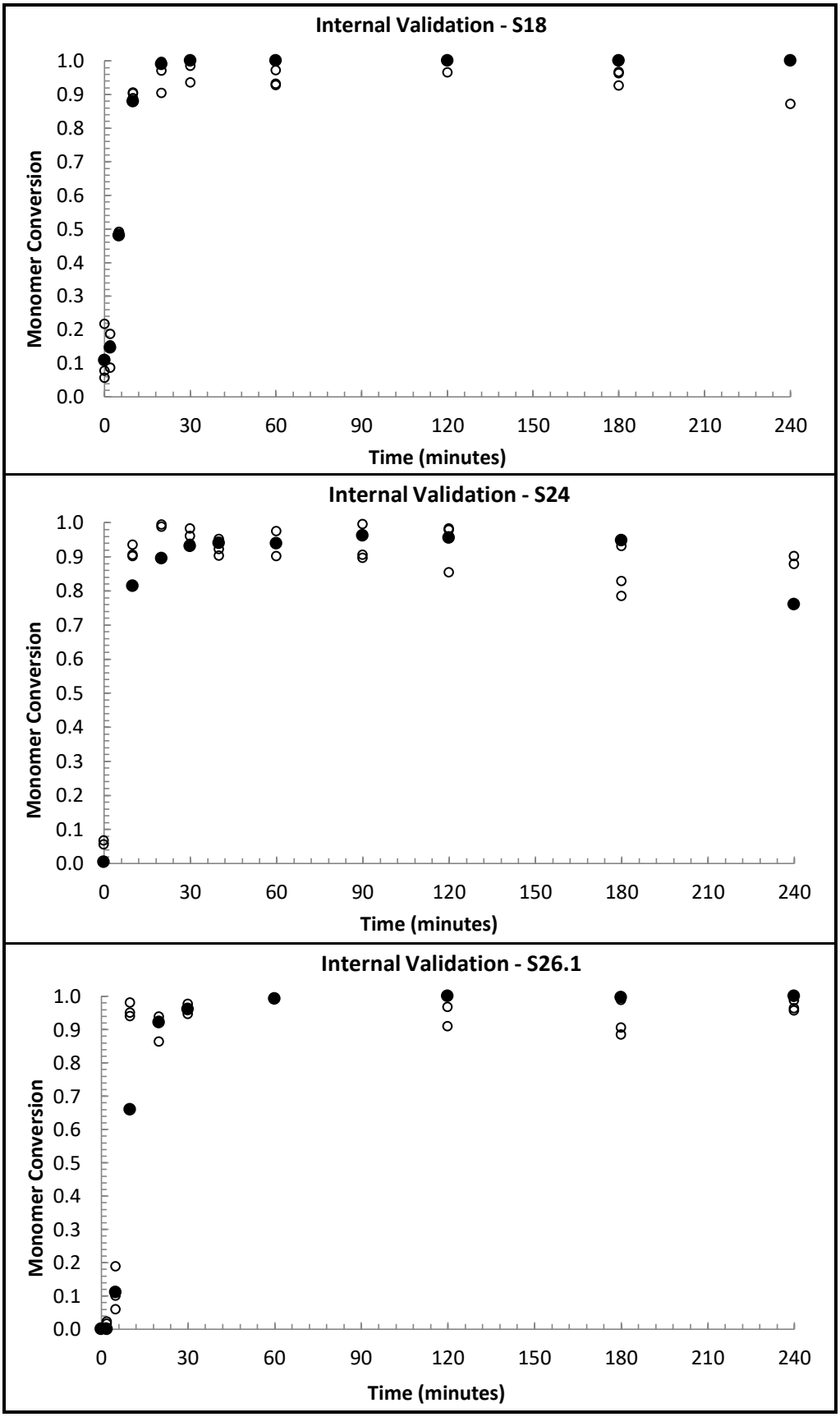

Figure 3.24 and Figure 3.25 compare the NIR prediction model with the experimental data from the set not used in the calibration step. The intention of these validations was evaluated the model performance.

Figure 3.24 - External validation. Full circle: Experimental data; Empty circle: NIR Prediction

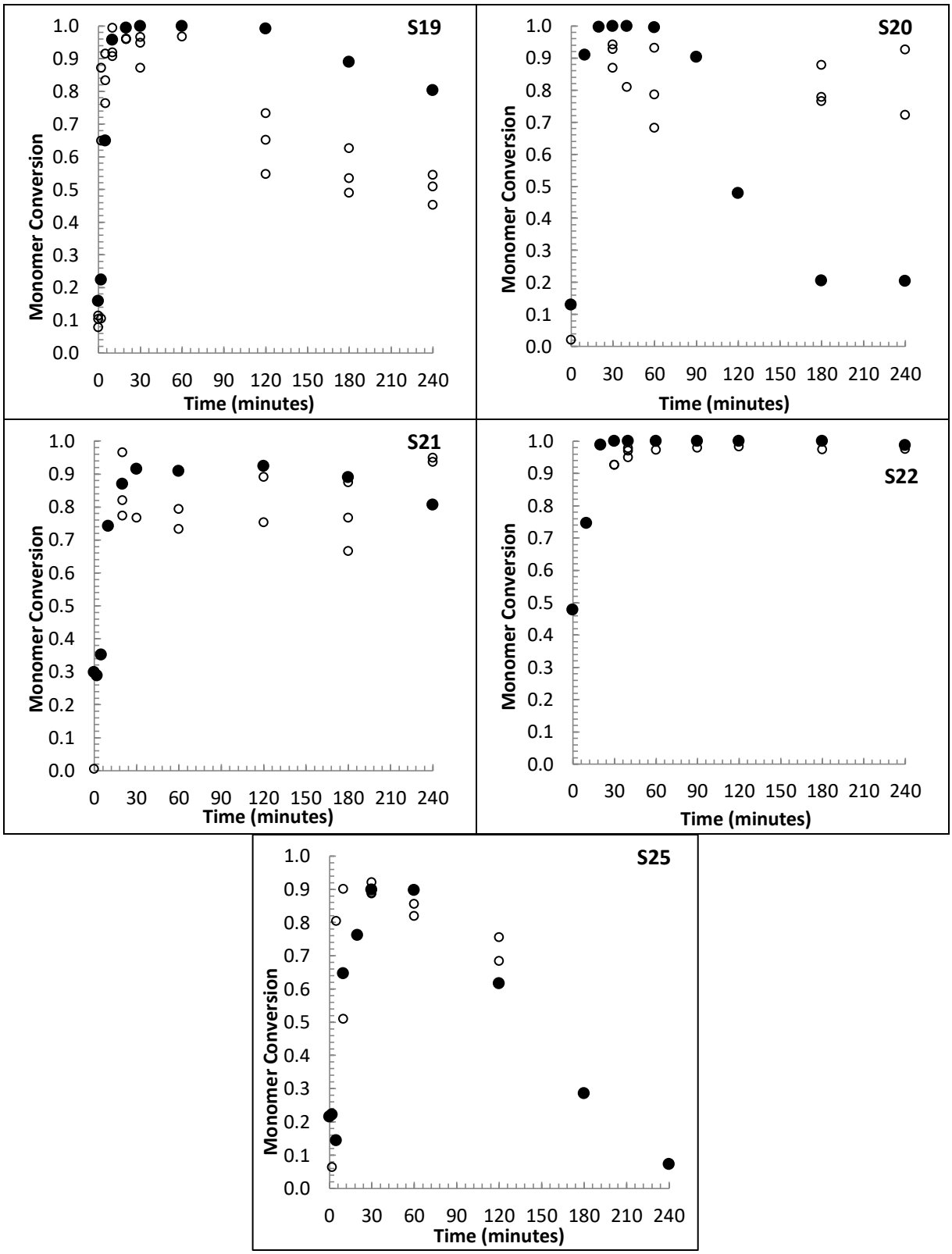

Figure 3.25 – Continuation of results of external validation. Full circle: Experimental data; Empty circle: NIR Prediction

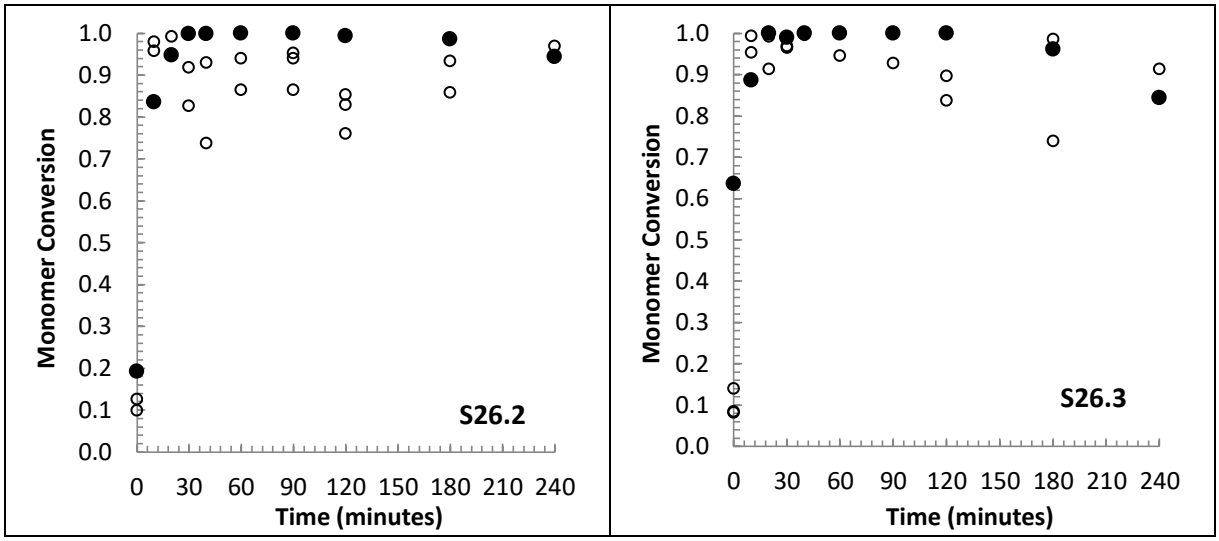

According to the results of external validation show in Figure 3.24 and Figure 3.25, it can be noted that the predicted data follow the profile of experimental values. However, in some samples, there is a significant difference between the values of offline analysis and the predicted data. This weak correlation can be attributed to the higher sensitivity of the experimental data due to the low concentration of monomer and particles in the reaction medium, and the high speed of reaction.

Another observation that can be done about the results is that the calibration model for monomer conversion is sensitive to the heterogeneity of the reaction medium. In the case of samples S19, S20 and S25, it is possible to observe a decrease in the value of monomer conversion in the last two hours of reaction. Theoretically, the conversion of a batch polymerisation cannot decrease. Therefore, a plausible explanation for this behaviour can be supported in the fact that the model is more sensitive to the concentration of the microgel particle in the reaction medium than the global conversion.

This decrease in the concentration of the microgel was caused by the formation of two phases in the reaction system, one with aggregated particles in the bottom and sides of the reactor, and another with the aqueous medium with some microgel particles in suspension. Based on the results, the probe has measured the particles in the aqueous medium. In the case of S20 and S25, some points of NIR prediction are missing due to the formation of a thin

microgel film around the probe. Consequently, the spectra had to be omitted, since they presented noise, not representing the exact kinetic behaviour of these reactions.

About the influence of the reagent concentration, there is a limit of the total mass of monomers associated with the initiator concentration that the reaction system remains stable. However, when the system tends to the instability, and consequently, there is a formation of aggregated particles inside the reactor, the monomer conversion model showed capable of identifying this phenomenon, and the reaction can be stopped.

3.3.2.3. Elaboration of the NIR calibration model for average particle size

For the construction of the NIR calibration model for average particle size, it was adopted the same criteria for the development of the calibration model for monomer conversion, that is, the points of the experimental design corresponding to the minimum, central and maximum. We also tried to cover a wide range of particle size, capable of representing different sizes throughout the polymerisation, although, some size results for validation show higher size diameter than for calibration, these values probably represents a deviation of the profile, and in some cases the effects of particle aggregation.

Table 3.13 shows the initial and final average particle size of the samples used in the calibration and validation model.

Table 3.13 - Experimental results for initial and final values of average particle size for the samples used in the calibration and validation of the model.

Sample (run)	AA (wt%)	Nipam (wt%)	MBA (wt%)	KPS (wt%)	Y_{mo} (wt%)	Initial Dh (nm)	Final Dh (nm)
Calibration							
S24	0.28	2.20	0.03	0.13	2.52	314.7	278
S18	0.07	1.34	0.03	0.14	1.44	122.8	301.3
S26.1	0.18	1.33	0.06	0.20	1.57	180.9	302.5
Validation							
S26.3	0.18	1.77	0.06	0.20	2.00	314.2	265.2
S26.2	0.18	1.77	0.06	0.20	2.00	282.1	339.1
S19	0.07	1.33	0.09	0.27	1.49	235.1	192.8
S21	0.07	2.21	0.09	0.13	2.37	224.1	394.9
S25	0.28	2.20	0.08	0.26	2.56	219.9	524.5

The reference average particle sizes were measured offline using the dynamic light scattering technique. As expected at the beginning of the polymerisation (for the two first samples, the time equal to 0 and 2 min, respectively), there are no particles in the medium,

in this way, it was not possible to measure the particle size by DLS. For this reason, the calibration was constructed without these samples. This is in agreement with the NIR spectra that do not show baseline offset, confirming the absence of light scattering.

Figure 3.26 shows the evolution of the diameter during the reaction time in the samples used in the calibration and validation model.

Figure 3.26 - Experimental data for average particle size. Samples used in (A) the calibration model and internal validation, and (B) external validation.

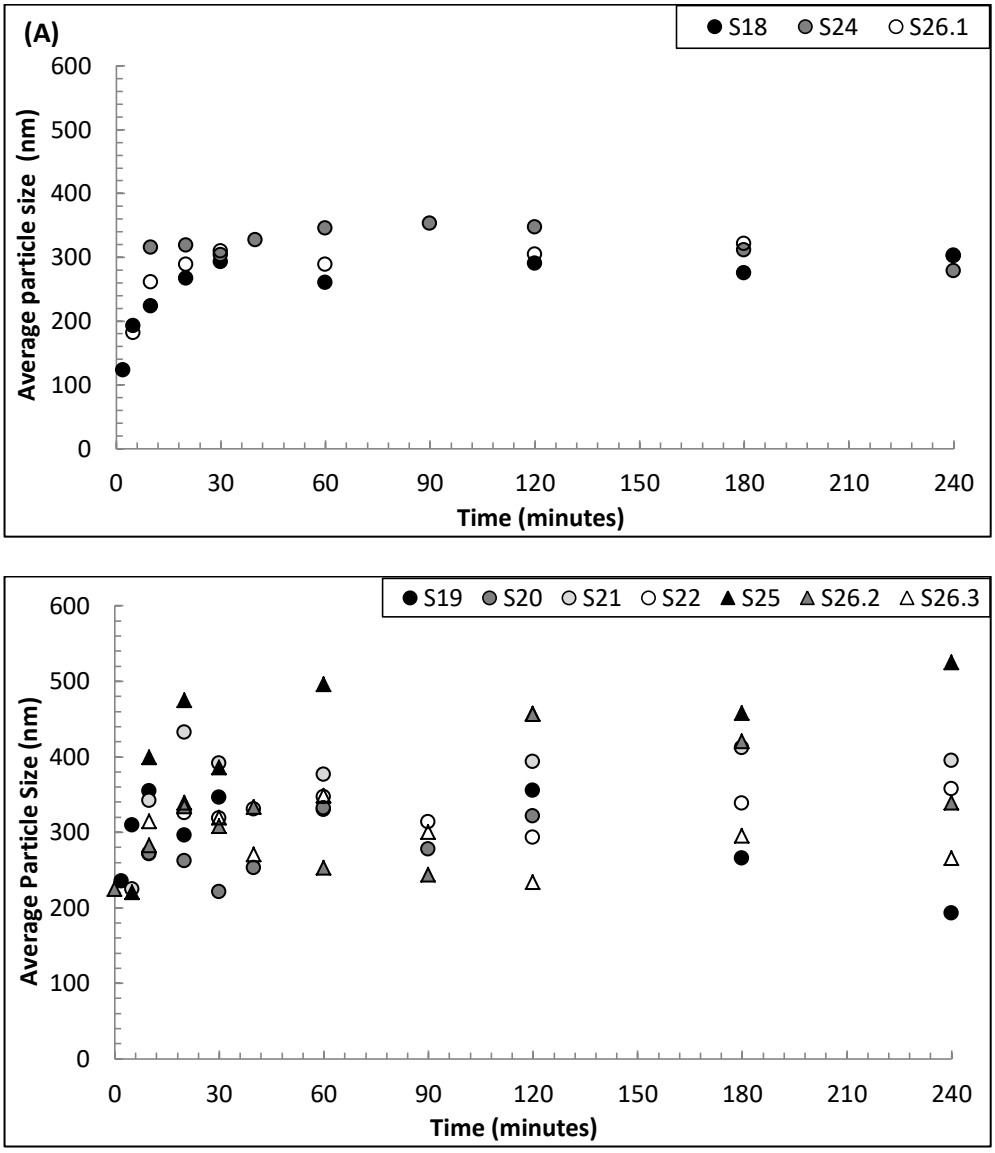

A calibration model based on the spectral range from 12501.7 to 4599.9 cm^{-1} was constructed to evaluate the viability of the NIR to monitor the average particle size during the precipitation polymerisation. The interval between 12501.7 and 7498.7 cm^{-1} corresponds to the region of significant deviations in the spectra baseline; these deviations can be

attributed to the manifestation of the physical phenomenon of light scattering, where the absorption is predominant.

For the choice of the calibration model, different spectral pre-processing and spectral range were evaluated. The better results for the chemometric parameters were in the frequency range from 12501.7 to 4599.9 cm^{-1}. Table 3.14 presents the tests validation with different pre-processing treatment for this spectral band.

Table 3.14 - Comparison of different pre-processing data in the spectral range from 12501.7 to 4599.9 cm^{-1}. These calibration models were constructed without the points 18-1.1, 18-1.2, 18-1.3 and 24-9.3.

Validation	Method	Rank	RMSECV	R^2
1	NSDP	2	20.7	74.89
2	COE	2	22.3	70.84
3	VN	1	20.9	74.51
4	M-M N	2	20.8	74.66
5	MSC	1	18.4	80.24
6*	IS		22.2	71.27

*with one point of the outlier (26-9.3). NSDP: No Spectra Data Pre-Processing; COE: Constant Offset Elimination; VN: Vector Normalisation; M-M N: Min-Max Normalization; MSC: Multiplicative Scatter Correction; IS: Internal Standard.

According to Table 3.14, the best calibration model for average particle size was the validation 5, based on MSC preprocessing method, which gave a reasonable combination of low Rank (1), high R^2 (80.24), and low RMSECV (18.4). Figure 3.27 shows the cross-validation parity plot for validation chosen.

Figure 3.27 - Cross-validation parity plot for average particle size. Empty circle: Experimental values; Straight line: NIR Prediction.

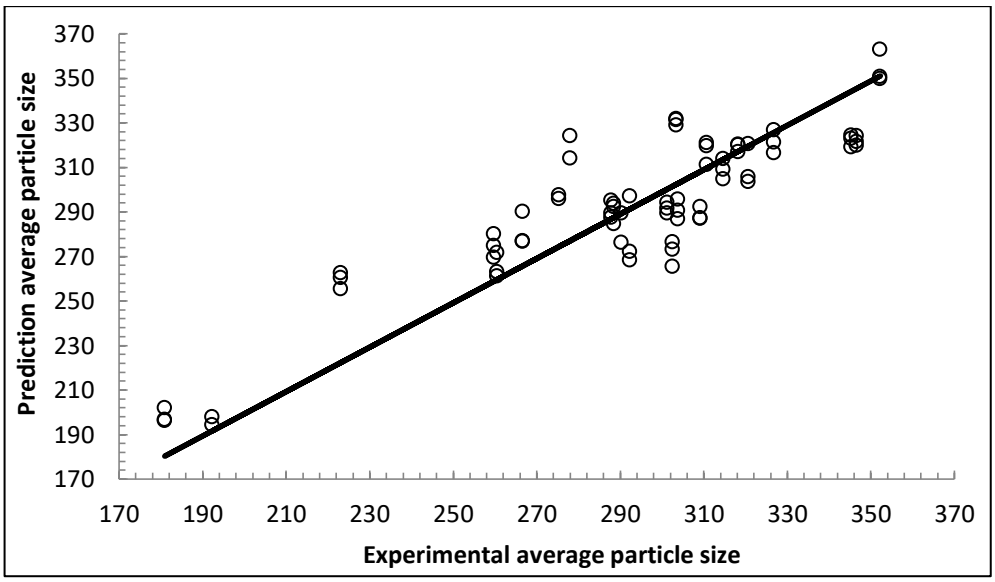

For the construction of this calibration model, the number of factors necessary to maintain the quality of the chemometric model was 1 (Figure 3.28). With the rank equal to 1, the model has maximum R^2 and minimum RMSECV.

Figure 3.28 - Rank for average particle size calibration model. The relationship between (A) determination coefficient and (B) root mean square error of cross-validation with rank.

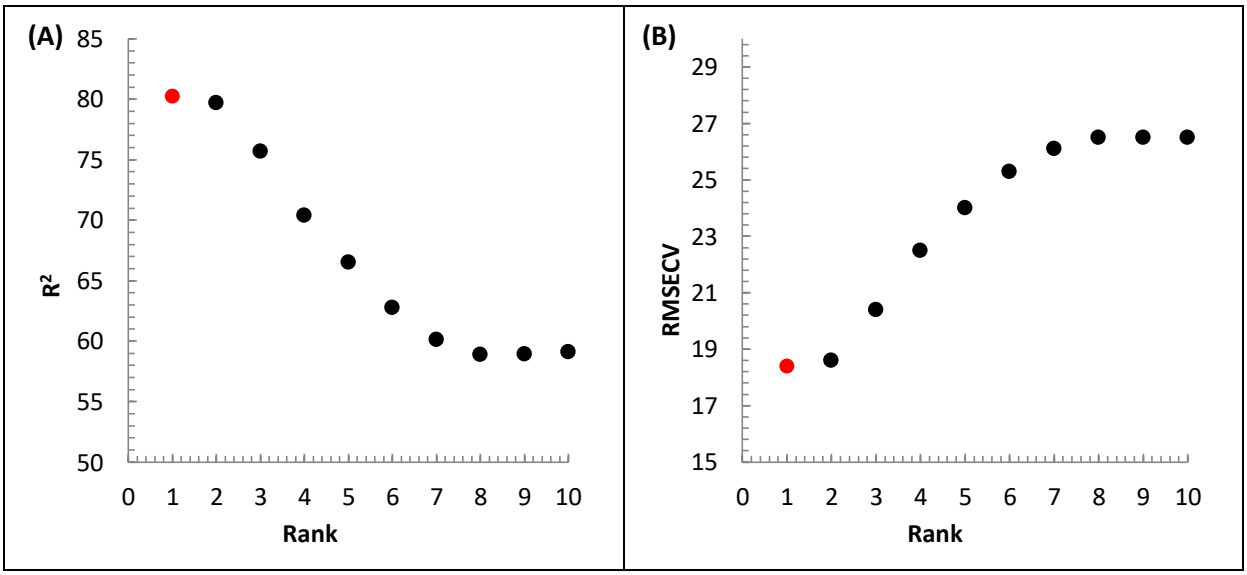

Figure 3.29 shows the internal validation (validation with the samples used in the construction of the calibration model). The results show that NIR spectra data follow very well the experimental data (by DLS), as expected.

Figure 3.29 – Internal validation for average particle size. Full circle: experimental data, empty circle: NIR prediction.

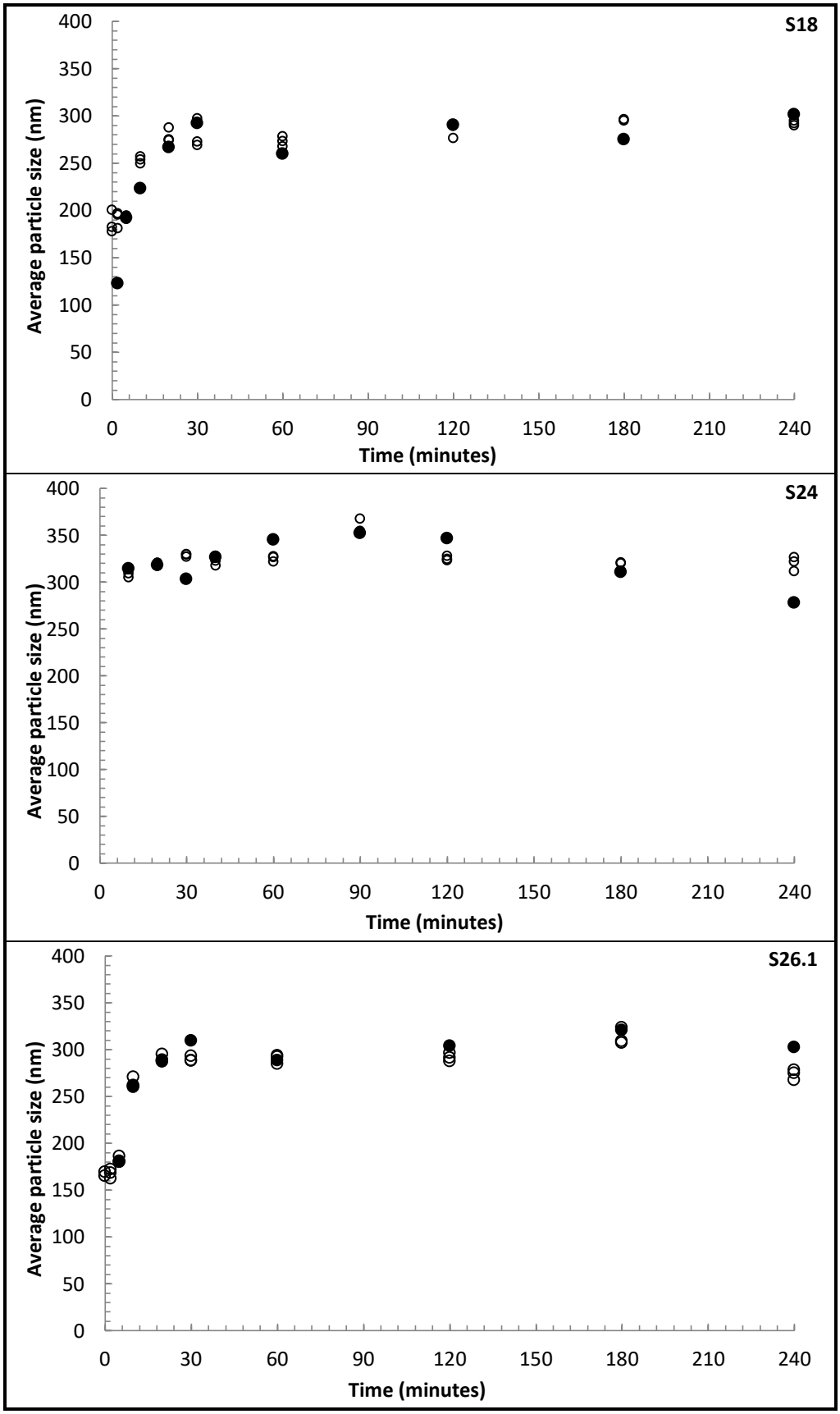

Figure 3.30 and Figure 3.31 compare the NIR prediction model with the experimental data from the samples not used in the calibration step. The intention of these validations has evaluated the similarity of the data predicted by the NIR model and the experimental data.

Figure 3.30 - External validation. Full circle: Experimental data; Empty circle: NIR Prediction.

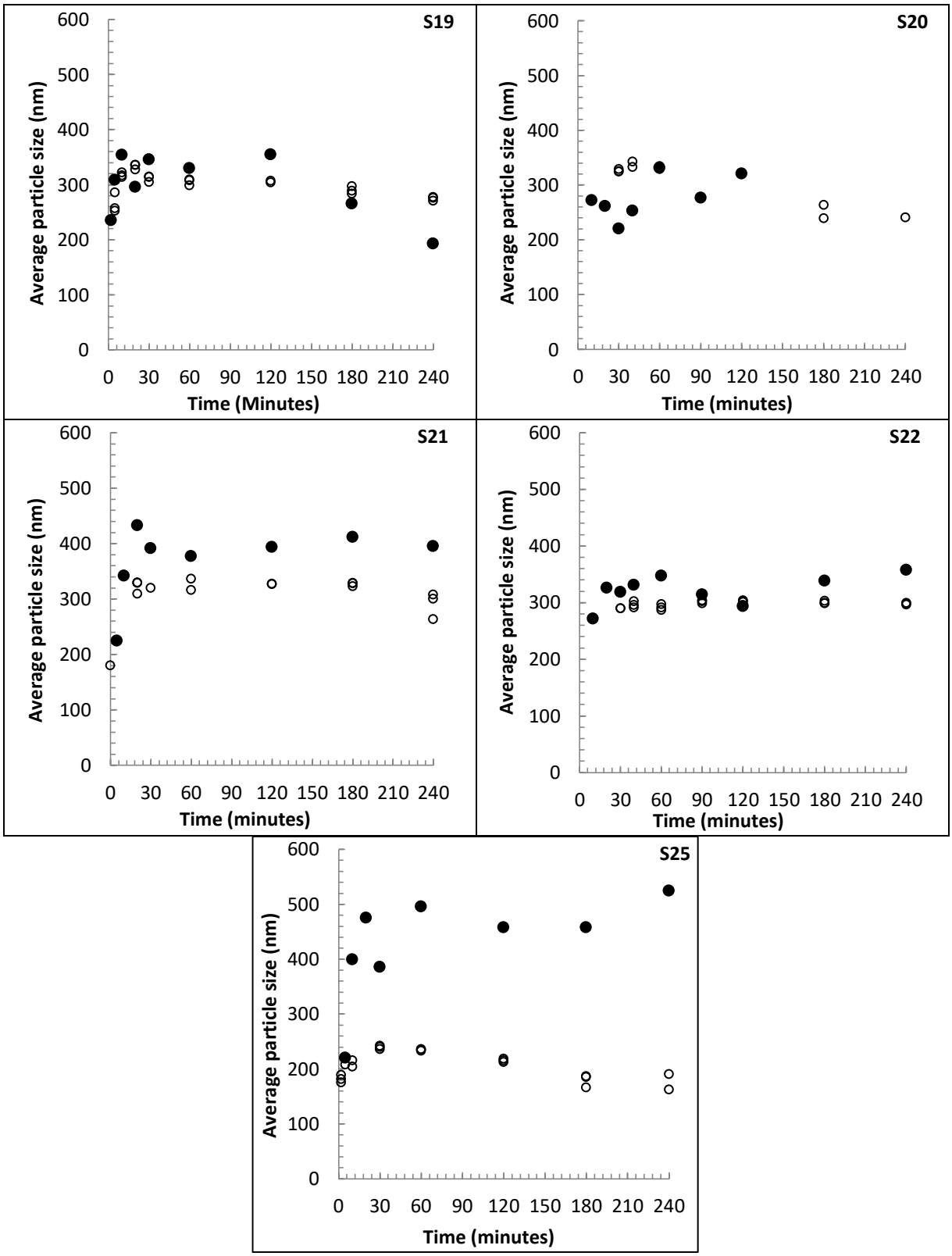

Figure 3.31 - Continuation of external validation results. Full circle: Experimental data; Empty circle: Nir Prediction

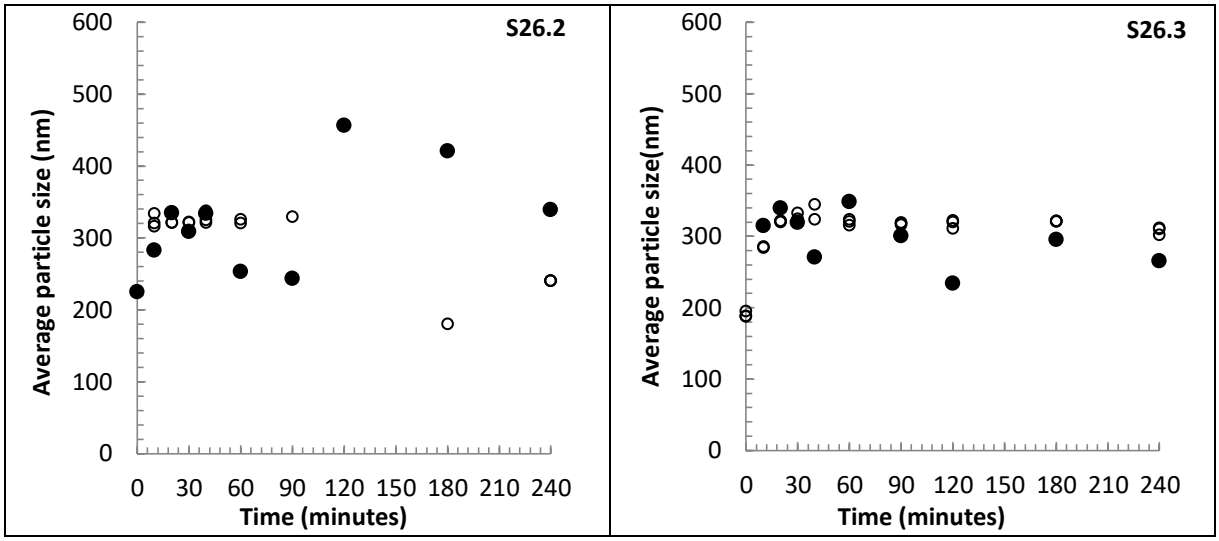

Figure 3.30 and Figure 3.31 shows the results of external validation, which compare the average particle size estimated from the NIR spectra using the calibration model with the reference values of average particle size measured off-line by DLS.

According to the results, in general, the NIR predicted following reasonably the qualitative trend of the experimental data. However, there are some differences between experimental values and the data predicted by the NIR model; in some cases (as in run S21 and S25); the DLS values are higher than NIR data.

As the results of average particles size monitoring by UV-VIS-NIR spectrophotometer (sub-section 3.3.1), this difference observed in the runs S21 and S25 can be explained by the higher initial concentration of monomers (equal to 2.37 and 2.57 wt%, respectively), which consequently may occur in a more considerable amount of polymer particles in the reaction medium. This higher concentration of microgels in the medium may result in greater instability of the system, causing particle aggregation. In this way, it means that the NIR spectra and calibration model probably represent the real size of the particles inside the reactor during the reaction, while the off-line DLS data show the results of this aggregation. This difference between the off-line measurements and the NIR predictions can indicate another advantage of using an in-line probe during the polymerisation, which measures are not affected by the problems involved in the sampling (that, under certain conditions may

not be representative of the reaction medium inside the reactor) and/or sample preparation (as delays in analyses and sample dilution), that may favour changes in the sample.

3.3.3. Comparison of the monitoring methods

In general, the developed models for at-line and in-line monitoring of process variables monomer conversion and average particle size of the microgel particles production by precipitation polymerisation using UV-Vis-NIR and NIR (Full region) spectrophotometer, respectively, have similarities.

However, some differences can be observed in the predicted data for runs S19, S21 and S25 (Figure 3.32). This difference is more evident for the monitoring results of global conversion, in which it is possible to observe that the NIR model following the experimental data better than models developed from the UV-Vis-NIR. This means that the models developed by UV-Vis-NIR are less sensitive to the concentration of the particles in the sample, which decreased due to the formation of two different phases in the reactor (the aggregate particles and the dispersed particle in the aqueous part). This heterogeneity caused by the formation of aggregate particles in the reactor becomes difficult the proper collection of samples during the reaction time. For this reason, these samples cannot represent the real global conversion of the polymer, but the concentration of microgel particles in the analysed sample.

Taking into account that the conversion of a batch polymerisation cannot decrease, it is interesting to observe this difference in the trend of the models, because it was expected that the experimental data had a closer profile with UV-VIS-NIR spectra than with the NIR spectra, because the NIR spectra are obtained inside the reactor, while the UV-VIS-NIR spectra belong to samples collected at certain times of the reaction, which were the same samples used to obtain the experimental data.

Although the NIR spectra for microgel formulations with specific concentration of reagents do not represent the real conversion of the microgel polymer in the last hours of the polymerisation, this indeed can be a good warning about the reaction system, because this sensibility about the heterogeneity of the reaction medium can be that the aggregates are being formed inside the reactor and actions need to be taken.

In the case of monitoring results for average particle size, the models show good agreement between them and with the experimental data. However, as discussed previously, experiments S21 and S25 show values for experimental data higher than the predicted by the models. The hypothesis raised to explain these differences was that the off-line measurements by DLS probably represent the values of particle size aggregation and not the real size of the microgel particles inside the reactor during the polymerisation. This is due to the time elapsed, and medium changed during the sample preparation. This hypothesis can be strengthened when observing quantitative differences in the evolution of particle sizes during the experiment S25. The results obtained in-line by NIR probably represents the real size of the microgels during the reaction, but when samples were collected from the reactor and analysed at-line by UV-VIS-NIR spectrophotometer (no more than 2 min later) there is an increase in the values of average particle size, this increase in the size values is even higher when the samples are analysed off-line by DLS (hours later).

Figure 3.32 – Comparison of the models obtained for the at-line and in-line monitoring of monomer conversion and average particle size.

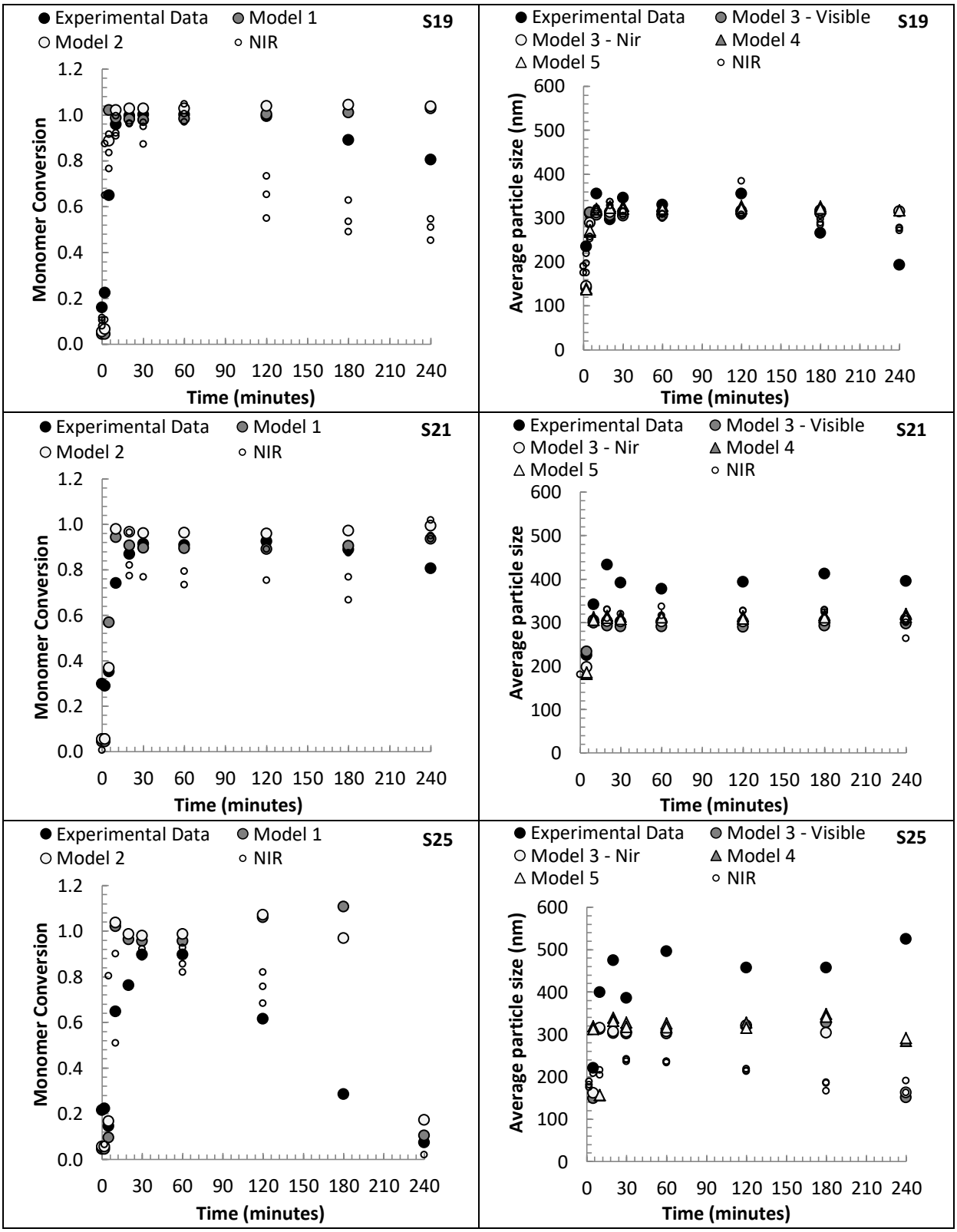

3.4. Partial Conclusions

The objective of this chapter was to evaluate the ability of spectroscopic techniques, in the region of Ultraviolet (200-400 nm), Visible (400-800) and Near-infrared (800-2500 nm), to monitor the process variables monomer conversion and average particle size of microgel particles formed during the precipitation polymerisation.

Monitoring the formation of microgel particles is very important to control the quality of the product and to improve the final characteristics of the particles according to the desired application. However, although the control of microgel features to be necessary, there are few studies focused on understanding the mechanism involved in microgel formation using spectroscopic techniques to monitoring the polymerisation kinetics, mainly about average particle size.

UV-VIS-NIR high-resolution spectrophotometer was used for at-line monitoring, and five calibrations models were constructed (two models for monomer conversion and three for average particle size). For the construction of the models, a simple linear relationship was applied to relate the information contains in the spectra (the area corresponds to a specific wavelength range), and the parameters monitored. The calibrations models for monomer conversion was constructed based on Visible (R^2=0.9196) and NIR (R^2=0.9219) regions, and two models for average particle size were obtained in NIR region with a determination coefficient above 0.84. A third model was constructed based on the observed linear relationship between monomer conversion and average particle size with a determination coefficient of 0.665, and this model was used to predict the size of the microgels from the visible region.

According to the results of external validation, the models are similar; that is, any part of the spectrum (visible and Near-infrared) can be used for predicting the analysed parameters. Although the predictive capability of the models shows agreement with the experimental data, when occurs formation of microgel aggregates, they are not capable of identifying this difference and continues to show the conversion profile without losing the correlation.

The PLS regression method was used for the construction of the calibration models of the in-line monitoring using Near-infrared spectrophotometer. The calibration model for monomer conversion was based on the spectral range 12501.7-10000.2 and 6204.5-5695.4 cm^{-1}, and a

min-max normalisation pre-processing was applied. The cross-validation gives the rank equal to 3, R^2 equal to 0.934, and RMSECV equal to 0.0939. Already for the calibration model for average particle size, the spectral range was from 12501.7 to 4599.9 cm^{-1}, with an MSC preprocessing. The rank was 1, the R^2 was 0.8024, and the RMSECV was 18.4 nm. In both cases, a broad spectrum band was used; this was possible due to the "Full spectrum" nature of the PLS method. In addition to the presence of water which makes it challenging to construct the model for monomer conversion in the regions related to the chemical bonds present in the monomers and polymers, the model for average particle size was also not limited to the region belonging to "Physical Information", the better calibrations tested took practically the entire spectral range. This tendency can mean that the global monomers conversion is directly related to the particle size, proving the importance of knowing how the changes in formulations (differences in the concentration of the reagents that have different ratios reactivity and consequently different monomers conversion) can affect the physical properties of the microgel (as the structure and particle size).

The results for external validation show that the predictions from the NIR spectra and the calibration models follow the trends of the experimental results. It is important to highlight the sensitivity of the global conversion model to identify the increase in the heterogeneity of the reaction medium that occurs when microgel aggregates are formed into the reactor. This behaviour raises the question that the model is more sensitive to the concentration of the microgel particle into the reaction medium than the monomer conversion. If the model only recognises the concentration of the particles, this means that the models constructed are sensitive just for physical changes in the spectra, as expected.

Comparing the models obtained from UV-Vis-NIR and NIR (Full spectrum) spectrophotometer, they show similarities. However, in some cases, they show different results predicted about experimental data. For monomer conversion, the main difference between them was found in the first minutes of the polymerisation. This discrepancy can be explained by two hypotheses; (i) due to inaccuracy of the experimental data causing by the possible existence of the unreacted monomers in the dried polymer samples and/or low concentration of polymers, and (ii) due to the instability of the reaction medium at the beginning of the polymerisation, the homogeneous medium becomes heterogeneous due to particles formation by homogeneous nucleation.

In the case of average particle size monitoring, the difference between the predicted and experimental data can be seen in runs S21 and S25. In these two cases, although the evolution of particle sizes are qualitatively the same, the experimental data is higher than the predicted by the models. In run S25, this difference stands out even more, even among the predicted models, the longer it took for the samples to be analysed, the greater the average particle size obtained for the microgels. The results obtained in-line by NIR represents the real size of the microgels during the reaction, when samples were collected from the reactor and analysed at-line by UV-VIS-NIR spectrophotometer (no more than 2 min later). There is an increase in the values of average particle size, this increase in the size values is even higher when the samples are analysed off-line by DLS (hours later), that is, as time passes, what is observed is not the real value of size, but rather its aggregation.

The main difference between UV-Vis-NIR (at-line) and NIR (in-line) monitoring was about their predictive ability for monomer conversion, in which it is possible to observe that the NIR model followed the experimental data better than models developed from the UV-Vis-NIR in the case of microgel aggregates in the reactor. This sensibility of in-line monitoring to the heterogeneity of the reaction medium can be a good warning about the reaction system, allowing that actions can be taken.

About the influence of the reagent concentration in the monitoring of the monomer conversion and average particle size, there is a limit of the total percent mass of monomers associated with the initiator that it is possible to follow the kinetics of the process without losing the correlation. This loss of correlation is due to the instability of the reaction system that forming aggregated particles inside the reactor.

In conclusion, the spectroscopic techniques used in this work showed good applicability and proved to be important tools for monitoring the kinetic parameters of microgel particles during the precipitation polymerisation, mainly for monitoring the evolution of average particle size, and to identify the formation of microgel aggregates in the system. Another advantageous point of this monitoring was that the combination of these different spectroscopic techniques allows a better comprehensive overview of the microgel formation.

4. Characterisation of microgel particles based on Acrylic acid, N-isopropylacrylamide and Chitosan for use in biological application

Abstract

This chapter focus on the characterisation of pH- and temperature-sensitive microgel particles with potential application as an oral drug delivery system. Microgels with different composition were synthesised by free-radical precipitation polymerisation, and the influence of the reagents (AA, NIPAM, MBA, KPS and Cs) in their physicochemical properties and swelling behaviour were investigated. Dynamic light scattering was used to characterise the microgel size and size distribution, and the responsive behaviour under various conditions of pH and temperature. Electrophoretic light scattering was used to determinate the zeta potential of the samples at 25 °C and 37 °C, and the influence of pH at 37 °C. The particle morphology and qualitative composition of microgels were analysed by scanning electron microscopy, and Fourier transform infrared spectroscopy, respectively. The stability of the microgel particles during the storage time (180 days) was monitored through the measurement of size, size distribution, zeta potential and pH of the samples. The polymer particles [Poly(AA), poly(NIPAM), poly(NIPAM-co-AA) and poly(NIPAM-co-AA)-Cs] synthesised in this work have sizes from 275.6 to 7288 nm, the minimum and maximum values represent the microgels of only poly(NIPAM) (minimum amount: 133 mmol.L^{-1}) and polymers with chitosan in their formulation (maximum amount: 0.24 g), respectively. The PDI values ranged from 0.014 to 0.476, except for samples with a higher amount of AA (S1 and S2) and Cs (S27, S28, S29 and S30) in their composition that present these values above 0.5. The samples show negative charges for zeta potential, and the pH varies from 2.0 to 3.0. However, for sample S30 that has a higher amount of chitosan (cationic biopolymer), the zeta potential presents positive charges and the pH value equal to 4.58. The poly(NIPAM-co-AA) show spherical morphology for samples with a proper proportion between the monomers. The FTIR spectra proved the presence of the monomers in the microgels structure, and the study of the swelling behaviour in different mediums verified the sensibility of the microgel particles to temperature and pH. The monitoring of the stability of the particles showed that the selected microgels did not have variations in their physicochemical characteristics during the storage time. In conclusion, with an adequate understanding of the influence of the reagents in the physicochemical properties of the

microgels, it is possible to tailor the multi-sensitive microgels for the desired application. In the case of this work, samples S15, S17-S19, S21, S22 and S24 showed characteristics more suitable for being used as an oral drug delivery system.

4.1. Introduction

The characterisation of the polymer particles produced by the precipitation polymerisation plays an essential role in this work since it allows evaluating the influence of parameters related to the polymer synthesis, such as the concentration of reagents, on the final characteristics of the material. In this way, it is possible to optimise the process to obtain particles with characteristics suitable for the desired application.

However, due to their colloidal nature, technical difficulties can be found in the physicochemical characterisation of the particles. Given these difficulties, it is important to use several characterisation techniques to understand the behaviour and features of these particles.

In this chapter, the influence of the formulation on the physical and chemical characteristics of the microgel particles was investigated. These polymeric particles were analysed in terms of their size, size distribution, zeta potential, pH, morphology, qualitative composition, behaviour in medium with different pHs and temperatures, and stability during the storage.

The techniques used in the characterisation include dynamic light scattering (DLS), electrophoretic light scattering (ELS), scanning electron microscopy (SEM), and Fourier transforms infrared spectroscopy (FTIR). The following subtopics explain the theory behind these analytical methods.

4.1.1. Dynamic Light Scattering (DLS)

Dynamic light scattering (DLS) (also known as photon correlation spectroscopy (PCS) and quasi-elastic light scattering (QELS)) is a non-invasive and well-established technique used to measure the size of particles and macromolecules in the submicron scale.

DLS measures the diffusion of the suspended particles that move through the solvent molecules under Brownian motion and converts this to the hydrodynamic diameter (D_H) using the Stokes-Einstein relationship (4.1).

$$D_H = \frac{K_B T}{3\pi\eta D} \tag{4.1}$$

where K_B is the Boltzmann's constant, T is the absolute temperature, η is the viscosity of the dispersing medium, and D is the translational diffusion coefficient of the particles.

The diameter obtained by DLS is defined as "the size of a hypothetical hard sphere that has same translational diffusion coefficient as that of the particle being measured, assuming a hydration layer surrounding the particle or molecule (Figure 4.1), and it is called the hydrodynamic diameter (D_H) (MALVERN INSTRUMENTS LIMITED, 2014). It is important to note that DLS gives an intensity-weighted particle size distribution, where the contribution of each particle in the distribution relates to the intensity of light scattered by the particle, which means that the presence of oversized particles can dominate the particle size result (MALVERN INSTRUMENTS LIMITED, 2014).

Figure 4.1 - Definition of hydrodynamic diameter.

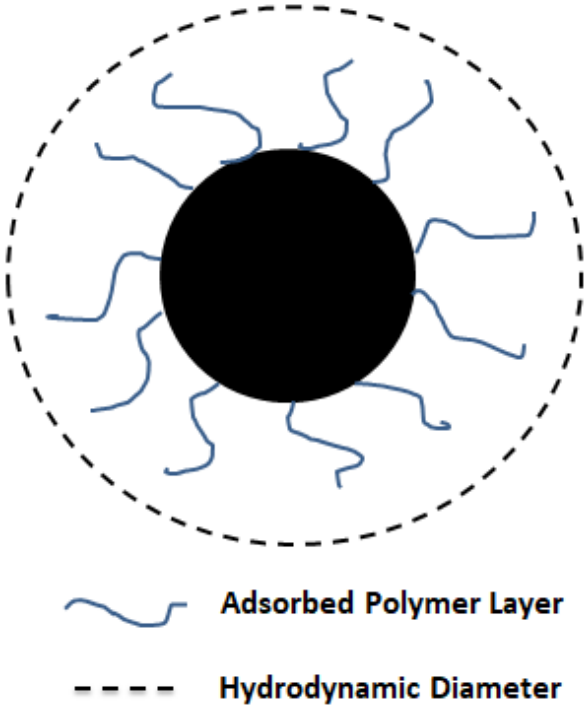

Source: Author

A conventional dynamic light scattering instrument uses a monochromatic He-Ne laser with a wavelength of 633 nm as the light source, which converges to a focus in the sample using lens. Light is scattered by the particles at all angles. However, the DLS instrument has a

single detector at a fixed angle, traditionally placed at 90° to the laser beam. The intensity fluctuations of the scattered light are converted into electrical pulses, which are fed into a digital correlator. This generates the autocorrelation function, G(t), from which it is related to the translational diffusion coefficient of the particles, and particle size is calculated (MALVERN INSTRUMENTS LIMITED, 2014). Figure 4.2 shows a schematic of the DLS principle to obtain the hydrodynamic diameter of suspended particles.

Figure 4.2 - Principle of measurement of particle size by dynamic light scattering (DLS) technique for small and large particles. (A) Intensity fluctuations of the scattered light; (B) Correlation function, G1; (C) Size distribution.

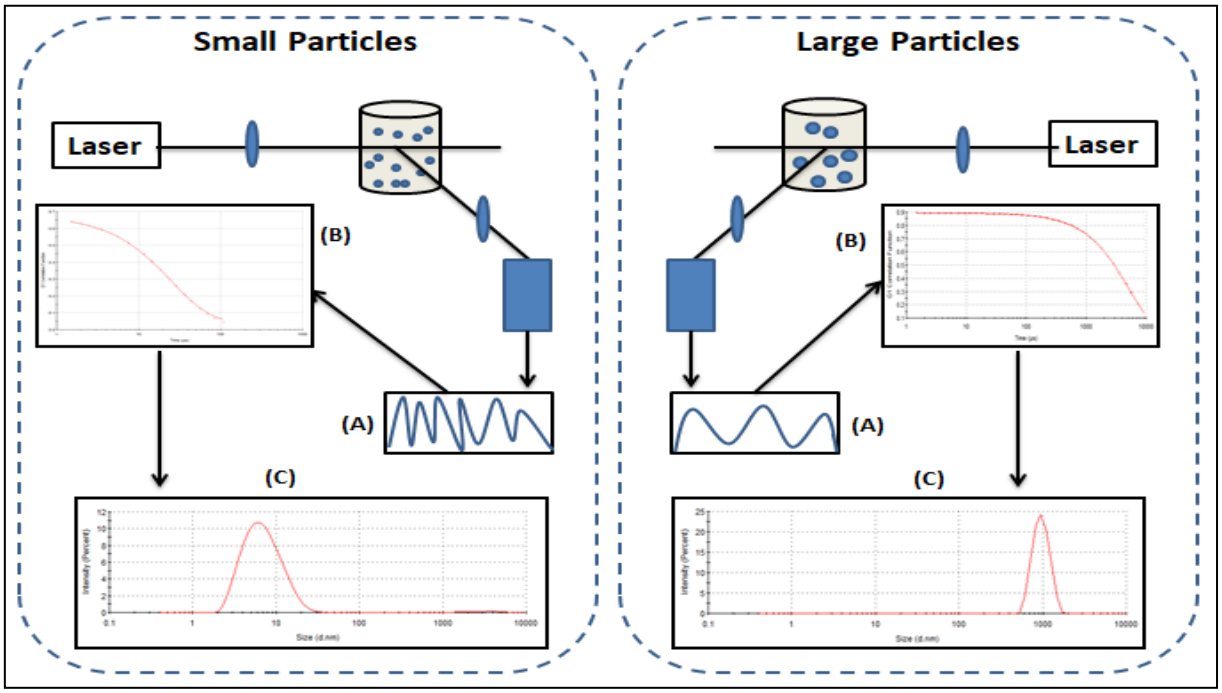

Source: Author

The particles diffuse in the medium with diffusion constants that depend on the size of the particles. The smaller the particle, it is “kicked” further by the solvent molecules and move more rapidly and passes for the detector more often within a time interval. The light intensity scattered from particles will fluctuate in time as a result of particle diffusion (A). From the temporal intensity autocorrelation function, G(t), of the scattered light (B), the particle diffusivity can be evaluated, which, in turn, can be related to particle “average” diameter and diameter distribution (C) (ALSAYED; HAN; YODH, 2011).

Mathematically this autocorrelation of scattered light is presented as follows (4.2) (COLMÁN, 2013):

$$G(t) = \langle I(t_0) + I(t_0 + t) \rangle \tag{4.2}$$

Where $I(t_0)$ and $I(t_0 + t)$ are the scattered light intensities at instants (t_0) and $(t_0 + t)$. At time $t = t_0 = 0$, the scattering intensity is $I(0)$ and the autocorrelation function has a maximum value. Over time, the scattering intensity at a time $(t_0 + t)$ will have less and less correlation with the initial scattering intensity, and the average on the products of the intensities, which is $G(t)$, tends to zero. It is usually assumed that $G(t)$ decays exponentially as a function of time, as shown in item B of Figure 4.2.

For spherical and monodisperse particles, $G(t)$ is given by Equation 4.3:

$$G(t) = A' e^{-2\Gamma t} + B' \tag{4.3}$$

where A' is the baseline constant and B' is the intercept constant, both of the autocorrelation function, Γ is the decay constant of the exponential curve generated by the autocorrelation function, defined by Equation 4.4:

$$\Gamma = D \cdot q^2 \tag{4.4}$$

where D is the translational diffusion constant of the particles, q is the light scattering wave vector, which is given by Equation 4.5:

$$q = \left(\frac{4\pi n}{\lambda_0}\right) \cdot \sin\left(\frac{\theta}{2}\right) \tag{4.5}$$

where n is the refractive index of the dispersant, θ is the scattering angle and λ_0 is the wavelength of the incident light.

For the calculation of the Equations 4.1-4.5, the software of the equipment finds the curve that best fits the points originated by the autocorrelation function, that is, it finds an appropriate value for Γ. Then, it is replaced in Equation 4.4 in which it results in a value for D. Finally, by means of the Equation 4.1, the hydrodynamic average diameter (D_H) of the particles is obtained.

The first order result from DLS is typically the mean value of the intensity distribution (called the Z-average size) and the polydispersity index (PDI) to describe the distribution width. It is possible to convert the results of intensity into a volume or number distribution to compare to other techniques, such as laser diffraction or microscopy (HORIBA SCIENTIFIC, 2012). The Z-average size will only be comparable with the size measured by other techniques if the sample has a monomodal distribution (i.e., only one peak), monodisperse distribution (i.e., very narrow width of distribution), spherical or near-spherical particles, and the sample is prepared in a suitable dispersant (MALVERN INSTRUMENTS, 2011a). It should be noted that converting an intensity result from DLS to a volume or number basis can lead to undefined errors.

The polydispersity index (PDI) is a dimensionless number of the width of the particle size distribution, ranging from 0 to 1, which indicates the extent to which the particles in dispersion are a uniform size (MALVERN INSTRUMENTS, 2011a). This index is calculated from a simple two-parameter fit to the correlation data (the cumulant analysis). It can be interpreted as follows:

- 0.00 - 0.05: standards or monodisperse particles;
- 0.05 – 0.08: nearly monodisperse samples;
- 0.08 – 0.70: mid-range polydispersity;
- higher than 0.7 indicate that the sample has a broad size distribution and is probably not suitable for the DLS technique.

The various algorithms to calculate the size distribution operate better in the interval corresponding to the mid-range (0.08 and 0.70). The calculations for these parameters are defined in the ISO standard document 22412:2017 (MALVERN INSTRUMENTS, 2011a).

4.1.2. Electrophoretic Light Scattering (ELS)

Zeta Potential (ZP) is a physical property exhibited by any particles in suspension (MALVERN INSTRUMENTS, 2011b), that reflects their surface potential, which is influenced by the changes in the interface with the dispersion medium and the stationary layer of fluid attached to the dispersed particles, due to the dissociation of functional groups on the surface of the particles or the adsorption of ionic species present in the aqueous medium (HONARY; ZAHIR, 2013a). That is, the zeta potential is a measure of the magnitude of the electrostatic or charges repulsion or attraction between particles in a liquid suspension (MALVERN INSTRUMENTS LIMITED, 2014). Figure 4.3 shows the schematic representation of the zeta potential.

Figure 4.3 - Schematic representation of the zeta potential for the negatively charged particle. (A) Stern Layer; (B) Diffuse Layer; (C) Electrical Double Layer; (D) Surface Potential; (E) Stern Potential; (F) Zeta Potential.

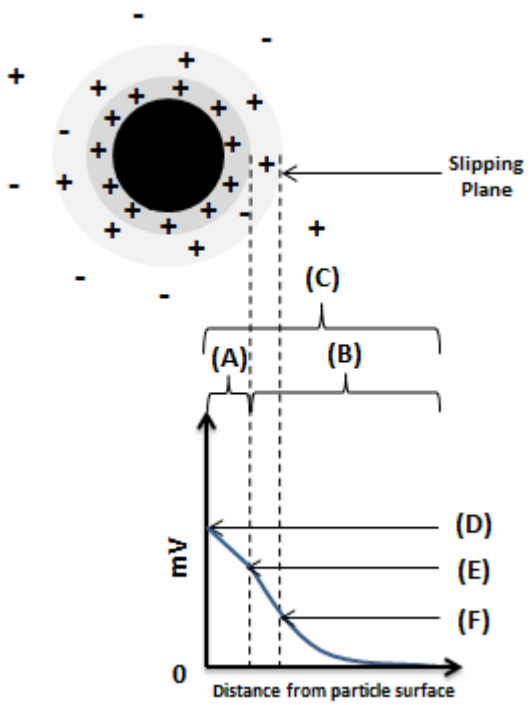

Source: adapted from Malvern Instrument (2011b)

Figure 4.3 shows that a layer (denominated as an electrical double layer) exists around each particle. The electrical double layer is composed of two parts; an inner region (Stern layer) where the ions are strongly bound and an outer region (diffuse layer) where the ions are less firmly associated (MALVERN INSTRUMENTS, 2011b).

The interaction of the particles is given by the magnitude of the zeta potential and not by their surface charge. In this way, this magnitude brings detailed insight into the causes of dispersion, aggregation or flocculation, and can be applied to improve the formulation of dispersions, emulsions and suspensions and hence to minimise the time and cost of testing as well as improving shelf life (MALVERN INSTRUMENTS LIMITED, 2014). Zeta potential of low magnitude, most especially relatively close to 0, indicates that particles are likely to attract and consequently aggregate. Zeta potential of high magnitude, ideally greater than ± 30 mV, is associated with greater stability, since large repulsive forces tend to avoid aggregation due to occasional collisions of adjacent particles, and consequently, instability is reduced.

Several factors can influence the zeta potential of a particle, such as pH of the medium, ionic strength (concentration and type of ions present in the medium) and the concentration of charged molecules that may exist in the dispersant medium. In this way, knowing the influence of these factors on the ZP provides useful information for the formulation of a more stable product. For this reason, zeta potential has long been recognised as a useful index for the stability of the colloidal system.

Zeta potential is not measurable directly but can be calculated using theoretical models (HONARY; ZAHIR, 2013a). There are two different experimental techniques used to quantify ZP: microelectrophoresis which has the advantage of yielding an image of the moving particles, and electrophoretic light scattering (ELS) technique (or Laser Doppler Microelectrophoresis), which is based on dynamic light scattering (HONARY; ZAHIR, 2013b). Figure 4.4 shows a zeta potential measurement system by electrophoresis.

Electrophoresis technique consists in the application of an electric field across an electrolyte into a cell containing two electrodes (A). Firstly, a laser is used to provide a light source to illuminate the particles suspension sample; this light is divided into two beams: an incident and a reference beam. The incident laser beam goes through the centre of the cell sample, and the scattered light is detected. The equipment measures the phase change (B) in light scattered by particles moving under the influence of the electric field applied to the cell, any charged particles or molecules suspended in the electrolyte will attract towards the electrode of opposite charge. The velocity which these particles move is known as the electrophoretic mobility (C); the change phase is proportional to the electrophoretic mobility

of the particles, and this mobility (U_E) can be related to zeta potential (ζ) (D) by the Henry Equation (4.6).

$$U_E = \frac{\varepsilon\zeta}{\eta}\frac{2}{3}f(ka) \tag{4.6}$$

where ε is the dielectric constant of the medium, η is the viscosity of the medium, $f(ka)$ is the Henry function (k is the reciprocal of the Debye length, and a is the radius of the particle). In the case of aqueous solutions with moderate electrolyte concentration, where ka >>1, the Smoluchowski approximation $f(ka)$=1.5 is used. For small particles in a low dielectric constant medium (i.e. non-aqueous medium), the Huckel approximation $f(ka)$=1.0 is used.

Figure 4.4 - Electrophoresis Fundamental Physical Principle. (A) Capillary Cell with electrodes; (B) Phase Plot; (C) Electrophoretic Mobility Distribution; (D) Zeta Potential Distribution.

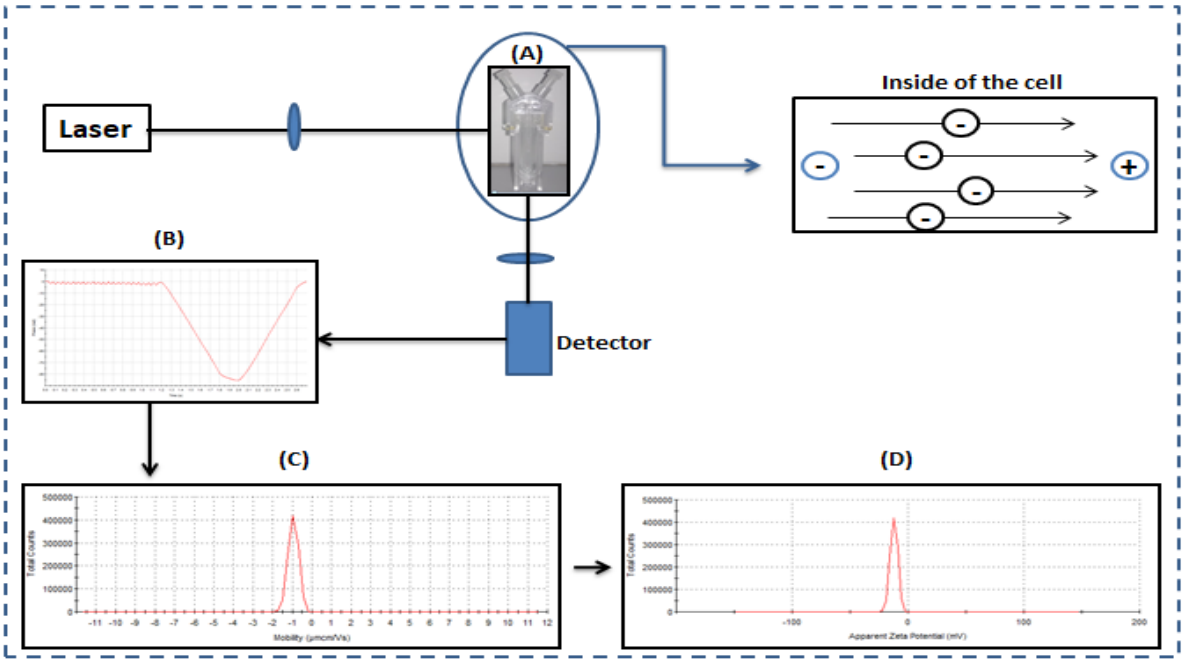

Source: Author

4.1.3. Scanning Electron Microscopy (SEM)

Scanning electron microscopy (SEM) can be used to determine information about the particle morphology, particle size and dispersity. It is a technique commonly used to observe

the surface of particles (greater than 2 nm in size) that are under high vacuum (THORNE, 2012).

The principle of scanning electron microscopy (Figure 4.5) consists of generating a beam of 2 to 3 nm of electrons through an electron gun, which is focused on and scanned across the particle surface on a point-by-point basis, interacting with its atoms, and producing different signals. When the electron beam ejects, loosely bound conduction electrons (less than 50 eV) from the surface of the particle, secondary electrons, are produced from the valence electrons of sample atoms at the surface and therefore provide accurate and good resolution topographic information. Therefore, they are used to form the surface image of the samples. Elastically scattered electrons may also be generated (creating a back-scattered signal). The back-scattered electrons possess greater energy (above 50 eV) than the secondary electrons, and therefore provide information from a relatively larger sample depth, providing information related to the topography as to the composition of the material analysed. Together, these two sources create signals picked up by a secondary electron detector, which is amplified and converted into an image on the display screen. The image formed in the SEM gives the impression of three dimensions (AZEVEDO, 2012; THORNE, 2012).

Figure 4.5 – Principle of scanning electron microscopy

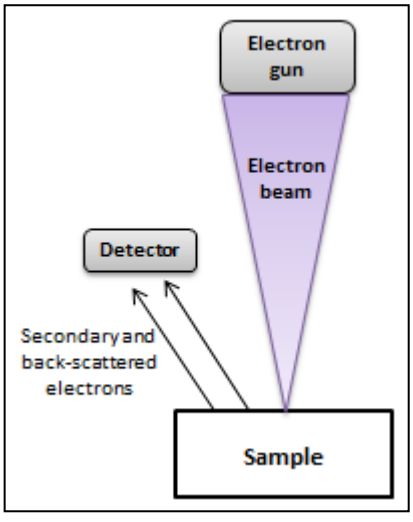

Source: Author

4.1.4. Fourier Transform Infrared Spectroscopy (FTIR)

Infrared (IR) spectroscopy is one of the most important and widely used analytical techniques available for qualitative and quantitative composition determination of diverse kind of materials (STUART, 2004).

The IR spectroscopy is based on the vibrations of the atoms of a molecule. At ordinary temperatures, molecules are in a constant state of vibrations, each bond having its characteristic stretching and bending frequencies. When infrared electromagnetic radiation between 4000-400 cm^{-1} are passed through a sample, some of these radiations are absorbed by the sample and are converted into energy of molecular vibrations. The other radiations which do not interact with the sample are transmitted through the sample without being absorbed (KUMAR, 2006). The energy of each peak in an absorption spectrum corresponds to the frequency of the vibration of a molecule part, thus allowing qualitative identification of certain bond types in the sample (STUART, 2004; KUMIRSKA et al., 2010).

The total spectrum is analysed by an interference process and converted into the frequency or wavenumber range using a mathematical process known as Fourier transform (KUMIRSKA et al., 2010). Fourier-transform infrared (FTIR) spectroscopy is based on the idea of the interference of radiation between two beams to yield an interferogram. The radiation emerging from the source is passed through an interferometer to the sample before reaching a detector. Upon amplification of the signal, in which high-frequency contributions have been eliminated by a filter, the data are converted to digital form by analog-to-digital converter and transferred to the computer for Fourier-transformation (STUART, 2004). FTIR spectroscopy has dramatically improved the quality of infrared spectra and minimised the time required to obtain data (KUMIRSKA et al., 2010).

As spectroscopic techniques were extensively studied in Chapter 3, comparing FTIR and NIR (both belong to the collection of analytical techniques known as “vibrational spectroscopy”), the IR spectral region that presents peaks corresponding to fundamental vibrations of primary chemical bonds have narrower and better-defined peaks than the bands in the NIR region (where the bands correspond to overtones and combinations of the fundamental vibrations).

4.2. Materials and Methods

4.2.1. Materials

Three titrant solutions were prepared for the study of the size and zeta potential of the particles at different pHs: aqueous solutions of sodium hydroxide (0.025 M and 0.25 M) and hydrochloric acid (0.25 M). An aqueous solution of sodium chloride (0.1M) was also used to provide charge to the particles during the analysis of the zeta potential.

The reagents were purchased from Sigma Aldrich and Vetec.

4.2.2. Experimental Sets

To understand the influence of the polymerisation reagents on the final characteristics of the microgel particles, several sets of polymerisation were performed. It is important to emphasise that some sets represent preliminary tests with the purpose of knowing the system and verify the reproducibility, as well as to compare the results with the literature (ZHANG et al., 2009). Other set of experiments were planned according to an experimental design (Full and Fractional Factorial Experiment) based on the preliminary results and other literature (SNOWDEN et al., 1996; KRATZ; HELLWEG; EIMER, 2000; FAROOQI et al., 2013; MARQUES et al., 2013; VENEGAS-SANCHEZ et al., 2013) (Table 4.1).

Table 4.1 shows all the assays used in this work. Runs S1-S5 (Set 1) have a total concentration of monomers (AA and NIPAM) fixed at 160 mmol.L^{-1}, with different ratios of concentration between these monomers. This set was performed to understand the influence of these ratios in the final characteristics of the microgel particles. In runs S4 and S6-S8 (Set 2), the concentration of the monomer NIPAM was fixed at 133 mmol.L^{-1}, and the concentration of AA was varied. These experiments had the intention to understand how different concentrations of AA influence the properties of poly(NIPAM-co-AA) microgels. Runs S9-S17 (Set 3) form a set of Full Factorial Design of Experiments, with variation in the monomer (AA), cross-linking agent (MBA) and initiator (KPS). Runs S18-S26 (Set 4) form a set of Fractional Factorial Design of Experiments, with variation in the monomers (AA and NIPAM), cross-linking agent (MBA) and initiator (KPS). Finally, runs S27-S30 (Set 5) have chitosan (Cs) in their formulation. In this last case, only the Cs concentration is varied. The samples of all set were characterised (Chapter 4), the samples of set 4 were used in the

synthesis monitoring (Chapter 3), and some samples of set 2 and 3 were tested as oral drug carrier (Chapter 5).

Table 4.1 - Formulations used to produce microgel particles by free-radical precipitation polymerisation.

Runs	Microgel Particle	Reagents Concentration (mmol.L^{-1})				
		AA	NIPAM	MBA	KPS	Cs
S1	AA	160	0	7	5	-
S2	AA/Nipam	133	27	7	5	-
S3	AA/Nipam	80	80	7	5	-
S4	AA/Nipam	27	133	7	5	-
S5	Nipam	0	160	7	5	-
S6	Nipam	0	133	7	5	-
S7	AA/Nipam	54	133	7	5	-
S8	AA/Nipam	108	133	7	5	-
S9	AA/Nipam	20	120	2	2.5	-
S10	AA/Nipam	20	120	2	5	-
S11	AA/Nipam	20	120	4	2.5	-
S12	AA/Nipam	20	120	4	5	-
S13	AA/Nipam	40	120	2	2.5	-
S14	AA/Nipam	40	120	2	5	-
S15	AA/Nipam	40	120	4	2.5	-
S16	AA/Nipam	40	120	4	5	-
S17[a]	AA/Nipam	30	120	3	3.75	-
S18	AA/Nipam	10	120	2	5	-
S19	AA/Nipam	10	120	6	10	-
S20	AA/Nipam	10	200	2	10	-
S21	AA/Nipam	10	200	6	5	-
S22	AA/Nipam	40	120	2	10	-
S23	AA/Nipam	40	120	6	5	-
S24	AA/Nipam	40	200	2	5	-
S25	AA/Nipam	40	200	6	10	-
S26[a]	AA/Nipam	25	160	4	7.5	-
S27	AA/Nipam/Cs	20	120	2	2.5	0.03[b]
S28	AA/Nipam/Cs	20	120	2	2.5	0.06[b]
S29	AA/Nipam/Cs	20	120	2	2.5	0.12[b]
S30	AA/Nipam/Cs	20	120	2	2.5	0.24[b]

[a]Central point of the factorial experimental design (n=3). [b]Values in grams (g).

4.2.3. Methodology

4.2.3.1. Determination of size and size distribution of microgels

The Z-average particle size of the microgels was determined by the Dynamic Light Scattering method (or photon correlation spectroscopy) using a Zetasizer Nano ZS90 (Malvern Instruments, Malvern, UK) fitted with a 4 mW laser (λ= 633 nm) and a detector placed at 90°. The diffraction pattern analysis was performed according to the Mie theory, with a refractive

index of 1.33 for the diluent (water). For size analyses, the samples were diluted in MiliQ water to reach the appropriate concentration for the reading range of the equipment. At least three replicates were conducted for each sample to give an average hydrodynamic diameter (D_h) and size distribution (PDI).

4.2.3.2. Zeta Potential determination

Zeta potential (ζ) of the microgels was determined by Electrophoretic Light Scattering (ELS) using a Zetasizer Nano ZS90 Malvern equipment and disposable capillary cells (cuvettes containing two electrodes). The applied field strength was 20 V/cm. Sample preparation was done by dilutions with MilliQ water and a 0.1 M sodium chloride solution (0.1 M NaCl), to reach the appropriate concentration for the reading range of the equipment. The solution of NaCl was employed to produce the required ionic strength in the microgel particles.

The technique used in the Zetasizer Nano ZS90 is a combination of laser Doppler velocimetry and phase analysis light scattering (PALS) in a patented technique called M3-PALS. Further information discussing this technique is available in the Malvern Instruments website (MALVERN INSTRUMENTS, 2011b).

4.2.3.3. Determination of the hydrogenionic potential (pH) of the microgel suspensions

Relevant information on the stability of suspensions can be obtained by monitoring the pH as a function of storage time. The change in pH may be an indication of polymer degradation. For example, the decrease in the pH values of polymer colloidal suspensions, in a short period, can be attributed to ionisation of carboxylic groups present in the polymer (SCHAFFAZICK et al., 2003).

In this work, the determination of the pH of the microgel suspensions was performed using a potentiometer (pHmeter Tec-3MP, Tecnal), previously calibrated with buffer solutions of pH 10.0, 7.0, and 4.0 (Neon Comercial Ltda.). The measurements were performed at room temperature. The pH of the samples was measured at predefined time intervals during storage.

4.2.3.4. Morphological evaluation of microgel particles

The morphology of the microgel particles (S1-S17) was observed by scanning electron microscopy on a Nova NanoSEM 400 (Fei Company) instrument with field emission gun (SEM-FEG) operated at 10 kV, belonging to the "*Laboratório de Sistemas Integrados do*

Departamento de Engenharia Elétrica da Escola Politécnica da Universidade de São Paulo". The detector used was a secondary electron detector (SED).

However, due to a period of technical problems with this equipment, some samples (namely, S17-S18 and S24-S26) were analysed using the equipment Tescan Vega3 (Oxford Instruments) with X-act detector, belonging to the "*Laboratorio de Eletroquímica e Corrosão do Departamento de Engenharia Química da Escola Politécnica da Universidade de São Paulo".*

Sample preparation was performed on the day before the analysis when one drop of the sample (approximately ten µL) was placed on a silica grid and left overnight to dry. On the day of the analysis, the support of the dried sample was coated with gold vapour. The metallization conditions were: 20 mA current for 1 min. Coating with gold is required on non-metallic samples to increase sample conductivity and protect against localised heating (increase the contrast and quality of the images).

4.2.3.5. Qualitative identification of microgels composition by Fourier Transform Infrared (FTIR)

FTIR was used to identify the presence of the different functional groups present in microgels (Table 4.2). In this way, the previously dried samples of the microgels were mixed with spectroscopy-grade potassium bromide (KBr) in the proportion of 1:100. With this mixture, a semi-transparent disc (or pellet) was formed by compression and analysed by an IRPrestige-21 Shimadzu spectrophotometer (Figure 4.6). The spectral scan was performed over a wavenumber range of 800 - 4000 cm^{-1} with a resolution accuracy of 4 cm^{-1}.

Figure 4.6 – FTIR Spectrophotometer setup and sample preparation apparatus.

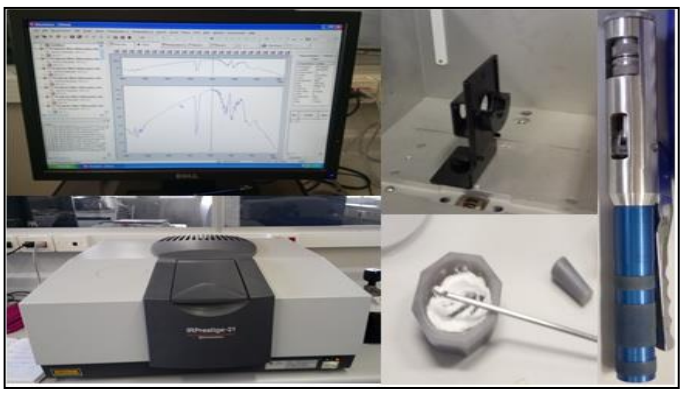

Source: Author

Table 4.2 gives the characteristic frequencies/bands in the IR spectra of the synthesised microgels.

Table 4.2 - Summary of the absorption bands of different chemical bonds of the microgels based on AA, Nipam and Cs cross-linked with MBA.

Chemical binding/ functional group	Wave Frequencies range (cm^{-1})	Information
aliphatic C-N	1180-1280	-
C-O of carboxylic acid	1200-1300 and 1420	Two axial bands appear due to the coupling of the angular deformation in the plane of the O-H bond and the axial deformation of C-O
CH_2	1430-1470	Angular deformation of -$(CH_2)_n$, where for n greater than 3 the band appears in the region around 720 cm^{-1} (angular chain deformation)
N-H	1495-1580	a weak band of angular deformation
C=C	1645-1675	Intensity usually weak to medium. Bands are absent in symmetrical alkenes. The presence of one or two additional bands of 1650-1600 occurs in conjugated alkenes.
C=0 of amide groups	1630-1700	-
C=0 of carboxylic acid	1710-1760	The monomer has the band of ~ 1760 and the dimer ~ 1710
aliphatic C-H	2852-2960 and 2880-2890	CH_3 and CH_2 CH
N-H	3070-3320	-
O-H (chelate)	2500-3200	Intramolecular hydrogen bonding with C = O. Broad band, of normally weak intensity, and frequency generally proportional to the binding force
O-H (associated)	3200-3400	Strong, wide band resulting from the polymer association

4.2.3.6. Influence of the external environment: pH and temperature

In order to determine the behaviour of the microgels in different conditions of pH and temperature, DLS and ELS analysis were applied for monitoring the hydrodynamic diameter and potential zeta, respectively, of the microgel particles as a function of pH (1.5-8.5) at a

constant temperature (37 °C), and the hydrodynamic diameter was also monitored across the temperature range from 20 to 50 °C.

To determine the influence of temperature on the particle size of microgels, the samples were pre-diluted at a concentration of 1:100 in MilliQ water and the measures were controlled by the Zetasizer Software (Temperature trend SOP). The samples were equilibrated at each temperature for 2 min before data collection. Three measurements were conducted for each point of temperature to give an average hydrodynamic diameter and size distribution.

The influence of pH on particle size and zeta potential were obtained by combining the Zetasizer Nano with a Multipurpose Titrator (MPT-2) (Figure 4.7-A). This combination provides extensive automation for some measurements and improves productivity by proving a complete measurement using a stored method (Standard Operating Procedures, SOP). The software controls all aspects of titration and measurement. The MPT-2 titrator incorporates an integral peristaltic pump to circulate the sample from the sample container through the flow cell in the optics unit of the Zetasizer, a pH probe and measurement electronics, and 3 syringes for 3 different titrants. The sample container uses a magnetic stirrer to mix the sample and titrants and to ensure pH equilibration in the shortest possible time (MALVERN INSTRUMENTS). For the measurement of zeta potential, it was used the standard ZEN1070 folded capillary cell (Figure 4.7-B), and the size and size distribution were measured by the ZEN0023 quartz flow cell (Figure 4.7-C). Each pH was adjusted using the following solutions: NaOH (0.025 M and 0.25M) and HCl (0.25M). The microgels were diluted in MilliQ water using a proportion of 1:10. Each point of pH consists of three measurements.

Figure 4.7 – (A) Zetasizer Nano ZS90 with multipurpose titrator MPT2. (B) ZEN1070 folded capillary cell. (C) ZEN0023 quartz flow cell.

4.2.3.7. Storage and stability kinetic of the microgel suspension

Colloidal suspensions usually do not tend to aggregation, even after a few months. This stability occurs because the sedimentation rate is slow for submicron particles, minimised by Brownian motion. However, over longer times, agglomerations of the particles can happen and, consequently, the sedimentation. For this reason, it is essential to monitor the stability of the particles during storage time. In polymeric samples, this stability can be monitored through the control of some physicochemical parameters, such as particle size, particle size distribution, zeta potential, pH and distribution of polymer molar mass (SCHAFFAZICK et al., 2003).

In this work, the kinetic stability study of the microgel suspensions was carried out within a range of 180 days. The samples were stored in a refrigerator at a temperature of 4.0 ± 0.5 °C. The measurements of size, size distribution and zeta potential were performed at 25 and 37 °C, and the pH measurements were performed at room temperature. In all measurements, aliquots were taken at random locations of the samples.

4.3. Results and Discussion

This section presents the results and discussion of the microgel characterisations and begins with an overview of the main physicochemical characteristics of these particles. It is followed by the results and discussion of particle size diameter (D_H) and particle size distribution (polydispersity index, PDI), zeta potential evaluation, final batch pH evaluation, morphological analysis by scanning electron microscopy (SEM), analysis of the qualitative composition by Fourier Transform Infrared (FTIR), analysis of the microgel swelling behaviour at different temperatures and pHs, and, finally, the study of the microgels stability at the storage time. In each subsection, the relationship between the studied characteristics and the sample formulations are explained in more detail.

As previously said, there are several works in the literature about microgel characterisation, mainly concerning the influence of the external environment on the swelling and shrinking behaviour of these polymer particles. Besides that, the characterisations presented in this chapter aim to understand the influence of synthesis conditions upon the microgel properties and select the best formulations for the desired application (as oral drug carrier). At the same time, all results were compared with literature, to verify the reproducibility of the properties and behaviours of microgels.

4.3.1. General characteristics of the microgel particles

Table 4.3 shows the results regarding the characteristics of the particles obtained in each formulation of this work. Particle size diameter (D_H), particle size distribution (PDI) and zeta potential (ZP) results were obtained at 37 °C, while pH values were measured at room temperature. The option to show these general results at 37 °C was because at this temperature the microgel particles are in their shrunken state, that is, they present a smaller amount of water in their structure; consequently, they exhibit a size closer to the unswollen microgel particles.

Table 4.3 shows that the values for all synthesised microgels vary from 275.6 to 7288 nm; according to Table 4.1, this minimum and maximum values represent the microgels composed only by NIPAM (minimum amount: 133 $mmol.L^{-1}$) and with chitosan in their composition (maximum amount: 0.24 g), respectively. In general, the size values for poly(NIPAM-co-AA) particles ranged from 280 to 680 nm, except for the particle with the higher amount of AA compared to the amount of NIPAM (S2), and for particles with chitosan

in their composition (S27, S28, S29 and S30). Excluding S1, S2, S27 and S30, all other samples showed suitable sizes for the desired application.

Table 4.3 – Overview of the main physicochemical characteristics of microgel particles.

Experimental Set	Sample Code	D_h ± Std Dev[a] (nm)	PDI± Std Dev[a]	ZP± Std Dev[a] (mV)	pH[b]
	S1	2958±2054	0.86±0.25	-11.2±4.1	2.3
	S2	1315±80.3	1.00±0.00	-5.2±0.5	2.4
1	S3	536.6±25.9	0.10±0.01	-7.0±0.7	2.3
	S4	439.6±138.0	0.30±0.02	-9.7±1.2	2.5
	S5	476.6±118.4	0.22±0.20	-4.9±1.1	1.9
	S6	275.6±11.5	0.04±0.03	-6.8±1.6	2.4
2	S4	439.6±138.0	0.30±0.02	-9.7±1.2	2.5
	S7	472.0±27.7	0.40±0.16	-8.1±1.3	2.5
	S8	473.2±19.4	0.48±0.04	-10.5±1.3	2.4
	S9	341.1±31.6	0.24±0.02	-7.6±1.3	3.0
	S10	317.3±19.8	0.11±0.09	-9.8±2.5	2.4
	S11	300.1±25.8	0.19±0.02	-6.6±1.4	2.1
	S12	448.3±28.6	0.20±0.06	-7.6±1.6	2.3
3	S13	283.9±4.2	0.11±0.06	-5.0±1.6	2.7
	S14	395.1±19.8	0.14±0.09	-7.7±1.0	1.9
	S15	382.9±4.5	0.09±0.07	-15.5±1.1	2.5
	S16	414.9±29.1	0.22±0.23	-8.8±0.7	2.2
	S17[c]	436.3±10.3	0.15±0.04	-8.5±0.3	2.0
	S18	358.3±3.3	0.04±0.03	-8.6±2.1	2.3
	S19	662.4±15.1	0.05±0.01	-6.6±1.3	2.0
	S20	395.7±42.8	0.11±0.09	-6.9±0.9	2.2
	S21	582.3±7.9	0.10±0.07	-9.3±1.3	2.5
4	S22	374.0±9.5	0.10±0.02	-8.9±1.7	2.3
	S23	412.0±17.9	0.05±0.06	-8.3±1.2	2.4
	S24	542.1±8.8	0.01±0.01	-7.8±1.0	2.5
	S25	604.6±15.9	0.04±0.04	-8.2±2.3	2.2
	S26[c]	477.1±118.2	0.17±0.23	-9.1±0.9	2.1
	S9	341.1±31.6	0.24±0.02	-7.6±1.3	3.0
	S27	1462±1121	0.87±0.23	-4.8±0.6	2.4
5	S28	566.0±34.2	0.96±0.06	-4.8±1.4	1.7
	S29	862.7±25.5	0.95±0.07	-2.3±1.6	2.5
	S30	7288±4815	0.57±0.44	4.5±2.2	4.6

The analysis was done at [a] 37°C and [b] room temperature. [c] Central point of the factorial design (n=3).

The uniformity and dispersity of the microgel particles were presented by the polydispersity index (PDI). As defined previously, the polydispersity index (PDI) is a dimensionless number that expresses the width of the particle size distribution, ranging from 0 to 1; values close to 0 indicate that samples are monodisperse, while larger values suggest that the sample is increasingly polydisperse. The results of PDI show agreement with the particle size values, i.e., particles with higher size (S1, S2, S27, S28, S29 and S30) present higher PDI (upper 0.5), probably caused by aggregation. For other samples, the PDI ranged from 0.01 to 0.48. According to the results shown in Table 4.3, only samples belonging to the experimental sets number 2 (S6) and number 4 (S18, S19, S23, S24 and S25) were less or equal than 0.05; taking into account the definitions given in section 4.1.1., this indicates that the particles were monodisperse. However, for application as a drug delivery system, these particles may have a PDI of up to 0.2 (DANAEI et al., 2018); thus, according to this criterion, the samples suitable for the desired application were S3, S6, S10, S13, S15, S17-S25.

The zeta potential values were negative for all samples, as expected, except for the sample S30 (4.5±2.2) that have a higher amount of chitosan, a cationic biopolymer. The absolute values ranged from 2.3 to 15.5.

The pH values for microgel suspension varied from 2.0 to 3.0. The only sample that distances from this interval was S30 that has pH equal to 4.58 due to the higher amount of chitosan in the microgel structure.

Observing the results presented in Table 4.3, and taking into account the works found in the literature for similar systems (ZHANG et al., 2009; FAROOQI et al., 2013), it is concluded that microgels particles obtained by the precipitation polymerisation method present coherent properties.

4.3.2. Size and polydispersity (DP and PDI)

Size controllability and narrow size distribution are two important parameters for use in the biological/pharmaceutical applications. Microgel sizes have a significant effect on their distribution in the body and affect the interaction between the particles and cells. Furthermore, narrowly dispersed particles can bring the same stimuli-response behaviours, which will result in a coincident drug release profile. Thus it becomes easy to manipulate the drug release kinetics and to design a more suitable drug delivery system (WANG et al.,

2013). In the scope of this work, the desired size range of the microgel particles to be used in the controlled release of drugs are between 100 to 1000 nm, with a narrow size distribution (PDI less than 0.2).

Table 4.4 shows the average particle size (D_h) and polydispersity index (PDI) of microgel particles measured at 25 and 37 °C.

Table 4.4 - Particles sizes and polydispersity index of microgels based on AA, NIPAM and Cs at 25 and 37 °C.

Sample Code	25 °C		37 °C	
	D_h ± Std Dev (nm)	PDI	D_h ± Std Dev (nm)	PDI
S1	-	-	2958±2054	0.86±0.25
S2	1219±171.5	0.28±0.02	1315±80.3	1.00±0.00
S3	923.8±20.1	0.08±0.03	536.6±26.0	0.10±0.01
S4	829.3±15.0	0.09±0.07	439.6±138.0	0.30±0.02
S5	748±3.2	0.25±0.01	476.6±118.4	0.22±0.20
S6	535.3±18.5	0.11±0.02	275.6±11.5	0.04±0.03
S4	829.3±15.00	0.09±0.07	439.6±138.0	0.30±0.02
S7	981.2±66.7	0.09±0.08	472.0±27.7	0.40±0.16
S8	556.7±33.8	0.95±0.10	473.2±19.4	0.48±0.04
S9	326.1±84.21	0.96±0.07	341.1±31.6	0.24±0.02
S10	1001±30.5	0.22±0.01	317.3±19.8	0.11±0.09
S11	593.5±17.8	0.07±0.06	300.1±25.8	0.19±0.02
S12	1081±12.1	0.10±0.03	448.3±28.6	0.20±0.06
S13	592.9±8.5	0.21±0.03	283.9±4.2	0.11±0.06
S14	930.0±22.0	0.01±0.01	395.1±19.8	0.14±0.09
S15	879.6±44.2	0.09±0.08	382.9±4.5	0.09±0.07
S16	978.0±56.5	0.11±0.01	414.9±29.1	0.22±0.23
S17[a]	1028.4±142.2	0.08±0.04	436.3±10.3	0.15±0.04
S18	944.0±41.1	0.04±0.03	358.3±3.3	0.04±0.03
S19	1025±15.31	0.07±0.02	662.4±15.1	0.05±0.01
S20	579.0±37.9	0.92±0.11	395.7±42.8	0.11±0.09
S21	897.9±23.8	0.09±0.09	582.3±7.9	0.10±0.07
S22	752.6±43.0	0.63±0.09	374.0±9.5	0.10±0.02
S23	898.0±18.2	0.03±0.02	412.0±17.9	0.05±0.06
S24	1189±76.2	0.07±0.04	542.1±8.8	0.01±0.01
S25	1266±101.2	0.40±0.10	604.6±15.9	0.04±0.04
S26[a]	1046.4±129.8	0.10±0.03	477.1±118.2	0.17±0.23
S27	617.7±123.9	1.00±0.00	1462±1121	0.87±0.23
S28	2490±63.1	0.95±0.07	566.0±34.2	0.96±0.06
S29	726.7±39.7	0.60±0.04	862.7±25.5	0.95±0.07
S30	37.81±15.7	0.49±0.02	7288±4815	0.57±0.44

In general, the results presented in Table 4.4 show that the microgel particles have a smaller size at 37 °C than at 25 °C, as expected. In some case, the PDI is also smaller at 37°C (Figure 4.8). This may reflect the fact that above the volume phase transition temperature (VPTT), in this case, upper 32°C, the microgel particles adopt a collapsed state, hard, latex-like spherical conformation, which is less likely to show size variation than particles below the VPTT with a softer, more porous, flexible network-like structure (PICH; RICHTERING, 2010; FERNANDEZ-NIEVES et al., 2011). This behaviour will be explained better in item 4.3.7.

Figure 4.8 – Size distribution by intensity. Sample S25 was measure at (A) 25 °C and (B) 37 °C. The polydispersity index values obtained at these two temperatures are 0.40 and 0.04, respectively.

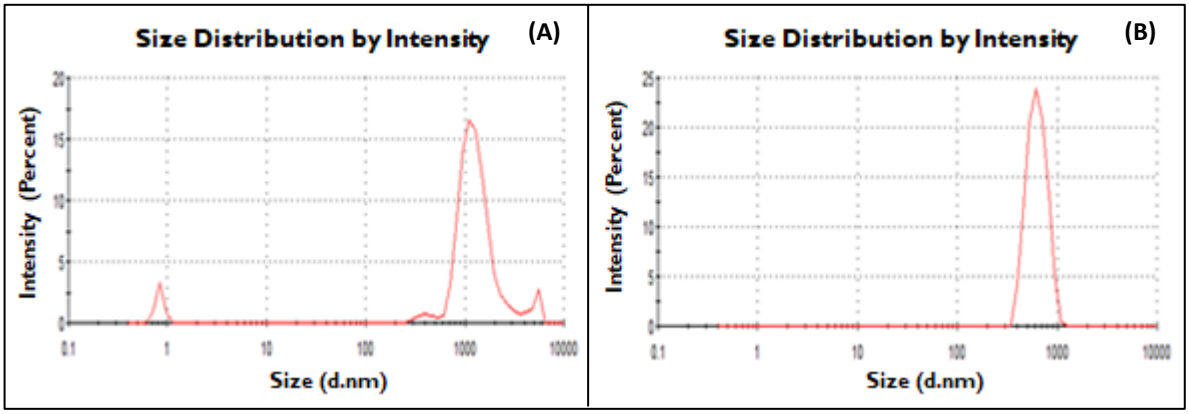

Conclusions about the influence of the components of the reaction process on the size and particle size distribution of microgel particles are shown following.

4.3.2.1. Evaluation of the influence of AA monomer

Figure 4.9 shows the influence of AA molar concentration in the results of the average particle size and polydispersity index of microgel particles. The concentrations of NIPAM, MBA and KPS were kept constant and equal to 133, 7 and 5 mmol.L^{-1}, respectively.

In general, it is possible to observe that the introduction of hydrophilic AA group causes an increase in the particle size. With the amount of AA varying from 0 to 54 mmol.L^{-1}, only a large increase at 25 °C can be observed, while a slight increase in the particle size at 37 °C can be observed. However, at 25 °C, a large decrease could be found when the amount of AA increased from 54 to 108 mmol.L^{-1}. Probably, this behaviour was caused by the higher amount of AA concerning NIPAM, thus occurring inhibition of the temperature effect in this sample (S8); there is no significant difference between the diameters in both temperatures.

Zhang et al. (2009) show this same behaviour in particles of poly(NIPAM-co-AA) synthesised by batch polymerisation, with increasing the amount of AA from 0 to 5 mol% of NIPAM monomer, the hydrodynamic diameter increases, suggesting that the introduction of a small amount of the hydrophilic AA group cause an increase in the particles size, the same difference in the diameter could be observed with the amount of AA increases from 10 to 20% of NIPAM monomer. However, for poly(NIPAM-co-AA) microgel produced by semi-batch polymerisation, a large decrease could be found when the amount of AA increase. The authors explain this behaviour due to more stabilisation stemming from carboxylic ions.

Figure 4.9 - Influence of AA concentration in (A) average particle size and (B) polydispersity index of microgel particles. The samples have the following AA concentration: S4 (27 mmol.L^{-1}), S6 (0 mmol.L^{-1}), S7 (54 mmol.L^{-1}) and S8 (108 mmol.L^{-1}).

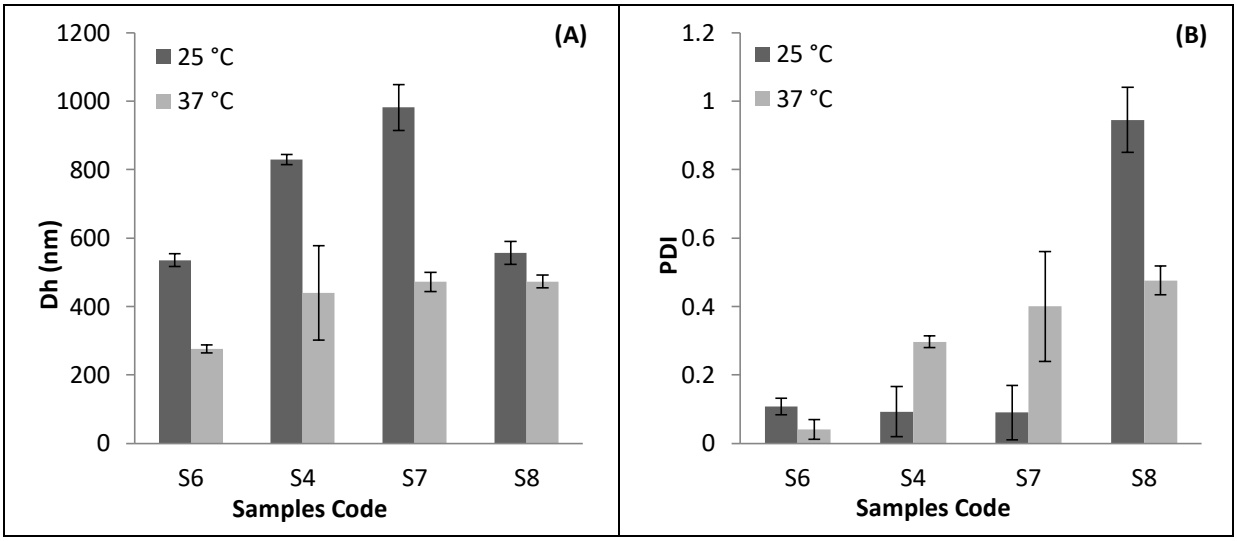

(n=3, +-sd)

According to the theory (GALAEV; MATTIASSON, 2008), microgel particles based on poly(NIPAM) that are temperature-sensitive, the polydispersity index should be smaller above the VPTT, as in sample S6. However, when AA is added to the microgel structure (samples S4, S7 and S8), the PDI values show smaller values at 25°C than 37°C, except for sample S8. As can be seen in Figure 4.9 and Table 4.4, the values for PDI cannot be associated only to the temperature, because, probably, there is an influence of other factors, such as the total concentration of monomers, pH of the medium, among other ones.

Figure 4.10 compares the average particle size and polydispersity index of the formulation with different AA concentration (20 and 40 mmol.L^{-1}), but with the same concentration of NIPAM, MBA and KPS. The results were obtained at 37°C.

Figure 4.10 - Influence of AA concentration in (A) average particle size and (B) polydispersity index of microgel particles. Sample formulations: S9 and S13 (MBA: 2.0 mmol.L^{-1}; KPS: 2.5 mmol.L^{-1}); S10 and S14 (MBA: 2.0 mmol.L^{-1}; KPS: 5.0 mmol.L^{-1}); S11 and S15 (MBA: 4.0 mmol.L^{-1}; KPS: 2.5 mmol.L^{-1}); S12 and S16 (MBA: 4.0 mmol.L^{-1}; KPS: 5.0 mmol.L^{-1}). All samples have the same Nipam concentration (120 mmol.L^{-1}). The AA concentration is represented in the bar graph: dark grey bar (20 mmol.L^{-1}); light grey bar (40 mmol.L^{-1}).

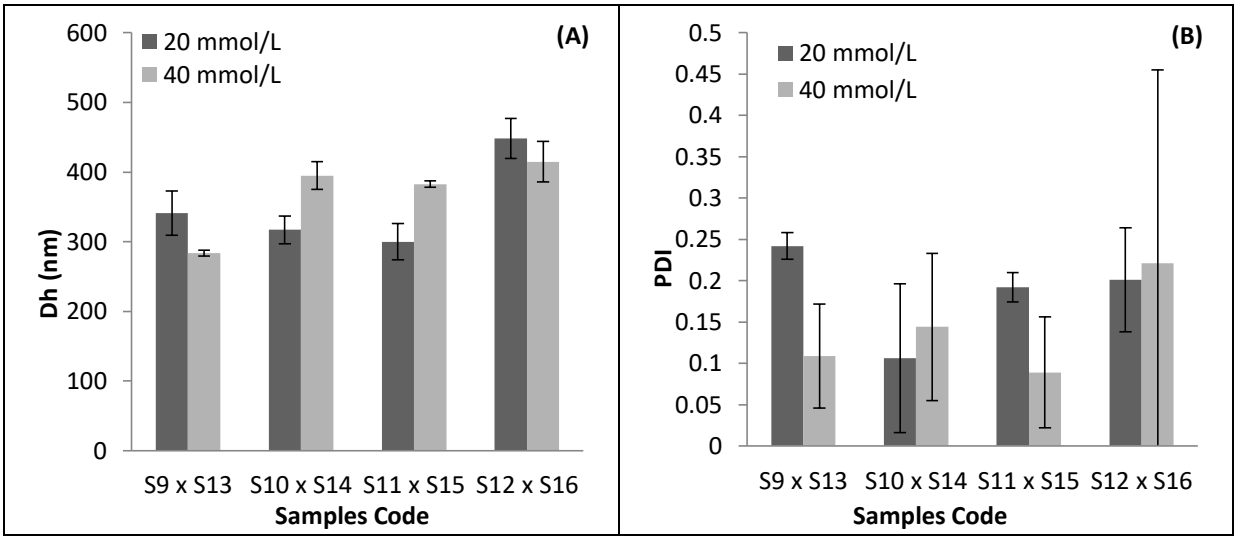

(n=3, +-sd)

According to Figure 4.10, in general, the increase in the AA amount increases the microgel average particle size (S10xS14 and S11xS15). In the case of samples S9xS13 and S12xS16, considering the standard deviation, there is no difference between them. It is known that the AA has a stabilising effect in the formation of the particles; however, in this case, the polymerisation was done in a medium with pH smaller than the pKa of the polymer, making this stabilisation difficult. In this way, for a better understanding of the AA influence, other formulations with a higher difference between the concentrations need to be done.

The PDI values did not show correlation with the behaviour and values for particle size, but it is possible to observe that there is more variability in its values for particles with AA concentration equal to 40 mmol.L^{-1} than with 20 mmol.L^{-1}.

Figure 4.11 also shows the results for average particle size and polydispersity index of microgel particles with different AA concentration. The samples studied have the following concentration in mmol.L^{-1}: 10 (S18), 20 (S10), and 40 (S14). The concentrations of NIPAM, MBA and KPS were kept constant and equal to 120, 2 and 5 mmol.L^{-1}, respectively. The results were obtained at 37°C.

Figure 4.11 - Influence of AA concentration in average particle size and polydispersity index of microgel particles. The Nipam, MBA and KPS concentration are 120, 2 and 5 mmol.L^{-1}, respectively.

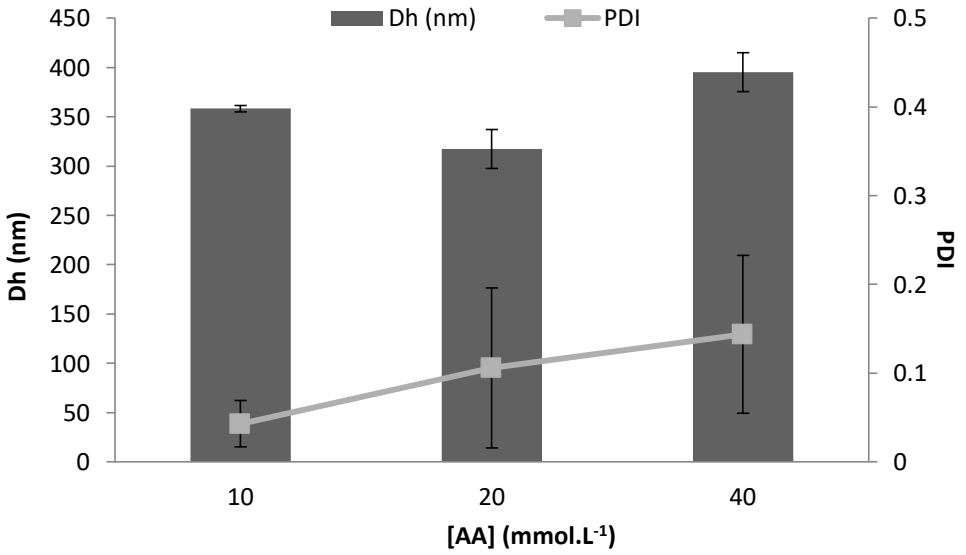

In the case of formulations shown in Figure 4.11, taking into account the standard deviation, they confirmed that the range of acrylic acid concentration studied did not show significant influence in microgel average particle size. However, it is possible to observe that increasing the AA concentration also increases the polydispersity index, which means that if we continue to increase the AA concentration, taking into account the tendency of PDI, the aggregation of the particles can occur, consequently increasing their sizes.

Figure 4.12 shows the results of the average particle size of microgels with different NIPAM concentrations.

Figure 4.12 - Influence of NIPAM concentration in average particle size and polydispersity index of microgel particles. Samples (A) without and (B) with AA in their microgels composition.

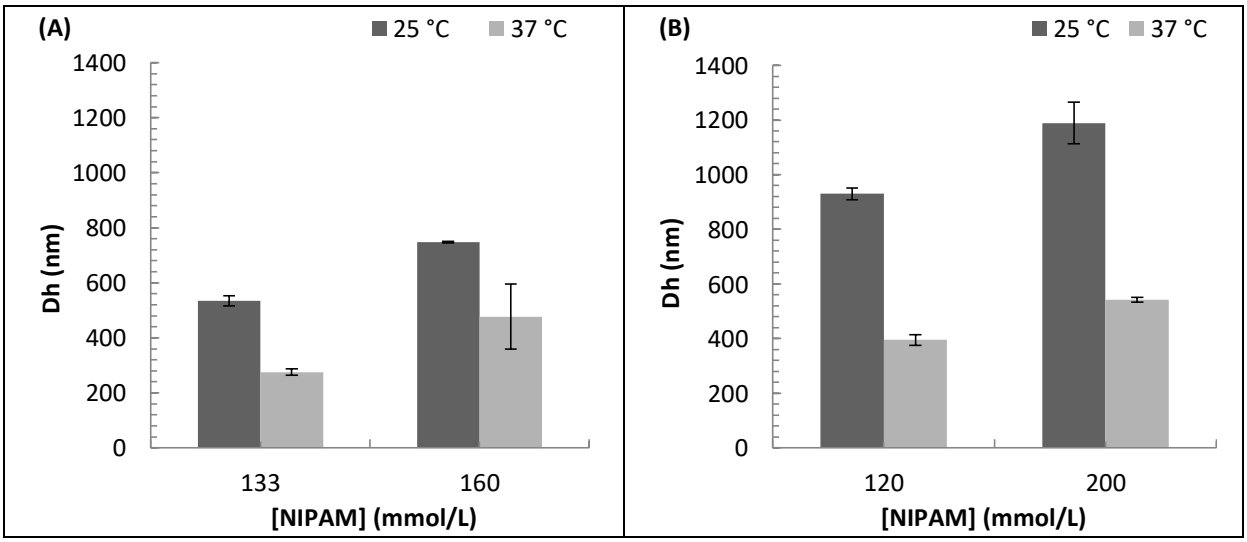

As expected, the microgels have a smaller size at 37 °C than 25 °C, and as the concentration of NIPAM increases the particle size also increases. Another observation is that the presence of AA monomer in the microgels (Figure 4.12 – B) increases the size of poly (NIPAM-co-AA) particles.

Figure 4.13 shows the results of size and polydispersity index of samples with a total concentration of AA and NIPAM in the reaction medium equal to 160 mmol.L^{-1}, varying only the ratio between them (AA:NIPAM). Thus, it was sought to understand how the proportion of the concentrations of these two monomers influence the size and distribution of the particles. The results were measured at 37 °C.

Figure 4.13 - Influence of proportion between AA and NIPAM concentration in average particle size and polydispersity index of microgel particles. The samples have the following AA and NIPAM concentration (AA:NIPAM) in mmol.L^{-1}: S1 (160:0), S2 (133:27), S3 (80:80), S4 (27:133) and S5 (0:160). All samples have the same MBA and KPS concentration, respectively, 7 and 5 mmol.L^{-1}.

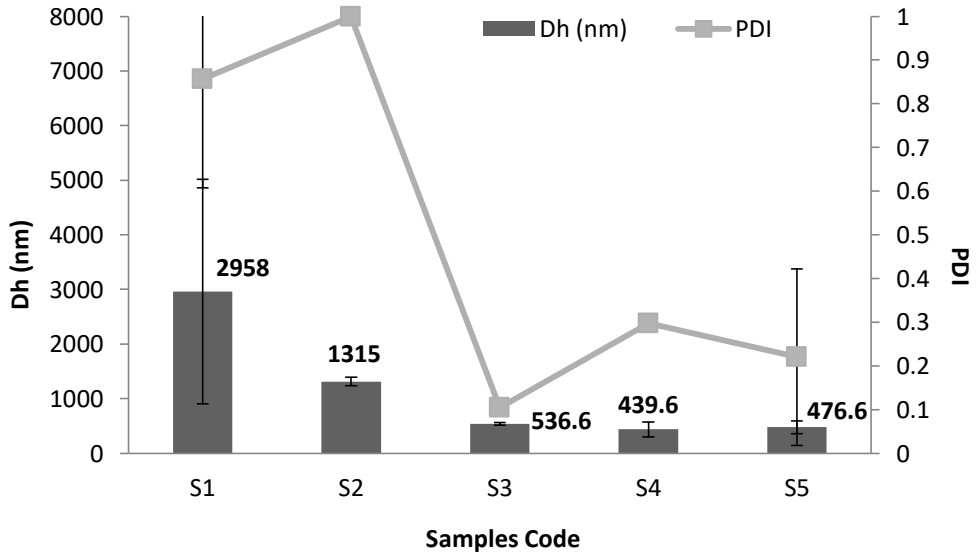

The results show that, for the same molar concentration (160 mmol.L^{-1}), the AA microgels (S1) present particles larger than the NIPAM microgels (S5), respectively 2958 and 476.6 nm at 37 ° C. About microgel particles based on AA and NIPAM monomers (S2, S3 and S4), the higher the ratio of NIPAM to acrylic acid, the smaller the particle size obtained. This behaviour can be explained by the contribution of NIPAM monomer in the formation of more stable and uniform microgel particles, while microgels with more concentration of AA than NIPAM in their composition; the particles show low colloidal stability (tending to higher polydispersity) and non-spherical morphology. In the subtopic 4.3.5, this trend will be better visualised.

About the results for the polydispersity index, it is possible to observe that the samples with a large AA/NIPAM ratio have a high polydispersity index. This parameter indicates that these systems have microgel particles with different sizes, which can cause the instability and aggregation of these particles. In the sample S1, this aggregation was verified visually, and the formation of a gelatinous film (microgel aggregates) in the sample could be observed.

In conclusion, according to the results for the influence of AA monomer in the particle size and polydispersity index, the increases in the AA increases the average particle size, mainly when the AA amount is higher than NIPAM, causing instability and aggregation. However, for a better understanding of the AA influence, an in-depth study needs to be done. About the influence of NIPAM concentration, the higher the amount of NIPAM in the copolymer formulation, the higher the average particle size of microgels.

4.3.2.2. Evaluation of the influence of the cross-linker (MBA)

The cross-linking of polymer chains is of crucial importance in the production of microgel particles (ELAISSARI; MAHDAVIAN, 2011). According to the literature (MEDEIROS, 2010), the increase of the MBA concentration leads to an increase in the average particle diameter, due to the higher reactivity of the MBA compared to the other monomers that can increase the critical chain size of the particles during the precipitation process and microgel formation. Another work that discusses this behaviour was done by Wu et al. (1994); they reported that, during the formation of the microgel particles by precipitation polymerisation, the cross-linking agent was consumed faster compared to the other monomers and therefore preferentially incorporated into the microgels at the beginning of the polymerisation.

Figure 4.14 compares the average particle size and polydispersity index of the formulation with different MBA concentration (2 and 4 mmol.L^{-1}), but with the same concentration of AA, NIPAM and KPS. The results were obtained at 37°C.

According to the results, they agree with the literature about the MBA influence in the microgel average particle size synthesised by precipitation polymerisation (ELAISSARI; MAHDAVIAN, 2011), in which the increases in the MBA amount increases the particle size. This difference in the particle size was significant when S10 and S13 (2 mmol.L^{-1}) were compared with S12 and S15 (4 mmol.L-1), respectively. For the comparison between other

samples (S9 x S11 and S14 x S16), there is no difference between the hydrodynamic values when the standard deviation is considered. The variation of MBA concentration did not show influence in the PDI values.

Figure 4.14 - Influence of MBA concentration in (A) average particle size and (B) polydispersity index of microgel particles. Sample formulations: S9 and S11 (AA: 20 mmol.L^{-1}; KPS: 2.5 mmol.L^{-1}); S10 and S12 (AA: 20 mmol.L^{-1}; KPS: 5.0 mmol.L^{-1}); S13 and S15 (AA: 40 mmol.L^{-1}; KPS: 2.5 mmol.L^{-1}); S14 and S16 (AA: 40 mmol.L^{-1}; KPS: 5.0 mmol.L^{-1}). All samples have the same NIPAM concentration (120 mmol.L^{-1}). The MBA concentration is represented in the bar graph: dark grey bar (2 mmol.L^{-1}); light grey bar (4 mmol.L^{-1}).

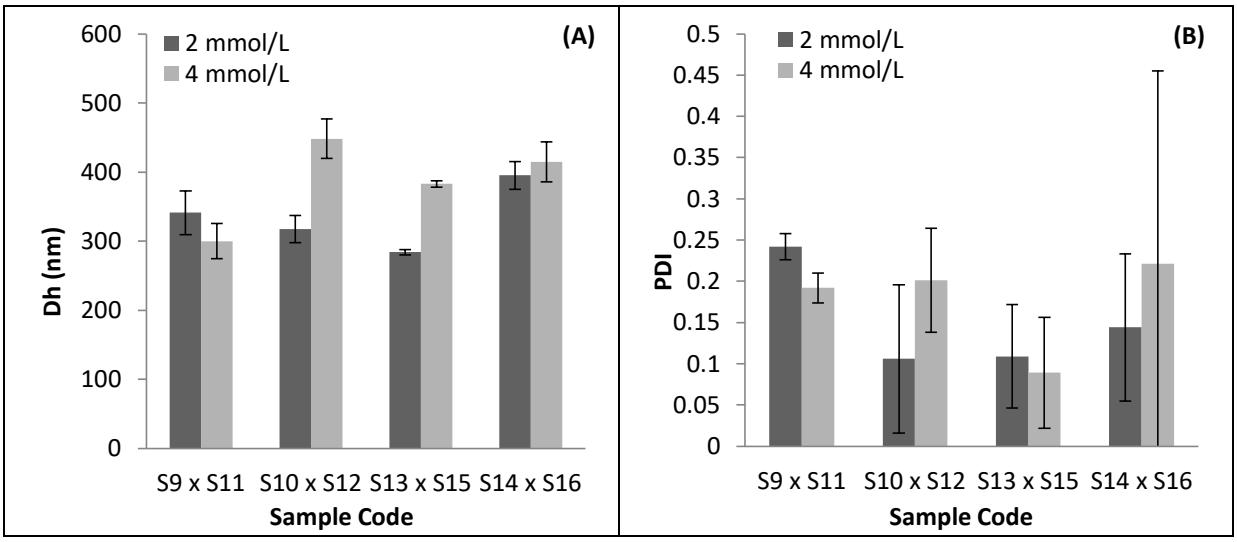

4.3.2.3. Evaluation of the influence of initiator (KPS)

Figure 4.15 compares the average particle size and polydispersity index of the formulation with different KPS concentration (2.5 and 5.0 mmol.L^{-1}), but with the same concentration of AA, NIPAM and MBA. The results were obtained at 37°C.

According to the theory of the formation of polymer particles (MATYJASZEWSKI; DAVIS, 2002; FERNANDES; LONA, 2004), the increase of the concentration of initiator increases the concentration of free radicals. Consequently, a decrease in the final diameter of the particles occurs, due to the rise in the number of particles formed at the beginning of the polymerisation. However, according to Figure 4.15, an increase in the average diameter of the particles upon increasing the concentration of the initiator is observed. A hypothesis about this opposite fact can be related to the difference in reactivity ratio of the reagents (AA, NIPAM and MBA) during the reaction, in which in the initial stages, particle growth occurs mostly due to the reaction of radicals with the molecules of the crosslinking reagent, in this case, MBA, due to its greater reactivity compared to NIPAM and AA. Thus, if the

concentration of growing radicals is very high, the probability of the formed radicals to react with the MBA molecules is higher. Consequently, the final diameter of the particles increases. Similar behaviour was reported in other studies (MEDEIROS, 2010) with particles with other compositions, but having MBA as the crosslinking agent and KPS as the initiator.

Figure 4.15 - Influence of KPS concentration in (A) average particle size and (B) polydispersity index of microgel particles. Sample formulations: S9 and S10 (AA: 20 mmol.L^{-1}; MBA: 2.0 mmol.L^{-1}); S11 and S12 (AA: 20 mmol.L^{-1}; MBA: 4.0 mmol.L^{-1}); S13 and S14 (AA: 40 mmol.L^{-1}; MBA: 2.0 mmol.L^{-1}); S15 and S16 (AA: 40 mmol.L^{-1}; MBA: 4.0 mmol.L^{-1}). All samples have the same NIPAM concentration (120 mmol.L^{-1}). The KPS concentration is represented in the bar graph: dark grey bar (2.5 mmol.L^{-1}); light grey bar (5.0 mmol.L^{-1}).

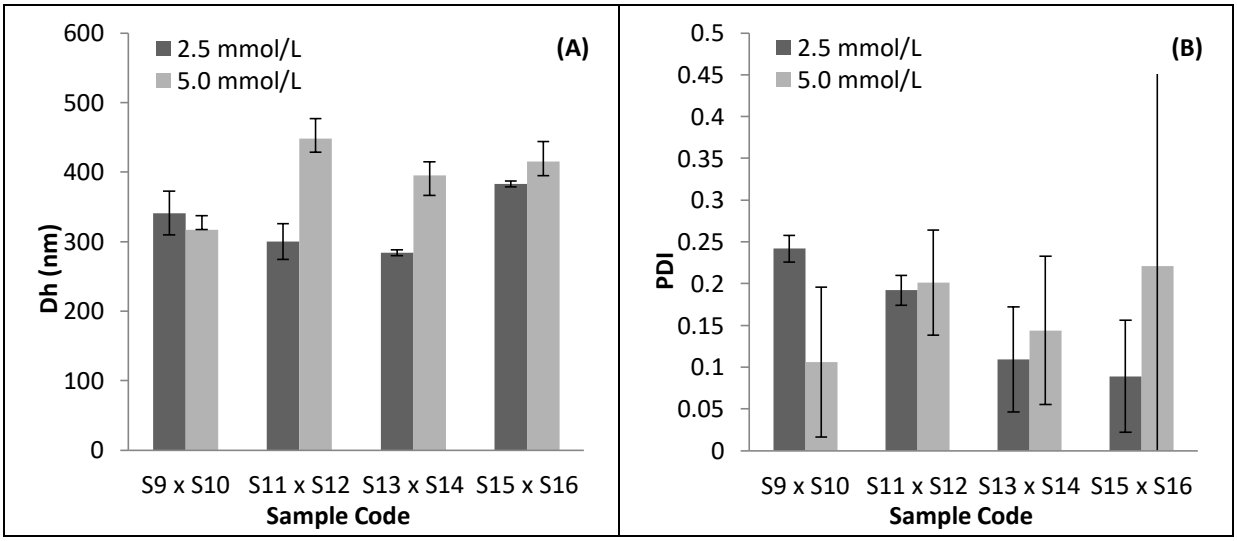

4.3.2.4. Evaluation of the influence of chitosan

Figure 4.16 shows the influence of Cs amount in the average particle size and polydispersity index in poly(NIPAM-AA-Cs). Based on the results shown previously, the microgels with Cs in their structure have a higher size and a large polydispersity index.

Figure 4.16 - Influence of Cs in (A) average particle size and (B) polydispersity index of microgel particles. Samples with different amount of chitosan in grams: S9 (0.00), S27 (0.03), S28 (0.06), S29 (0.12) and S30 (0.24). All samples have the same AA, NIPAM, MBA and KPS concentrations, respectively, 20, 120, 2 and 2.5 mmol.L^{-1}.

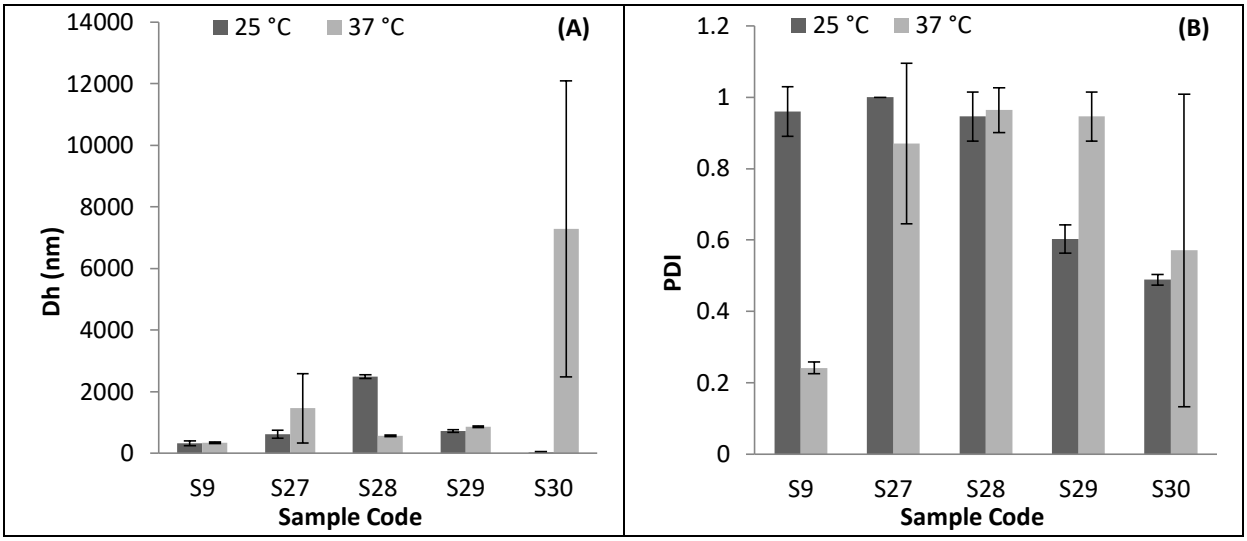

4.3.3. Evaluation of Zeta Potential (ZP)

In addition to size and size distribution, it is essential to analyse the surface charge of the microgel particles, because these particles can interact with the surface of the biological cells when administered to a biological system (NAGASHIMA et al., 1998).

Table 4.5 – Zeta potential of microgel particles based on AA, NIPAM and Cs at 25 and 37 °C.

Sample Code	25 °C	37 °C
	ZP (mV)	ZP (mV)
S1	-5.2±0.7	-11.2±4.1
S2	-5.0±0.8	-5.2±0.5
S3	-6.7±0.7	-7.0±0.7
S4	-4.7±0.7	-9.7±1.2
S5	-3.3±0.2	-4.9±1.1
S6	-2.5±0.8	-6.8±1.6
S4	-4.7±0.7	-9.7±1.2
S7	-5.6±0.3	-8.1±1.3
S8	-9.7±0.4	-10.5±1.3
S9	-5.3±0.2	-7.6±1.3
S10	-8.6±0.6	-9.8±2.5
S11	-5.1±0.4	-6.6±1.4
S12	-11.2±0.9	-7.6±1.6
S13	-2.0±0.4	-5.0±1.6
S14	-8.0±0.6	-7.7±1.0
S15	-11.3±1.8	-15.5±1.1
S16	-10.4±0.5	-8.8±0.7
S17	-9.6±3.8	-8.5±0.3
S18	-5.2±0.2	-8.6±2.1
S19	-3.7±0.3	-6.6±1.3
S20	-2.9±0.4	-6.9±0.9
S21	-6.0±0.7	-9.3±1.3
S22	-8.6±0.2	-8.9±1.7
S23	-6.7±0.2	-8.3±1.2
S24	-7.1±1.1	-7.8±1.0
S25	-6.3±0.1	-8.2±2.3
S26	-5.3±0.9	-9.1±0.9
S9	-5.3±0.2	-7.6±1.3
S27	-4.0±0.5	-4.8±0.6
S28	-2.2±0.3	-4.8±1.4
S29	-3.7±0.5	-2.3±1.6
S30	3.1±0.9	4.53±2.2

Table 4.5 shows the zeta potential of microgel particles in a NaCl solution (0.1 M) at 25 and 37 °C. The results indicated that the microgel particles were negatively charged, and in most cases, they are more negative at 37 °C than 25°C. The zeta potential values can vary substantially between the swollen (25 °C) and shrunken (37°C) particles because volume changes alter the surface charge density of the particles and hence their mobilities.

In radical polymerisation, the main sources of the electrically charged groups are the ionic free radical initiator and/or ionic monomers copolymerised into the polymer network (PELTON; HOARE, 2011). In this case, the negative zeta potentials are coming from the dissociation of the carboxylic acid groups of AA on microgel surfaces and the ionic free radical initiator (KPS). Taking into account the previously described, it is very important to analyse how the variation in the concentration of the reagents present in the samples influences the zeta potential. Figure 4.17 and Figure 4.18 show the influence of reagents concentrations (AA, KPS and Cs) in zeta potential values. The experimental data were measured in the suspending medium at neutral pH and 37 °C.

Figure 4.17 shows the zeta potential of microgel particles with different AA molar concentration.

Figure 4.17 – Influence of AA concentration in the zeta potential of microgel particles. The samples have the following AA concentration: (A) S6 (0 mmol.L^{-1}), S4 (27 mmol.L^{-1}), S7 (54 mmol.L^{-1}) and S8 (108 mmol.L^{-1}). All samples have the same NIPAM, MBA and KPS concentration that have the following values 133, 7 and 5 mmol.L^{-1}, respectively; (B) S18 (10 mmol.L^{-1}), S10 (20 mmol.L^{-1}) and S14 (40 mmol.L^{-1}). All samples have the same NIPAM, MBA and KPS concentration that have the following values 120, 2 and 5 mmol.L^{-1}, respectively.

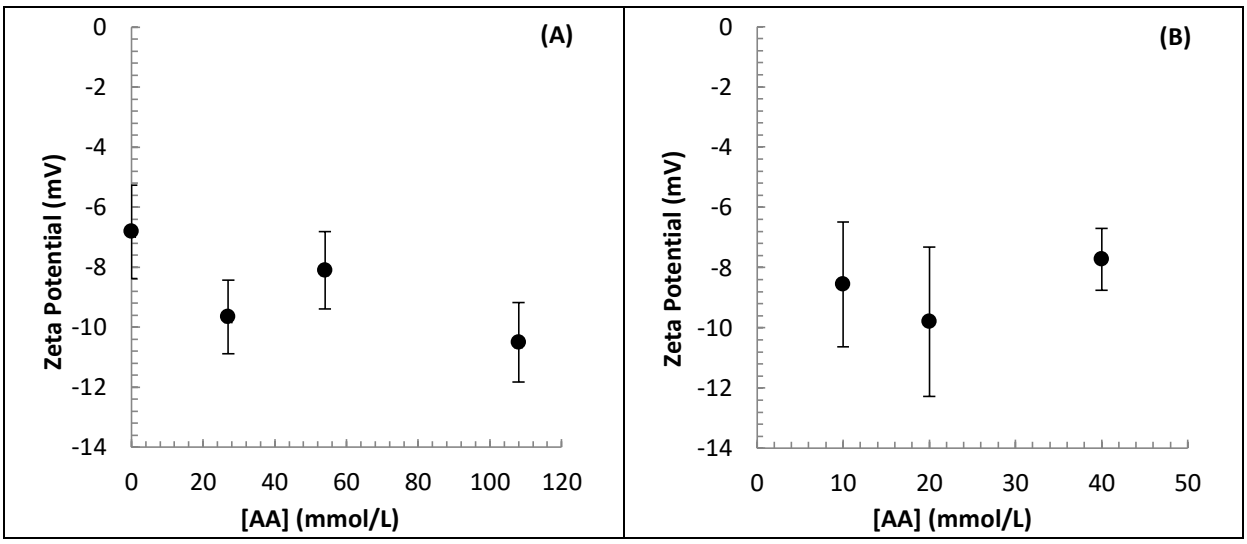

According to Figure 4.17, taking into account the standard deviation, there is not significative variation in zeta potential values for the range of AA concentration analysed. However, in general, the increases in AA amount increases the magnitude of the negative charge due to the higher concentration of AA at the surface layer of the microgels.

Figure 4.18 shows the zeta potential of microgel particles with different potassium persulfate molar concentration (A) and chitosan mass (B).

Figure 4.18 – (A) Influence of KPS concentration in the zeta potential of microgel particles. The samples have the following KPS concentration: S13 (2.5 mmol.L^{-1}), S14 (5.0 mmol.L^{-1}) and S22 (10 mmol.L^{-1}). All samples have the same AA, NIPAM and MBA concentration that have the following values 40, 120 and 2.0 mmol.L^{-1}, respectively; (B) Influence of Cs concentration in the zeta potential of microgel particles. The samples have the following Cs concentration: S9 (0.00 g), S27 (0.03 g), S28 (0.06 g), S29 (0.12 g) and S30 (0.24 g). All samples have the same AA, NIPAM, MBA and KPS concentration that have the following values 20, 120, 2.0 and 2.5mmol.L^{-1}, respectively.

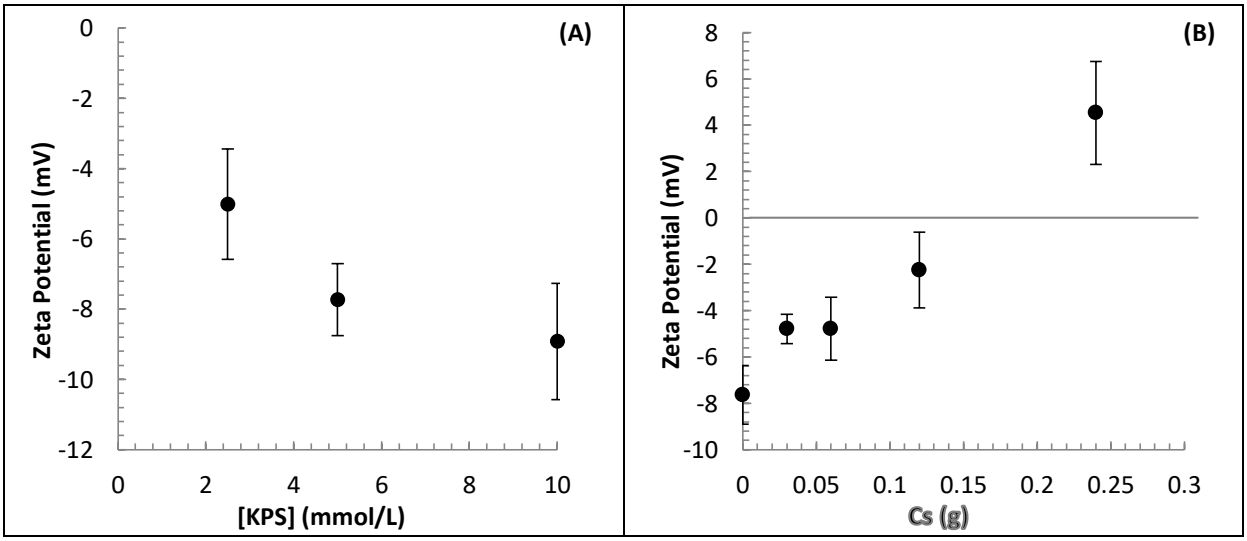

According to Figure 4.18, both the initiator (KPS) and the biopolymer (Cs) influence the zeta potential. However, as the initiator is ionic, the increased in its concentration causes the increase of the zeta potential value towards negative charges. While for rising of the chitosan concentration, which is a cationic biopolymer, the zeta potential values tend to positive charges.

4.3.4. Final Batch pH Evaluation

Figure 4.19 shows the pH of microgel suspensions for all samples present in this chapter.

Figure 4.19 – pH of the microgel particles.

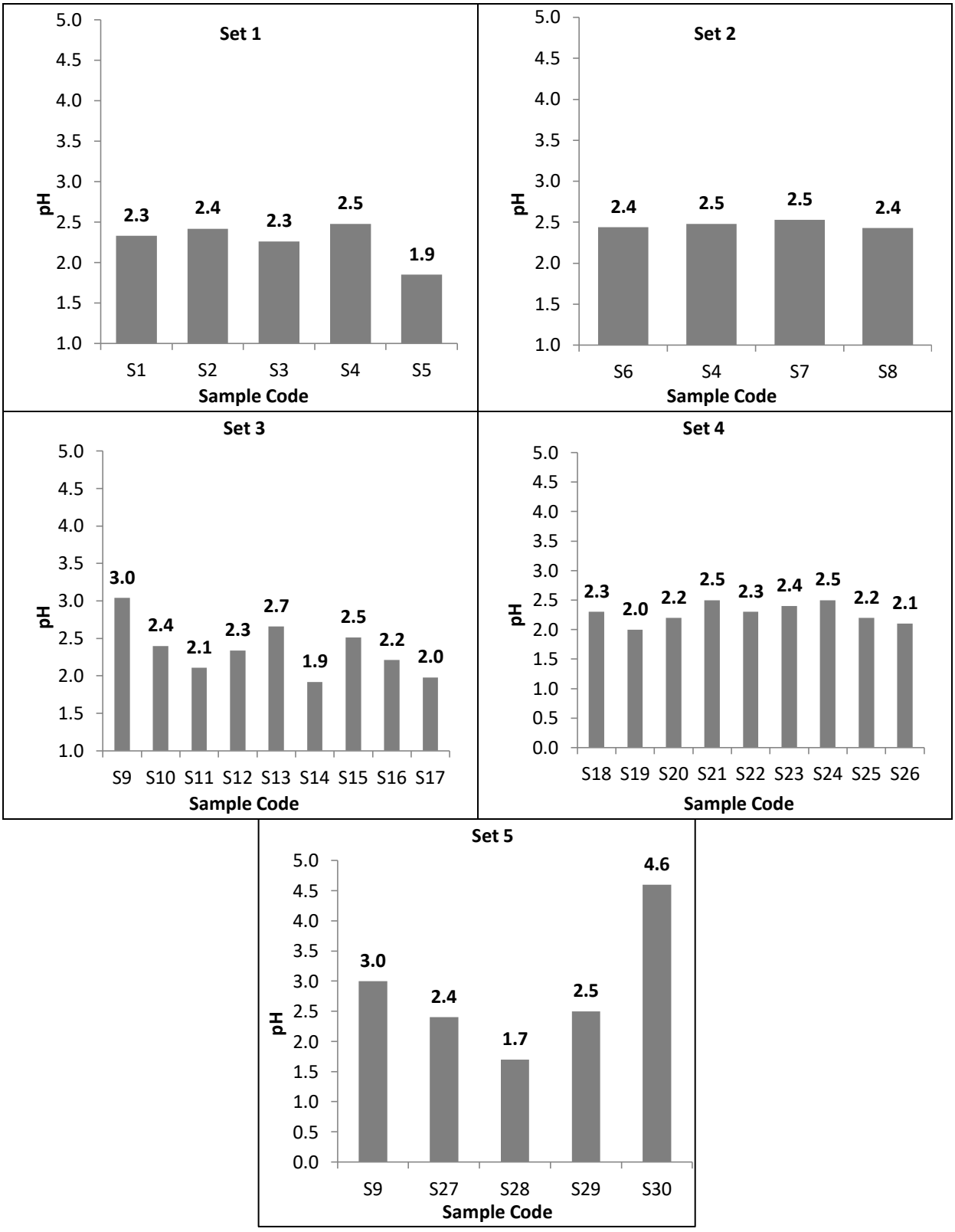

As previously reported, the microgel suspensions have pH values from 2.0 to 3.0. In general, no significant changes were observed in pH values with changes in formulation, except for sample S30, which has a larger amount of chitosan (a cationic biopolymer) in its formulation.

4.3.5. Morphological analysis by scanning electron microscopy (SEM)

The characterisation of particle size can be conducted, either indirectly by dynamic light scattering or through direct observation by microscopy (SEM, MEV, AFM). Scanning electron microscopy (SEM) was used in this work to confirm if the obtained particles had a spherical morphology and showed monodisperse distribution.

It is important to say that the SEM images of the microgels were obtained in their dehydrated state (collapsed conformation), because of the high vacuum in the equipment. Therefore, SEM measurements can only be compared with observations from other techniques made for particles in the collapsed state, that is, above the VPTT (THORNE, 2012). Furthermore, additional caution must be taken because the dehydrated particles are analysed in the (almost) total absence of solvent, while other techniques like DLS do so for the particles that are still dispersed in a solvent (above the VPTT).

Moreover, when comparing particle size data for the same sample measured by different techniques, it is important to realise that the types of distribution being measured and reported will not necessarily give precisely the same result for the particle diameter, because different measurement techniques use different equivalent sphere models (MALVERN INSTRUMENTS, 2011a).

Figure 4.20 shows the micrographs of samples with different AA molar concentration. The concentration of NIPAM, MBA and KPS is 133, 7 and 5 mmol.L^{-1}, respectively, for all samples. In this figure, it is possible to observe that the increase of the AA concentration causes the particle aggregation, and consequently, the microgels lose their spherical morphology. This aggregation is well visible in samples S7 and S8, where some points of the samples, the formation of a more homogeneous surface occur, in which the limits between the particles are not observed.

Figure 4.20 - SEM images of microgels with different amount of AA. AA concentration in mmol.L^{-1}: S6 (0), S4 (27), S7 (54), and S8 (108). The concentration of NIPAM, MBA and KPS is 133, 7 and 5 mmol.L^{-1}, respectively, for all samples.

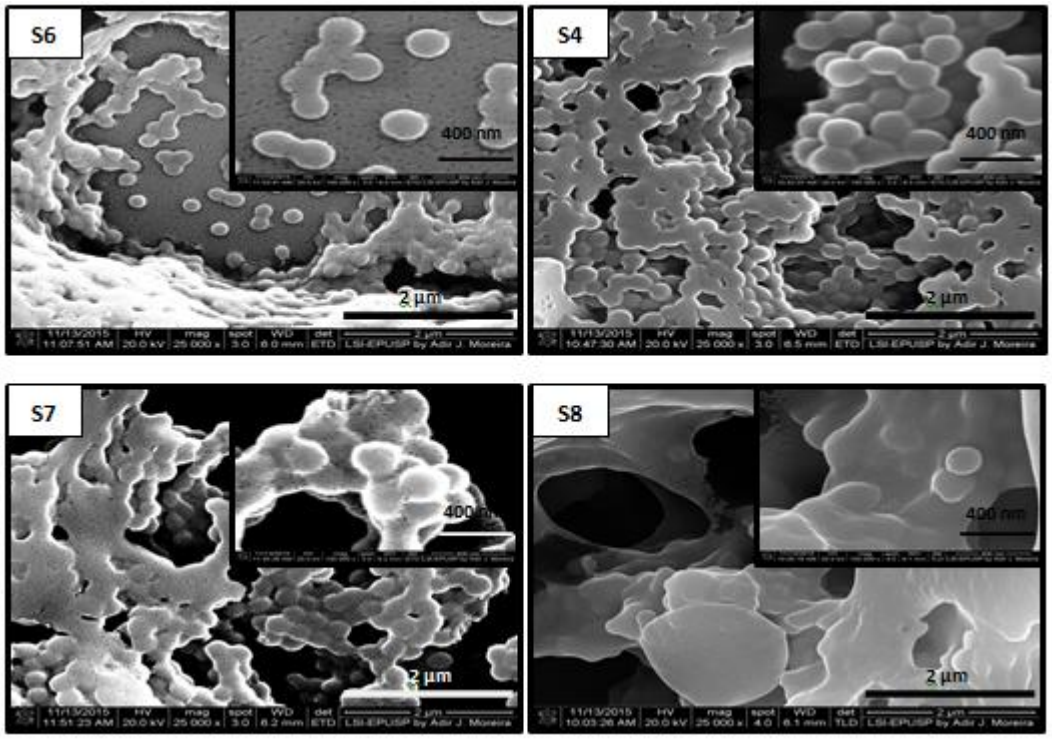

This aggregation behaviour of microgel particles was also confirmed by the size distribution (in number) results obtained by DLS (Figure 4.21), whereas the concentration of AA increases, it is possible to observe a second size distribution of particles with higher values. In the case of sample S8, the results only show one distribution with a size equal to 132 ± 119.8 nm, but according to PDI value (0.476), there is another distribution (maybe out of the range of the equipment) with large particles size, proving that the DLS technique is not the most suitable technique for determining the size of non-spherical particles.

Figure 4.21 – Size distribution by number of microgels with different amount of AA. AA molar concentration in mmol.L^{-1}: S6 (0), S4 (27), S7 (54), and S8 (108).

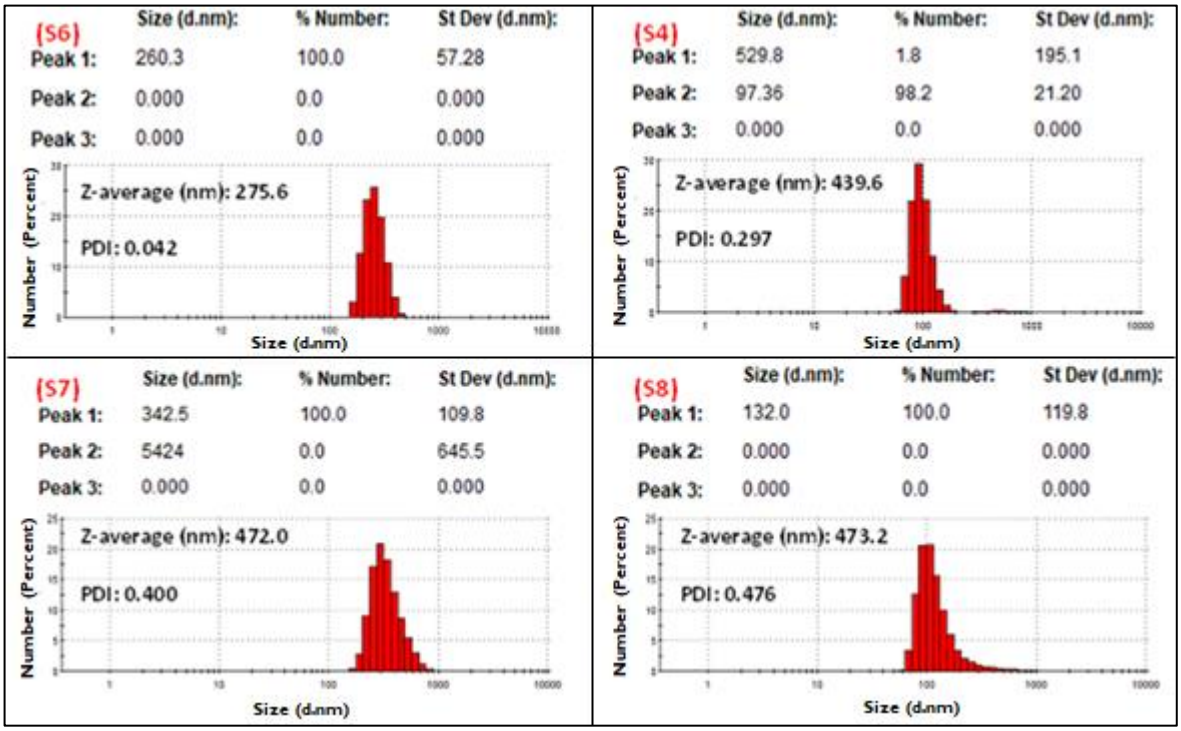

Figure 4.22 shows the micrographs of samples with a different amount between AA and NIPAM monomers. The molar concentration of MBA and KPS is 7 and 5 mmol.L^{-1}, for all samples.

Figure 4.22 - SEM images of microgels with different proportions between AA and NIPAM. AA and NIPAM concentration in mmol.L^{-1}: S2 (133:27), S3 (80:80), S4 (27:133), and S5 (0:160). The concentration of MBA and KPS is 7 and 5 mmol.L^{-1} for all samples.

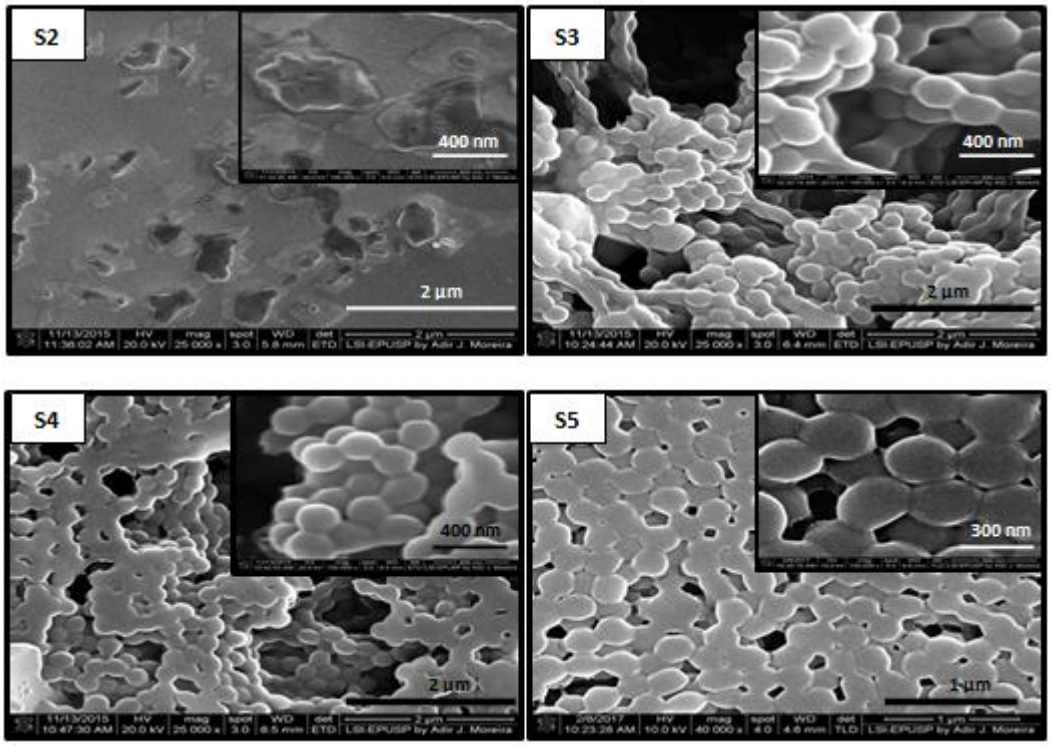

Based on the images shown in Figure 4.22, it can be seen that the microgels produced with 133 mmol.L^{-1} of AA and 27 mmol.L^{-1} of NIPAM (S2) have a non-spherical morphology and a high polydispersity. As the proportion of AA decreases relative to NIPAM, the formation of more spherical particles with fewer tendencies to aggregation was observed. According to the scale presented in the micrographs, the particles of poly(NIPAM-co-AA) are smaller than those of poly(NIPAM), confirming that by inserting AA together with NIPAM during precipitation polymerization, the oligomers of poly(NIPAM-co-AA) reach the critical size of their chains earlier and precipitate with smaller size, due to the stabilizing effect of AA.

Thus, through these micrographs, it was possible to better understand the influence of the AA and NIPAM monomers on the formation of more spherical and monodisperse particles. In that, NIPAM favours the formation of poly(AA) microgels with more spherical morphology, while AA helps to stabilise poly(NIPAM) oligomers faster, forming particles with smaller sizes. However, despite the stabilising effect of AA on NIPAM microgels, if this monomer is in

excess, it can cause the opposite effect of destabilisation and aggregation of the particles, and when the pH of the polymerisation is lower than the pKa of the polymer the stabilising effect is minimised.

Figure 4.23 shows the micrographs of the microgel particles belong to the full experimental design with variation in the molar concentration of AA (20, 30 and 40 mmol.L^{-1}), MBA (2, 3 and 4 mmol.L^{-1}) and KPS (2.5, 3.75 and 5 mmol.L^{-1}). The molar concentration of NIPAM was equal to 120 mmol.L^{-1} for all samples.

In general, the formulations used in this experimental design produced particles with spherical morphology. However, for some samples (S9, S10, S12 and S14), there is a stronger tendency for aggregation, which can be observed through the formation of a more homogeneous surface, in which boundaries between the particles are not clearly observed. Samples S13 and S15 look to be more monodisperse and with less tendency to aggregate, what agrees with the results of the polydispersity index (PDI) measured by DLS. At 37 °C, the value of PDI was 0.110 and 0.089, respectively.

It is important to say that the micrographs of sample S17 (Figure 4.23), S18, S19, S24, S25 and S26 (Figure 4.24) were analysed by another MEV equipment, for which it was not possible to obtain a good resolution. In this way, these micrographs are present in this work only to reinforce the tendency of precipitation polymerisation of acrylic acid and N-isopropylacrylamide to form spherical particles.

Figure 4.23 - SEM images of microgels belong to full experimental design with variation in AA, MBA and KPS molar concentration.

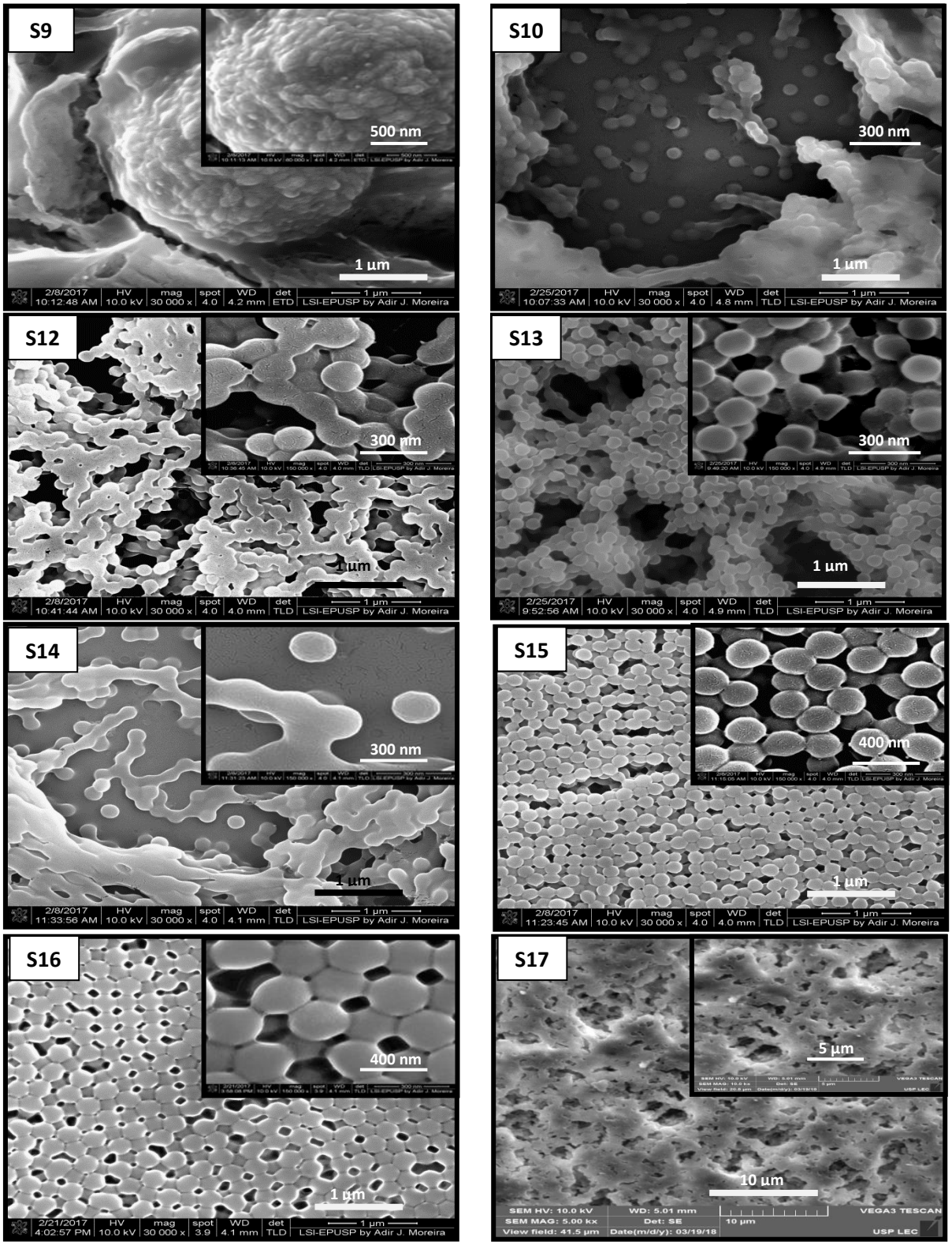

Figure 4.24 - SEM images of microgels belong to fractional experimental design.

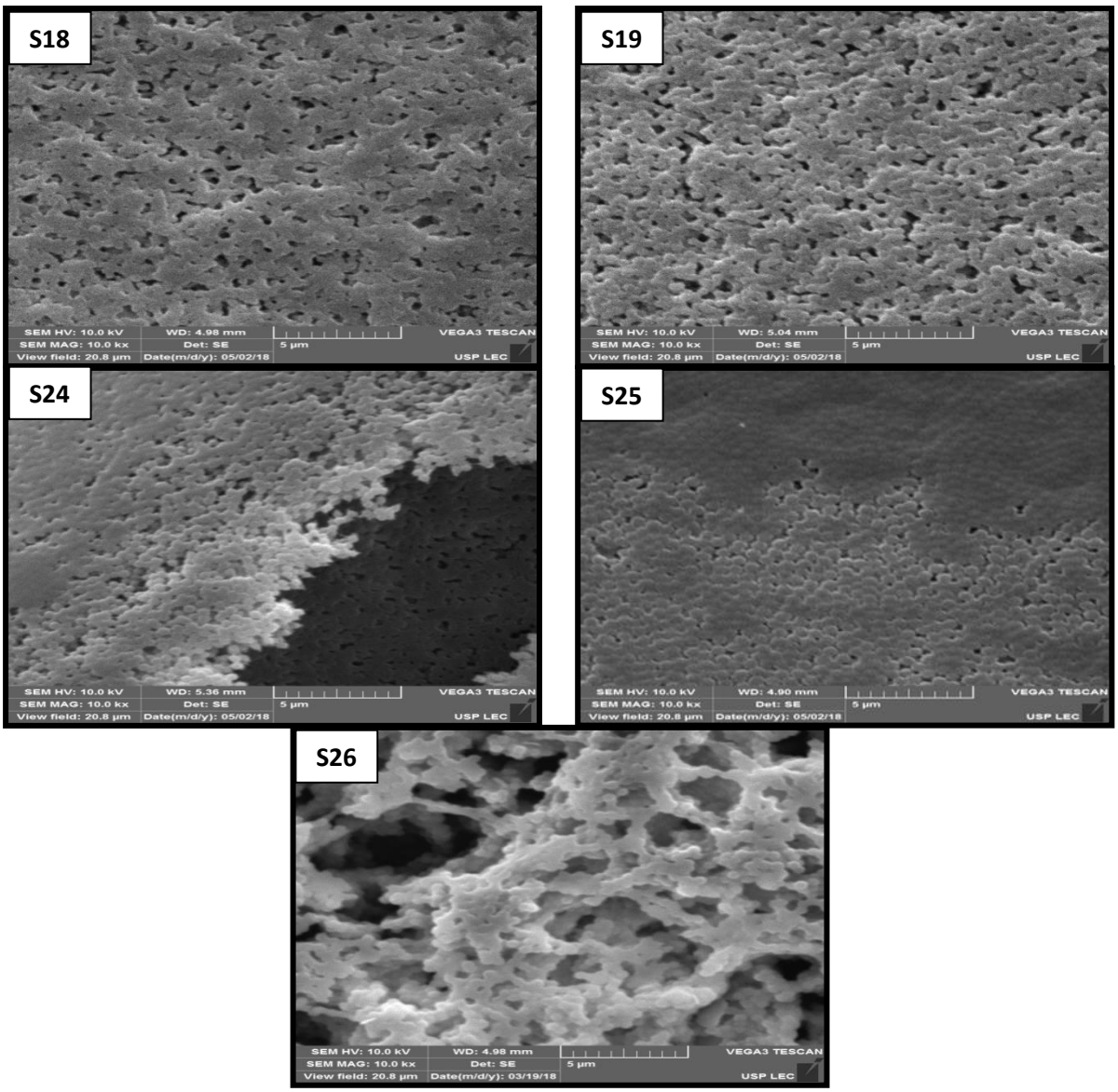

Based on the results presented in this subtopic, it can be seen that, in general, SEM images of the microgels show that the poly(NIPAM-co-AA) particles are spherical, and some formulations have the tendency to aggregate. This aggregation was shown to be stronger, especially when there is a very large amount of AA in relation to NIPAM.

4.3.6. Analysis of the qualitative composition of microgels by FTIR

Fourier transform infrared spectroscopy was used to detect functional groups of the reagents (AA, NIPAM, MBA and Cs) used to synthesise microgel particles.

Figure 4.25 shows the FTIR spectra for the solid reagents used in the production of poly(AA), poly(NIPAM), poly(NIPAM-co-AA) and poly(NIPAM-co-AA)-Cs.

Figure 4.25 – FTIR spectra of the solid reagents (NIPAM, MBA and Cs) used in the production of microgel particles: (A) NIPAM, (B) MBA and (C) Cs.

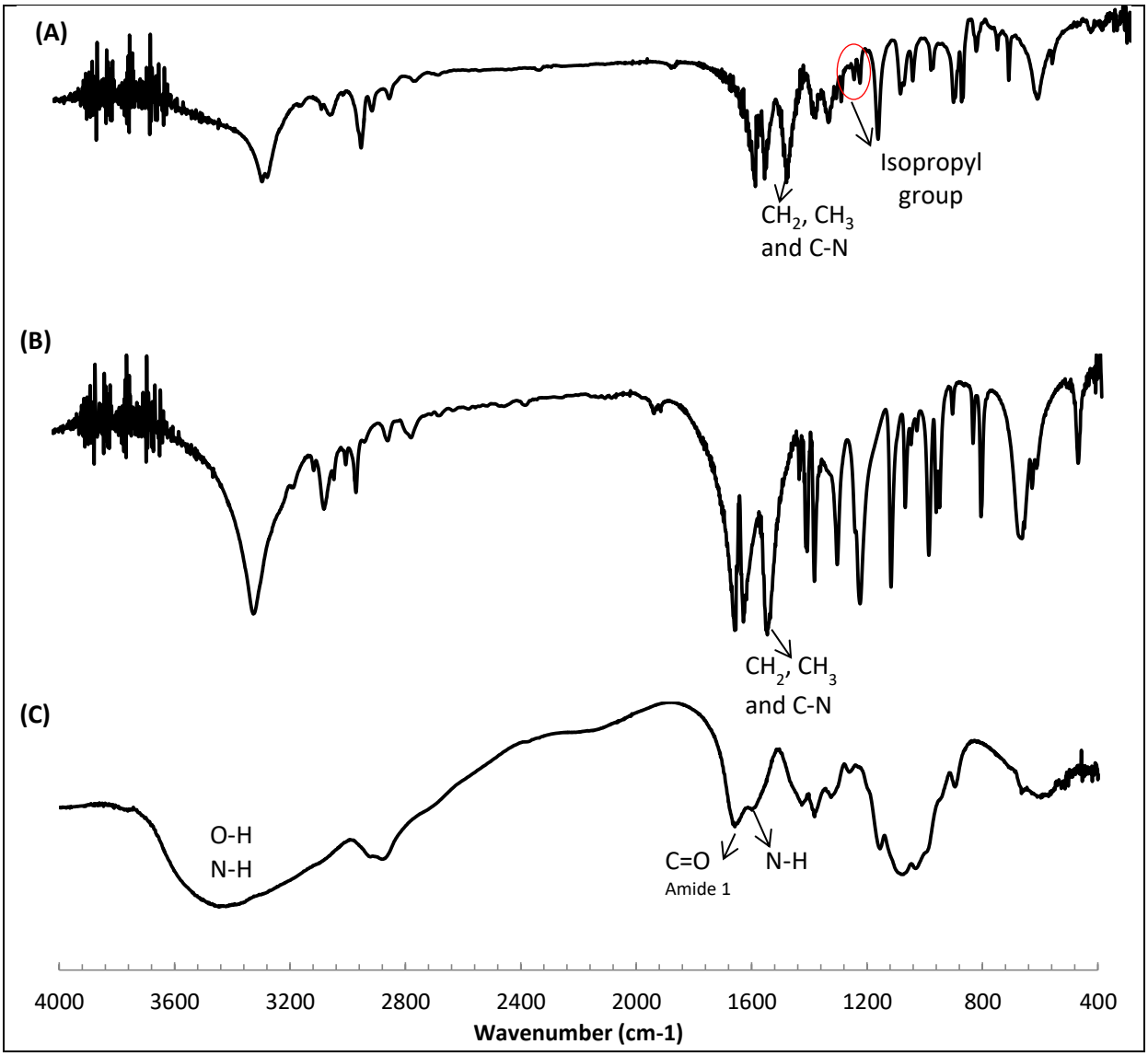

According to Figure 4.25 there is a CH_3 antisymmetric bending, CH_2 scissoring and C-H stretching of amide groups at about 1545 cm^{-1} belonged to NIPAM and MBA. Besides, the NIPAM exhibited two peaks representing the symmetric bend (or umbrella band) of isopropyl groups at 1365 and 1385 cm^{-1} (gem-dimethyl groups). The spectrum of chitosan

displays a broad band around 3400 cm^{-1} that is attributed to overlapped N-H and O-H group stretching vibrations, and peaks at approximately 1645 and 1535 cm^{-1} corresponding to absorptions of C=O stretching (primary amide) and N-H bending, respectively (THOMAS, 1994; MARQUES et al., 2013).

Figure 4.26 illustrates the FTIR spectrum of microgel particles based on AA, NIPAM and Cs. Some samples were selected as representative of all reactions.

In the spectrum of S2, which has a more significant amount of AA, there is a peak at 1710.5 cm^{-1} attributed to the stretching vibration of C=O bond of carboxylic acid, as the amount of NIPAM increases concerning AA, this band practically disappears. Another explanation for this decrease at the vibration frequency of AA peak, it is due to the hydrogen bonding between the carboxylic groups and amide groups of MBA.

The presence of the bands at 1644.25 cm^{-1} to the vibration of the C=O groups can be attributed to the primary amide of NIPAM, MBA and/or Cs. The presence of NIPAM in the microgel particles can also be identified from the double peak at 1387.48 and 1394.07 cm^{-1} related to symmetrical bending vibration and coupling split originating from bimethyl of isopropyl group.

In general, despite the low intensities of some peaks, it can be said that all spectra contain the typical bands of carboxylic acid (stretching peak at 1720 cm^{-1}) and amide groups (1650 cm^{-1}, C=0 stretching; 1540 cm^{-1}, N-H plane bending vibration), confirming the presence of the monomers.

Figure 4.26 - FTIR spectra of microgels particles: (A) S2, (B) S3, (C) S13 and (D) S30.

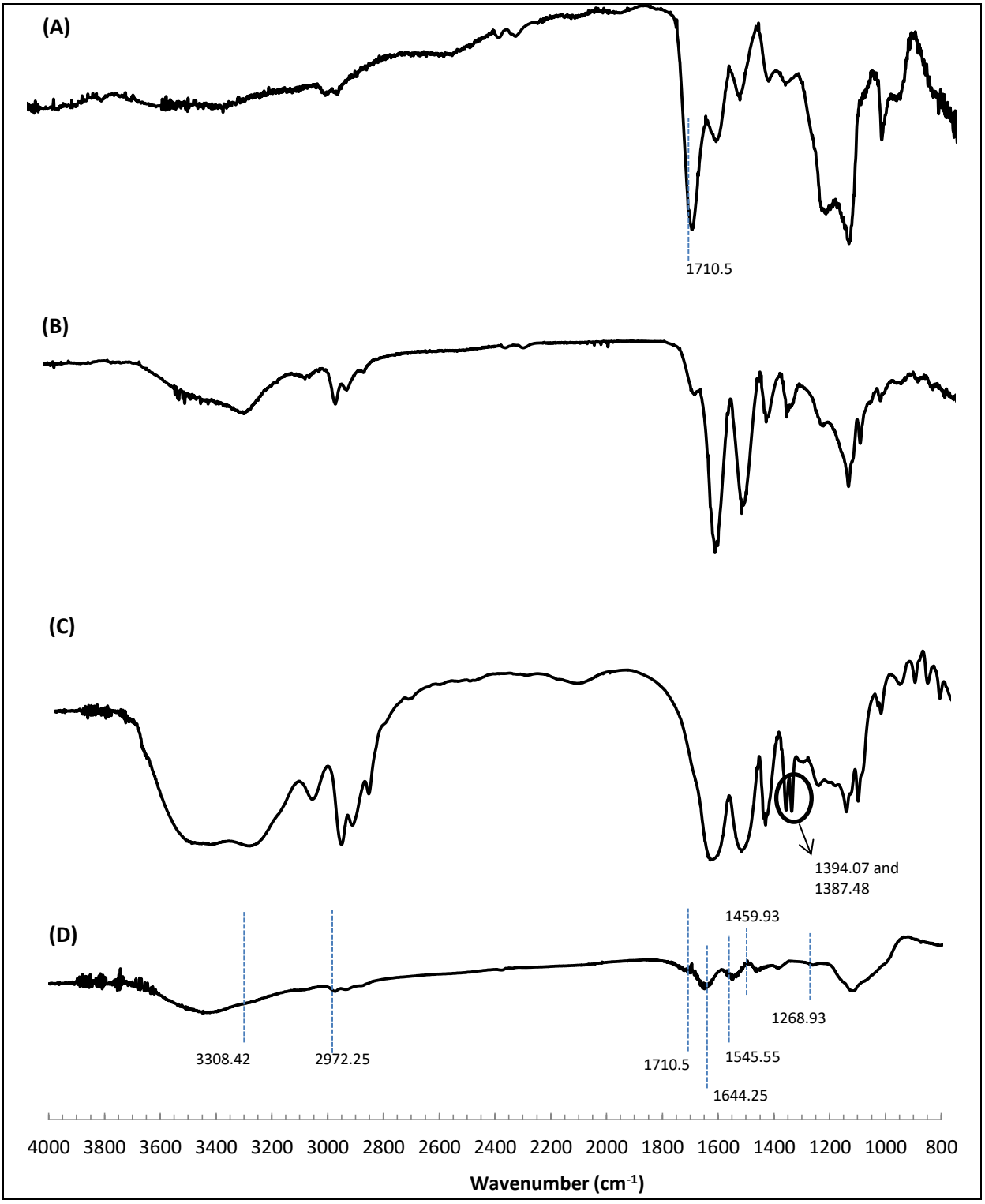

4.3.7. The behaviour of the particles at different temperatures and pHs (Dp and PZ)

The main characteristic of microgel is the capability to change their shape in various media, and understanding the phase behaviour of microgel particles is one of the central points for the application of such systems (BALLAUFF; LU, 2007).

As previously mentioned, acrylic acid microgels exhibit sensitivity to pH, a fundamental property for the desired application (as a drug delivery system for oral administration). However, the poly(acrylic acid) microgels do not present excellent colloidal stability, being able to undergo agglomeration easily; besides that, their particles show a non-spherical morphology. Thus, the strategy used was copolymerised the monomers NIPAM and AA through precipitation polymerisation, thus forming poly(NIPAM-co-AA) microgels. The obtained particles show a spherical morphological, smaller polydispersity and greater stability, dependent on the relation between the amount of the reagents.

Another important factor is that the copolymerisation of AA and NIPAM forms particles sensitive to both pH and temperature, that are the most useful factors in controlling the shrinkage and swelling of microgels, and often applied in the biomedical-pharmaceutical area, such as drug delivery system.

There are many studies about the influence of pH and temperature in poly(NIPAM-co-AA) microgels (SNOWDEN et al., 1996; KRATZ; HELLWEG; EIMER, 2000; ZHANG et al., 2009; FAROOQI et al., 2013). Some studies have been concentrated on the comparison between the influences of hydrophilic monomers in the LCST of NIPAM microgels in different pHs (ZHANG; LIU; ZHA, 2011; FAROOQI et al., 2013). In this study, we focus on the effect of temperature (20-50 °C) and pH (1.5-8.5) in the hydrophilicity/hydrophobicity transition of the poly(NIPAM-co-AA) microgels in water. The results were compared with the literature.

4.3.7.1. Temperature effect on the particle size

Figure 4.27Figure 4.30 exhibit the temperature dependence of the average particle size of microgel particles and their volume phase transition temperature (VPTT). In general, it is possible to observe that when the temperature increases, the particles collapse, adopting a tightly packed structure more like a hard particle such as a poly(styrene) latex (PICH; RICHTERING, 2010; FERNANDEZ-NIEVES et al., 2011). This behaviour results from the temperature dependence of hydrogen bonding and hydrophobic interactions between

polymer chains and solvent. When the temperature increases, the polymer-solvent hydrogen bonds weaken, while the interactions between the hydrophobic isopropyl groups of the polymer become stronger, leading to contraction of the chains (PICH; RICHTERING, 2010; FERNANDEZ-NIEVES et al., 2011).

The point at which the particle switches between swollen and collapsed conformations is known as VPTT. The VPTT is a fundamental physicochemical property reported for microgel particles. At temperatures below the VPTT, the polymer-solvent interactions dominate and water is therefore considered to be a suitable solvent for these microgel particles, and the swollen particles can contain a large volume of water, typically more than 80%, so substantial hydrogen bonding occurs between the solvent and the functional groups (amide) backbones, that is, Van der Walls attraction between the swollen particle is low. Also, some extend outwards from the particle into the solvent, providing steric stabilisation and creating what is known as the hairy layer. Longer -range electrostatic repulsions between the charged groups primarily at the particle surfaces also help to ensure the colloidal stability of the particles in an aqueous medium (GALAEV; MATTIASSON, 2008; PICH; RICHTERING, 2010; FERNANDEZ-NIEVES et al., 2011).

As the temperatures rise above the VPTT, hydrogen bonds between the polymer and solvent are disrupted, and water molecules become poorer solvent for the microgel chains. Hydrophobic interactions between the polymer chains increase, as do inter- and intra-polymer hydrogen bonding, and, together, these lead to the collapse of the particle structure. Electrostatic repulsion between particles increases because the charge density of the surface groups grows as the particles collapse (GALAEV; MATTIASSON, 2008; PICH; RICHTERING, 2010; FERNANDEZ-NIEVES et al., 2011).

In this work, the values of VPTT were obtained by the first derivative (FD) method. FD was calculated from the results of average particle size obtained for each temperature, where the peak on the FD plot represents the point of inflexion of the hydrodynamic diameter *versus* temperature curve and indicates the VPTT of the microgel samples (BALACEANU et al., 2013).

Figure 4.27 shows the temperature dependence of average particles size of pure poly(AA) (sample S1) and pure poly(NIPAM) (Samples S5 and S6).

Figure 4.27 - Average particle size variation in water as a function of temperature and VPTT values. Poly(AA) with 160 mmol.L^{-1} of AA (S1); Poly (NIPAM) with (S5) 160 and (S6) 133 mmol.L^{-1} of NIPAM.

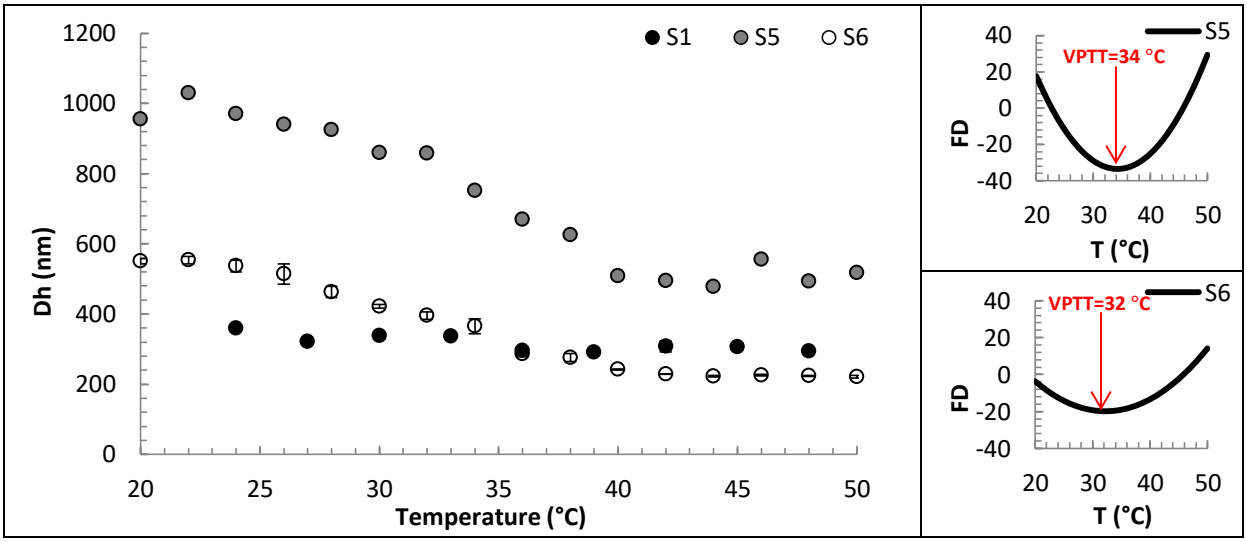

According to results shown in Figure 4.27, the pure poly(AA) microgels (without NIPAM in their composition) are not sensitive to changes in temperature, as expected. It is important to say that the average particle sizes for S1 are only qualitative because they do not represent precisely the particle size of these microgels that are non-spherical particles.

On the other hand, microgels based on NIPAM are known to be temperature-sensitive, with a VPTT around 31-34°C (KRATZ; HELLWEG; EIMER, 2000). Observing the results, samples S5 and S6 exhibit temperature sensitivity, and have VPTT at 34°C and 32°C, respectively, which is in good agreement with the literature (SNOWDEN et al., 1996; KRATZ; HELLWEG; EIMER, 2000). It is also possible to observe that the average particle sizes of S5 are higher than S6, as shown in Table 4.4.

Figure 4.28 and Figure 4.29 compare the influence of the reagent amounts, respectively, AA and MBA, on the average particle size of microgels at different temperatures, and on the VPTT value.

Figure 4.28 - Average particle size variation in water as a function of temperature and VPTT values. Samples with variation in AA concentration in mmol.L^{-1}: (A) S6 (0), S4 (27), S7 (54) and S8 (108); (B) S18 (10), S10 (20) and S40 (40).

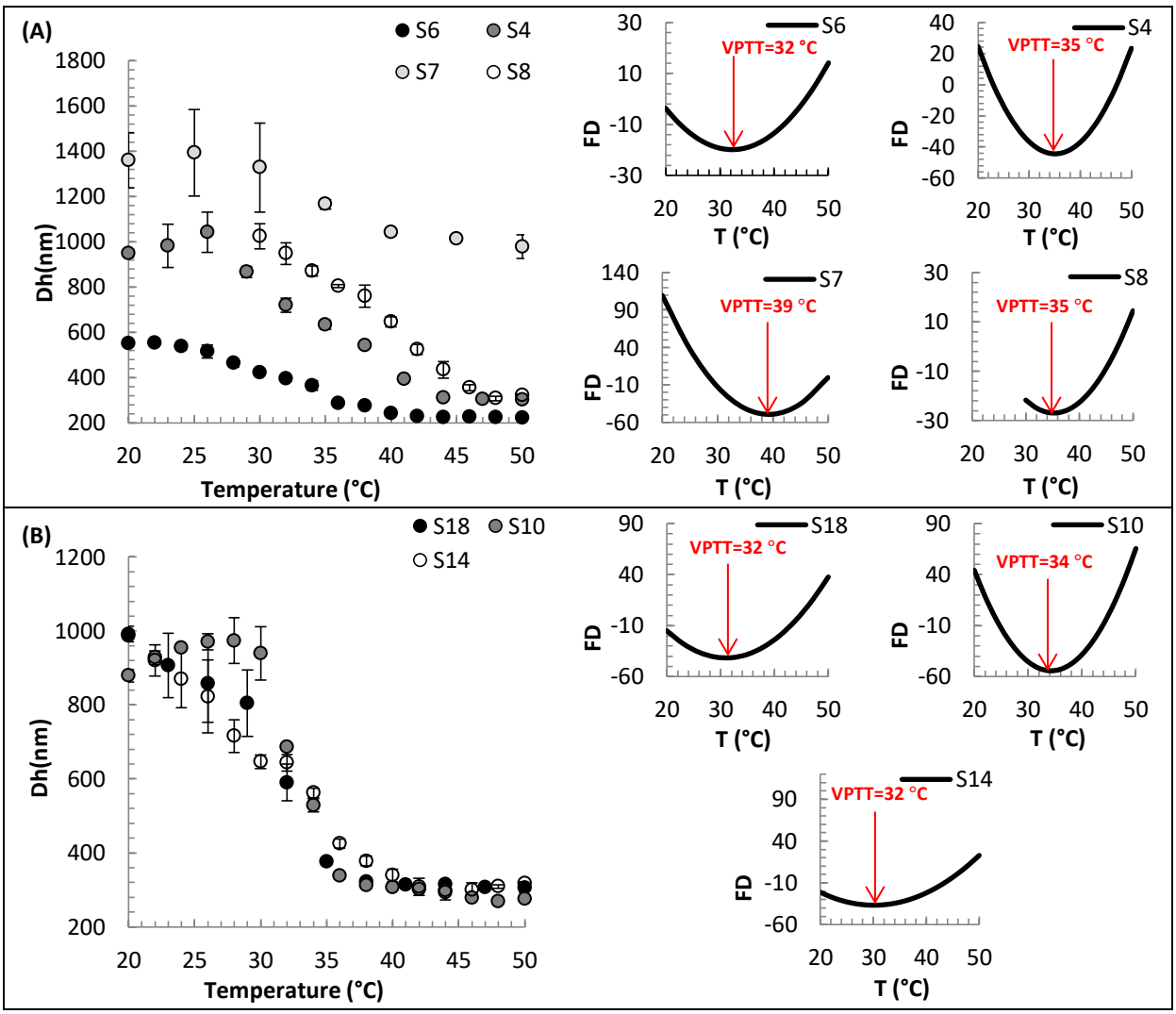

According to Figure 4.28, the VPTT of the samples S6 is centred at 32 °C, as expected. Some samples with AA in their composition showed the VPTT above 32 °C. This slight increase in comparison with linear poly(Nipam) occurs due to the increase in the hydrophilic nature of the microgel particles, which is in good agreement with other publications that showed that the transition temperature increases with the incorporation of ionic groups (ZHANG et al., 2009; SAMAH; HEARD, 2013).

Figure 4.29 - Average particle size variation in water as a function of temperature and VPTT values. Samples with variation in MBA concentration in mmol.L^{-1}: S14 (2.0), S16 (4.0) and S23 (6.0).

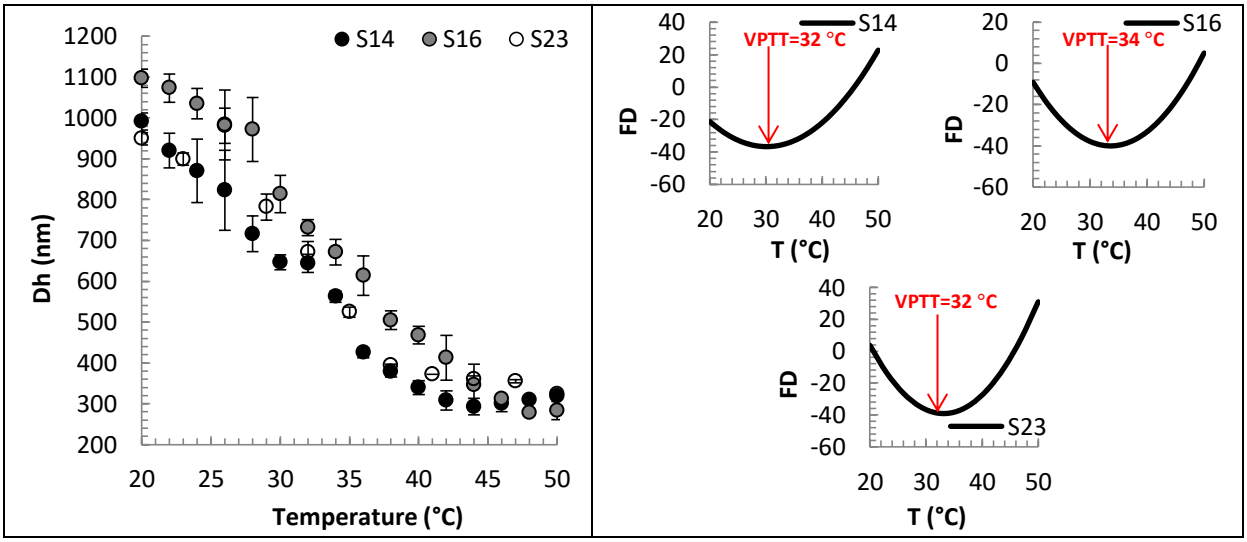

In general, the decrease in the cross-linker agent concentration leads to a significant increase in the swelling behaviour of the particles at temperatures below the VPTT (VARGA et al., 2001; BURMISTROVA et al., 2011; FERNANDEZ-NIEVES et al., 2011). The extent of swelling is mainly controlled by the elasticity of the polymer network, which is directly related to the cross-linker concentration, that is, the swelling ratio of microgels with higher cross-linker content is smaller than that of less cross-linked microgels. Cross-linkers also influence the rate of conformational change, with a higher cross-linking density, ensuring the polymer chains are held more closely together and resulting in more rapid collapse (FERNANDEZ-NIEVES et al., 2011).

Figure 4.30 shows the temperature behaviour of microgel particles with chitosan in their composition.

S29 and S30 show a decrease in the particle size below the VPTT, an increase around the VPTT, and re-decrease above the VPTT. This same behaviour was verified by Jung et al. (2009), which they synthesised nanoparticles based on NIPAAm-AA core and lower molecular weight water-soluble chitosan shell. They explained this increase around the VPTT, which are not observed in poly(NIPAM-co-AA) microgels, may due to some nanoparticles aggregation caused by PNIPAAm polymer chair shrinkage.

Figure 4.30 - Average particle size variation in water as a function of the temperature. Samples with variation in Cs amount in grams: S9 (0.00), S27 (0.03), S28 (0.06), S29 (0.12) and S30 (0.24).

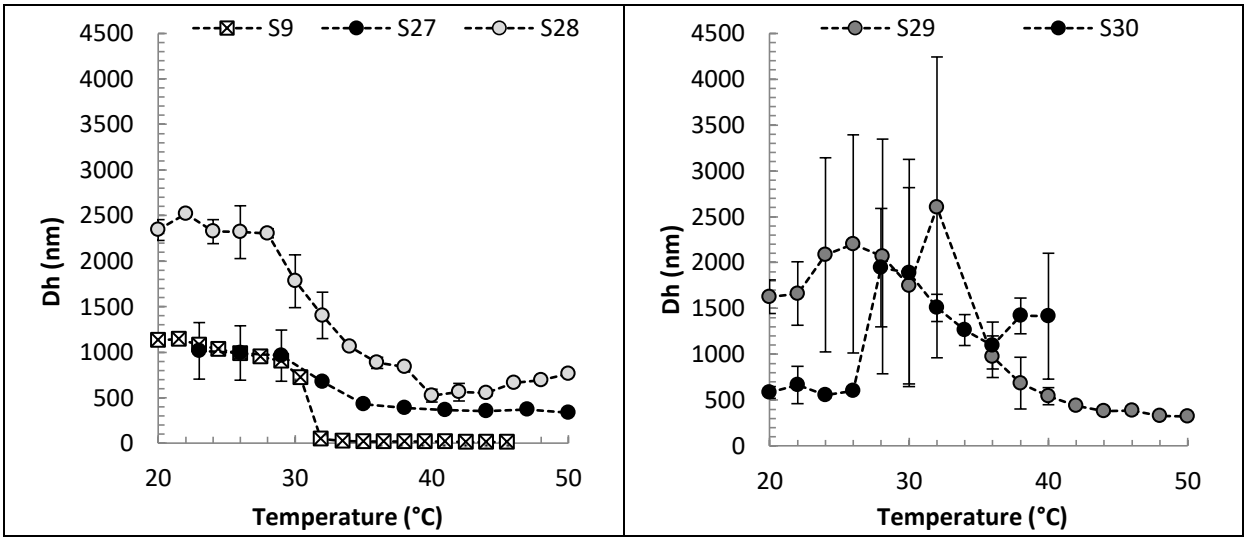

4.3.7.2. pH effect on the particle size and zeta potential

Swelling of the polymer in response to the external pH plays a significant role in the drug release kinetics (SHAH; PATEL, 2014). For the microgels compound for the anionic monomer, the dependence of swelling behaviour on pH is largely derived from the long-range electrostatic interactions among the ionic functional groups (CHEN, 2015).

For example, for microgels based on acrylic acid monomer (pKa of carboxylic groups, approximate 4.2), when exposed in an acidic environment (pH values below the pKa of the carboxylic groups), they are in the molecular state and become hydrophobic due to the formation of hydrogen bonds between the polymer chain, which causes shrinkage of the particles, in turn, restrict the release of the drug in the medium. On the other hand, in alkaline medium (above the pKa of the carboxylic groups), the carboxylic acid groups (-C00H) became progressively more ionised ($-COO^-$). In this case, hydration of the microgels increased due to a large swelling force created by the electrostatic repulsive forces, and the drug is released (JABBARI; NOZARI, 2000; SHAH; AGRAWAL; PARIKH, 2010; SAMAH; HEARD, 2013).

The microgel particles developed in this work were designed as a potential drug delivery system for oral administration. The results shown in this subtopic are focused on the

understanding of the pH dependence (1.5-8.5) of the average particle size (hydrodynamic diameter) and zeta potential of the poly(NIPAM-co-AA) microgel particles at 37 °C.

One of the main factors influencing the value of the zeta potential of the particles is the pH of the medium in which they are dispersed. As poly(NIPAM-co-AA) is stabilised by sulphate and carboxylic groups, and their carboxylic acid group are weakly acidic, the ionisation degree depends on the pH of the medium and thus can be evaluated by zeta potential. Through the construction of the zeta potential curve as a function of pH, it is possible to identify the isoelectric point of the particles. The isoelectric point is the pH at which the particles have an electric charge equal to 0; that is, there is a balance between positive and negative charges (MALVERN INSTRUMENTS LIMITED, 2016). In this way, it is possible to identify the best pH range to work, so that the particles are as stable as possible.

Figure 4.31 shows the influence of pH in the average particle size and zeta potential of microgel poly(NIPAM-co-AA) with different AA concentrations.

According to Figure 4.31, the increase in the acrylic acid concentration in the structure of microgel particles strongly affects the swelling behaviour with increasing pH. For samples S14, S15 and S16 that have higher concentration of AA (40 $mmol.L^{-1}$), this swelling force is more evident due to the high concentration of free ions within the ionic network and the surrounding solution that causing a high electrostatic repulsion between the ionised acid groups and the osmotic pressure (JAFARI; MODARRESS, 2005; SAMAH; HEARD, 2013).

In the case of S14, there is a slight decrease in average particle size at pH value 7 and 8; this behaviour may be due to the electrostatic screening effect between the ionised carboxylic groups resulting from high OH- concentration due to the additional NaOH. Similar effects have been observed by Kratz and co-workers (2000) and Zhang and co-workers (2009).

Another different behaviour about average particle size was observed at pH value 1.5 and 3.5; on what the microgel particles show a higher size. In this case, the greater sizes are not caused by swelling, but probably, by the aggregation of the particles (inter-particle interactions) due to the higher hydrophobicity of the system. This hydrophobicity is caused due to the low pH, and temperature above the VPTT of the particles (microgel are in the collapsed state). This phenomenon has been verified in other studies presented in the literature (KRATZ; HELLWEG; EIMER, 2000; FAROOQI et al., 2013).

Figure 4.31 - Evaluation of the influence of AA concentration in the average particle size and zeta potential of poly(NIPAM-co-AA) at different pHs. Samples formulation: (A) S18, S10 and S14 have the following AA concentration 10, 20, 40 mmol.L^{-1}, respectively. The samples have MBA and KPS concentration equal to 2 and 5 mmol.L^{-1}, respectively. (B) S11 and S15 have the following AA concentration 10 and 20, respectively. The samples have MBA and KPS concentration equal to 4 and 2.5 mmol.L^{-1}, respectively. (C) S12 and S16 have the following AA concentration 10 and 20, respectively. The samples have MBA and KPS concentration equal to 4 and 5 mmol.L^{-1}, respectively. All samples have NIPAM concentration equal to 120 mmol.L^{-1}.

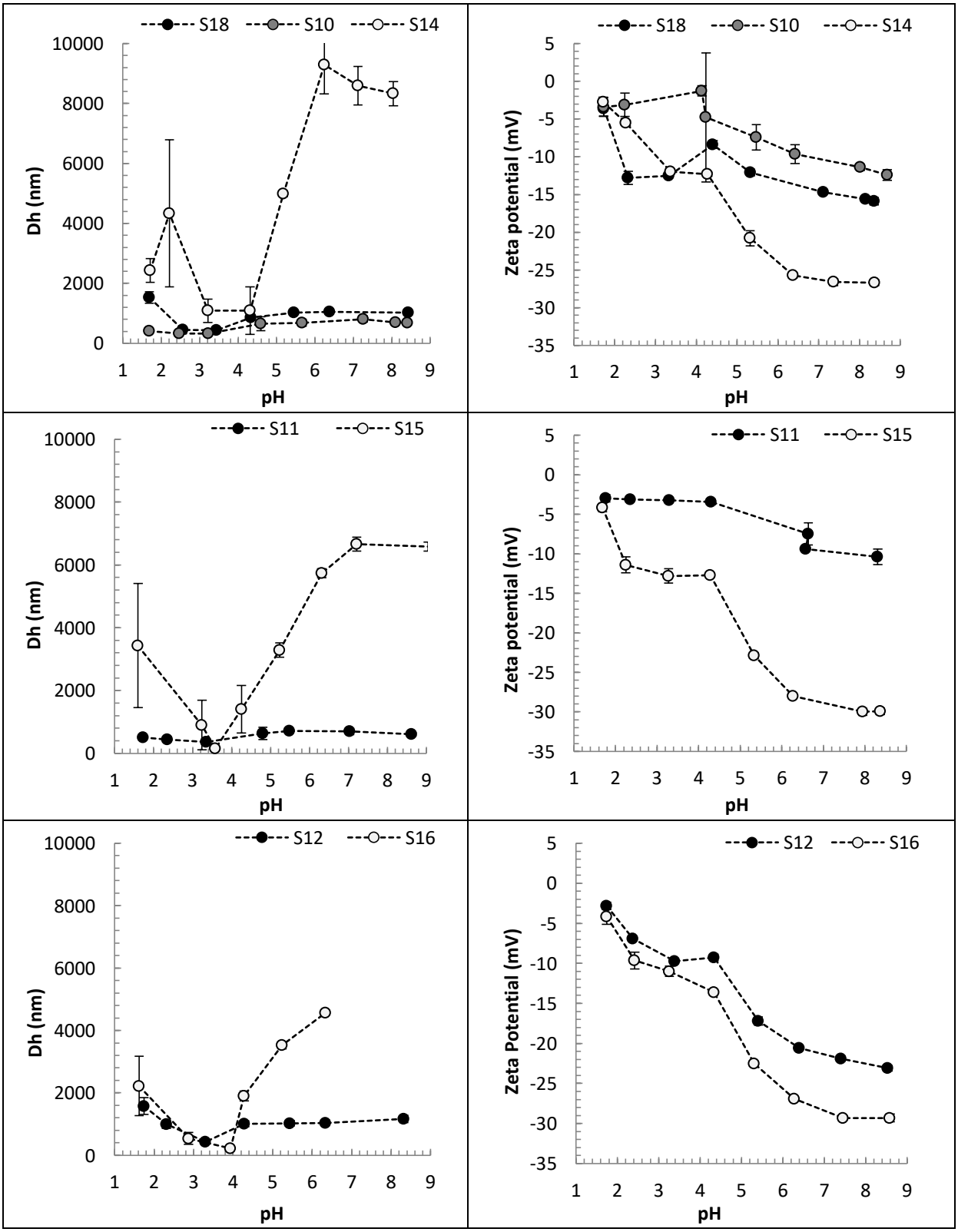

Furthermore, the AA concentration also showed to has influenced the size of the aggregates. The larger the amount of AA, the larger the average particle size measured by DLS. A reasonable explanation for this effect was given by Kratz et al. (2000) that take into account inter-particle hydrogen bonding interactions between the carboxyl group of the AA side chain and the amide group of NIPAM, which can exist only in the neutral form of the carboxylic moiety. The increasing amount of AA allows for more hydrogen bonds with NIPAM side chains, which seems to favour larger aggregates.

About the zeta potential results, it is possible to observe that they follow the behaviour of the average particle size. In this case, as the pH increases and the particles swell, the zeta potential also increases. This means that in the fully swollen state, the dispersion of microgel particles are more stable. This stability occurs due to the weakening of the Van der Waals attraction between the particles (SAUNDERS; VINCENT, 1999).

Figure 4.32 shows the influence of pH in the average particle size and zeta potential of microgel poly(NIPAM-co-AA) with different NIPAM concentrations.

Figure 4.32 - Evaluation of the influence of NIPAM concentration in the average particle size and zeta potential of poly(NIPAM-co-AA) at different pHs. Samples formulation: S14 and S24 have the following NIPAM concentration 120 and 200 mmol.L^{-1}, respectively. The samples have AA, MBA and KPS concentration equal to 40, 2 and 5 mmol.L^{-1}, respectively.

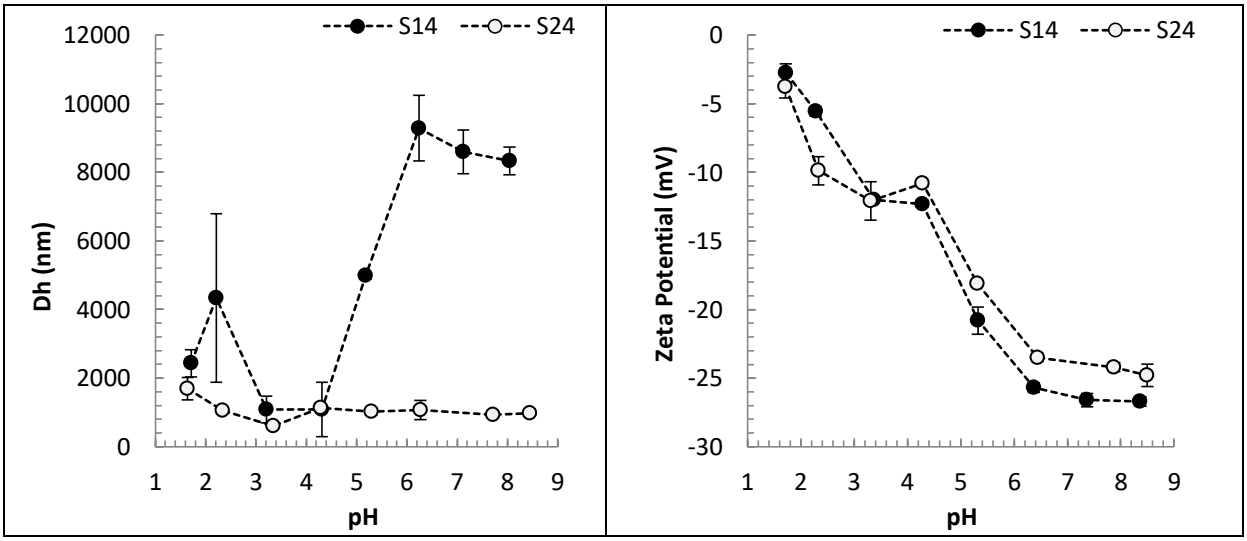

According to the results shown in Figure 4.32, the increase in NIPAM amount resulted in a decrease in the swelling behaviour of microgel particles at higher pHs, due to the presence of less AA in comparison with NIPAM. About the zeta potential, as AA and KPS are the

reagents that provide the negative charges, variation in the zeta potential values does not occur with an increase in the NIPAM concentration, as expected.

Figure 4.33 shows the influence of pH on the particle size and potential zeta on the microgel particles with a variation between AA and NIPAM concentration.

Figure 4.33 - Average particle size and zeta potential of microgel particles with different proportion between AA and NIPAM.

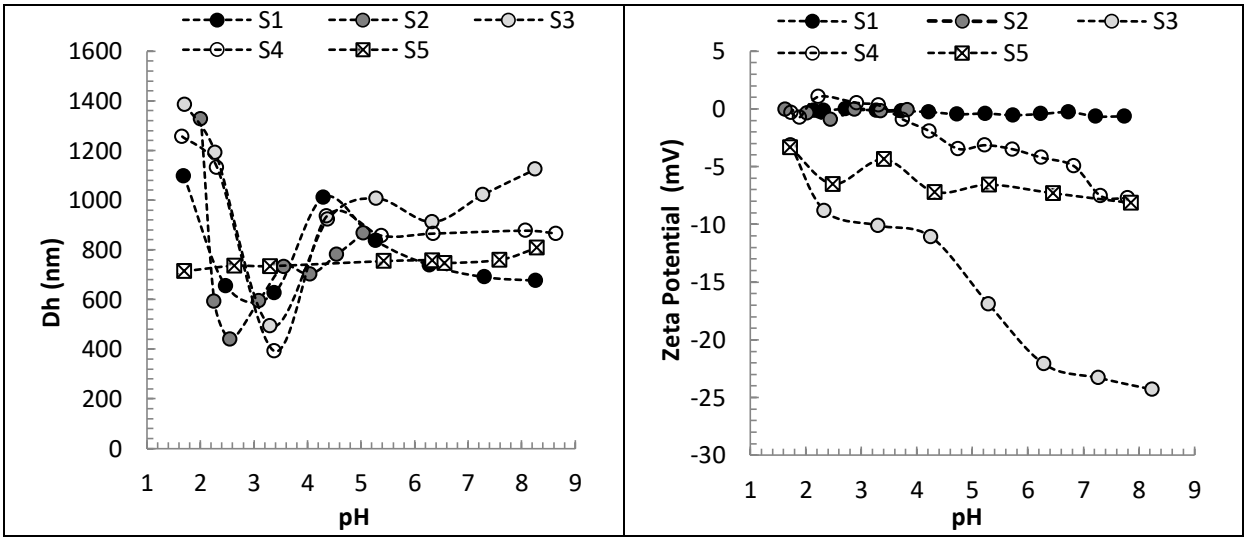

In Figure 4.33, it can be observed that the microgel without AA in its composition (S5) does not show swelling behaviour as the pH increases, confirming that microgels composed only of NIPAM monomer are not pH sensitive. On the other hand, microgel particles with AA in their composition show an increase in their size as the pH increases. In the case of samples S1 and S2, although they are pH-sensitive, the results are only qualitative, due to the imprecision in the DLS analyses in non-spherical and higher polydispersity particles.

All samples were found to have negative values of zeta potential due to the dissociation of the carboxylic acid groups at the surface of the particles. In samples S1 and S2, the pH did not have a significant influence on the zeta potential of the microgel particles for the whole pH range analysed, the poly(AA) microgels have their zeta potential always close to 0. On the other hand, for the samples S3 and S4, that has NIPAM amount equal to and/or above the AA molar concentration, it is observed that above pH 4.0-4.5 the absolute value of the zeta potential begins to increase, confirming that the proper union of the NIPAM and AA monomers confers better stability to the particles.

Figure 4.34 compares the pH behaviour of microgels with different crosslinked concentration.

Figure 4.34 - Evaluation of the influence of MBA concentration in the average particle size and zeta potential of poly(NIPAM-co-AA) at different pHs. Samples formulation: (A) S10 and S12 have the following MBA concentration: 2 and 4 mmol.L^{-1}, respectively. The samples have AA and KPS concentration equal to 20 and 5 mmol.L^{-1}, respectively; (B) S14, S16 and S23 have the following MBA concentration 2, 4 and 6, respectively. The samples have AA and KPS concentration equal to 40 and 5 mmol.L^{-1}, respectively. All samples have NIPAM concentration equal to 120 mmol.L^{-1}.

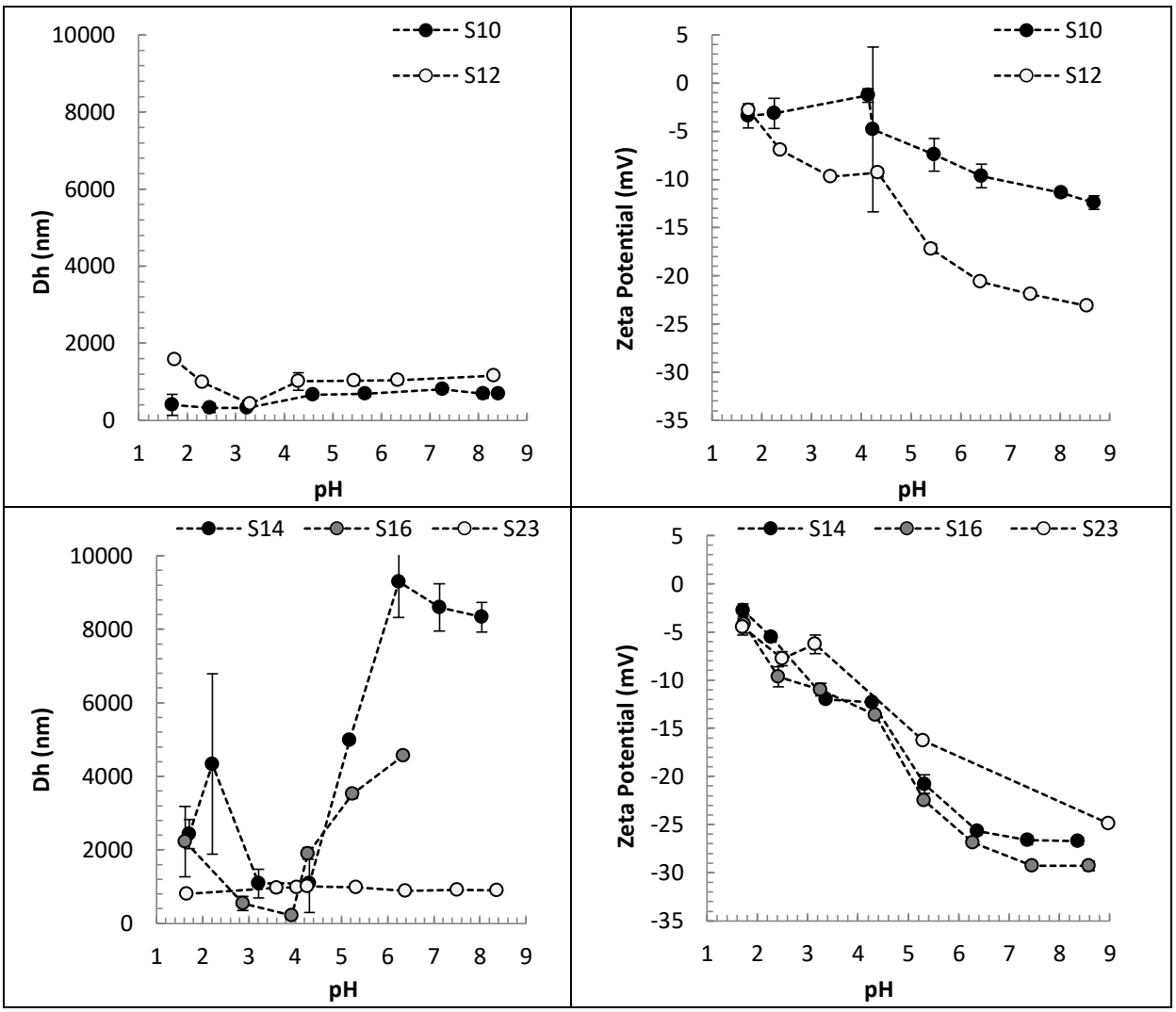

Comparing samples S14, S16 and S23, the swelling was observed to decrease with increasing of MBA concentration, which was attributed to the topological constraints introduced by an increasing number of crosslinking points, raising the rigidity of polymer structure. In the case of samples S10 and S12, it is not observed a significant difference in the swelling behaviour between the concentrations studied.

Figure 4.35 shows the pH behaviour of formulation with different KPS concentration.

Figure 4.35 – Evaluation of the influence of KPS concentration in the average particle size and zeta potential of poly(NIPAM-co-AA) at different pHs. Samples formulation: (A) S11 and S12 have the following KPS concentration of 2.5 and 5 mmol.L^{-1}, respectively. The samples have AA and MBA concentration equal to 20 and 4 mmol.L^{-1}, respectively; (B) S14 and S22 have the following KPS concentration 5 and 10 mmol.L^{-1}, respectively. The samples have AA and MBA concentration equal to 40 and 2 mmol.L^{-1}, respectively. (C) S15 and S16 have the following KPS concentration 2.5 and 5, respectively. The samples have AA and MBA concentration equal to 40 and 4 mmol.L^{-1}, respectively. All samples have 120 mmol.L^{-1} of NIPAM.

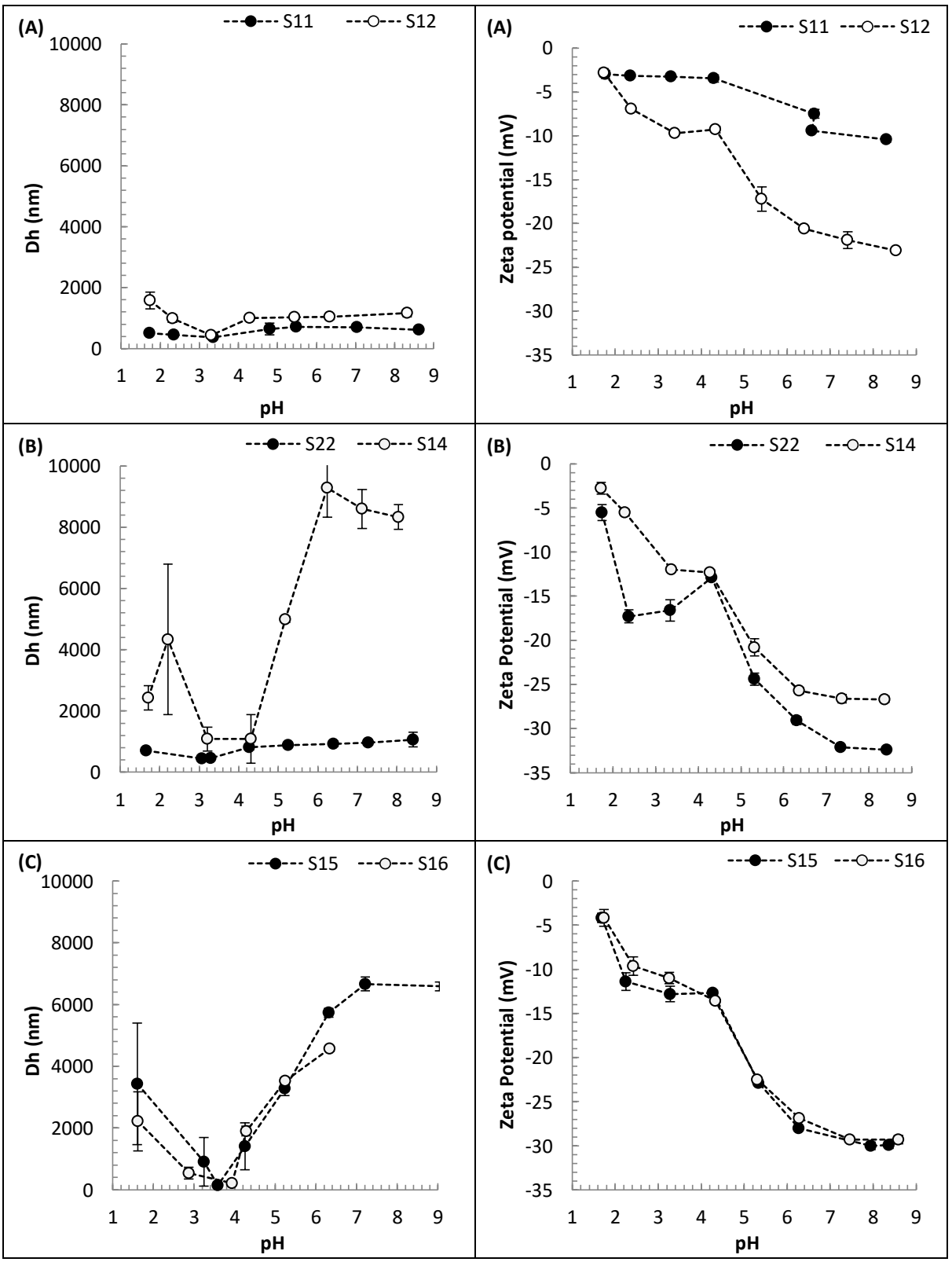

Samples produced with higher KPS concentration showed better swelling behaviour than samples with less KPS in their formulation, probably because the KPS not only initiates polymerisation as well as acts as the source of charge required to stabilise the particles (GAO; FRISKEN, 2003). Consequently, particles can be stabilised earlier and with less MBA in their structure, increasing the swelling capability.

Figure 4.36 – Average particle size and zeta potential of microgel particles with different amount of Cs.

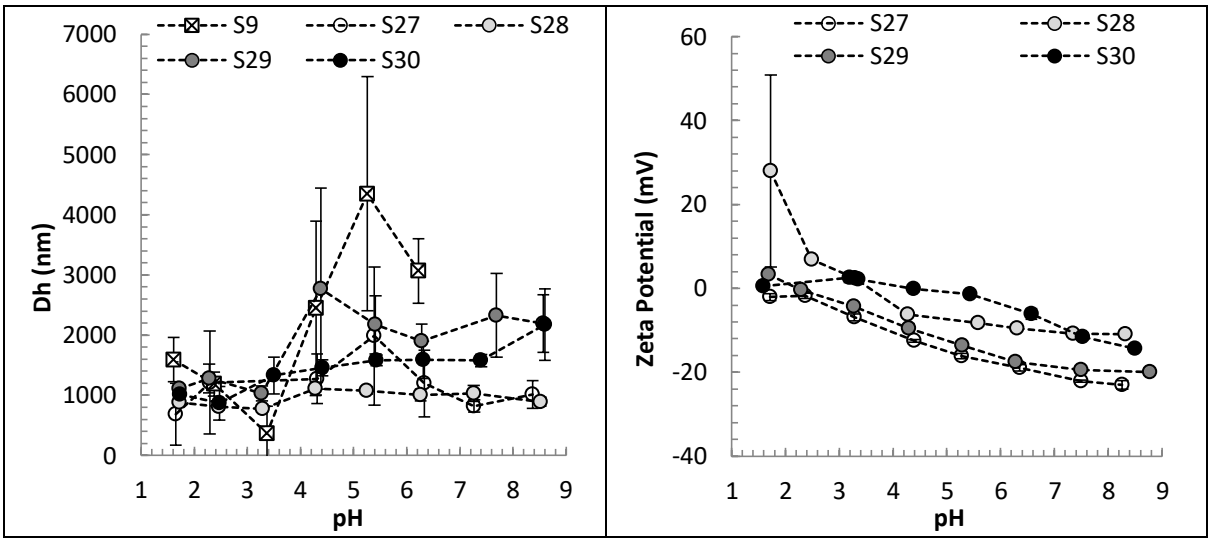

According to results about the influence of Cs in the swelling behaviour of poly(NIPAM-co-AA)-Cs at different pHs, it is possible to conclude that the presence of Cs diminishes the swelling ratio in alkaline mediums, and gives more stability. This stability at high pH values is caused by the rigidity of the polysaccharide chain that is chemically bound to the polymer network, due to the deprotonated state of the Cs amine groups (MARQUES et al., 2013).

According to the previous studies about the average particle size, polydispersity index and particle morphology that taking into account the features needs for an oral carrier that should be a size between 100 to 1000 nm, a PDI up to 0.2 and a spherical morphology, the formulations suitable for the desired application were S13, S15, S17-S25. However, samples S13, S20, S23 and S25 did not show proper sensitivity to pH (Figure 4.37), being necessary to discard them as potential particles for oral administration.

In general, according to the results shown in this subtopic, we can conclude that the poly(NIPAM-co-AA) microgel particles exhibited good pH and temperature-sensitivity, and

the majority of the particles presented stability in the pH range from 3.5 to 8.5 at 37°C. As expected, the particle size tends to increase upon increasing the pH of the external medium.

Figure 4.37 – Poly(NIPAM-co-AA) microgel particles with poor pH sensibility.

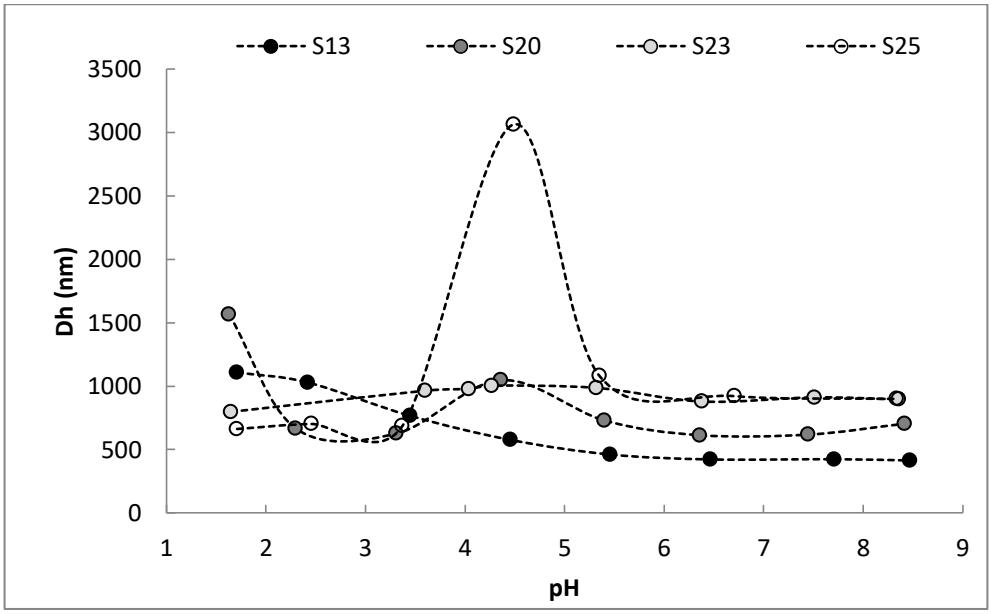

4.3.8. Stability behaviour of the microgels at the storage time

Regardless of the preparation method, the microgel particles are obtained in the form of aqueous colloidal suspensions. Despite the good stability of the final product, during the storage time, the particles can aggregate, resulting in the formation of precipitates. The consequence of this limited physicochemical stability, as a function of storage time, is an obstacle to the industrial applicability of aqueous suspensions of nanoparticles (SCHAFFAZICK et al., 2003).

Thus, monitoring the effect of the storage time of the microgel particles on their stability becomes necessary. In this work, the stability of the microgels was monitored following the size, size distribution and zeta potential of the particles, and the pH of the suspension medium at predetermined times during storage, for a total of 180 days.

Figure 4.38-Figure 4.41 show changes in the physicochemical parameters during the storage time for samples suitable for oral administration of the drug.

Figure 4.38 shows the average particle size of poly(NIPAM-co-AA), and it can be seen that the samples did not suffer significant variation in their size comparing the size in the beginning and at the end of the 180 days of storage.

Figure 4.38 – Average particle size (D_H) of microgel particles during the storage time.

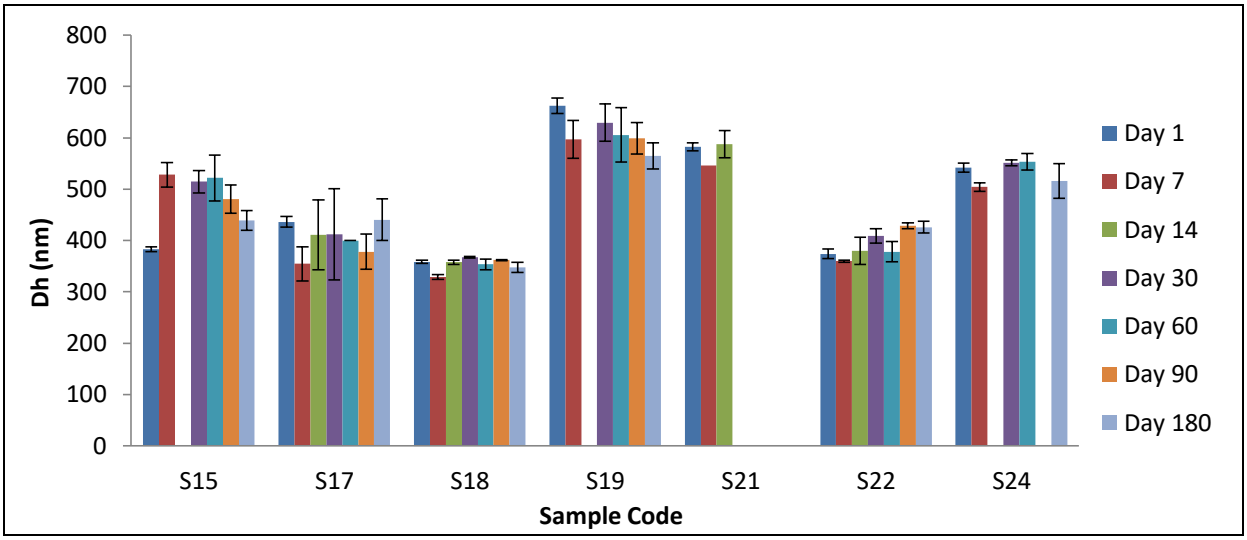

As important as the average value of the particle size is the value of the polydispersity of the particle distribution. The homogeneity in the mean diameter of the particles can be evaluated through the polydispersity index, which indicates the broadness of the particle size distribution, and values smaller than 0.2 are considered good indicators of homogeneity.

Figure 4.39 shows the polydispersity index of poly(NIPAM-co-AA) microgel particles during the storage time. In general, despite the high standard deviation for some samples, they remain with PDI values within the acceptable range to be considered particles with narrow polydispersity.

Figure 4.39 – Polydispersity index (PDI) of microgel particles during the storage time.

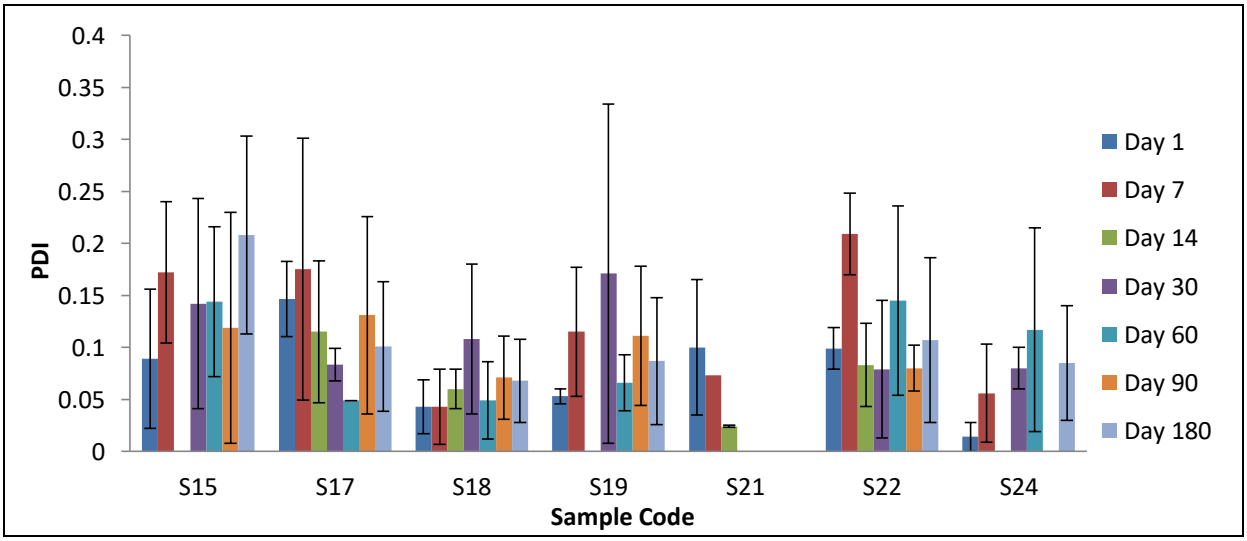

Figure 4.40 presents the zeta potential for microgel particles during storage time.

Figure 4.40 – Zeta potential (ZP) of microgel particles during the storage time.

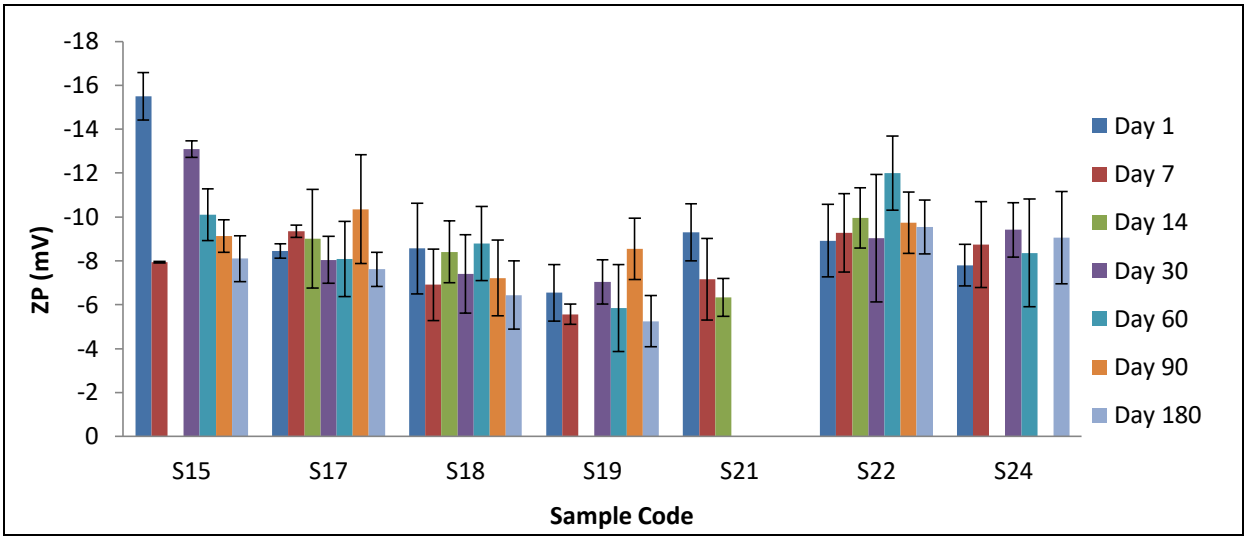

Despite some differences in the absolute value of the zeta potential, it remained negative for all the monitored samples, indicating that even during storage the residual charge of the acrylic acid chains present on the surface of the particles continued negative. In general, except for sample S15, the zeta potential values remain practically constant during the storage time.

Finally, according to Figure 4.41, the pH of the microgel suspension did not suffer significant variations, remaining with pH values between 2.0 and 3.0.

Figure 4.41 – pH of microgel suspensions during the storage time.

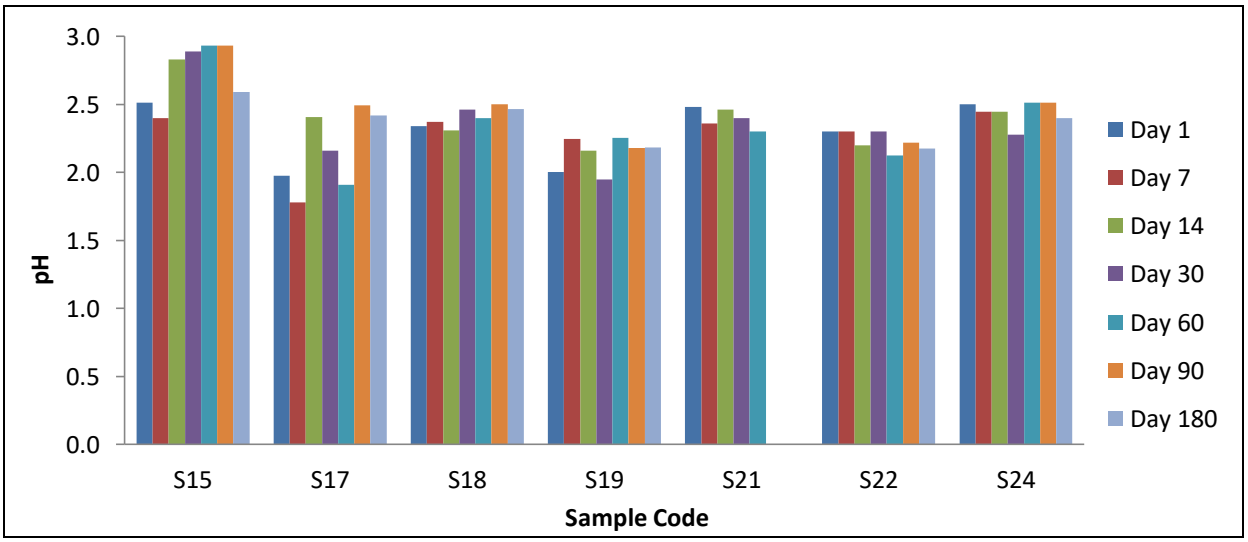

In conclusion, taking into account the results obtained, it was observed that the poly(NIPAM-co-AA) physicochemical characteristics monitored during the storage time suffering slight variations. Thus, the selected samples (S15, S17-S19, S21, S22 and S24) may be considered to have a suitable formulation for maintaining the stability of the colloidal dispersion without the formation of aggregates or precipitates.

4.4. Partial Conclusions

The understanding of the physicochemical behaviour of the polymer particle is the subject of numerous researches. However, when particles are small in size, difficulties are encountered for their fair characterisation. Thus, the physicochemical characterisation of these particles is only possible by combining several analytical techniques.

In this chapter, we characterised microgel particles about their size, size distribution, zeta potential, pH of the suspension, morphology, qualitative composition, swelling behaviour in different temperatures and pHs, and stability at the storage time. For this, the analytical techniques used were Dynamic Light Scattering (DLS), Electrophoretic Light Scattering (ELS), Scanning Electron Microscopy (SEM) and Fourier Transform Infrared (FTIR) spectroscopy.

The results showed that the poly(NIPAM-co-AA) microgel particles synthesised in this work and analysed by DLS at 37 °C have an average size from 280 to 680 nm, and a polydispersity index between 0.01 and 0.48. The zeta potential charges showed to be negative for all samples, and the pH varied from 2.0 to 3.0. Samples with chitosan in their formulation show higher size and broader polydispersity. In particular, for sample S30 that has a higher amount of chitosan, a cationic biopolymer, the zeta potential was positive, and the pH of microgel suspension was less acidic.

The micrographs obtained by MEV revealed that the microgel particles are spherical and have low dispersity in their size. However, for samples with higher amount of AA, it was observed a tendency to aggregate. This aggregation was better visualised in S7 and S8, where at some points of the samples, the formation of more homogeneous surface occurs, in which the visualisation of the boundaries between the particles became difficult. For the formulation with higher AA amount than NIPAM (S2), the particles did not have a spherical morphology and showed high polydispersity. The FTIR spectra proved the presence of the monomers in the microgels structure, which were identified through bands characteristics of

the functional groups belonging to acrylic acid (C=O), and to NIPAM (C=O, N-H and isopropyl group).

The study of the swelling behaviour in different mediums verified the sensibility of the microgel particles to both temperature and pH. The poly(NIPAM-co-AA) microgels showed a decrease in their size with the increase in temperature, and a VPTT around 32 and 34 °C. In some case, the presence of AA showed increases the VPTT. About the behaviour of microgel particles at different pHs, the poly(NIPAM-co-AA) particles showed an increase in the average particle size and zeta potential as the pH increased, being that the majority of the particles have stability in the pH range from 3.5 to 8.5 at 37°C. However, at low pH (1.5-3.5), a higher hydrophobicity of the system manifested due to the combination with the temperature above the VPTT of the microgels, and the particles tended to aggregate. The monitoring of the stability of the particles showed that the selected microgels did not have variations in their physicochemical characteristics during the storage time.

It was observed that the concentration of the reagents has a significant influence in physicochemical characteristics of microgel particles based on AA, NIPAM and CS, and having MBA and KPS as cross-linker agent and initiator, respectively. The amount of AA showed to have two different effects in the average particle size of the microgels that are dependent on its concentration, and the concentration of other polymerisation reagents. The results also showed that higher the amounts of NIPAM and KPS, higher the average particle size. For MBA, the effect was the same for some formulations, but in other cases, the increase in MBA amount did not affect the average particle size. The presence of chitosan caused some instability and, consequently, aggregation of the particles.

Some reagents also showed to influence the swelling capacity of the particles in basic medium; the increase in acrylic acid concentration showed strongly effect in the swelling ratio due to the high concentration of free ions within the ionic network and the surrounding solution that causing a high electrostatic repulsion between the ionised acid groups and the osmotic pressure. On the other hand, the increase in the MBA concentration decreases the swelling of the particles.

In summary, it is concluded that the microgels based on acrylic acid and N-isopropylacrylamide, sensitive to temperature and pH, were successfully synthesised. It was observed that, by varying the synthesis conditions (reagents concentration: AA, NIPAM, MBA

and KPS), control of the final properties of the microgels could be obtained according to the desired application, in this case, as an oral drug carrier. From the results of particle size, polydispersity index, pH sensitivity and stability of the formulations studied, it can be concluded that the samples suitable for the desired application are: S15, S17-S19, S21, S22 and S24.

5. Poly(NIPAM-co-AA) microgel particles with potential application as an oral drug delivery system of insulin

Abstract

Diabetes mellitus is a disorder of the endocrine system characterised by the insufficient insulin production by the pancreas or inefficient use of insulin by the body. The diabetes treatment is accomplished by insulin therapy, which is currently administrated by a parenteral route that causes pain and discomfort for the patients. In this way, many efforts have been made for new routes of insulin application, being the oral route the most attractive. However, some challenges are found in the oral application of insulin, such as physical (absorption in the intestinal epithelium) and enzymatic barriers (digestive enzymes in the stomach and the small intestine lumen), and the stability of the protein. In this way, some alternatives to overcome these barriers have been studied, such as permeation enhancers, protease inhibitors, enteric coatings and polymeric microspheres formulations. Thereby, this chapter shows the preliminary study about the potential of pH- and temperature-sensitive microgels based on acrylic acid and N-isopropylacrylamide as drug delivery system for oral insulin administration. The insulin was loaded into poly(NIPAM-co-AA) microgel particles to evaluate their potential for the oral delivery of hydrophilic drugs and/or proteins. The entrapment efficiency and drug release profile were analysed by Lowry method and UV-Visible spectroscopy. For this, a calibration curve for insulin concentration was constructed with a linear coefficient equal to 0.9939. The insulin entrapment efficiency (EE) was between 95 and 100 % for analyses conducted with an initial concentration of insulin equal to 0.4 $UI.mL^{-1}$, and loading time of 24 hours. The increase in acrylic acid and KPS concentration on the microgel showed to improve the EE, while the increase of MBA decreases this efficiency. The results of insulin release in the acidic and basic medium indicated that further studies need to be carried out in this area, to increase release efficiency. The study about the influence of insulin in the physicochemical characteristic of microgel particles showed that there is a slight increase in the average particle size and potential zeta and a slight decrease in the polydispersity index when the particles with insulin are analysed, but these differences are not significant. The particles carrying insulin in their structure also showed to remain pH-sensitive, presenting higher sizes in the alkaline medium due to the swelling behaviour of the microgels. Although the release results were

not as desired, this does not mean that the particles designed in this work are not suitable to be used as an oral drug delivery system for insulin, but a more in-depth study between the interaction of the drug with the particles as well as the method of release is recommended.

5.1. Introduction

Diabetes is a major disorder of the endocrine system resulting from insufficient insulin (a hormone that regulates blood sugar, or glucose) production by the pancreas or inefficient use of insulin by the body. Diabetes is a significant public health problem; the prevalence of diabetes has increased worldwide and has become an epidemic, mostly resulting from population ageing. However, physical inactivity, an inadequate diet and the increase in obesity are also responsible for the global expansion of diabetes (SCHMIDT et al., 2009).

Diabetes mellitus caused 1.5 million deaths in 2012; it was the eighth most common cause of death in the world. According to the World Health Organization (WHO), 422 million adults aged over 18 years had been detected with diabetes mellitus in 2014, the number of people in the world with diabetes has quadrupled since 1980 (108 million) (WORLD HEALTH ORGANIZATION, 2016). In Brazil, there was a prevalence of 8.7% of patients with diabetes mellitus in the adult population in 2017 (INTERNATIONAL DIABETES FEDERATION, 2019), which generates high expenses with the acquisition and distribution of medicines by the Ministry of Health.

As previously stated, diabetes is an insulin deficiency in the body. Insulin was discovered by Fedrick Banting, Macleod, and Collip in 1921, they received the Nobel Prize in 1923 for this discovery. Insulin is a peptide hormone composed of 51 amino acid residues and has a molecular weight of 5808 Da. It is composed of two peptide chains referred to as an A and B chain. The A and B chains are linked together by the two disulphide bonds, and an additional disulphide is formed within the A chain. In most species, the A chain consists of 21 amino acids, and the B chain consists of 30 amino acids.

Insulin therapy is currently done by daily subcutaneous administration, where insulin injections are inconvenient for patients. The usual duration of action is relatively short; i.e., 4-8 hours and therefore daily 2 to 4 injections are required for proper control of severe diabetic condition (SHAH; AGRAWAL; PARIKH, 2010). These daily injections can cause much physical and psychological damage, such as stress, pain, inconvenient, infection, among

others. For this reason, there are many works that focus on developing a safe and effective non-invasive route of insulin delivery. Despite the considerable advance in the field of pharmaceutical research, the development of an appropriate insulin delivery system remains a major challenge.

Potential routes for insulin administration are oral, pulmonary, buccal, rectal, transdermal, nasal and vaginal. In particular, oral administration of insulin has been the most attractive option due to the ease of administration and the absence of pain, leading to greater convenience, greater compliance and a reduced risk of infection compared to injections. The great advantage of this route of administration is that insulin can diffuse across the intercellular tight junctions of intestinal, colonic and rectal mucosa. After being absorbed by the intestine, would be delivered directly to the liver in a high concentration, simulating the physiological secretion pattern of the pancreas and exerting a direct effect on the hepatic production of glucose (SHAH; AGRAWAL; PARIKH, 2010).

However, there are still many challenges regarding oral insulin administration, because insulin has several well-known properties which are not suitable for oral absorption. Insulin is quickly denatured and degraded by proteolytic enzymes in the gastrointestinal tract (GI); these include rapid enzyme degradation in the stomach, deactivation and digestion with the influence of proteolytic enzyme on the lumen of the intestine and poor intestinal permeability throughout the epithelium due to the high molecular weight and hydrophilicity. These proteolytic enzymes (pepsin, trypsin, chymotrypsin and carboxypeptidase) are responsible for about 20% degradation of ingested proteins. Because of these barriers, the oral bioavailability of most peptides and proteins is less than 1-2% (CARINO; MATHIOWITZ, 1999; IYER; KHEDKAR; VERMA, 2010). Many authors have attempted to improve this bioavailability (LOWMAN et al., 1999; CARINO; JACOB; MATHIOWITZ, 2000; MORISHITA et al., 2004; WU et al., 2012).

Thus, different approaches have been developed for improving the oral bioavailability of peptides and proteins, mainly insulin. This approaches consist of the use of permeation enhancers (detergents, fatty acids or bile salts which improve the permeability through the mucus and the epithelial layers and open the intercellular tight junctions), protease inhibitors, enteric coatings, and formulations of smart release system, such as microspheres and nanoparticles (SHAH; AGRAWAL; PARIKH, 2010).

Particularly, several research groups have attempted to use polymeric carriers as oral delivery systems for insulin. Compare with other drugs carriers, polymeric micro- and nanoparticles offer higher protection and release of the drug in the desired location. In particular, hydrophilic smart polymers like microgels provide relatively mild network fabrication and drug encapsulation conditions that make them suitable for protein delivery (LIN; METTERS, 2006).

In literature, there are some studies about the use of sensitive materials with potential application in oral delivery of insulin. Lowman et al. (1999) studied the release of insulin as a function of pH; they incorporated insulin into pH-responsive polymeric microspheres of cross-linked copolymers of poly(methacrylic acid) grafted with ethylene glycol, P(MAA-g-EG), and administered orally to healthy and diabetic rats. The results show that in the acidic environment of the stomach, theses microspheres (hydrogels) did not swell due to the formation of intermolecular polymer complexes. In this way, the insulin was retained in the hydrogel. On the other hand, in the basic and neutral environments of the intestine, the intermolecular polymer complexes were dissociated, which resulted in a rapid swelling of the hydrogels and consequently release of insulin. In the *in vivo* studies (Wistar rats), the insulin-loaded P(MAA-g-EG) microspheres and the control solutions were administered via the mouth using a gelatin capsule. The researchers observed that after the absorption of insulin in the GI tract, the blood glucose levels in these animals were decreased significantly for at least 8 hours. In conclusion, hydrogels based on methacrylic acid and ethylene glycol showed to be a potential oral carrier for biological active insulin.

Taking into account the potential application of the P(MAA-g-EG) microspheres and intending to improve the delivery system for later clinical application, Morishita et al. (2004) investigated the effect of polymer particle size in the release of insulin in the intestine. They show that the lower the particle size, the higher insulin absorption, because of the greater contact area of the hydrogel with the mucosa, resulting in greater hypoglycemic effects without detectable mucosal damage. So, these results show that by reducing the particle size, there is an improvement in the bioavailability of insulin in oral administration.

Foss et al. (2004) investigated the release of insulin incorporated in nanospheres of crosslinked networks of methacrylic acid grafted with poly(ethylene glycol) [P(MA-g-PEG)], and acrylic acid grafted with poly(ethylene glycol) [P(AA-g-PEG)] with different concentration

ratio between the monomers. The authors show that these copolymers carriers have a high affinity for loading the insulin, and also increased protein transport across the cellular barrier in the upper small intestine. In conclusion, the best candidates for oral insulin delivery were the P(MAA-g-PEG) with comonomer feed ratios of 1:1 MAA:EG and the P(AA-g-PEG) carriers prepared with comonomer feed of 2:1 AA:EG. The results of insulin studies showed that P(AA-g-PEG) nanospheres present a better release profile, they released a tiny percentage of their load insulin at low pH, and an excellent ratio of total insulin released at high pH to the total of insulin initially charged.

Mundargi, Rangaswamy and Aminabhavi (2011) prepared pH-sensitive hydrogels based on N-vinylcaprolactam and methacrylic acid for being used for oral insulin delivery. The results show 52% of encapsulation efficiency, and the *in vitro* experiments show that there is no release of insulin in the first 2 hours in acidic pH. On the other hand, in basic pH, almost 100% insulin was released in 6 hours. The *in vivo* studies of alloxan-induced diabetic rats showed the biological inhibition up to 50%, and glucose tolerance testes exhibited 44% inhibition. Based on the results, the authors concluded that the polymer formulations used in their work are promising carriers for oral delivery of insulin.

Bai et al. (2012) developed thermo- and pH-responsive microgel particles based on hydroxypropylcellulose and acrylic acid to be used in the controlled release of insulin. The results showed that the microgel diameters increase with increasing pH, exhibiting a higher swelling ratio at higher pH in aqueous solution. The *in vitro* data demonstrated that the amount of insulin released from the microgels is higher in the basic medium than in acidic medium, as desired. In this way, according to the authors, the microgel synthesised show great potential as intelligent oral drug delivery.

In our research group, the experimental (SOUZA, 2013; RAYMUNDI et al., 2016) and mathematical modelling (RAYMUNDI et al., 2016) study of the insulin release through the hydrogels of acrylic acid (AA) crosslinked with trimethylolpropane triacrylate (TMPTA) was studied. The release study was performed in acidic and basic media, and the mathematical model was capable to represent the experimental profiles with fitted values of diffusivity of insulin through the hydrogels in the range of 6.0×10^{-7}-1.3×10^{-6} $cm^2.s^{-1}$. The experimental and predicted results also show that the release of insulin is higher in the basic medium than in the acidic medium, as desired for the application.

In this work, we have used a pH- and temperature-sensitive microgels designed to protect the insulin in an acidic environment (stomach) and release them in a basic medium (small intestine). The advantage of these particles is their monodisperse size and spherical morphology which are important parameters for the control of the release kinetics of the drug; also the pH-sensitive monomer (acrylic acid) used in the synthesis of these particles present excellent binding efficiency in the intercellular junctions of intestine improving the absorption of the drug.

5.2. Experimental Section

5.2.1. Reagents and Materials

5.2.1.1. Reagents

Insulin is the model drug used in this work to test the efficiency of the microgel particles as an oral drug carrier. The insulin used was recombinant human insulin derived from recombinant ADN (Humulin® 100 µL.mL^{-1}, Ely Lilly and Company).

The reagents used to simulate the gastrointestinal system were: sodium hydroxide (NaOH, 97%) and hydrochloric acid (HCl, 36.5-38%).

The reagents used in the development and validation of the analytical method for insulin quantification (by Folin-Lowry method) were: Folin & Ciocalteu's phenol (2N) reagent, sodium carbonate, sodium hydroxide, cupric sulphate pentahydrate, potassium sodium tartrate tetrahydrate (99%).

The reagents were purchased from Sigma-Aldrich, Labsynth and F. Maia, and were used as received. Deionised water was used for the preparation of all solutions.

5.2.1.2. Materials and equipment

Materials used for validation of insulin quantification method, insulin loading and release profile were: test tubes (10 mL), volumetric flasks, quartz cuvette, Amicon filter with Eppendorf (10 kD, 500 µL). The other materials used were: micropipettes and tips, spatulas, stopwatch, and a digital thermometer.

The main equipment used were: analytical balance, magnetic stirrer, thermostatic bath, pHmeter, centrifuge, and UV-visible spectrophotometer.

5.2.2. Measurements

5.2.2.1. Insulin Calibration Curve

The insulin calibration curve was constructed based on the Lowry method using UV-Visible spectrometer at 750 nm.

Figure 5.1 - Calibration curve for insulin concentration.

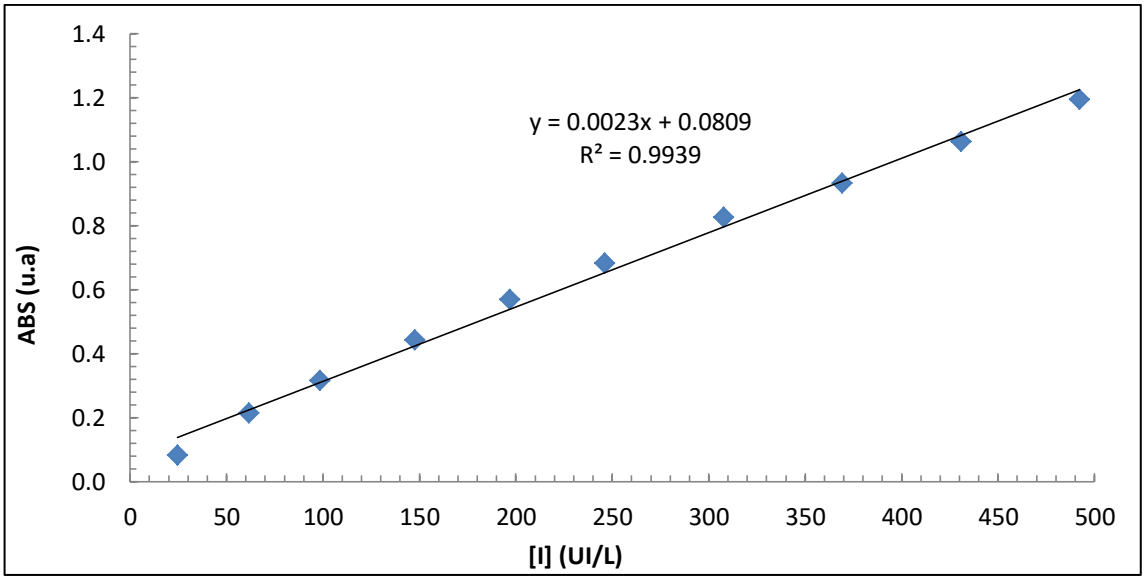

Applying a linear regression between the known concentrations of insulin and the related absorbance, the following equation is obtained with a linear correlation equal to 0.9939:

$$[I] = \frac{ABS - 0.0809}{0.0023} \tag{5.7}$$

where $[I]$ is the insulin concentration, and ABS is the absorbance at 750 nm.

5.2.2.2. Insulin loading and entrapment efficiency

There are two ways to load drugs or active substances into the smart polymer matrices: post-loading or *in situ* loading (LIN; METTERS, 2006). In the first method (post-loading), the drug is added to the medium when the polymer matrix is already formed. If an inert polymer system is used, diffusion is the major driving force for drug uptake, and release will be determined by diffusion and/or swelling (LIN; METTERS, 2006). In the second strategy (*in situ* loading), the drug is solubilised in the polymerisation reaction medium before the addition of the monomer, and the polymerisation causes the trapping of the drug within the matrix,

i.e., the microgel network formation and drug encapsulation are accomplished simultaneously. In these systems, the release of drugs can be controlled by diffusion, polymers swelling, reversible drug-polymer interactions, or degradation of labile covalent bonds (LIN; METTERS, 2006).

The easiest (and most used) methods to charge a drug into the carrier is the classical post-loading (or swelling-diffusion method), which consists of placing the two materials in contact. This method is more used for hydrophilic drug, and for active substances that degrade and/or lose their activity at high polymerisation temperatures, such as, proteins.

Thus, given the literature and the nature of the drug (hydrophilic and denaturation in higher temperatures), the insulin was loaded into the polymer particles (microgels) by the swelling-diffusion method, in which the particles were placed in contact with an aqueous solution of insulin at a known concentration for a pre-determination time. In this step, the insulin concentration and loading time were varied; and the proportion between the insulin solution and microgel suspension was 1:20.

After the time of insulin loading, the mixture was put in an Amicon filter (10 kD) with an Eppendorf tube, and centrifuged (5000 x g for 10 minutes at room temperature). The entrapment efficiency was analysed by the indirect method through the quantification of remaining insulin concentration in the filtered sample. The determination of free insulin concentration was performed according to the Lowry method, and absorbance was measured using an ultraviolet-visible (UV-Vis) spectrophotometer at 750 nm (Figure 5.2). Each sample was analysed in triplicate.

Figure 5.2 - Experimental procedures for insulin loading in poly(NIPAM-co-AA) microgels and for the analysis of the entrapment efficiency.

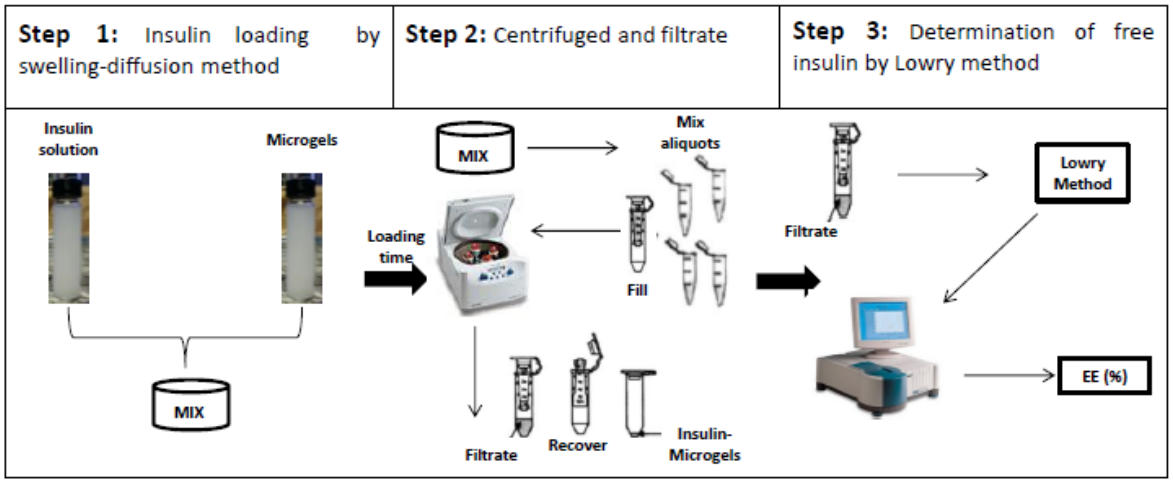

Source: author

The entrapment efficiency (EE) of insulin was calculated using Equation 5.8:

$$EE(\%) = \frac{[I]_{initial} - [I]_{free}}{[I]_{initial}} \times 100 \quad (5.8)$$

where $[I]_{initial}$ is the concentration of insulin in solution before the loading, and $[I]_{free}$ is the concentration of insulin in solution after the loading, i.e., the insulin that did not associate with the microgel particles.

5.2.2.3. Kinetic of insulin release

The drug release from polymeric particulate systems depends on different factors, such as the desorption of the drug from the surface of the particles, the diffusion of the drug through the matrix of the sphere particles or through the polymeric wall of the capsule, the erosion of the polymer matrix, and/or the combination of the diffusion and erosion processes (UHRICH et al., 1999; LIN; METTERS, 2006).

The most common methods used to study the drug release through the particles (microspheres) are the “sample and separate” and the “dialysis” method. The more conventional method is the “sample and separate”, which consists of incubation of drug-loaded particles in an Eppendorf tube and at predetermined time intervals, the solution is

sampled and centrifuged using an Amicon filter to separate the free drug from the particles (CHOPRA, 2017).

In this work, release studies were performed by placing the insulin-loaded microgel carriers in contact with acid and basic solutions with pH 1.2 and 6.8, respectively. The low pH was used to simulate the conditions of the stomach, while the high pH was used to simulate the intestine conditions. The acidic and basic solutions with the loaded-particles were divided into test tubes and were placed in an environment at 37 °C. Each tube was taken at given time intervals to measure the insulin released from the microgel carriers. The insulin concentration was measured according to the methodology used in the entrapment efficiency. Each sample was analysed in duplicate.

5.2.2.4. Physicochemical characteristics of microgel particles with and without the insulin

The average particle size (D_h), polydispersity index (PDI) and zeta potential (ZP) of the microgel particles with (Insulin-Microgels) and without (Blank-Microgels) the drug were determined as described in Chapter 4, using a Zetasizer Nano ZS-90 (Malvern) instrument. For size analyses, the samples were diluted in MiliQ water, and for zeta potential the dilutions were done in a 0.1 M of sodium chloride solution, respecting the appropriate concentration for the reading range of the equipment. To determine the behaviour of the microgels in different pHs, the Blank-Microgels and Insulin-Microgels were diluted in solutions with pHs 1.5, 3.9, 5.2 and 6.9. At least three replicates were conducted for each sample, and all analysed were conducted at 37 °C.

5.3. Results and Discussion

The results shown in this chapter represent a preliminary study about the insulin entrapment efficiency into the poly(NIPAM-co-AA) microgel particles, the *in vitro* kinetic release of insulin through the microgels, and the physicochemical characteristics of these particles with and without the drug.

As these results belong to a preliminary study, these analyses were not carried out with all the samples selected in Chapter 4 as the most suitable ones as oral carriers of drugs, but with some samples belonging to sets 2 and 3 that have different formulations.

5.3.1. Insulin Entrapment Efficiency

One of the crucial goals in the design of micro- and nanoparticles to be used as a drug delivery system is to achieve higher encapsulation/entrapment of drug into the particles. The efficiency of encapsulation/entrapment can be improved by changing some conditions during the loading process of the drug into the particles, for example, the ratio of the polymer and the drug, the concentration and type of drug, pH and temperature conditions, stirring speed rate, and the loading time.

In this work, the study of insulin entrapment efficiency was conducted with variation in two parameters; (i) the initial concentration of insulin and (ii) the loading time. The experiments were conducted with a volumetric ratio of insulin and particles solutions equally to 1:20. Figure 5.3 shows the results for these analysed parameters for three different samples.

Figure 5.3 - Influence of insulin concentration and loading time in entrapment efficiency (EE) of insulin into the microgel particles. (A) Results of EE (%) for sample S4 that was analysed with two different insulin concentration (0.5 and 1.0 IU.ml^{-1}) and loading time (24 and 48 hours); (B) Results of EE (%) for samples S10 and S13 that was analysed with two different insulin concentration (0.4 and 0.5 IU.ml^{-1}) and a loading time of 24 hours.

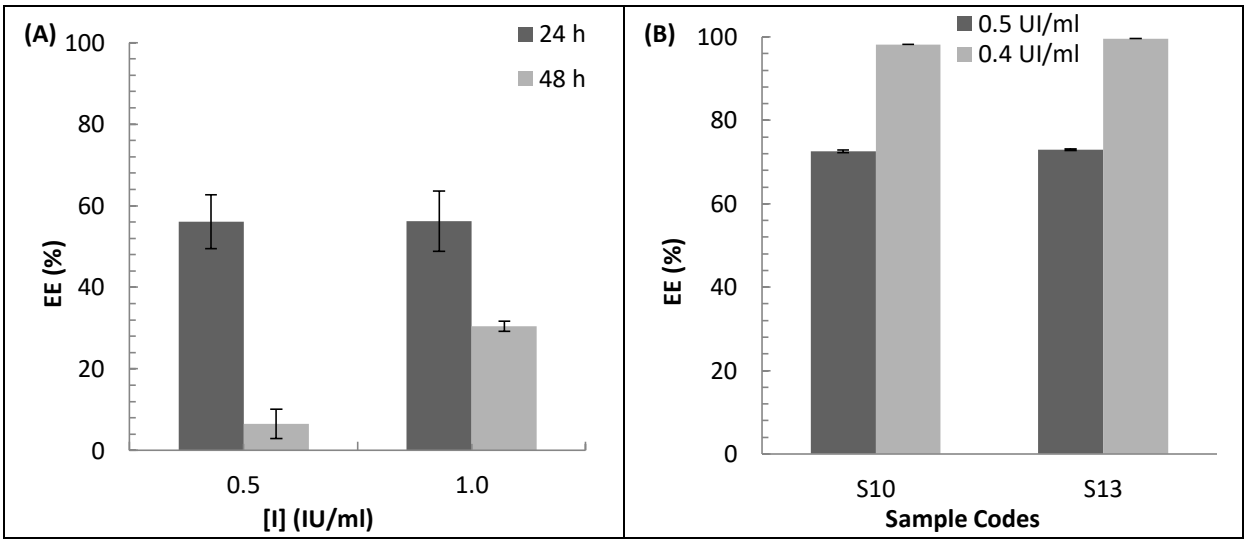

According to Figure 5.3 (A), it is possible to observe that the particles have better loading efficiency in 24 hours than in 48 hours. Theoretically, the amount of insulin entrapped into the particles during the loading time should have one of two behaviours: (i) increase in the entrapment efficiency over time or; (ii) remain constant until the end of loading time from the moment that the limit of drug amount into the particles is reached. However, as mentioned above, a third behaviour was observed, in which there was a decrease in the entrapment efficiency of the drug with the increase in the loading time.

One hypothesis to explain this behaviour may be associated with the fact that the entrapment tests were performed by placing two aqueous mediums in contact; one with insulin and another with polymer particles, both with different pHs. In the first moment, due to the slightly higher pH of insulin solution, the microgels can swell, and the insulin can be entrapment into the particles. However, an unbalance in the osmotic equilibrium between the external and internal phase can occur, thus facilitating the insulin diffusion to the external phase, and diminishing the insulin entrapment efficiency.

About the influence of the concentration of insulin, the particles loading initially with 0.5 and 1.0 $IU.mL^{-1}$ show entrapment efficiency between 56 – 73%. This percentage was improved for values close to 100% when the insulin concentration suffers a slight decrease to 0.4 $IU.mL^{-1}$.

Based on the results shown previously, other samples (with the formulation shown in Table 5.1) were loaded with an insulin concentration equal to 0.4 $IU.mL^{-1}$ during 24 hours (Figure 5.4). The results show a significant entrapment of insulin in the microgel matrix that varied between 95-100%.

Table 5.1 - Formulations of poly(NIPAM-co-AA) microgel particles that were loaded with insulin.

Sample Codes	AA ($mmol.L^{-1}$)	NIPAM ($mmol.L^{-1}$)	MBA ($mmol.L^{-1}$)	KPS ($mmol.L^{-1}$)
S9	20	120	2	2.5
S10	20	120	2	5.0
S12	20	120	4	5.0
S13	40	120	2	2.5
S14	40	120	2	5.0
S15	40	120	4	2.5
S16	40	120	4	5.0

Figure 5.4 - Insulin entrapment efficiency in poly(NIPAM-co-AA) microgel particles. Mean±SD (n=3)

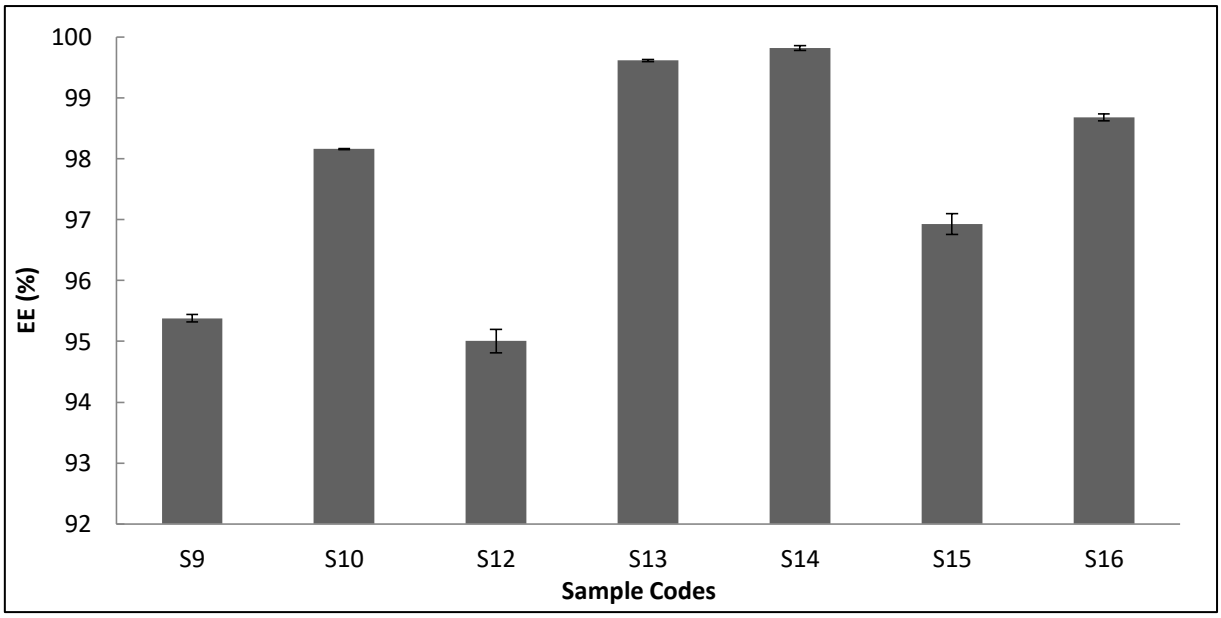

The samples have different reagent concentrations in their composition (Table 5.1); thus, a comparison of the influence of the reagents in the entrapment efficiency can be made. In this way, it is possible to observe that the comonomer (AA) and crosslinked agent (MBA) are the reagents with the most influence on the entrapment efficiency: particles with higher MBA concentration have the smallest entrapment ratio, as expected. MBA strengthens the polymer network by increasing the crosslinking density, reducing the swelling, and consequently decreasing the entrapment capability of the particles.

On the other hand, the increase in the AA concentration increases the entrapment efficiency. This could be attributed to the hydrophilic interaction of insulin and the carboxylic groups of acrylic acid, that favours the entrapment of the drug into the particles. The increase in the initiator concentration also increases the entrapment efficiency.

5.3.2. *In vitro* insulin release kinetics

In vitro release of insulin through poly(NIPAM-co-AA) microgel particles was measured according to the method mentioned in section 5.2.2.3. Figure 5.5 shows the results of *in vitro* insulin release kinetics for three samples in the acidic and basic medium that simulates the stomach and intestine pH, respectively.

Figure 5.5 - Results for *in vitro* insulin release in (A) Acid medium and (B) Basic medium.

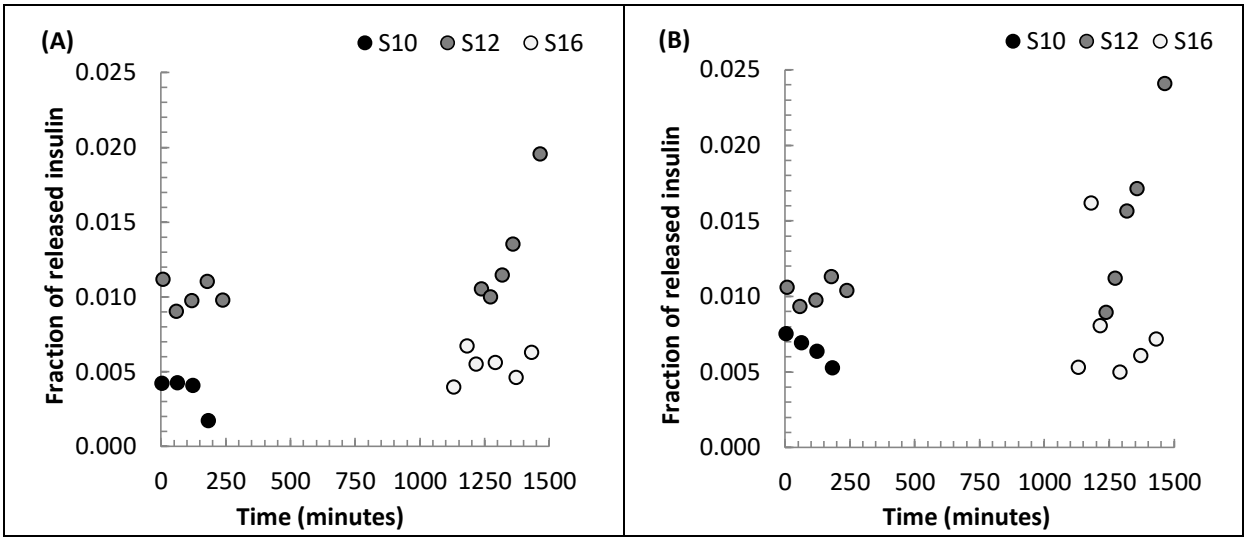

Observing Figure 5.5, the results are far from desirable, mainly for basic medium. The fact of the release fractions is close to zero can raise several hypotheses: first, the sensitive particles are not releasing the drug, a slow diffusion is happening, or the system reached the equilibrium, and the values observed for the released fraction correspond to the insulin that was on the surface of the particles, and that was dissolved in the medium. Secondly, insulin loss may have occurred due to inadequate procedures in the *in vitro* insulin release measurement protocols, in which various losses of the material may have occurred during manipulation of the particles with the insulin in their structure by the various steps until the results are obtained.

These inaccurate results related to the insulin release by the sample and separate method was also observed by Chopra (2017) that was unable to estimate the insulin release profile successfully. The hypotheses rose for this event were that some insulin was getting trapped in the washing device due to adsorption on the cellulose filter instead of being in the solution in the supernatant or the filtrate. This hypothesis was proven through analyses of the insulin release using the filtrate and the supernatant from the same nanoparticles that show different results. To understand that the filtrate or the supernatant is the most reliable source to analyse the release data, the study about the effect of replacing the Amicon filter after every washing step was done. The results confirmed that the amount of insulin released from the filtrate data gives a lower and inaccurate value (CHOPRA, 2017).

In this way, it is crucial to develop a suitable release system for the measure and characterises the insulin release from the microgel particles, as well as understanding the process of insulin diffusion through the particles.

5.3.3. Physicochemical characteristics of microgel particles with and without the insulin

In Chapter 4, the influence of the microgel compositions in their physicochemical characteristics was analysed. Here, the intention is to investigate whether the inclusion of insulin into the poly(NIPAM-co-AA) microgels affects the properties of the particles.

According to Figure 5.6, considering the standard deviation, for some samples there is no significant difference between the values obtained for the samples with and without the drug, but it is possible to observe that there is a trend for the increase of the average particle size and zeta potential, while the polydispersity index undergoes a slight decrease. A hypothesis for this increase in size can be associated with the growth in the polymeric net when the insulin was associated, and not due to particle agglomeration process, the increase in zeta potential and the decrease in PDI help to corroborate this hypothesis.

Figure 5.6 - Physicochemical characteristics of Insulin-Microgels (light grey bar) and Blank-Microgels (dark grey bar). (A) Average particle size, Dh; (B) Polydispersity index, PDI; and (C) Zeta Potential, ZP.

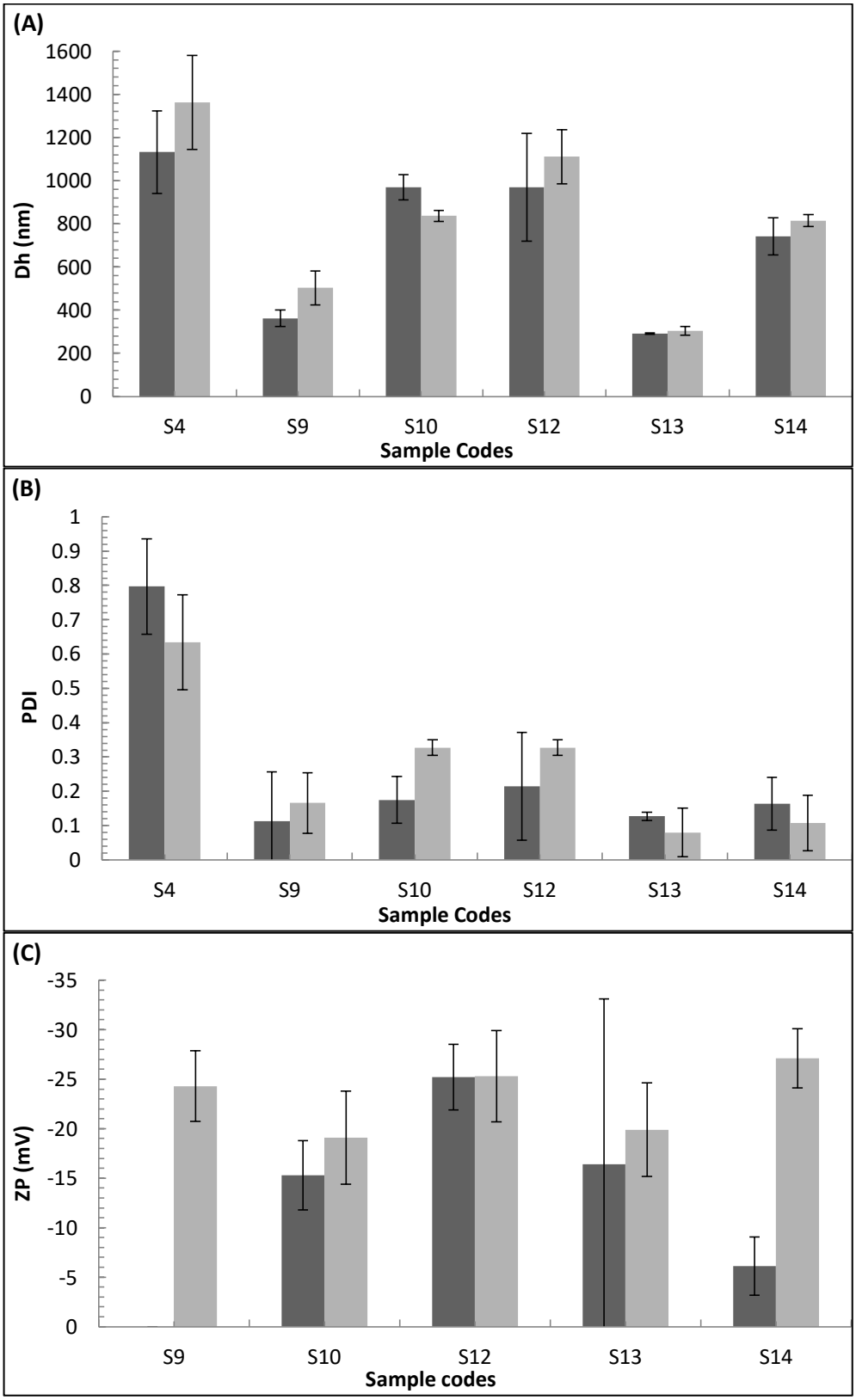

Figure 5.7 shows the average particle size and zeta potential of (A) Blank-Microgels and (B) Insulin-Microgels at different pHs. The results were obtained at 37 °C.

Figure 5.7 - Physicochemical characteristics of (A) Blank-Microgels and (B) Insulin-Microgels at different pHs. The results for average particle size and zeta potential are represented by index 1 and 2, respectively.

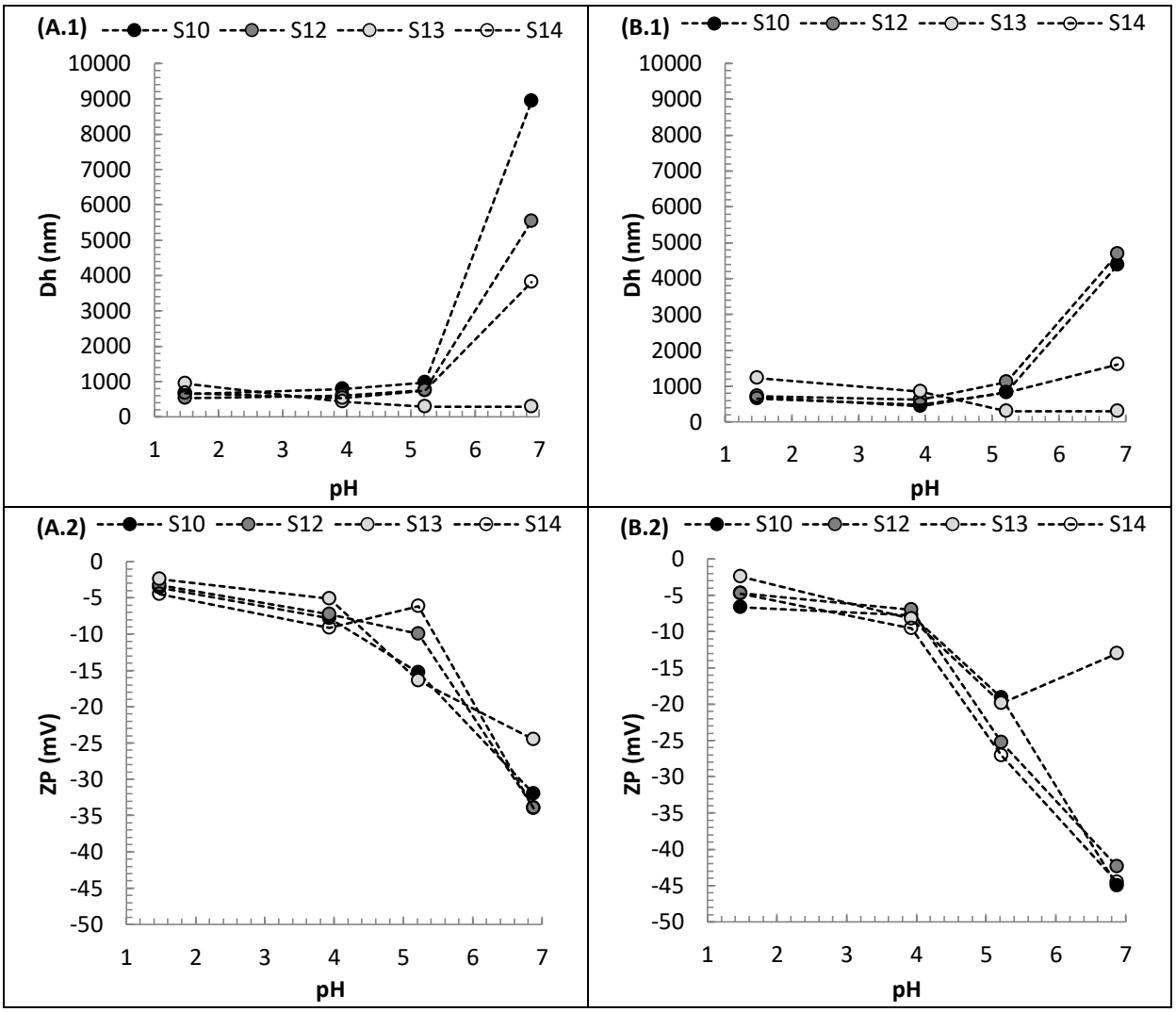

According to the results, the particles with insulin in their structure continue to present sensitivity to pH, presenting higher sizes in the basic medium due to the swelling behaviour of microgels. The only sample that did not show an increase in size in alkaline medium (both with and without insulin) was sample S13, the one that presented a different behaviour as discussed in Chapter 4 (Section 4.3.7.2). About the results for Blank-Microgels shown in this chapter and Chapter 4, although they show similar behaviour, there is a more significant difference in the values for average particle size, mainly for data in pH 7.0. There are two hypotheses for this: firstly, as these data were obtained for too long times late so, particle aggregation may have occurred. However, by analysing the stability results on storage time,

the samples are reasonably stable, except for S14, which was stable only for the first 90 days. Secondly, the study about the behaviour of microgel particles at different pHs presented in Chapter 4 was done through automatic pH adjustments and with an initial dilution of the samples equal to 1:10, while the results presented in Figure 5.6 were diluted in 1:100 in solutions with pH previously adjusted. Thus, perhaps dilution had a more significant effect on results, in that in the case presented in this chapter, the particles were in a more diluted medium, consequently had their swelling capacity improved.

In general, the average size and zeta potential are similar for both kind of particles (Blank-Microgel and Insulin-Microgel), shown a slight difference only in the results after pH equal 5.5 (above the pKa of AA). After this pH, the Blank-Microgels have higher size and smaller zeta potential than Insulin-Microgels, this means that when insulin molecules are inside the microgels, the swelling behaviour is more slow, due to the existence of barriers for the external solution to enter in the particles, which are dependent on the insulin diffusion to the external medium.

5.4. Partial Conclusions

The study in development in this chapter aimed to test the potential of the pH- and temperature-sensitive poly(NIPAM-co-AA) microgel particles as an oral drug delivery system for insulin.

The Insulin-Microgels were analysed for the insulin entrapment efficiency into the poly(NIPAM-co-AA) microgel particles, the *in vitro* kinetic release of insulin through the microgels, and the physicochemical characteristics of microgels with and without loaded insulin.

The influence of the insulin concentration initially loaded, and the loading time in the entrapment efficiency was evaluated. The better results for entrapment efficiency (EE) of insulin into the microgels was obtained with an insulin concentration equal to 0.4 $IU.mL^{-1}$ and a time loading of 24 hours; the EE varied between 95 and 100%. A great decrease in the entrapment efficiency was observed when the particles and insulin solutions were in contact for 48 hours. A hypothesis for this behaviour was based on the possible existence of an osmotic imbalance between the internal and external phases of the particles after they had reached their capacity of loading the drug, facilitating the insulin diffusion to the external

phase, and consequently diminishing the insulin entrapment efficiency. The decrease in the concentration of insulin in the external solution initially improved the entrapment efficiency from 56% to values close to 100%. The composition and structure of the microgels, expressed by the composition of the reagents used in the microgel production, also showed to have an influence on entrapment efficiency, in which EE increased upon increasing of acrylic acid and KPS, while the increase in MBA had an opposite effect. Despite the good results for the insulin entrapment efficiency, future investigations must be carried out to define the real capacity of the particles for entrapping insulin in their interior, so that the EE can be optimised to be able to release appropriate values of insulin for the human organism.

The *in vitro* release of insulin at acidic and basic pH presented poor results, mainly for alkaline medium, for which a more intense release would be expected. The fractions of insulin released during the 24 hours of the experiment were close to zero, indicating that the particles are not releasing the drug due to slow diffusion of insulin through the microgels or the existence an equilibrium between the external environment and the particles loaded with insulin. Another explanation for this undesirable release results are associated with accumulation of experimental errors during the procedures in the *in vitro* insulin release measurement by “sample and separated” associated with the Lowry method that require many steps until the results are obtained, and loss of material (Insulin-Microgels) may occur during handling. The possibility of insulin loss during sample and separate method was observed by Chopra (2017).

Considering the standard deviation, in general, insulin did not alter the physicochemical characteristics of poly(NIPAM-co-AA) microgel particles significantly. However, a trend for the increase of the average particle and zeta potential, and a decrease in the polydispersity index can be observed. As the insulin-loaded into the microgel particles was governed by the swelling-diffusion method, probably during the loading procedure the polymeric network becomes more flexible due to their hydrophilicity, and a slight increase in the hydrodynamic diameter can occur. The results of the swelling behaviour of microgel particles with insulin in their structure exhibited the desired pH response, presenting higher sizes in alkaline medium.

In general, the study presented in this chapter allowed a preliminary understanding of the interaction between the insulin and the poly(NIPAM-co-AA) microgel particles, and about

the issues related to drug diffusivity, system equilibrium and *in vitro* drug release measurements protocol. In this way, it is crucial to carry on further investigations for a better understanding of these problems, and for circumventing them to improve the release system of the drug through the particles.

To conclude, although the *in vitro* release results were not as desired, without the necessary studies on the problems faced in this work, the poly(NIPAM-co-AA) microgel particles cannot be ruled out as potential candidates for an oral drug delivery carrier for insulin.

6. General Conclusions and Future Works

The research topics developed in this thesis were motivated by the increasing interest in the microgel particles, mainly in the biomedical and pharmaceutical field, which during the last decades have been the object of numerous studies. In this way, taking into account the needs for designing microgels with different features suitable for the desired application, it becomes necessary to understand the influence of process conditions and formulation on the microgel characteristics. Especially the particle size is an important characteristic in the final product as well as is essential for the stability of particles during the microgel formation.

In this way, this thesis aimed at bringing a better understanding of the microgel formation process during precipitation polymerisation using real-time monitoring by spectroscopic techniques. Besides, the influence of reaction conditions in the physicochemical characteristics of microgel particles was extensively investigated as well as their potential as an oral drug carrier for insulin.

A new approach was proposed to monitoring the process variables, monomer conversion and average particle size of the microgel particles, during precipitation polymerisation using NIR and UV-VIS-NIR high-resolution spectrophotometers coupled with a probe. The UV-VIS-NIR spectra were collected at-line, and five calibrations models (two models for global conversion and three for average particle size) were constructed based on a simple linear relationship between the spectra (the area corresponds to a specific wavelength range), and the monitored variables (monomer conversion and average particle size). The NIR spectra were collected in-line, and two calibrations models (one for global conversion and another for average particle size) were constructed based on PLS regression. The determination coefficients for global conversion obtained in all models were above 0.91, while the average particle size models showed lower values, with the lowest value equal to 0.665. Also, the PLS cross-validation models gave an RMSECV equal to 0.0939 for global conversion, and equal to 18.4 nm for average particle size.

The results for external validation showed good agreement between the predictions and the experimental data, and similarities between the models. However, when microgel aggregates occur inside the reactor, the NIR calibration model for monomer conversion was more capable of identifying this phenomenon than the calibration model developed for UV-

VIS-NIR. In conclusion, the developed models showed that monitoring using NIR and/or UV-VIS spectroscopy with a probe is capable of detecting physical and chemical changes in the reaction medium during the production of microgel particles by precipitation polymerisation. Although it was not possible to separate the physical information from the chemical information, the results pointed out the enormous potential of these techniques to monitor the precipitation polymerisation process, allowing control over the polymerisation reaction with quickly and directly acquisition of data in real-time.

We also reported the detailed characterisation of the microgel particles, as well as the influence of reagent concentrations in their physicochemical characteristics and swelling behaviour. The pH- and temperature-sensitive microgels based on acrylic acid and N-isopropylacrylamide synthesised in this work show a range of size between 284 and 1315 nm and a polydispersity index from 0.01 to 1.00 when measured at 37 °C by DLS. The particles with the greatest size and polydispersity index were those with a higher molar ratio of acrylic acid to N-isopropylacrylamide in the formulation. The poly(AA) and poly(NIPAM-co-AA) with a higher amount of acrylic acid also showed a non-spherical morphology or tendency to aggregate. In general, the poly(NIPAM-co-AA) microgels present negative charge, spherical morphology and the dispersion pH in the range from 2.00 to 3.00. The FTIR spectra identified the chemical composition of the microgels. The studies of the influence of temperature and pH in the swelling behaviour of the samples showed that poly(NIPAM-co-AA) microgels are sensitive to both temperature and pH. In general, the microgels showed good stability during the storage time, and the higher the total concentration of polymers suspended in the medium, the higher the tendency for particle aggregation. The particles synthesised with chitosan showed to be unstable and easily aggregated, as expressed by their higher polydispersity index. The sample with a higher amount of chitosan presented positive charge and higher pH compared to other samples. In summary, it is concluded that the microgels based on acrylic acid and N-isopropylacrylamide, sensitive to both temperature and pH, were synthesised successfully, and many formulations showed to be suitable for application as oral drug carriers.

The study about the entrapment efficiency of insulin into poly(NIPAM-co-AA) microgels showed good values for assays with 0.4 $IU.mL^{-1}$ of insulin initially loaded and loading time of 24 hours. These values were improved by decreasing the initial concentration of insulin

loading and the loading time. The composition of the microgels (formulation employed in the microgel synthesis) also showed an influence on entrapment efficiency, which increases upon an increase of acrylic acid and KPS while an increase in MBA had an opposite effect. The results of insulin release in the acidic and basic medium indicate that further studies are needed to increase release efficiency. The study about the influence of insulin in the physicochemical characteristics and swelling behaviour of microgel particles showed that this drug did not alter significantly these features of the particles. The results of the swelling behaviour of microgel particles with insulin in their structure exhibited the desired pH response, presenting higher sizes in alkaline medium.

Overall, our investigations allowed a better understanding of the influence of some reaction conditions in the microgel properties, making possible to design particles with properties more suitable for the desired application. The monitoring results showed the enormous potential of using spectroscopic techniques during the precipitation polymerisation for better control and knowledge of the process, mainly for real-time monitoring of the physical properties. Last but not least, although the preliminary *in vitro* release results were not satisfactory, we believe that pH- and temperature-sensitive poly(NIPAM-co-AA) microgel particles continue to be a potential candidate as an oral drug delivery carrier for insulin and/or other proteins and hydrophilic drugs.

Given the challenges and complexity encountered throughout this research, further studies are needed. In this sense, some suggestions for futures works are given:

- To use Raman spectroscopy to monitor the precipitation polymerisation, and compare the results with the NIR and UV-Vis-NIR;
- To study and compare different calibration methods based on the linear and non-linear regression method for improving the relationship between the spectra and the experimental data, mainly for the information acquired by UV-VIS-NIR spectrophotometer;
- To develop a mathematical model for a better understanding of the reaction mechanism involved in precipitation polymerisation;
- To continue the study about the physicochemical characteristic and swelling behaviour of microgel particles with chitosan in their structure;

- To use microfluidic technology for better control of the microgel features, and for drug encapsulation during the formation of the particles, improving the encapsulation/entrapment efficiency;
- To complete the study of drug loading for improving the entrapment efficiency and drug release;
- To use the dialysis method and compare with the sample and separate method;
- To adjust a mathematical model for *in vitro* release of the drug from the microgel particles;
- To relate the calibration based on the Lowry method with the direct reading of the UV-Visible spectra, allowing to take advantage of the use of the probe for the in-line quantification of insulin during the release assays.

Due to the potentialities and interdisciplinarity of the research, many other related topics beyond the chemical engineering field can be further studied.

REFERENCES

Chapter 1

AJMAL, M.; FAROOQI, Z. H.; SIDDIQ, M. Silver Nanoparticles Containing Hybrid Polymer Microgels with Tunable Surface Plasmon Resonance and Catalytic Activity. **Korean Journal of Chemical Engineering**, v. 30, n. 11, p. 2030–2036, 2013.

AL-MANASIR, N. **Preparation and Characterization of Cross-Linked Polymeric Nanoparticles for Enhanced Oil Recovery Applications**. 2009. University of Oslo, 2009.

BAI, Y.; ZHANG, Z.; DENG, M.; CHEN, L.; HE, C.; ZHUANG, X.; CHEN, X. Thermo- and pH-Responsive Microgels for Controlled Release of Insulin. **Polymer International**, v. 61, n. 7, p. 1151–1157, 2012.

BALACEANU, A.; VERKH, Y.; DEMCO, D. E.; MÖLLER, M.; PICH, A. Correlated Morphological Changes in the Volume Temperature Transition of Core-Shell Microgels. **Macromolecules**, v. 46, n. 12, p. 4882–4891, 2013.

CHATURVEDI, K.; GANGULY, K.; NADAGOUDA, M. N.; AMINABHAVI, T. M. Polymeric Hydrogels for Oral Insulin Delivery. **Journal of Controlled Release**, v. 165, n. 2, p. 129-138, 2013.

DIMITROV, I.; TRZEBICKA, B.; MULLER, A. H. E.; ANDRZEJ; DWORAK; TSVETANOV, C. B. Thermosensitive Water-Soluble Copolymers with Doubly Responsive Reversibly Interacting Entities. **Progress in Polymer Science**, v. 32, n. 11, p. 1275–1343, 2007.

ELSAYED, A. M. Oral Delivery of Insulin: Novel Approaches. In: **Recent Advances in Novel Drug Carrier Systems**. [s.l: s.n] p. 281-314, 2012.

FAROOQI, Z. H.; KHAN, H. U.; SHAH, S. M.; SIDDIQ, M. Stability of Poly(N-Isopropylacrylamide-Co-Acrylic Acid) Polymer Microgels under Various Conditions of Temperature, PH and Salt Concentration. **Arabian Journal of Chemistry**, v. 10, n. 3, p. 329-335, 2013.

FAROOQI, Z. H.; NASEEM, K.; BEGUM, R.; IJAZ, A. Catalytic Reduction of 2-Nitroaniline in Aqueous Medium Using Silver Nanoparticles Functionalized Polymer Microgels. **Journal of Inorganic and Organometallic Polymers and Materials**, v. 25, n. 6, p. 1554–1568, 2015.

FERNÁNDEZ-NIEVES, A.; FERNÁNDEZ-BARBERO, A.; VINCENT, B.; NIEVES, F. J. de las. Osmotic De-Swelling of Ionic Microgel Particles. **The Journal of Chemical Physics**, v. 119, n. 19, p. 10383–10388, 2003.

GANGULY, K.; CHATURVEDI, K.; MORE, U. A.; NADAGOUDA, M. N.; AMINABHAVI, T. M. Polysaccharide-Based Micro/Nanohydrogels for Delivering Macromolecular Therapeutics. **Journal of Controlled Release**, v. 193, p. 162–173, 2014.

HAIDER, I.; SIDDIQ, M.; SHAH, S. M.; REHMAN, S. ur. Synthesis and Characterization of Multi-Responsive Poly (NIPAm-Co-AAc) Microgels. **International Symposium on Advanced Materials**, v. 60, n. 1, p. 012046, 2014.

HAN, D.; ZHANG, Q. M.; SERPE, M. J. Poly(N-Isopropylacrylamide)-Co-(Acrylic Acid) Microgel/Ag Nanoparticle Hybrids for the Colorimetric Sensing of H2O2. **Nanoscale**, v. 7, n. 6, p. 2784–2789, 2015.

IQBAL, Z.; SHAH, L. A.; SAYED, M.; HALEEM, A.; SIDDIQ, M. Responsive Polymer Hybrid Gel Cross-linked by N,N-(1,2-Dihydroxyethylene) Bisacrylamide for Catalytic Application. **Journal of the Chilean Chemical Society**, v. 61, n. 3, p. 3061–3065, 2016.

KANTER, M. De; MEYER-KIRSCHNER, J.; VIELL, J.; MITSOS, A.; KATHER, M.; PICH, A.; JANZEN, C. Enabling the Measurement of Particle Sizes in Stirred Colloidal Suspensions by Embedding Dynamic Light Scattering into an Automated Probe Head. **Measurement**, v. 80, p. 92–98, 2016.

KAWAGUCHI, H. Thermoresponsive Microhydrogels: Preparation, Properties and Applications. **Polymer International**, v. 63, n. 6, p. 925–932, 2014.

LALLY, S.; MACKENZIE, P.; LEMAITRE, C. L.; FREEMONT, T. J.; SAUNDERS, B. R. Microgel Particles Containing Methacrylic Acid : pH-Triggered Swelling Behaviour and Potential for Biomaterial Application. **Journal of Colloid and Interface Science**, v. 316, n. 2, p. 367–375, 2007.

LU, C.; LIU, X.; ZHA, L. Investigation of Au Nanoparticles Loading Temperature Responsive Hybrid Microgels. **Advanced Materials Research**, v. 650, p. 268–272, 2013.

MALMSTEN, M. Soft Drug Delivery Systems. **Soft Matter**, v. 2, n. 9, p. 760–769, 2006.

MALMSTEN, M.; BYSELL, H.; HANSSON, P. Biomacromolecules in Microgels — Opportunities and Challenges for Drug Delivery. **Current Opinion in Colloid & Interface Science**, v. 15, n. 6, p. 435–444, 2010.

MÉNAGER, C.; SANDRE, O.; MANGILI, J.; CABUIL, V. Preparation and Swelling of Hydrophilic Magnetic Microgels. **Polymer**, v. 45, n. 8, p. 2475–2481, 2004.

MEYER-KIRSCHNER, J.; KATHER, M.; KSIAZKIEWICZ, A.; PICH, A.; MITSOS, A.; VIELL, J. Monitoring Microgel Synthesis by Copolymerization of N-Isopropylacrylamide and N-Vinylcaprolactam via In-Line Raman Spectroscopy and Indirect Hard Modeling. **Macromolecular Reaction Engineering**, v. 12, n. 3, p. 1–8, 2018.

MEYER-KIRSCHNER, J.; KATHER, M.; PICH, A.; ENGEL, D.; MARQUARDT, W.; VIELL, J.; MITSOS, A. In-Line Monitoring of Monomer and Polymer Content during Microgel Synthesis Using Precipitation Polymerization via Raman Spectroscopy and Indirect Hard Modeling. **Applied Spectroscopy**, v. 70, n. 3, p. 416–426, 2016.

MEYER-KIRSCHNER, J.; MITSOS, A.; VIELL, J. Polymer Particle Sizing from Raman Spectra by Regression of Hard Model Parameters. **Journal of Raman Spectroscopy**, v. 49, n. 8, p. 1402–1411, 2018.

MUNDARGI, R. C.; RANGASWAMY, V.; AMINABHAVI, T. M. Poly (N-Vinylcaprolactam-Co-Methacrylic Acid) Hydrogel Microparticles for Oral Insulin Delivery. **Journal of Microencapsulation**, v. 28, n. 5, p. 384–394, 2011.

NOJD, S.; MOHANTY, P. S.; BAGHERI, P.; YETHIRAJ, A.; SCHURTENBERGER, P. Eletric Field Driven Self-Assembly of Ionic Microgels. **Soft Matter**, v. 9, n. 38, p. 9199-9207, 2013.

PELTON, R.; HOARE, T. Microgels and Their Synthesis: An Introduction. In: **Microgel Suspensions Fundamentals and Applications**. [s.l: s.n.]p. 2–32.

PICH, A.; RICHTERING, W. Microgels by Precipitation Polymerization: Synthesis, Characterization, and Functionalization. In: **Chemical Design of Responsive** Microgels. [s.l: s.n.]p. 1–37, 2010.

RWEI, S.; WAY, T.; CHANG, S.; CHIANG, W.; LIEN, Y. Thermo- and PH- Responsive Copolymers : Poly(N -Isopropylacrylamide- Co-IAM) Copolymers. **Journal of Applied Polymer Science**, v. 42367, p. 7, 2015.

SAMAH, N. H. A.; HEARD, C. M. Enhanced in Vitro Transdermal Delivery of Caffeine Using a Temperature- and PH- Sensitive Nanogel, Poly(NIPAM-Co-AAc). **International Journal of Pharmaceutics**, v. 453, n. 2, p. 630-640, 2013.

SAUNDERS, B. R.; VINCENT, B. Microgel Particles as Model Colloids: Theory, Properties and Applications. **Advances in Colloid and Interface Science**, v. 80, n. 1, p. 1–25, 1999.

SCHMALJOHANN, D. Thermo- and PH-Responsive Polymers in Drug Delivery. **Advanced Drug Delivery Reviews**, v. 58, n. 15, p. 1655–1670, 2006.

SMEETS, N. M. B.; HOARE, T. Designing Responsive Microgels for Drug Delivery Applications. **Journal of Polymer Science Part A: Polymer Chemistry**, v. 51, n. 14, p. 3027–3043, 2013.

SNOWDEN, M. J.; CHOWDHRY, B. Z.; VINCENT., B.; MORRIS, E. G. Colloidal Copolymer Microgels of N-Isopropylacrylamide and Acrylic Acid: pH, Ionic Strength and Temperature Effects. **Journal of the Chemical Society- Faraday Transactions**, v. 92, n. 24, p. 5013–5016, 1996.

VEGA, J. C. D. La; ELISCHER, P.; SCHNEIDER, T.; HAFELI, U. O. Uniform Polymer Microspheres: Monodispersity Criteria, Methods of Formation and Applications. **Nanomedicine**, v. 8, n. 2, p. 265–285, 2013.

YUAN, Z.; WANG, Y.; CHEN, D. Preparation and Characterization of Thermo-, PH-, and Magnetic-Field-Responsive Organic/Inorganic Hybrid Microgels Based on Poly(Ethylene Glycol). **Journal of Material Science**, v. 49, n. 8, p. 3287–3296, 2014.

ZHANG, C.; LIU, X.; ZHA, L. Preparation and Characterization of pH Sensitive Microgels with Semi-Interpenetrating Polymer Network Structure. **Advanced Materials Research**, v. 332, p. 1836–1839, 2011.

Chapter 2

ACCIARO, R.; GILÁNYI, T.; VARGA, I. Preparation of Monodisperse Poly (N - Isopropylacrylamide) Microgel Particles with Homogenous Cross-Link Density Distribution. **Langmuir**, v. 27, n. 2, p. 7917–7925, 2011.

AHMAD, N.; CAIRUL, M.; MOHD, I.; MAHALI, S. M.; ISMAIL, I.; TUAN, V.; CHUANG, G. Biocompatible and Mucoadhesive Bacterial Cellulose -g- Poly (Acrylic Acid) Hydrogels for

Oral Protein Delivery. **Molecular Pharmaceutics**, v. 11, n. 11, p. 4130–42, 2014.

AL-MANASIR, N. **Preparation and Characterization of Cross-Linked Polymeric Nanoparticles for Enhanced Oil Recovery Applications**. 2009. University of Oslo, 2009.

BAI, F.; YANG, X.; LI, R.; HUANG, B.; HUANG, W. Monodisperse Hydrophilic Polymer Microspheres Having Carboxylic Acid Groups Prepared by Distillation Precipitation Polymerization. **Polymer**, v. 47, n. 16, 5775–5784, 2006.

BAKER, W. O. Microgel, a New Macromolecule. Relation to Sol and Gel as Structural Elements of Synthetic Rubber. **Rubber Chemistry and Technology**, v. 41, n. 3, p. 511–520, 1949.

BALACEANU, A.; VERKH, Y.; DEMCO, D. E.; MÖLLER, M.; PICH, A. Correlated Morphological Changes in the Volume Temperature Transition of Core-Shell Microgels. **Macromolecules**, v. 46, n. 12, p. 4882–4891, 2013.

BURMISTROVA, A.; RICHTER, M.; UZUM, C.; KLITZING, R. Effect of Cross-Linker Density of P(NIPAM-Co-AAc) Microgels at Solid Surfaces on the Swelling/Shrinking Behaviour and the Young's Modulus. **Colloid and Polymer Science**, v. 289, n. 5-6, p. 613–624, 2011.

CHEN, X.; CHEN, S.; WANG, J. A pH-responsive Poly(N-isopropylacrylamide-co-acrylic acid) Hydrogel for the Selective Isolation of Hemoglobin from Human Blood. **Analyst**, v. 135, n.7, p. 1736-1741, 2010.

CUI, H.; CHEN, H.; QU, R.; WANG, C.; SUN, C.; ZHOU, W.; YU, M.; JIANG, H. Highly Crosslinked Poly(Styrene-Co-Divinylbenzene) Microspheres Prepared by Precipitation Polymerization: Effects of the Polymerization Parameters on the Characteristics of the Particles. **Journal of Applied Polymer Science**, v. 111, n. 6, p. 3144–3149, 2009.

DIMITROV, I.; TRZEBICKA, B.; MULLER, A. H. E.; ANDRZEJ; DWORAK; TSVETANOV, C. B. Thermosensitive Water-Soluble Copolymers with Doubly Responsive Reversibly Interacting Entities. **Progress in Polymer Science**, v. 32, n. 11, p. 1275–1343, 2007.

DON, T.; HUANG, M.; CHIU, A.; KUO, K.; CHIU, W.; CHIU, L. Preparation of Thermo-Responsive Acrylic Hydrogels Useful for the Application in Transdermal Drug Delivery Systems. **Materials Chemistry and Physics**, v. 107, n. 2-3, p. 266–273, 2008.

FAN, K.; BRADLEY, M.; VINCENT, B. Photo-Responsive Properties of Poly (NIPAM-Co-AAc) Microgel Particles with Absorbed, Hydrophobically Modified Organic Salts. **Journal of Colloid and Interface Science**, v. 368, n.1, p. 287–291, 2012.

FAROOQI, Z. H.; KHAN, H. U.; SHAH, S. M.; SIDDIQ, M. Stability of Poly(N-Isopropylacrylamide-Co-Acrylic Acid) Polymer Microgels under Various Conditions of Temperature, pH and Salt Concentration. **Arabian Journal of Chemistry**, v. 10, n. 3, p. 329-335, 2013.

FAROOQI, Z. H.; NASEEM, K.; BEGUM, R.; IJAZ, A. Catalytic Reduction of 2-Nitroaniline in Aqueous Medium Using Silver Nanoparticles Functionalized Polymer Microgels. **Journal of Inorganic and Organometallic Polymers and Materials**, v. 25, n. 6, p. 1554–1568, 2015.

GALAEV, I.; MATTIASSON, B. **Smart Polymers: Application in Biotechnology and Biomedicine**. [s.l: s.n.].

GANGULY, K.; CHATURVEDI, K.; MORE, U. A.; NADAGOUDA, M. N.; AMINABHAVI, T. M. Polysaccharide-Based Micro/Nanohydrogels for Delivering Macromolecular Therapeutics. **Journal of Controlled Release**, v. 193, p. 162–173, 2014.

GONÇALVES, I. C.; MARTINS, M. C. L.; BARBOSA, M. A.; RATNER, B. D. Biomaterials Protein Adsorption and Clotting Time of PHEMA Hydrogels Modified with C18 Ligands to Adsorb Albumin Selectively and Reversibly. **Biomaterials**, v. 30, n. 29, p. 5541–5551, 2009.

HAIDER, I.; SIDDIQ, M.; SHAH, S. M.; REHMAN, S. ur. Synthesis and Characterization of Multi-Responsive Poly (NIPAm-Co-AAc) Microgels. **International Symposium on Advanced Materials**, v. 60, n. 1, p. 012046, 2014.

HAN, D.; ZHANG, Q. M.; SERPE, M. J. Poly(N-Isopropylacrylamide)-Co-(Acrylic Acid) Microgel/Ag Nanoparticle Hybrids for the Colorimetric Sensing of H2O2. **Nanoscale**, v. 7, n. 6, p. 2784–2789, 2015.

HU, Y.; DING, Y.; DING, D.; SUN, M.; ZHANG, L.; JIANG, X.; YANG, C. Hollow Chitosan / Poly (Acrylic Acid) Nanospheres as Drug Carriers. **Biomacromolecules**, v. 8, n. 4, p. 1069–1076, 2007.

IQBAL, Z.; SHAH, L. A.; SAYED, M.; HALEEM, A.; SIDDIQ, M. Responsive Polymer Hybrid Gel Cross-linked by N,N-(1,2-Dihydroxyethylene) Bisacrylamide for Catalytic Application. **Journal of Chilean Chemical Society**, v. 61, n. 3, p. 3061–3065, 2016.

KLINGER, D.; LANDFESTER, K. Stimuli-responsive Microgels for the Loading and Release of Functional Compounds: Fundamental Concepts and Application. **Polymer**, v. 53, n. 23, p. 5209-5231, 2012.

LANZALACOS, S.; ARMELIN, E. Poly(N-isopropylacrylamide) and Copolymers: A Review on Recent Progress in Biomedical Applications. **Gels**, v.3, n. 36, p. 1-32, 2017.

LAY, M. M.; AUNG, T.; NAING, K. M. Chitosan-g-Poly (Acrylic Acid) Hydrogel as Superabsorbent. **Universities Research Journal**, v. 4, n. 3, p. 75–88, 2011.

LIN, C.; METTERS, A. T. Hydrogels in Controlled Release Formulations : Network Design and Mathematical Modeling. **Advanced Drug Delivery Reviews**, v. 58, n. 12-13, p. 1379–1408, 2006.

LYON, L. A.; HENDRICKSON, G. R.; MENG, Z.; IYER, A. N. S. J. Exploiting the Optical Properties of Microgel and Hydrogels as Microlenses and Photonic Crystals in Sensing Applications. In: **Microgel Suspensions - Fundamentals and Applications**. [s.l: s.n.]p. 357–374.

MAHKAM, M.; ASSADI, M. G. New PH-Sensitive Hydrogels for Oral Delivery of Hydrophobic Drugs. **Phosphorus, Sulfur, and Silicon and the Related Elements**, v. 185, n. 4, p. 842–847, 2010.

MALMSTEN, M. Microgels in Drug Delivery. In: **Microgel Suspensions - Fundamentals and Applications**. [s.l: s.n.]p. 375–405.

MALMSTEN, M.; BYSELL, H.; HANSSON, P. Biomacromolecules in Microgels — Opportunities and Challenges for Drug Delivery. **Current Opinion in Colloid & Interface Science**, v. 15, n. 6, p. 435–444, 2010.

MATEESCU, A.; WANG, Y.; DOSTALEK, J.; JONAS, U. Thin Hydrogel Films for Optical Biosensor Applications. **Membranes**, v. 2, n. 1, p. 40–69, 2012.

OLIVEIRA, M. A. M. de. **Produção de Micropartículas e Nanopartículas Poliméricas para Aplicações Biomédicas em Sistemas Heterogêneos de Polimerização**. 2011. Universidade Federal do Rio de Janeiro, 2011.

PELTON, R. H.; CHIBANTE, P. Preparation of Aqueous Latices with N- Isopropylacrylamide. **Colloids and Surface**, v. 20, n. 3, p. 247–256, 1986.

PELTON, R.; HOARE, T. Microgels and Their Synthesis: An Introduction. In: **Microgel Suspensions Fundamentals and Applications**. [s.l: s.n.]p. 2–32.

PEPPAS, N. A.; BLARCOM, D. S. Van. Hydrogel-Based Biosensors and Sensing Devices for Drug Delivery. **Journal of Controlled Release**, v. 240, p. 142-150, 2016.

PEPPAS, N.; LEOBANDUNG, W.; ICHIKAWA, H. Hydrogels in Pharmaceutical Formulations. **European journal of pharmaceutics and biopharmaceutics**, v. 50, n. 1, p. 27–46, 2000.

PICH, A.; RICHTERING, W. Microgels by Precipitation Polymerization: Synthesis, Characterization and Functionalization. In: **Chemical Design of Responsive Microgels**. [s.l: s.n.]p. 1–37.

SAMAH, N. H. A.; HEARD, C. M. Enhanced in Vitro Transdermal Delivery of Caffeine Using a Temperature- and PH- Sensitive Nanogel, Poly(NIPAM-Co-AAc). **International Journal of Pharmaceutics**, v. 453, n. 2, p. 630-640, 2013.

SAMGENKO, Y.; ULBERG, Z.; KOROTYCH, O. Multipurpose Smart Hydrogel System. **Advances in Colloid and Interface Science**, v. 168, n. 1–2, p. 247–262, 2011.

SAUNDERS, B. R.; VINCENT, B. Microgel Particles as Model Colloids: Theory, Properties and Applications. **Advances in Colloid and Interface Science**, v. 80, n. 1, p. 1–25, 1999.

SCHAFFAZICK, S. R.; GUTERRES, S. S.; FREITAS, L. de L.; POHLMANN, A. R. Caracterização e Estabilidade Físico-Química de Sistemas Poliméricos Nanoparticulados Para Administração de Fármacos. **Quimica Nova**, v. 26, n. 5, p. 726–737, 2003.

SCHNEIDER, F.; BALACEANU, A.; FEOKTYSTOV, A.; PIPICH, V.; WU, Y.; ALLGAIER, J.; PYCKHOUT-HINTZEN, W.; PICH, A.; SCHNEIDER, G. J. Monitoring the Internal Structure of Poly(N - Vinylcaprolactam) Microgels with Variable Cross-Link Concentration. **Langmuir**, v. 30, n. 50, p. 15317–15326, 2014.

SIMÕES, S.; FIGUEIRAS, A.; VEIGA, F. Modular Hydrogels for Drug Delivery. **Journal of Biomaterials and Nanobiotechnology**, v. 3, n. 2, p. 185–199, 2012.

SNOWDEN, M. J.; CHOWDHRY, B. Z.; VINCENT., B.; MORRIS, G. E. Colloidal Copolymer Microgels of N-Isopropylacrylamide and Acrylic Acid: pH, Ionic Strength and Temperature Effects. **Journal of the Chemical Society- Faraday Transactions**, v. 92, n. 24, p. 5013–5016,

1996.

UHRICH, K.; CANNIZZARO, S.; LANGER, R.; SHAKESHEFF, K. Polymeric Systems for Controlled Drug Release. **Chemical Reviews**, v. 99, n. 11, p. 3181–3198, 1999.

VILLANOVA, J. C. O.; ORÉFICE, R. L.; CUNHA, A. S. Aplicações Farmacêuticas de Polímeros. **Polímeros**, v. 20, n. 1, p. 51–64, 2010.

YAO, Y.; WANG, Y.; LI, Z.; LI, H. Reversible On − Off Luminescence Switching in Self-Healable Hydrogels. **Langmuir**, v. 31, n. 46, p. 12736-12741, 2015.

YOSHIDA, R.; KANEKO, Y.; SAKAI, K.; OKANO, T.; SAKURAI, Y. Intelligent Thermo-Responsive Hydrogels-Mechanism of on-off Switches for Drug Release. **Advanced Materials**, v. 15A, p. 659–662, 1994.

ZHANG, J.; CHU, L. Y.; LI, Y. K.; LEE, Y. M. Dual Thermo- and pH-Sensitive Poly(N-Isopropylacrylamide-Co-Acrylic Acid) Hydrogels with Rapid Response Behaviors. **Polymer**, v. 48, n. 6, p. 1718–1728, 2007.

WICHTERLE, O.; LIM, D. Hydrophilic Gels for Biological Use. **Nature**, v. 185, n. 4706, p. 117-8, 1960.

Chapter 3

AENUGU, H. P. R.; SATHIS KUMAR, D.; SRISUDHARSON; PARTHIBAN, N.; GHOSH, S. S.; BANJI, D. Near Infra Red Spectroscopy- An Overview. **International Journal of ChemTech Research**, v. 3, n. 2, p. 825–836, 2011.

AMBROGI, M. P. N. **Polimerização de estireno em miniemulsão: Monitoramento em linha usando espectroscopia de Infravermelho Próximo e Raman e Modelagem Matemática do processo.** 2015. Universidade de São paulo, 2015.

AMBROGI, P. M. N.; COLMÁN, M. M. E.; GIUDICI, R. Miniemulsion Polymerization Monitoring Using Off-Line Raman Spectroscopy and In-Line NIR Spectroscopy. **Macromolecular Reaction Engineering**, v. 11, n. 4, p. 1–9, 2017.

ARAUJO, A. M.; SANTOS, L. M.; FORTUNY, M.; MELO, R. L. F. V; COUTINHO, R. C. C.; SANTOS, A. F. Evaluation of Water Content and Average Droplet Size in Water-in-Crude Oil Emulsions by Means of Near-Infrared Spectroscopy. **Energy & Fuels**, v. 22, n. 4, p. 3450–3458, 2008.

BAETEN, V.; DARDENNE, P. Spectroscopy: Developments in Instrumentation and Analysis. **Grasas y Aceites**, v. 53, n. 1, p. 45–63, 2002.

BASET, S.; AKBARI, H.; ZEYNALI, H.; SHAFIE, M. Size Measurement of Metal and Semiconductor Nanoparticles via UV-Vis Spectra Absorption Spectra. **Digest Journal of Nanomaterials and Biostructures**, v. 6, n. 2, p. 709–716, 2011.

BEGUM, R.; FAROOQI, Z. H.; NASEEM, K.; ALI, F.; BATOOL, M.; XIAO, J.; IRFAN, A. Applications of UV/Vis Spectroscopy in Characterization and Catalytic Activity of Noble Metal Nanoparticles Fabricated in Responsive Polymer Microgels : A Review. **Critical Reviews in Analytical Chemistry**, v. 48, n. 6, p. 503–516, 2018.

BOUTRIS, C.; CHATZI, E. G.; KIPARISSIDES, C. Characterization of the LCST Behaviour of Aqueous poly(N-Isopropylacrylamide) Solutions by Thermal and Cloud Point Techniques. **Polymer**, v. 38, n. 10, p. 2567–2570, 1997.

BRUKER OPTIK GMGH. **OPUS-NT Spectroscopy Software**, 2000. .

BURMISTROVA, A.; RICHTER, M.; UZUM, C.; KLITZING, R. Effect of Cross-Linker Density of P(NIPAM-Co-AAc) Microgels at Solid Surfaces on the Swelling/Shrinking Behaviour and the Young's Modulus. **Colloid Polymer Science**, v. 289, n. 5-6, p. 613–624, 2011.

CHERFI, A.; FÉVOTTE, G. On-Line Conversion Monitoring of the Solution Polymerization of Methyl Methacrylate Using near-Infrared Spectroscopy. **Macromolecular Chemistry and Physics**, v. 203, n. 9, p. 1188–1193, 2002.

CHICOMA, D.; CARRANZA, V.; SAYER, C.; GIUDICI, R. In Line Monitoring of VAc-BuA Emulsion Polymerization Reaction in a Continuous Pulsed Sieve Plate Reactor Using NIR Spectroscopy. **Macromolecular Symposia**, v. 289, n. 1, p. 140–148, 2010.

CHICOMA, D. L.; SAYER, C.; GIUDICI, R. In-Line Monitoring of Particle Size during Emulsion Polymerization under Different Operational Conditions Using NIR Spectroscopy. **Macromolecular Reaction Engineering**, v. 5, n. 3-4, p. 150–163, 2011.

COLMÁN, M. M. E.; CHICOMA, D. L.; GIUDICI, R.; ARAÚJO, P. H. H.; SAYER, C. Acrylamide Inverse Miniemulsion Polymerization: In Situ, Real-Time Monitoring Using Nir Spectroscopy. **Brazilian Journal of Chemical Engineering**, v. 31, n. 4, p. 925–933, 2014.

FAN, K.; BRADLEY, M.; VINCENT, B. Photo-Responsive Properties of Poly (NIPAM-Co-AAc) Microgel Particles with Absorbed, Hydrophobically Modified Organic Salts. **Journal of Colloid and Interface Science**, v. 368, n. 1, p. 287–291, 2012.

FONSECA, G. E.; DUBE, M. A.; PENLIDIS, A. A Critical Overview of Sensors for Monitoring Polymerizations. **Macromolecular Reaction Engineering**, v. 3, n. 7, p. 327-373, 2009.

FONTOURA, J. M. R.; SANTOS, A. F.; SILVA, F. M.; LENZI, M. K.; LIMA, E. L.; PINTO, J. C. Monitoring and Control of Styrene Solution Polymerization Using NIR Spectroscopy. **Journal of Applied Polymer Science**, v. 90, n. 5, p. 1273–1289, 2003.

GANGULY, K.; CHATURVEDI, K.; MORE, U. A.; NADAGOUDA, M. N.; AMINABHAVI, T. M. Polysaccharide-Based Micro/Nanohydrogels for Delivering Macromolecular Therapeutics. **Journal of Controlled Release**, v. 193, p. 162–173, 2014.

GELATI, P.; KOWASLSKI, B. R. Partial Least-Squares Regression: A Tutorial. **Analytica Chimica Acta**, v. 185, p. 1–17, 1986.

GOSSEN, P. D.; MACGREGOR, J. F.; PELTON, R. H. Composition and Particle Diameter for Styrene/Methyl Methacrylate Copolymer Latex Using UV and NIR Spectroscopy. **Applied Spectroscopy**, v. 47, n. 11, p. 1852–1870, 1993.

JUNIOR, J. M. de F. **Monitoramento in-situ e em tempo real de variáveis morfológicas do PVC com o uso de uma sonda NIR**. 2008. Universidade Federal do Rio de Janeiro, 2008.

KAASTRUP, K.; AGUIRRE-SOTO, A.; WANG, C.; BOWMAN, C. N.; STANSBURY, J. W.; SIKES, H.

D. UV-Vis/FT-NIR in Situ Monitoring of Visible-Light Induced Polymerization of PEGDA Hydrogels Initiated by Eosin/Triethanolamine/O 2. **Polymer Chemistry**, v. 7, n. 3, p. 592–602, 2016.

KAMMONA, O.; CHATZI, E. G.; KIPARISSIDES, C. Recent Developments in Hardware Sensors For the On-Line Monitoring of Polymerization Reactions. **Macromolecular Chemistry and Physics**, v. 39, n. 1, p. 57–134, 1999.

KANTER, M. De; MEYER-KIRSCHNER, J.; VIELL, J.; MITSOS, A.; KATHER, M.; PICH, A.; JANZEN, C. Enabling the Measurement of Particle Sizes in Stirred Colloidal Suspensions by Embedding Dynamic Light Scattering into an Automated Probe Head. **Measurement**, v. 80, p. 92–98, 2016.

KARA, S.; OKAY, O.; PEKCAN, O. Real-Time Temperature and Photon Transmission Measurements for Monitoring Phase Separation during the Formation of Poly (N - Isopropylacrylamide) Gels. **Journal of Applied Polymer Science**, v. 86, n. 14, p. 3589–3595, 2002.

KARA, S.; PEKCAN, O. In Situ Real-Time Photon Transmission Technique for Monitoring Formation of Polyacrylamide Gels at Various Crosslinker Contents. **Journal of Applied Polymer Science**, v. 80, n. 6, p. 823–830, 2001.

KUMAR, S. **Spectroscopy of Organic Compounds**, 2006.

MARQUES, N. N.; CURTI, P. S.; MAIA, A. M. S.; BALABAN, R. C. Temperature and PH Effects on the Stability and Rheological Behavior of the Aqueous Suspensions of Smart Polymers Based on N -Isopropylacrylamide, Chitosan, and Acrylic Acid. **Journal of Applied Polymer Science**, v. 129, n. 1, p. 334–345, 5 Jul. 2013.

METROHM. **NIR Spectroscopy: A guide to near-infrared spectroscopy analysis of industrial manufacturing processes**. [s.l: s.n.].

METROHM AG. **Metrohm NIRSystems Dedicated near-infrared solutions**, 2013. .

MEYER-KIRSCHNER, J.; KATHER, M.; KSIAZKIEWICZ, A.; PICH, A.; MITSOS, A.; VIELL, J. Monitoring Microgel Synthesis by Copolymerization of N-Isopropylacrylamide and N-Vinylcaprolactam via In-Line Raman Spectroscopy and Indirect Hard Modeling. **Macromolecular Reaction Engineering**, v. 12, n. 3, p. 1–8, 2018.

MEYER-KIRSCHNER, J.; KATHER, M.; PICH, A.; ENGEL, D.; MARQUARDT, W.; VIELL, J.; MITSOS, A. In-Line Monitoring of Monomer and Polymer Content during Microgel Synthesis Using Precipitation Polymerization via Raman Spectroscopy and Indirect Hard Modeling. **Applied Spectroscopy**, v. 70, n. 3, p. 416–426, 2016.

MEYER-KIRSCHNER, J.; MITSOS, A.; VIELL, J. Reliable Spectroscopic Process Monitoring Using an Optimal Acquisition Time Procedure Determined by Signal-to-Noise Ratio. **Measurement**, v. 122, p. 100–105, 2018a.

MEYER-KIRSCHNER, J.; MITSOS, A.; VIELL, J. Polymer Particle Sizing from Raman Spectra by Regression of Hard Model Parameters. **Journal of Raman Spectroscopy**, v. 49, n. 8, p. 1402–1411, 2018b.

NAES, T.; MARTENS, H. Principal Component Regression in NIR Analysis: Viewpoints, Background Details and Selection of Components. **Journal of Chemometrics**, v. 2, n. 2, p. 155–167, 1988.

NEBIOGLU, A.; SOUCEK, M. D. Reaction Kinetics and Microgel Particle Size Characterization of Ultraviolet-Curing Unsaturated Polyester Acrylates. **Journal of Polymer Science Part A: Polymer Chemistry**, v. 44, n. 22, p. 6544–6557, 2006.

PASQUINI, C. Review Near Infrared Spectroscopy : Fundamentals, Practical Aspects and Analytical Applications. **Journal of Brazilian Chemical Society**, v. 14, n. 2, p. 198–219, 2003.

PELTON, R. H.; CHIBANTE, P. Preparation of Aqueous Latices with N-isopropylacrylamide. **Colloids and Surfaces**, v. 20, n. 3, p. 247-256, 1986.

PELTON, R.; HOARE, T. Microgels and Their Synthesis: An Introduction. In: **Microgel Suspensions Fundamentals and Applications**. [s.l: s.n.]p. 2–32.

PEREIRA, H. L.; MACHADO, F.; LIMA, E. L.; PINTO, C. In-Line Monitoring of Vinyl Acetate / Acrylic Acid Batch Copolymerizations through Near Infrared Spectroscopy. **Macromolecular Symposia**, v. 299, n.1, p. 1–9, 2011.

PICH, A.; RICHTERING, W. Microgels by Precipitation Polymerization: Synthesis, Characterization, and Functionalization. In: **Chemical Design of Responsive Microgels** [s.l: s.n] p. 1–37.

QIN, S. J.; MCAVOY, T. J. Nonlinear PLS Modeling Using Neural Networks. **Computers & Chemical Engineering**, v. 16, n. 4, p. 379–391, 1992.

REY-BAYLE, M.; BENDOULA, R.; HENROT, S.; LAMIRI, K.; BACO-ANTONIALI, F.; CAILLOL, N.; GOBRECHT, A.; ROGER, J. Potential of Vis–NIR Spectroscopy to Monitor the Silica Precipitation Reaction. **Analytical and Bioanalytical Chemistry**, v. 409, n. 3, p. 785–796, 2017.

SAMAH, N. H. A.; HEARD, C. M. Enhanced in Vitro Transdermal Delivery of Caffeine Using a Temperature- and PH- Sensitive Nanogel, Poly(NIPAM-Co-AAc). **International Journal of Pharmaceutics**, v. 453, n. 2, p. 630-640, 2013.

SANTOS, A. F.; LIMA, E. L.; PINTO, J. C. In-Line Evaluation of Average Particle Size in Styrene Suspension Polymerizations Using Near-Infrared Spectroscopy. **Journal of Applied Polymer Science**, v. 70, n. 9, p. 1737–1745, 1998.

SANTOS, A. F.; SILVA, F. M.; LENZI, M. K.; PINTO, J. C. Monitoring and Control of Polymerization Reactors Using NIR Spectroscopy. **Polymer-Plastics Technology and Engineering**, v. 44, n. 1, p. 1–61, 2005.

SILVA, W. K.; CHICOMA, D. L.; GIUDICI, R. In-Situ Real-Time Monitoring of Particle Size, Polymer, and Monomer Contents in Emulsion Polymerization of Methyl Methacrylate by Near Infrared Spectroscopy. **Polymer Engineering & Science**, v. 51, n. 10, p. 2024–2034, 2011.

SMEETS, N. M. B.; HOARE, T. Designing Responsive Microgels for Drug Delivery Applications.

Journal of Polymer Science Part A: Polymer Chemistry, v. 51, n. 14, p. 3027–3043, 2013.

STANSBURY, J. W.; DING, X.; NEWMAN, S. M. Controlled Preparation of Nanogel Particles and Their Use as Macromonomers. **Am Chem Soc. Polym Prepr**, v. 47, n. 2, p. 825–826, 2006.

VEGA, J. C. D. La; ELISCHER, P.; SCHNEIDER, T.; HAFELI, U. O. Uniform Polymer Microspheres: Monodispersity Criteria, Methods of Formation and Applications. **Nanomedicine**, v. 8, n. 2, p. 265–285, 2013.

ZHANG, Q.; ZHA, L.; MA, J.; LIANG, B. A Novel route to prepare pH- and temperature-sensitive nanogels via a semibatch process. **Journal of Colloid and Interface Science**, v. 330, n.2, p. 330-336, 2009.

Chapter 4

ALSAYED, A. M.; HAN, Y.; YODH, A. G. Melting and Geometric Frustration in Temperature-Sensitive Colloids. In: **Microgel Suspensions - Fundamentals and Applications**. [s.l: s.n.]p. 229–281.

AZEVEDO, R. B. de. Microscopia Eletrônica. In: **Nanotecnologia: Introdução, preparação e caracterização de nanomateriais e exemplos de aplicação**. [s.l: s.n.]p. 101–109.

BALACEANU, A.; VERKH, Y.; DEMCO, D. E.; MÖLLER, M.; PICH, A. Correlated Morphological Changes in the Volume Temperature Transition of Core-Shell Microgels. **Macromolecules**, v. 46, n. 12, p. 4882–4891, 2013.

BALLAUFF, M.; LU, Y. 'Smart' Nanoparticles: Preparation, Characterization and Applications. **Polymer**, v. 48, n. 7, p. 1815–1823, 2007.

BURMISTROVA, A.; RICHTER, M.; UZUM, C.; KLITZING, R. Effect of Cross-Linker Density of P(NIPAM-Co-AAc) Microgels at Solid Surfaces on the Swelling/Shrinking Behaviour and the Young's Modulus. **Colloid and Polymer Science**, v. 289, n. 5-6, p. 613–624, 2011.

CHAN, K.; PELTON, R.; ZHANG, J. On the Formation of Colloidally Dispersed Phase-Separated Poly(N-isopropylacrylamide). **Langmuir**, v. 15, n. 11, p. 4018-4020, 1999.

CHEN, H. **Development of Environmentally Responsive Multifunctional Microgel Particles: Synthesis, Characterization and Applications**. 2015. Arizona State University, 2015.

COLMÁN, M. M. E. **Monitoramento da Polimerização de Acrilamida em Miniemulsão Inversa por Espectroscopia Raman e NIR**. 2013. Universidade Federal de Santa Catarina, 2013.

DANAEI, M.; DEHGHANKHOLD, M.; ATAEI, S.; DAVARANI, F. H.; JAVANMARD, R.; DOKHANI, A.; KHORASANI, S.; MOZAFARI, M. R. Impact of Particle Size and Polydispersity Index on the Clinical Applications of Lipidic Nanocarrier Systems. **Pharmaceutics**, v. 10, n. 57, p. 1–17, 2018.

ELAISSARI, A.; MAHDAVIAN, A. R. Polymerization Kinetics of Microgel Particles. In: **Microgel Suspensions - Fundamentals and Applications**. [s.l: s.n.]p. 33–51.

FAROOQI, Z. H.; KHAN, H. U.; SHAH, S. M.; SIDDIQ, M. Stability of Poly(N-Isopropylacrylamide-Co-Acrylic Acid) Polymer Microgels under Various Conditions of Temperature, PH and Salt Concentration. **Arabian Journal of Chemistry**, v. 10, n. 3, p. 329-335, 2013.

FERNANDES, F. A. N.; LONA, L. M. F. **Introdução à Modelagem de Sistemas de Polimerização**. [s.l: s.n.]

FERNANDEZ-NIEVES, A.; WYSS, H.; MATTSSON, J.; WEITZ, D. **Microgel Suspensions: Fundamentals and Applications**. [s.l: s.n.]

GALAEV, I.; MATTIASSON, B. **Smart Polymers: Application in Biotechnology and Biomedicine**. Second Edi ed. [s.l: s.n.]

GAO, J.; FRISKEN, B. J. Influence of Reaction Conditions on the Synthesis of Self-Cross-Linked N-Isopropylacrylamide Microgels. **Langmuir**, v. 19, n. 13, p. 5217–5222, 2003.

HONARY, S.; ZAHIR, F. Effect of Zeta Potential on the Properties of Nano - Drug Delivery Systems - A Review (Part 2). **Tropical Journal of Pharmaceutical Research**, v. 12, n. 2, p. 265–273, 2013a.

HONARY, S.; ZAHIR, F. Effect of Zeta Potential on the Properties of Nano-Drug Delivery Systems - A Review (Part 1). **Tropical Journal of Pharmaceutical Research**, v. 12, n. 2, p. 255–264, 2013b.

HORIBA SCIENTIFIC. **A Guidebook to Particle Size Analysis**. [s.l: s.n.].

JABBARI, E.; NOZARI, S. Swelling Behavior of Acrylic Acid Hydrogels Prepared by γ-Radiation Crosslinking of Polyacrylic Acid in Aqueous Solution. **European Polymer Journal**, v. 36, n. 12, p. 2685–2692, 2000.

JAFARI, S.; MODARRESS, H. A Study on Swelling and Complex Formation of Acrylic Acid and Methacrylic Acid Hydrogels with Polyethylene Glycol. **Polymer Journal**, v. 14, n. 10, p. 863–873, 2005.

JUNG, H.; JANG, M.; NAH, J.; KIM, Y. Synthesis and Characterization of Thermosensitive Nanoparticles Based on PNIPAAm Core and Chitosan Shell Structure. **Macromolecular Research**, v. 17, n. 4, p. 265-270, 2009.

KRATZ, K.; HELLWEG, T.; EIMER, W. Influence of Charge Density on the Swelling of Colloidal Poly(N-Isopropylacrylamide-Co-Acrylic Acid) Microgels. **Colloids and Surfaces A: Physicochemical and Engineering Aspects**, v. 170, n. 2–3, p. 137–149, 2000.

KUMAR, S. **Spectroscopy of Organic Compounds**, 2006.

KUMIRSKA, J.; CZERWICKA, M.; KACZYNSKI, Z.; BYCHOWSKA, A.; BRAZOZOWSKI, K.; THOMING, J.; STEPNOWSKI, P. Application of Spectroscopic Methods for Structural Analysis of Chitin and Chitosan. **Marine Drugs**, v. 8, n. 5, p. 1567–1636, 2010.

MALVERN INSTRUMENTS. **Autotitrator MPT2 - Technical information and SpecificationsMalvern zetasizer additional device**, [s.d.].

MALVERN INSTRUMENTS. Dynamic Light Scattering: Common Terms Defined. **Malvern Guides**, p. 1–6, 2011a.

MALVERN INSTRUMENTS. Zeta Potential: An Introduction in 30 Minutes. **Zetasizer Nano Series Technical Note. MRK654-01**, v. 2, p. 1–6, 2011b.

MALVERN INSTRUMENTS LIMITED. **A basic guide to particle characterization**, 2014. .

MALVERN INSTRUMENTS LIMITED. **Automatic determination of isoelectric points**, 2016.

MARQUES, N. N.; CURTI, P. S.; MAIA, A. M. S.; BALABAN, R. C. Temperature and PH Effects on the Stability and Rheological Behavior of the Aqueous Suspensions of Smart Polymers Based on N -Isopropylacrylamide, Chitosan, and Acrylic Acid. **Journal of Applied Polymer Science**, v. 129, n. 1, p. 334–345, 2013.

MATYJASZEWSKI, K.; DAVIS, T. P. **Handbook of Radical Polymerization**. [s.l: s.n.]

MEDEIROS, S. de F. **Obtenção de nanopartículas magnéticas sensíveis a estímulos para aplicações biomédicas**. 2010. Universidade de São Paulo, 2010.

NAGASHIMA, S.; ANDO, S.; MAKINO, K.; TSUKAMOTO, T.; OHSHIMA, H. Size Dependence of Polymer Composition in the Surface Layer of Poly(Acrylamide-Co-Acrylic Acid) Hydrogel Microspheres. **Journal of colloid and interface science**, v. 197, n. 2, p. 377–82, 1998.

PELTON, R.; HOARE, T. Microgels and Their Synthesis: An Introduction. In: **Microgel Suspensions Fundamentals and Applications**. [s.l: s.n.]p. 2–32.

PICH, A.; RICHTERING, W. Microgels by Precipitation Polymerization: Synthesis, Characterization, and Functionalization. In: **Chemical Design of Responsive Microgels.** [s.l: s.n.] p. 1–37.

SAMAH, N. H. A.; HEARD, C. M. Enhanced in Vitro Transdermal Delivery of Caffeine Using a Temperature- and PH- Sensitive Nanogel, Poly(NIPAM-Co-AAc). **International Journal of Pharmaceutics**, v. 453, n. 2, p. 630-640, 2013.

SAUNDERS, B. R.; VINCENT, B. Microgel Particles as Model Colloids: Theory, Properties and Applications. **Advances in Colloid and Interface Science**, v. 80, n. 1, p. 1–25, 1999.

SCHAFFAZICK, S. R.; GUTERRES, S. S.; FREITAS, L. de L.; POHLMANN, A. R. Caracterização e Estabilidade Físico-Química de Sistemas Poliméricos Nanoparticulados Para Administração de Fármacos. **Quimica Nova**, v. 26, n. 5, p. 726–737, 2003.

SHAH, D.; AGRAWAL, V.; PARIKH, R. Non-Invasive Insulin Delivery System: A Review. **International Journal of Applied Pharmaceutics**, v. 2, n. 1, p. 35–40, 2010.

SHAH, N.; PATEL, K. R. Formulation and Development of Hydrogel for Poly Acrylamide-Co-Acrylic Acid. **Journal of Pharmaceutical Science and Bioscientific Research (JPSBR)**, v. 4, n. 1, p. 114–120, 2014.

SNOWDEN, M. J.; CHOWDHRY, B. Z.; VINCENT., B.; GAYLE E. MORRIS. Colloidal Copolymer Microgels of N-Isopropylacrylamide and Acrylic Acid: pH, Ionic Strength and Temperature Effects. **Journal of the Chemical Society- Faraday Transactions**, v. 92, n. 24, p. 5013–5016,

1996.

STUART, B. **Infrared spectroscopy: Fundamentals and Applications**. [s.l.] John Wiley & Sons, Ltd, 2004.

THOMAS, E. V. A Primer on Multivariate Calibration. **Analytical Chemistry**, v. 66, n. 15, p. 795–804, 1994.

THORNE, J. B. **Controlling the Interfacial Behaviour of Colloidal Microgel Systems**. 2012. University of Greenwich, 2012.

VARGA, I.; GILÁNYI, T.; MÉSZÁROS, R.; FILIPCSEI, G.; ZRÍNYI, M. Effect of Cross-Link Density on the Internal Structure of Poly(N -Isopropylacrylamide) Microgels. **The Journal of Physical Chemistry B.**, v. 105, n. 38, p. 9071–9076, 2001.

VENEGAS-SANCHEZ, J. A.; KUSUNOKI, T.; YAMAMOTO, M.; KOBAYASHI, T. Sono-Respond on Thermosensitive Polymer Microgels Based on Cross-Linked Poly (N- Isopropylacrylamide-Co-Acrylic Acid). **Ultrasonic Sonochemistry**, v. 20, n. 5, p. 1271–1275, 2013.

WANG, Y.; QIN, J.; WEI, Y.; LI, C.; MA, G. Preparation Strategies of Thermo-Sensitive P(NIPAM-Co-AA) Microspheres with Narrow Size Distribution. **Powder Technology**, v. 236, p. 107–113, 2013.

WU, Z. M.; LING, L.; ZHOU, L. Y.; GUO, X. D.; JIANG, W.; QIAN, Y.; LUO, K. Q.; ZHANG, L. J. Novel Preparation of PLGA/HP55 Nanoparticles for Oral Insulin Delivery. **Nanoscale Research Letters**, v. 7, n. 1, p. 299, 2012.

ZHANG, C.; LIU, X.; ZHA, L. Preparation and Characterization of PH Sensitive Microgels with Semi-Interpenetrating Polymer Network Structure. **Advanced Materials Research**, v. 332–334, p. 1836–1839, 2011.

ZHANG, Q.; ZHA, L.; MA, J.; LIANG, B. A Novel Route to Prepare PH- and Temperature-Sensitive Nanogels via a Semibatch Process. **Journal of Colloid and Interface Science**, v. 330, n. 2, p. 330–336, 2009.

Chapter 5

BAI, Y.; ZHANG, Z.; DENG, M.; CHEN, L.; HE, C.; ZHUANG, X.; CHEN, X. Thermo- and PH-Responsive Microgels for Controlled Release of Insulin. **Polymer International**, v. 61, n. 7, p. 1151–1157, 2012.

CARINO, G. P.; JACOB, J. S.; MATHIOWITZ, E. Nanosphere Based Oral Insulin Delivery. **Journal of Controlled Release**, v. 65, n. 1-2, p. 261–269, 2000.

CARINO, G. P.; MATHIOWITZ, E. Oral Insulin Delivery. **Advanced Drug Delivery Reviews**, v. 35, n. 2-3, p. 249-257, 1999.

CHOPRA, S. **Development of Nanoparticles for Oral Delivery of Insulin**. 2017. Massachusetts Institute of Technology, 2017.

FOSS, A. C.; GOTO, T.; MORISHITA, M.; PEPPAS, N. A. Development of Acrylic-Based Copolymers for Oral Insulin Delivery. **European journal of pharmaceutics and**

biopharmaceutics, v. 57, n. 2, p.163-9, Mar. 2004.

INTERNATIONAL DIABETES FEDERATION. **IDF SACA Region**. Disponível em: <https://www.idf.org/our-network/regions-members/south-and-central-

IYER, H.; KHEDKAR, A.; VERMA, M. Oral Insulin – a Review of Current Status. **Diabetes, Obesity and Metabolism**, v. 12, n. 3, p. 179–185, 2010.

LIN, C.; METTERS, A. T. Hydrogels in Controlled Release Formulations : Network Design and Mathematical Modeling. **Advanced Drug Delivery Reviews**, v. 58, n. 12-13, p. 1379–1408, 2006.

LOWMAN, A. M.; MORISHITA, M; KAJITA, M.; NAGAI, T.; PEPPAS, N. A. Oral Delivery of Insulin Using pH-Responsive Complexation Gels. **Journal of Pharmaceutical Sciences**, v. 88, n. 9, p. 933–937, 1999.

MORISHITA, M.; GOTO, T.; PEPPAS, N. A.; JOSEPH, J. I.; TORJMAN, M. C.; MUNSICK, C.; NAKAMURA, K.; YAMAGATA, T.; TAKAYAMA, K.; LOWMAN, A. M. Mucosal Insulin Delivery Systems Based on Complexation Polymer Hydrogels: Effect of Particle Size on Insulin Enteral Absorption. **Journal of controlled release**, v. 97, n. 1, p. 115–24, 2004.

MUNDARGI, R. C.; RANGASWAMY, V.; AMINABHAVI, T. M. Poly (N-Vinylcaprolactam-Co-Methacrylic Acid) Hydrogel Microparticles for Oral Insulin Delivery. **Journal of Microencapsulation**, v. 28, n. 5, p. 384–394, 2011.

RAYMUNDI, V. C.; AGUIAR, L. G.; SOUZA, E. F.; SATO, A. C.; GIUDICI, R. Controlled Release of Insulin through Hydrogels of (Acrylic Acid)/Trimethylolpropane Triacrylate. **Heat and Mass Transfer**, v. 52, n. 10, p. 2193–2201, 2016.

SCHMIDT, M. I.; DUNCAN, B. B.; HOFFMANN, J. F.; MOURA, L. de; MALTA, D. C.; CARVALHO, R. M. S. V. de. Prevalence of diabetes and hypertension based on self-reported morbidity survey, Brazil, 2006. **Revista de Saúde Pública**, v. 43, p. 74–82, 2009.

SHAH, D.; AGRAWAL, V.; PARIKH, R. Noninvasive Insulin Delivery System : A Review. **International Journal of Applied Pharmaceutics**, v. 2, n. 1, p. 35–40, 2010.

SOUZA, E. F. **Estudo Experimental e Modelação Matemática do processo de Produção de Hidrogéis de Poly(Ácido Acrílico)**. 2013. Faculdade de Ciencias e Tecnologia da Universidade Nova de Lisboa, 2013.

UHRICH, K.; CANNIZZARO, S.; LANGER, R.; SHAKESHEFF, K. Polymeric Systems for Controlled Drug Release. **Chemical Reviews**, v. 99, n. 11, p. 3181–3198, 1999.

WORLD HEALTH ORGANIZATION. **Global Report on Diabetes**. [s.l: s.n.].

WU, Z. M.; LING, L.; ZHOU, L. Y.; GUO, X. D.; JIANG, W.; QIAN, Y.; LUO, K. Q.; ZHANG, L. J. Novel Preparation of PLGA/HP55 Nanoparticles for Oral Insulin Delivery. **Nanoscale Research Letters**, v. 7, n. 1, p. 299, 2012.